NEA
693.852
C397

Scientific Programme

PN-ABJ-240

posium on

Earthquake Engineering

Development

20523

held in ankara, november 1974

T

Earthquake engineering.

NEA
693.852 CENTO Symposium on Earthquake
C397 Engineering, Ankara, 1974.
Earthquake engineering. 1974.
240 p.
CENTO scientific programme report
no. 18.

1. Earthquakes and building - NEA. 2. Building materials - NEA. 3. Soil mechanics - NEA. 4. Disaster relief - NEA. 5. Engineering geology - NEA. 6. Seismology - NEA. I. Title.

PN-ABJ-240
73481

CENTO Scientific Programme

SYMPOSIUM ON

EARTHOUAKE ENGINEERING

held in Ankara
November 18 -- 20, 1974

Report No. 18

CENTO SCIENTIFIC SECRETARIAT

P.O. Box 1828, TEHRAN

Agency for International Development
Library
Room 1656 NS
Washington, D.C. 20523

CONTENTS

Welcoming Address 1
Professor Tarık G Somer

Opening Remarks 2
Mr. Morris Crawford

Stronger Masonry by Means of Reinforcing Plugs 4
Professor W.O. Keightley

Earthquake Design and Construction in Developing Countries 11
Mr. J.D.M. Lloyd

Engineering Report on the İzmir Earthquake 1974 15
Dr. Polat Gülkan and Dr. Mehmet Çelebi

Fatigue Crack Propagation and Earthquake Prediction 32
Dr. Uğur Kuran

Earthquake Analysis of Geometrically Nonlinear Systems 33
Dr. H. Faruk Karadoğan

Influence of Embedment on Vertical Foundation Response 49
Dr. Selçuk M. Erden and Professor Kenneth H. Stokce

Behaviour of Dry Sand Slopes Under Seismic Loading Conditions 62
Professor Vahit Kumbasar and Dr. Ali Erguvanlı

On the Application of Plane-Strain Analysis in Soil-Structure Interaction Problems 72
Professor W.D. Liam Finn, Dr. E. Varoğlu and Mr. T. Nogami

Some Soil Engineering Aspects for Construction Works in Earthquake Zones 84
Professor S. Nazır Ahmad

The Prediction of Earthquakes by an Electrical Method 85
Mr. Fikret Kaftanoğlu and Dr. Bilgin Kaftanoğlu

Non-Linear Wave Propagation in Soils 94
Dr. A. Askar and Dr. A.S. Çakmak

Photographs of the Lice Earthquake of 1975 107

Seismic Analysis of the Site of Soma-II Thermoelectric Plant 111
Professor Semih S. Tezcan and Dr. H. Turan Durgunoğlu

A Geodynamical Study for the Central Ankara Region 125
Dr. Çetin Soydemir, Dr. Aybars Gürpınar and Mr. Yener Özkan

The Stiffness of an Infilled Portal Frame Under Horizontal Load 141
Dr. S. Tanvir Wasti and Dr. Polat Gülkan

Free Vibration Analyses of the Bosphorus Suspension Bridge 151
Professor Semih Tezcan and Dr. Muzaffer İpek

A Model for Shear Pinched Hysteresis Loops 161
Dr. M. Çelebi

Analysis of a Hospital Damaged by the Burdur Earthquake 169
Mr. Alkut Aytun and Mr. Nejat Bayülke

Simple Zoning of North-East of Iran 179
Dr. K. Moazami Goudarzi and Dr. J. Hossein Javaheri

The Classification of Hazard Zones in Pakistan 186
Mr. Anwaruddin Ahmad

Motion Instrumentation in Iran 197
Dr. A.A. Moinfar

The Study of Past Earthquakes in Iran 203
Dr. M. Banisadr

The Correlations of Intensity with Ground Motion 206
Professor N.N. Ambraseys

Random Vibration of an Elastoplastic System 217
Dr. İbrahim Helvacı and Dr. Aybars Gürpınar

RECOMMENDATIONS 233

LIST OF PARTICIPANTS 234

WELCOMING ADDRESS

Professor Tarik G. Somer
Middle East Technical University, Ankara

It is with great pleasure that I welcome you to the Cento Symposium on Earthquake Engineering and Engineering Seismology. Disasters due to earthquake are one of the common problems faced by the CENTO countries. For this reason there must be a mutual objective and incentive amongst the scientists and engineers of these countries to search for better methods for the prevention of seismic disasters. Only then can cooperation on administrative levels lead to implementation of these methods for effective disaster prevention.

I hope that this occasion will mark the beginning of greater cooperation between the scientists of CENTO countries in relation to earthquake problems; such cooperation already exists between Iran, Pakistan and Turkey in many other scientific and technological fields under the sponsorship of CENTO.

In recent years, the field of earthquake engineering and engineering seismology has gained great momentum in Turkey. In the Middle East Technical University, this momentum has manifested itself in the formation of the earthquake engineering research group; the principal organizers of this symposium. Collective efforts in interdisciplinary fields such as earthquake engineering and engineering seismology have proved to be very successful both in pure and applied research as well as in implementation of the findings from such research. For this reason I am very hopeful that this symposium will be successful and fruitful.

I extend my best wishes to the scientists, engineers and architects gathered here in their future cooperation.

OPENING REMARKS

Mr. Morris Crawford
Deputy Secretary General (Economic)

I am delighted to welcome you this morning on behalf of the Secretary General of CENTO to the CENTO Symposium on Earthquake Engineering. At the same time, I want to express special appreciation to TUBITAK, METU and to our other Turkish hosts for making such excellent arrangements for this meeting.

Earthquakes are natural phenomena of the planet we live on. Like the weather, which Mark Twain once described as a subject that everyone talks about, but no one does anything about, earthquakes are more a matter of idle discussion than serious consideration. We in CENTO regard this as a mistaken view. There may be, as yet, nothing that we can do to prevent earthquakes; indeed it is difficult to see how the gigantic movements of the earth's surface that are a part of its natural evolution can ever be controlled.

There is much that can be done, however, to alleviate and to relieve the effects and consequences of earthquakes.

First, quick and effective help is essential for the people who live in towns and villages that are hit by earthquakes. Better ways of providing this help have already been developed under CENTO. Much more needs to be done, and both the Military and the Economic wings of CENTO are actively trying to work out improved schemes for bringing immediate relief—tents, medical supplies, emergency food supplies—to disaster areas.

Second, it is possible, if earthquake prone areas and sites are identified, to minimize the actual effects of earthquakes on people. New towns and villages can be developed or houses constructed where the danger from earthquakes is minimal or where the effect is less severe. Furthermore, those people who live in earthquake prone areas can better prepare themselves for the inevitable, and take precautions that will enable them to pass easily through what otherwise might be a calamitous and disastrous experience for themselves and their families. The geological and tectonic studies which CENTO is sponsoring alongside and in cooperation with major scientific bodies can indicate those areas and identify the localities where earthquakes are most likely, as well as those which are relatively immune to earthquakes.

The third approach is the main subject of this Symposium. Improving building construction and design is a critical part of coping with earthquakes. It is the engineering aspect of earthquakes that is the theme of this meeting. In many places houses are likely to collapse in a moderate or strong earthquake, and injuring or killing the inhabitants Public buildings are especially vulnerable. This is not necessary. This is avoidable. Better building technology can do much to strengthen houses, office buildings and apartment and hotel structures. Modern engineering can demonstrably show how structures can be built that will survive without damage even from the most severe earthquake disasters.

But it is not enough to prove that earthquake-immune structures can be built. It is also necessary to show how they can be built at an acceptable cost. For the cost factor is often —perhaps always— the paramount factor. It is usually the least prosperous, often the poorest, individuals who are the principle victims of earthquakes. It is they who are most in need of advice from earthquake engineers; it is they who need most help in building better and stronger houses, using materials that are available to them, using materials that exist in abundance and are relatively cheap to use, and which villagers can work with easily themselves. I am most gratified that this aspect of earthquake engineering will be a major topic for consideration by the experts and specialists at this symposium.

In short, CENTO is pursuing a three pronged attack of Relief, Science and Technology on earthquake disasters; of Relief to assist those who are suffering from the ravages of earthquakes; of Science to warn against the danger of the disaster striking; and of Technology to enable families to build houses that will protect them against the worst destructiveness of earthquakes.

This is an important meeting. I hope your discussions will be stimulating and productive. You have a vital contribution to make to the progress and well-being of the CENTO Region. I wish you the greatest success in your deliberations.

STRONGER MASONRY BY MEANS OF REINFORCING PLUGS

Professor W.O. Keightley

Brick masonry is at present one of the most common building materials in the urban areas of the Middle East but it is not an ideal material in areas where strong ground shaking is likely. Both bricks and mortar are brittle, and the tensile adhesive strength of mortar to brick is low, sometimes almost zero. Although the computed average stresses in walls due to earthquake loading might be very small, cracks propagate through the walls due to the law tensile strength and the brittleness of the mortar.

In much of the Middle East the clay is not well compressed or well fired, so the bricks are weak and highly absorbent. Unless they are well soaked before laying, too much moisture is sucked from the mortar and the joints are of low strength, even if the mortar was of good quality. Often the content is low and unwashed sand is used, so that joints crack at low levels of ground acceleration. Under sustained shaking the mortar is quickly reduced to powder, some of which falls from the joints, allowing bricks to bear unevenly against other bricks and they split under the concentrated vertical load. A ratchet phenomenon is caused by unequal friction in different directions, so cracks grow wider, and bricks are forced out individually or in groups, resulting in collapse.

A bearing wall in a seismic region should not only present a high resistance to initial cracking, but also carry vertical loads even though grossly cracked and distorted. This means the bricks must be held together beneath the load and the wall should be capable of gross deformation, but resist such deformation with great tenacity. Ideally every wall, whether load carrying or not, should possess these properties so that the building has more than one line of defence, and the walls should be tied to floor slabs above and below to transfer shear acting in the planes of the walls and also to prevent walls from toppling sideways.

The difficult problem with masonry is to create toughness out of brittle elements which are connected together through planes of weakness. The method should be economical and require only simple technical skill and knowledge by the builders.

This paper suggests short plugs which, as each course is laid, are inserted into holes in the bricks so that each brick is connected to those above and below. Every horizontal mortar joint is crossed by two plugs in the length of one brick. The plugs provide shear and some tensile resistance through their own strength, hold loosened

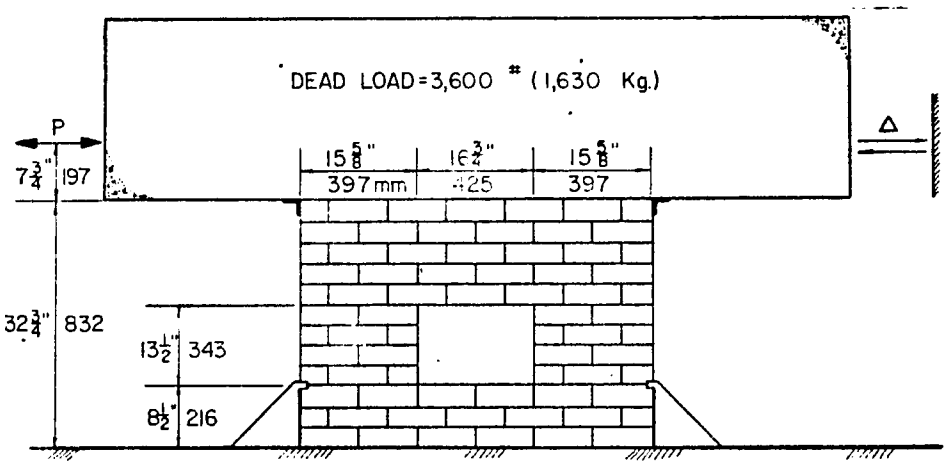

FIGURE 1. TEST PANEL FOR RECIPROCATING LOAD

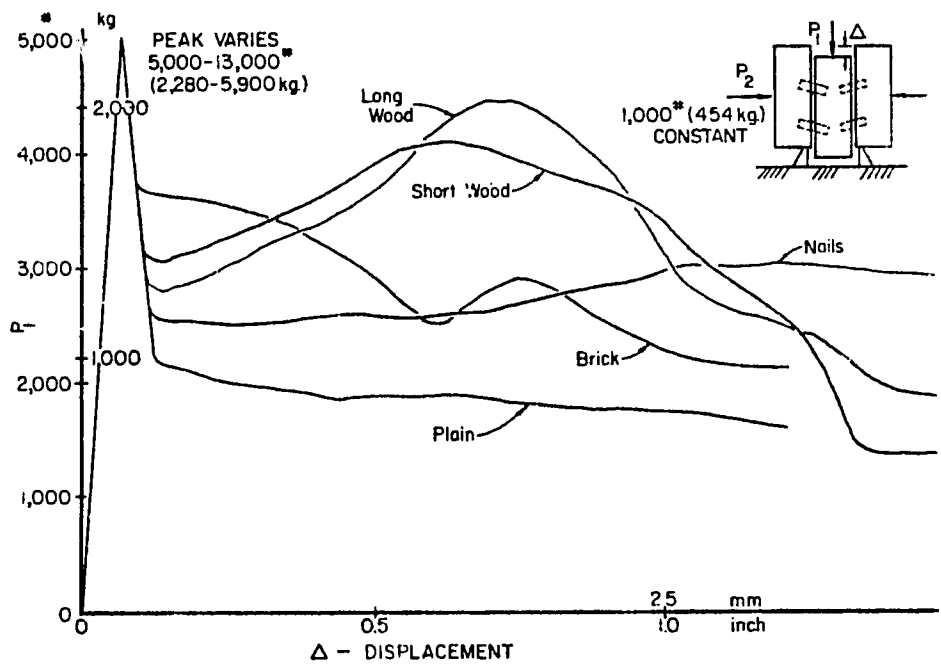

FIGURE 2. 3-BRICK SHEAR TEST

bricks from falling out, and cause cracking in a wall to appear as many small cracks rather than a few large cracks.

MATERIALS AND PROCEDURES

Two types of test specimens were prepared: panels one wythe thick, as shown in Figure 1, subjected to dead load compression and to reciprocating horizontal loads from an hydraulic ram; and 3-brick specimens, as shown in Figure 2, subjected to a constant clamping pressure and a unidirectional force which sheared the centre brick from between the outer two (see the preceding page).

The bricks, 194 x 92 x 57 mm, were hard and difficult to drill with a carbide-tipped masonry bit. Absorption after 24 hours in cold water was about 6%. The bricks were laid in a room dry condition.

Mortars of different strengths were used. Originally very strong mortar (2:5:1 cement:sand:lime), having tensile strength of 14.7 kg/cm^2 was used; however, with this the panels did not break in diagonal tension as usually observed in buildings which have been damaged by earthquakes, and the effects of the plugs were not significant. Panels were then laid in very weak mortar (1:6 cement:sand, tensile strength of 1.4–2.1 kg/cm^2) so that the desired type of failure could be obtained. Mortar quality was monitored by making 8 tension specimens and breaking these at the same time a panel was tested. Care was taken to see that the mortar was reasonably plastic (this was impossible with the lean mix) and all bricks were lightly tapped with the trowel to try to achieve bonding over all surfaces.

Figure 3 (page 7) illustrates the types of plugs which were investigated. The wood plugs were sawed from very soft pine, which showed a shearing strength of 210 kg/cm^2 when cylindrical specimens 19 mm diameter were broken in close-coupled shear. Hardwood plugs, used in one panel, were approximately twice as strong when tested in the same manner.

The double headed nails were made from commercial soft wire nails, 3.5 mm diameter and the brick plugs were sawed from the bricks used in the test specimens.

The walls were built as unsupervised workmen would by putting in the plugs, but taking no care beyond that. A bed of mortar was placed, bricks were laid in it, and then the plugs were inserted and pushed through the bed joint to penetrate halfway into the course below. With plastic mortar, the plugs were often fairly well anchored in mortar, probably the result of tapping with the trowel, something most workmen would not do. Larger clearances between the plugs and the holes would have probably resulted in better embedment of the plugs.

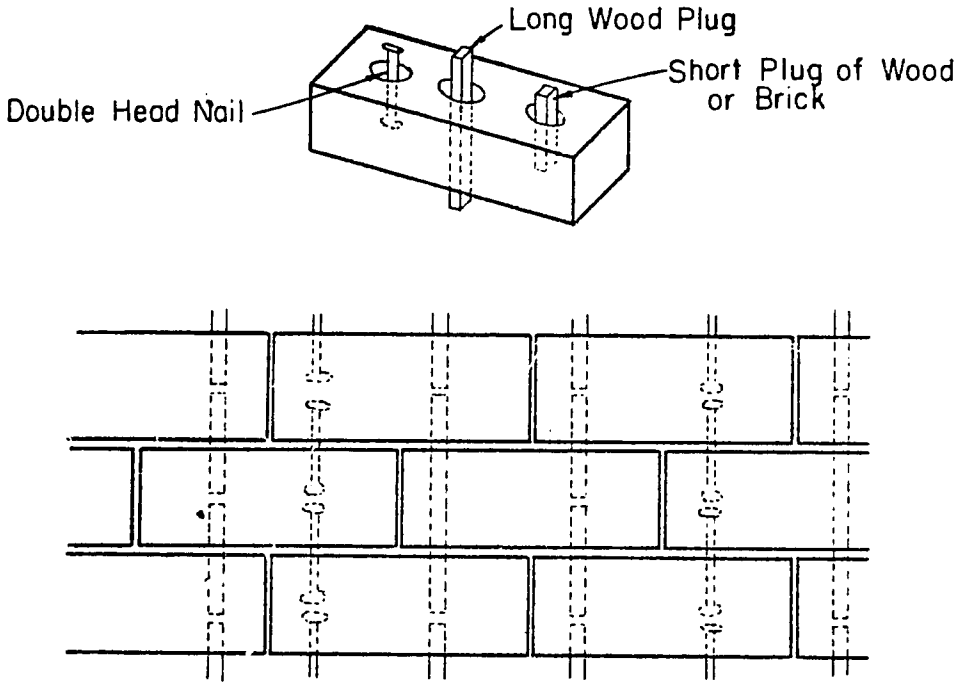

FIGURE 3. TYPES OF PLUGS TESTED

The amount of extra labour required to place short plugs is slight if the holes in the bricks are uniformly spaced, if the plugs are not too thick relative to hole size, and if the mason can make uniformly thick head joints. The author and a graduate student, rather novice masons, could build plug reinforced walls with little extra effort. The plugs used were 16 mm square in holes 32 mm diameter. It is estimated that labour costs for including short plugs should be increased by no more than 10%.

The cost of the plugs themselves is not insignificant. In the USA two wood plugs would cost 6 , about 2/3 the cost of a brick. Brick plugs would be cheaper, and although they do not possess the ductility of wood, they bond with mortar.

TEST RESULTS

Panels of hard bricks under constant vertical pressure of 2.2 kg/cm^2 and slowly reciprocating horizontal load were compared with an unreinforced panel laid in weak mortar. There was a modest increase in toughness when the joints were reinforced

with hardwood plugs and greater strength with brick plugs. The reinforced walls were capable of withstanding greater deformation within their planes, but they failed prematurely by buckling sideways, which would not be expected to happen to the thicker walls used in buildings. Figure 4 shows the force-deflection behaviour of these panels, and Figure 5 shows the cracking pattern in the wood reinforced wall. Only one panel of each type was tested.

The unreinforced wall failed, and the reinforced walls were progressing toward failure, by the vertical joints opening and bricks migrating toward one edge of the panel. The failure proceeded directly from cracks developed very early in the loading

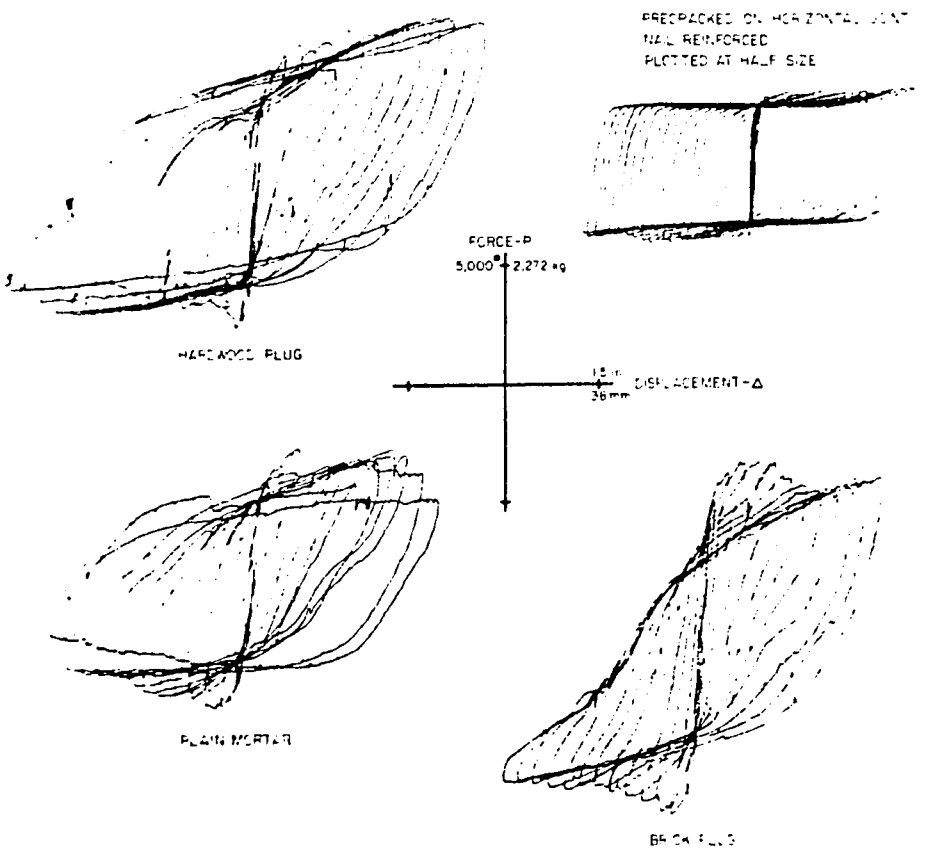

FIGURE 4. FORCE-DEFLECTION BEHAVIOUR OF PANELS

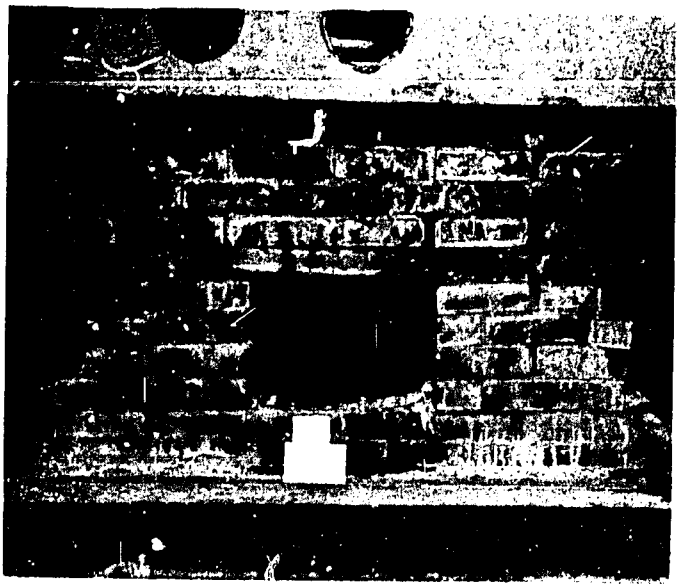

FIGURE 5. CRACKING OF WOOD-REINFORCED WALL

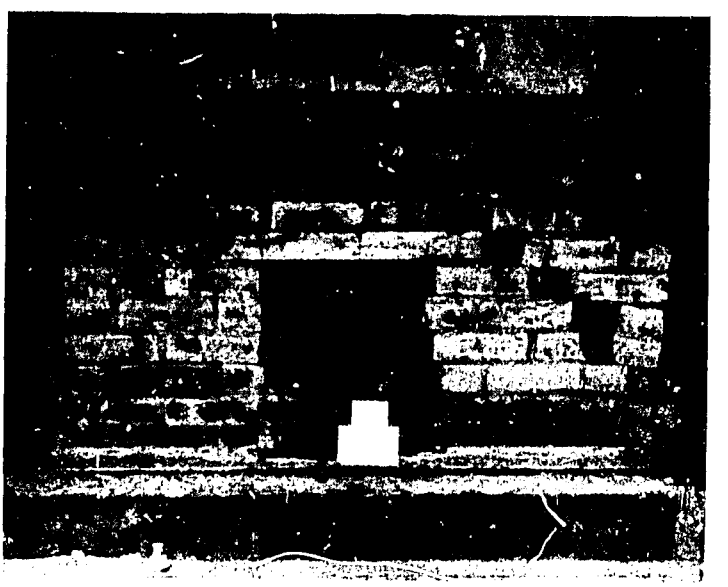

FIGURE 6. FAILURE OF UNREINFORCED WALL

although cracking also occurred later in other places.

Panels made with the strong mortar cracked into rather large blocks which then rocked back and forth with the reciprocating load. Softwood plugs did not appear to influence behaviour. Strong mortar was squeezed out in small plates from the active horizontal joints, but this was not sufficient to result in brick fracture. Failure was by displacement on a cracked surface of the upper portion of the wall in a direction perpendicular to the plane of the wall.

A panel reinforced with double-headed soft wire nails was cracked before the test along a horizontal joint at the top of the lintel. Under reciprocating load, the upper part of the panel simply slid back and forth in powdered mortar on the crack surface, without further damage. The nails appeared to add only slightly to the wall's resistance.

Unidirectional shear tests of joints of mortar consisting of 2:6:1 cement: sand:lime, tensile strength of 11.2 kg/cm^2 also carried out. In these a centre brick was pushed out under a constant normal pressure of 2.5 kg/cm^2, approximately the pressure found in the lower portion of a 2-storey wall-bearing residential building with window openings occupying 50% of the wall length. This shows that after fracture the peak resistance of joints reinforced with softwood plugs 17 mm square is about double the resistance due to friction only, the coefficient of friction varied from 0.75 to 1.0. This large increase was not shown in the tests of panels reinforced with wood plugs, probably because the plugs were not all fully activated simultaneously due to unequal clearances between the plugs and the sides of the holes, and because of the disintegration of the mortar in the holes surrounding the plugs.

Nails provided a modest increase in shear resistance in the 3-brick shear tests, but had negligible effect in a panel test.

Plugs 16 mm square, sawed from bricks, increased shear resistance significantly in the 3-brick tests just after the initial fracture, but the resistance decreased rather steadily with increasing displacement. Wedging and gouging of the broken plugs into the mortar resulted in an expansion of the mortar joints and necessitated continual loosening of the clamps to maintain constant normal pressure.

Peak breaking strengths of the joints, at first cracking, varied from 2,270-5,900 kg. Usually two closely spaced peaks were noted, one for fracture of each mortar joint. It is believed that variable wedging of the bricks against the lower supports caused the erratic peak values. After initial fracture, the effect of this wedging did not appear to be large.

Figure 2 presents the force-displacement behaviour of the 3-brick shear specimens. Most of the curves represent the averages of three tests.

CONCLUSIONS

Wood and brick plugs of the sizes used here appear to offer some increased earthquake resistance when used in lightly loaded walls laid in weak mortar. Under such circumstances the bricks would likely be cast wet rather than be extruded or dry pressed. The question of whether bricks with holes or bricks of different shape could be satisfactorily wet cast should be studied. Further work is also needed on the effect of larger plugs.

DISCUSSION

Dr. Çelebi asked what increase in stiffness of walls was obtained by various types of plugs. Dr. Keightley said that wood plugs did not bond with the mortar, and therefore did not have much effect until after the wall cracked. Brick plugs, on the other hand, bond with mortar and should produce slightly greater initial stiffness.

Dr. Wasti asked if extrusion of tongue-and-groove bricks was feasible, and if these could be used instead of plugs. Dr. Keightley said it would be necessary to test tongue-and-groove bricks, and thought it unlikely that strong bricks of this kind could be made by wet casting. He recommended that brick making plants be established to replace the numerous small wet casting operations. Dr. Bilgutay commented that Dr. Keightley had described structures built in the traditional way, with one brick half on the top of another; hexagonal bricks in panels would give extremely rigid structures.

EARTHQUAKE DESIGN AND CONSTRUCTION IN DEVELOPING COUNTRIES

Mr. J.D.M. Lloyd

The successful completion of any construction project calls for the exercise in an orderly sequence of a wide range of skills. While the interests of the architect are generally centred on aesthetics and the need for satisfactory spatial arrangements

and a comfortable occupation environment, those of the engineer are fundamental to durability and structural safety. He must ensure that the materials used meet structural requirements and are sufficiently durable to last the expected life of the building. He is also responsible for ensuring that the building will retain its integrity when subjected to the maximum stresses which it is likely to experience. In this, his duty lies not only to his client but also to the public at large.

There is a difference between the tasks of the analyst and designer although often these functions are carried out by the same person. The analyst is in a privileged position since for any given conditions of loading he is able with accuracy to evaluate stress conditions. The development of the computer has enabled him to do this more easily but the relevance of the answer still depends on the accuracy of the data used. This is determined by the designer who is called to make decisions often based on such indefinable factors as standards of construction, the degree of building maintenance acceptable and the extent to which effective control can be exercised over contractual or direct labour.

To facilitate structural analysis based on static theories, the UK and other national design codes make assumptions which are some way from the truth, for example that hinged joints have no rigidity, that steel reinforcement in columns has no capacity to undergo compression in excess of that on which the section is based and the horizontal cast in-situ members behave only as freely supported beams.

The dynamic analysis of structures based on the theory of simple harmonic motion was developed to explain vibration in machines and it also assumes, for example, that the materials of which the structure is built have characteristics as consistent as the steel in machines or the component parameters in electrical circuits. This is not so. Although it is possible to calculate the fundamental frequency of a well constructed building to within perhaps 20% of its actual value, actual periods increase with amplitude and only partially recover when the amplitude diminishes. This complicates analysis since it suggests that damping is amplitude—and frequency—dependent. Vertical accelerations also vary throughout the height of the structure by a factor of up to 3. Records of building response to the San Fernando earthquake show that in nearly identical buildings, closely located, vertical accelerations varied by a factor of about 1.5. The behaviour of large span suspended floors earthquake motion has seldom been considered but it would be unwise to assume they play no part in the overall pattern of events.

The parameters of ground motion used in the earthquake analysis of buildings are essentially derived from records of past events. These stretch back into the distant past in areas which have been populated for many centuries. Such records are of little help however, for analytical purposes and merely serve to emphasize the general background of seismic activity of the region. Developing countries in general have few

instrumental records of strong ground motion and where they are not available an assessment of the maximum ground motion is necessary from such data as is available. While an estimate of the likely magnitude of an event is possible from the records of international seismological centres, it is more difficult to decide possible intensities. Usually frequency characteristics are taken from strong motion records such as those of El Centro which may or may not be typical of local activity. Many uncertainties therefore confront the designer, so the benefits of complex and tedious dynamic calculations for "ordinary" buildings are doubtful since the basis on which they can be made is open to question.

In the UK the initial capital cost of accomodation in tall buildings is significantly greater than the same floor area in buildings of modest height; also tall buildings give rise to social and psychological problems and maintenance costs can be prohibitively expensive, perhaps 2 to 7 times those of lower rise structures. These factors have been chiefly responsible for their decline in appeal in the United Kingdom. The demands of national economy in a developing country would place even greater emphasis on these considerations. Also one must not overlook the risks of fire: in many cases unsuitable lining materials have aided the rapid spread of flame and the very dimensions of the structures have induced a chimney effect and made evacuation and fire fighting more difficult.

Some developing countries have restricted the height of buildings to 7 to 9 floors and are making vigorous efforts to improve the general standard of construction. To this end they have chosen to revise their building regulations and greatly strengthen their administrative and enforcement procedures while at the same time observing sound engineering principles in form of construction and layout.

Design parameters establish the performance of a building which is then expected to behave in a predictable manner for the rest of its life. However, the life span of a structure will vary according to the use to which it is put and prevailing economic climates. Industrial buildings will be almost entirely dependent on the economic climate for their life span but a period of about 60 years is normally considered as reasonable for domestic accomodation. Past experience shows that standards of accomodation are likely to change significantly within this period and changing fashions are likely to lead to minor structural alterations which of themselves will influence the fundamental period of the building and its response to earthquake motion. A lateral force analysis may, therefore, be appropriate for such buildings provided the forces taken are rationally based. Recent investigations of building movements during the San Fernando earthquake confirm that the appropriate lateral force is somewhat in excess of the 10% advocated by the 1970 Uniform Building Code. Well constructed buildings having no specially designed earthquake resistance should be capable of withstanding without significant damage an intensity of MM VI.

Implicit in the construction of buildings in the assumption that the materials of which they are built and the manner in which they have been assembled is such that they perform satisfactorily during the whole of their allotted life spans. This calls for an understanding by the engineer of the qualities and capabilities of the materials employed and the most efficient way of using them. There should be adequate site supervision and the regular testing of all materials incorporated in the structure. Many developing countries import processed materials such as steel and the source would depend on ruling prices. Although steel is manufactured to the standards of the country of origin, testing is always necessary and where the quality differs from that assumed during design a redesign will be necessary.

Most engineers underrate the variability of concrete and its quality should be closely controlled. There are more than 60 possible causes of variation although many of these may be eliminated for any given site. Variation of only one or two factors is sufficient to weaken the mix and adversely affect structural stability. For example, 5% voids caused by insufficient compaction or too high water content will cause a loss of strength by as much as 30%, accelerate the ingress of moisture and the corrosion of steel reinforcement, one of the main causes of loss of structural stability. The practice of obtaining concrete from ready mix suppliers has become increasingly popular throughout the world: this is sound provided the system has safeguards exercised by both the supplier and the engineer. It is always safe to assume that the supplier is as expert in the making of concrete as he makes out: often quality control is lacking and hoppers are not interlocked to deliver only the predetermined quantity of ingredients. These should be stated on the certificate of supply as should the amount and type of cement used, weight of aggregates, amount of water and designed strength. Variations can also occur due to travel times so that the only way of ensuring the quality of supply is by the continual making and checking of cubes.

Bar diameter and spacing is also a potent source of weakness and it is not unusual to find that there is insufficient space for the concrete to pass between the bars: then there is little bonding between the concrete and steel so that stress conditions are far removed from those assumed during design. Subsequent rendering after the removal of the formwork is only a short-term palliative since differential thermal expansion between the rendering and concrete quickly open cracks and provides access for moisture and premature corrosion of the reinforcement.

The profession of civil engineer is essentially that of the practical application of research and development and the examples cited above are only a few of many where the absence of proper supervision can lead to structures failing to meet their designed performance. Many codes are needed to cater for the wide range of construction needs and experience has proved them to be essential to the achievement of rec-

ognised standards of design and workmanship, but it must be borne in mind that the strength of any code rests on its efficient administration.

ENGINEERING REPORT ON THE IZMIR EARTHQUAKE, 1974

Dr. Polat Gülkan and Dr. Mehmet Çelebi

On February 1, 1974, a moderate earthquake of magnitude 5.2 on the Richter scale occurred in İzmir, the third largest city of Turkey. Immediately, an earthquake damage inspection and observation team of the Earthquake Engineering Research Group, Middle East Technical University went to the site. Subsequently two additional trips were undertaken by other teams. No strong motion records are available from this earthquake although two seismoscope traces were retrieved.

İzmir is built mainly on the small delta plain of the Kızılçullu river around the eastern end of the gulf, and on the height and ridges to the south. The population is about 600,000. Karşıyaka (pop. 175,000) lies across the gulf to the north, and is connected to the city by a chain of suburbs. The River Gediz discharges further on the northern shore of the gulf.

İzmir lies in the Aegean-Marmara earthquake zone which comprises a number of east-west trending grabens intersected by faults trending more or less north-south, parallel to the border of the Aegean basin. This system of grabens and faults extends eastward and southeastward from the islands of the Aegean Sea into the Turkish mainland.

Much of the surface geology of İzmir consists of fairly thick layers of sand, sand and gravel, silt with intermittent layers of clay and silty clays. The depth to bedrock is commonly greater than 150 m, and the water table is at a depth of 2 m although artesian wells have been drilled at a number of locations. Deep alluvial layers of similar materials are common also in the north of the bay.

The earthquake of 1st February, 1974 hit İzmir at 00h 01m 02s (GMT), or at about 2 a.m. local time, and lasted approximately 6 seconds. Patrolling policemen reported observing light phenomena, and "boiling" of the bay waters. The epicenter, determined by Bureau Central International de Seismologie, was at 38.6°N and 27.2°E.

The US Coast and Geodetic Survey[1] gave the coordinates as 38.6°N and 27.0°E with a depth of about 30 km. The estimated location of the epicenter is indicated in Figure 1. The magnitude of the earthquake, obtained[1] as the average of sixteen stations was 5.2 on the Richter scale. Although there were two strong motion accelerographs within İzmir province at the time, no records were available: the instrument in the city itself was not in operational order and that located in Salihli, a town 100 km east of İzmir, did not receive shocks strong enough to trip its starter circuit. There were, how-

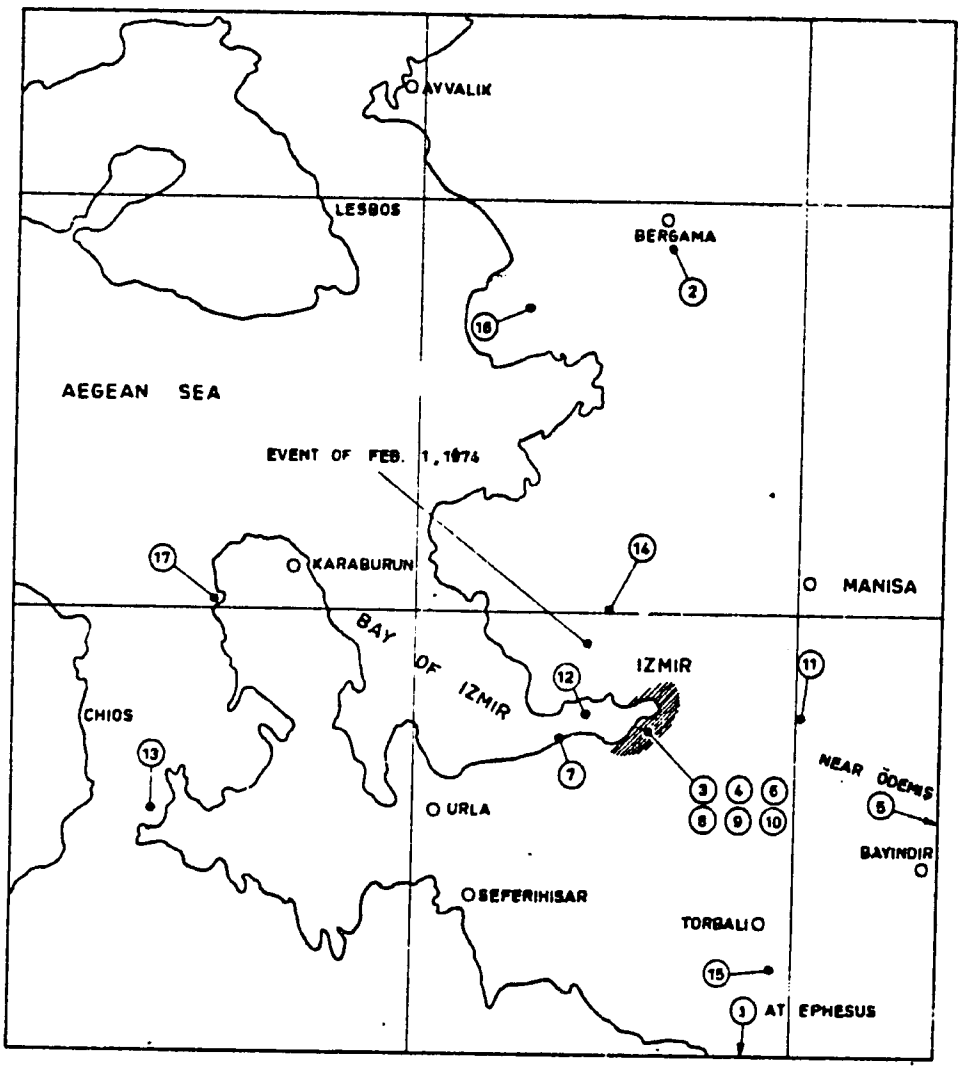

FIGURE 1. EARTHQUAKES IN THE IZMIR AREA

ever, two Wilmot SR-100 seismoscopes installed within the city limits by the Earthquake Research Institute of the Ministry of Reconstruction and Resettlement. Both of these instruments functioned during the strong ground motion. One instrument was on the bottom floor of a building founded on andesite, and the other was on a layer of alluvial deposit reaching a depth of about 200 m. The numerical information derived from these recordings is summarized in Table 1.

TABLE 1. INFORMATION DERIVED FROM TWO SEISMOSCOPES

Seismoscope Serial Number		755	765
Type of foundation material		Bedrock Andesite	Deep Alluvium
Undamped natural period, sec.		0.71	0.72
Fraction of critical damping		0.103	0.105
Tilt sensitivity, cm/rad		6.016 ± 0.164	6.019 ± 0.164
Maximum angular displacement, rad.	N–S	0.0581	0.1246
	E–W	0.0332	0.05
Maximum relative displacement, cm.	N–S	0.73	1.605
	E–W	0.4159	0.644
Maximum relative velocity, cm/sec.	N–S	6.456	14.0
	E–W	3.679	5.617
Maximum spectral acceleration, g	N–S	0.058	0.1246
	E–W	0.033	0.05

No surface faulting could be related to the shock, and within the city there were no reported landslides, foundation failures or water or gas main ruptures.

The ground motion was not very damaging but there were important varia-

tions of the extent of damage that was caused. 25 buildings were recorded after the shock as "heavily damaged", 183 as "moderately damaged" and 276 as "lightly damaged". These figures include damage in Karşıyaka but no categorization on building types was available. With several notable exceptions, buildings listed as "heavily damaged" after the earthquake were old, or of doubtful structural integrity originally. Most of the severe effects of the strong ground motion were concentrated in those areas of the city located on relatively recent alluvial fill material. The shock caused only two fatalities.

Soil Effects

A lack of precise information on soil types and their dynamic properties as well as the acceleration record of the strong ground motion makes it impossible to assess of soil conditions on structural response. There were buildings with superficial damage (cracked plaster, disintegration of cladding, etc.) in many parts of the city,

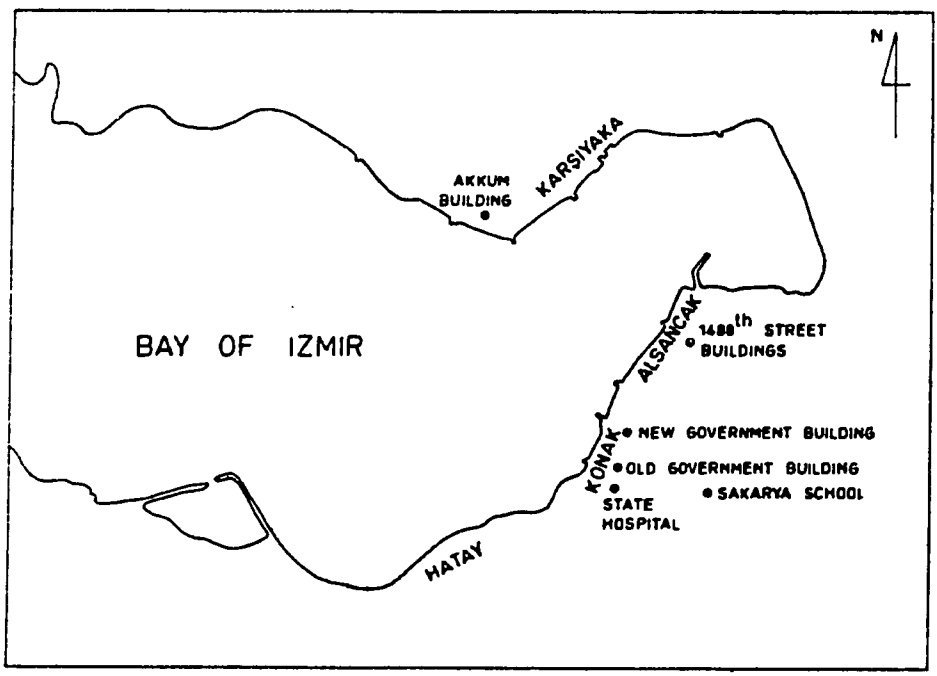

FIGURE 2. LOCATION OF DAMAGED STRUCTURES

and those that would later require repair were considerable distances apart. One possible case where "resonance" may have played an important role is the damage to a group of four-storey dwellings in or around 1488th Street. These buildings are said to have been built around 1953 for a cooperative housing group as two-storey units; they are all identical in plan and are all presumably constructed from similar quality materials. In 1962, a group of the owners applied for and received permission to build two additional floors above some of the original structures. All these units are load-bearing brick masonry with no reinforced concrete vertical load-carrying elements. The two-storey units suffered no damage, but all the four-storey once experienced various degrees of structural distress: some underwent extremely unsightly x-cracking at the first and second storey levels, and suffered considerable loss of structural integrity. The damage was due in part to the increased weight of the appended units but the fact that these houses are founded on deep alluvial fill may also have played a role in determining the magnitude of the accelerations developed in the longer period buildings.

Load bearing brick masonry buildings, other than those in 1488th Street fared well and no such building was considered in danger of collapsing. Two school buildings, both more than fifty years old, were damaged enough to be declared unsafe. One of these, a timber and mortar brick type, was probably not safe even before the earthquake. A state hospital, which lay in a semi-ruined state as a result of a previous fire, and a number of mosques appeared to have survived the shock with various degrees of cracking but none seemed to be an imminent danger of collapse. One structure which was badly damaged was the Akkum Building, as described below.

The Akkum Building

This residential five-storey reinforced concrete building was constructed in 1963. The structure is rectangular in plan. The concrete quality is indicated to have a minimum cylinder strength of 140 kgf/cm^2 and the undeformed steel was required to have a minimum yield strength of 2,200 kgf/cm^2. The structural computations for the floors were carried out for a two-way slab system with 12 cm thickness, although the actual floors were observed to have been 30 cm joists on 40 cm centrelines. The joists are formed by hollow lightweight cinder and cement blocks. In addition to the five regular stories, the building also has a penthouse which covers most of the plan area.

The Akkum Building is founded on a fill very close to the sealine and the foundation system is a two-way continuous strip foundation. The ground level, intended for use for commercial purposes contained very few walls in the column axes. Walls which did exist were made from hollow lightweight cinder cement blocks having very low structural strength. Floors above the ground housed eight flats per storey and the

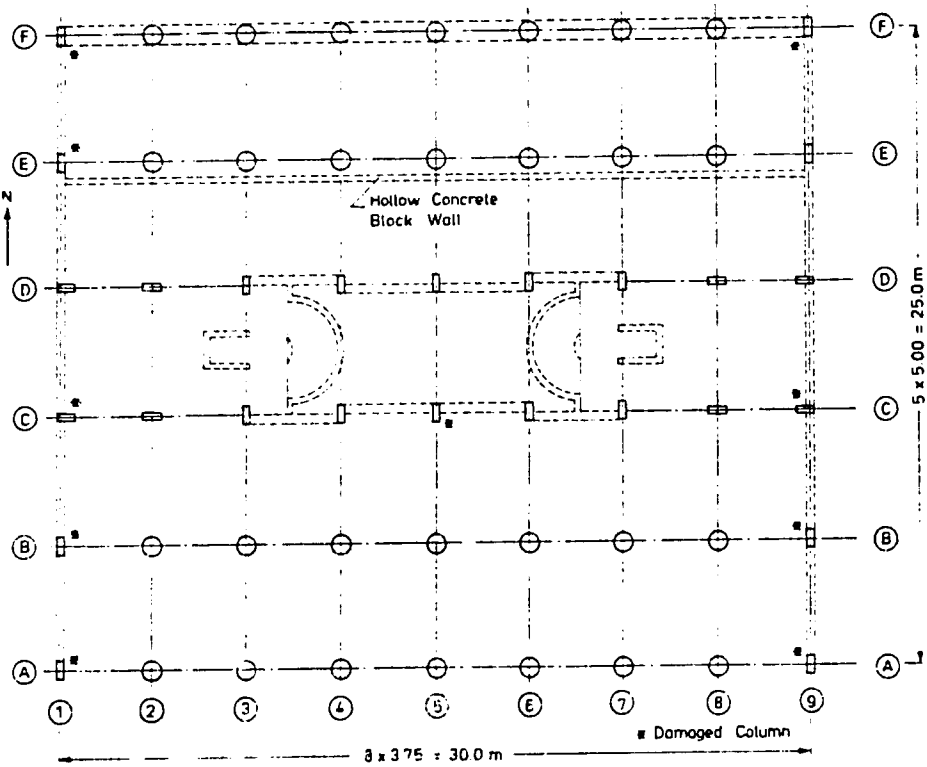

FIGURE 3. PLAN OF AKKUM BUILDING AND DAMAGED COLUMNS

liberal use of partition walls made these stories much stiffer against lateral loads than the ground level.

Damage to the building was concentrated at the ground floor and was confined mostly to the upper and lower ends of the columns. Columns A2, D2, D3, D4, E3, B5, A6 and B6 (Figure 3) had to be supported on timber stilts. The overall impression which column damage gave was that the building had swayed predominantly in the north-south direction essentially as a one-degree-of-freedom system: no column in the upper stories contained cracking to qualify it as having been damaged. That the structure was too flexible in the ground level compared with the upper floors supports this contention.

The axial loads on the ground level columns were calculated from the architectural drawings with tributary areas defined by panel centrelines. In determining

TABLE 2. GROUND LEVEL COLUMN PROPERTIES, AKKUM BUILDING

TYPE	b cm	h cm	D cm	Reinforcement	Columns with Equal Axial Load	Number (n)	l_4 dm	N (ton)	Nn (ton)
I	25	60	—	8ϕ18	A1,A9,F1,F9	4	180	55	220
II	35	60	—	16ϕ20	B1,B9,E1,E9	4	252	53	216
III	60	35	—	12ϕ20	C1,C9,D1,D9	4	85.6	67	268
					C2,C8,D2,D8	4	85.6	106	424
IV	30	60	—	12ϕ20	C3,C7,D3,D7	4	216	106	424
					C4,C6,D4,D6	4	216	80	320
					C5,D5	2	108	69	138
V	—	—	50	10ϕ20	A2,A3,A4,A5,A6,A7,A8 F2,F3,F4,F5,F6,F7,F8	14	429.8	70	980
VI	—	—	55	16ϕ20	B2,B3,B4,B6,B7,B8 E2,E3,E4,E6,E7,E8	12	538.8	82	984
					B5,E5	2	89.8	97	194
					TOTAL	54	2201.6		4168

these loads, concrete was assumed to have a unit weight of 2.4 t/m^3, and the live load at the time of earthquake was taken as 75 kg/m^2. The cumulative sum of the axial loads coming to the ground floor columns are indicated in Table 2 (see the preceding page). All columns at this level were further subclassified according to dimensions, reinforcement and configuration which resulted in recognizing six different types.

The capacity of column cross sections at the ground level to resist combinations of axial load and bending moment were calculated on the basis of the following material properties:

σ'_b = concrete cylinder strength = 100 kgf/cm^2 (measured by Schmidt hammer tests)

ε_u = maximum concrete strength in combined flexure and axial load = 0.003

σ_a = yield strength of steel = 2.200 kg/cm^2 (strain hardening ignored)

E_s = elastic modulus for steel = 2.1 $(10)^6$ kgf/cm^2

Assuming an equivalent rectangular distribution with 0.85 σ'_b stress and defining the bending moment about the plastic centroid, interaction curves given in Figure 4 were obtained for the column types defined in Table 2.

The structural system for the Akkum Building is symmetrical and simple. However, a reconstruction of the causes of damage must be limited because of the intermediate effect of walls at ground level on the structural behaviour, the lack of definite knowledge about the soil conditions, and the lack of adequate information about material properties and reinforcement details.

Since the damage pattern indicated a strong bias about the building shear in the north-south direction, we can consider only the effects of lateral forces in that direction. It is assumed that the ground level columns were fully restrained against rotation at either and although full details of their connections are not known.

The lateral load resisting mechanism of the building may be idealized simply as that of a box girder anchored at one end on fifty-four points (columns at the ground level). If axial deformations of the columns are ignored, the structure may be analyzed as a simple oscillator on account of the much greater rigidity of the floors above the first. The hollow concrete block walls and a brick wall around the elevator shaft at the ground level will be ignored in the following analysis and the full lateral load will be assigned to the columns in proportion to their relative stiffness.

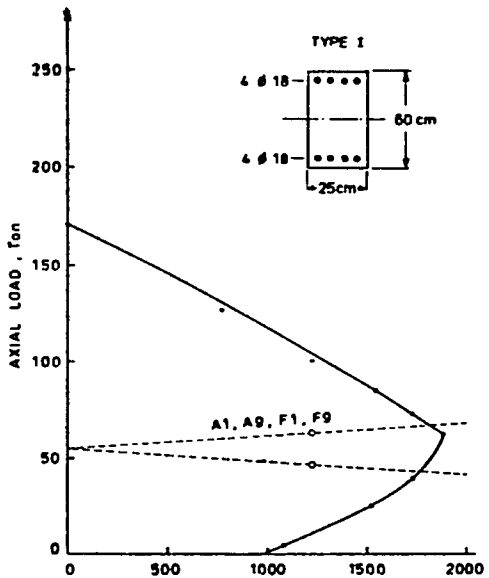

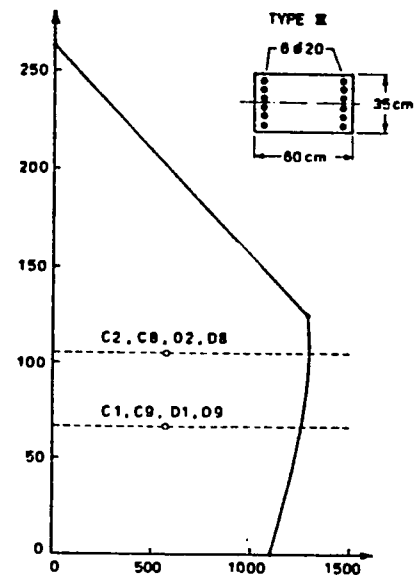

MOMENT , Ton - cm

FIGURE 4a. INTERACTION DIAGRAMS OF GROUND LEVEL COLUMNS

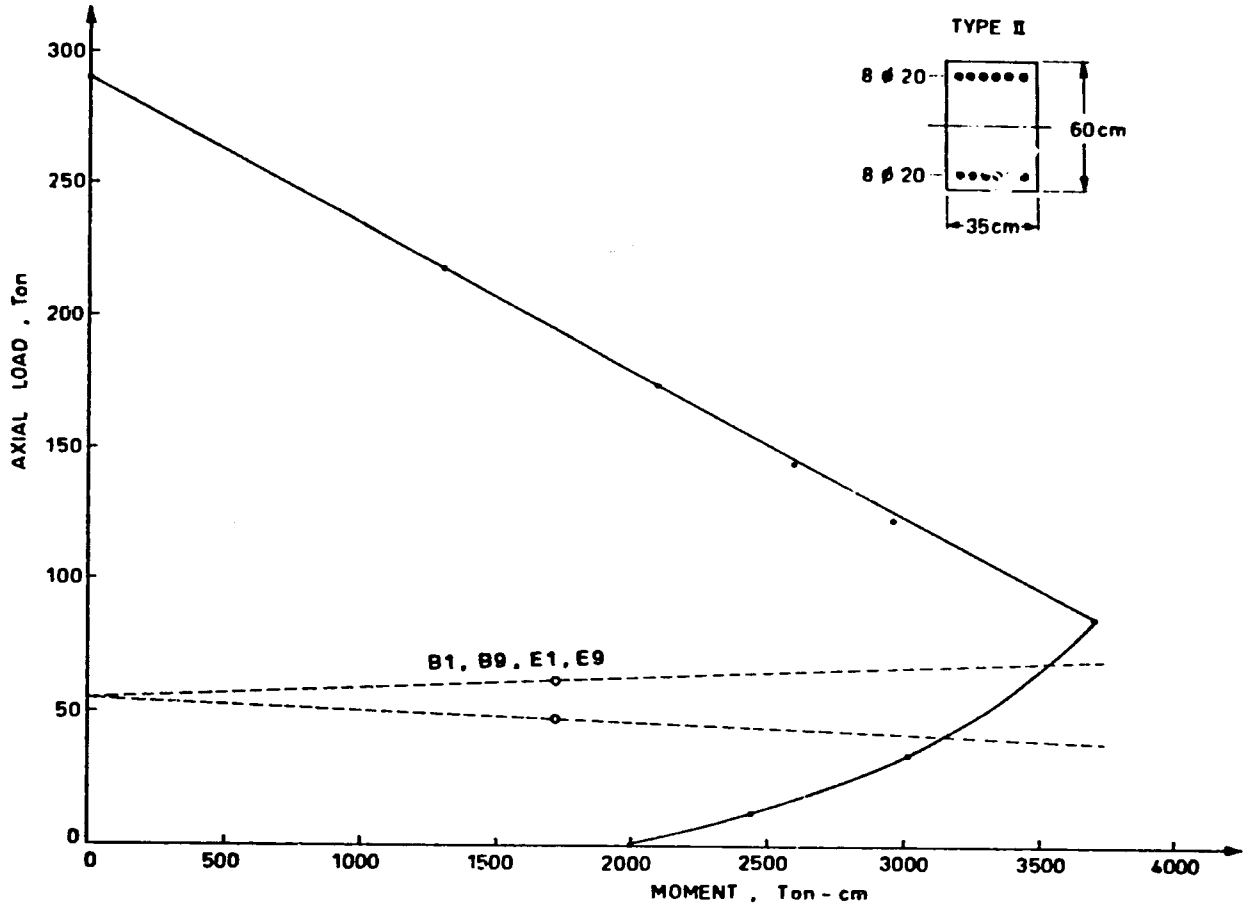

FIGURE 4b. INTERACTION DIAGRAMS OF GROUND LEVEL COLUMNS

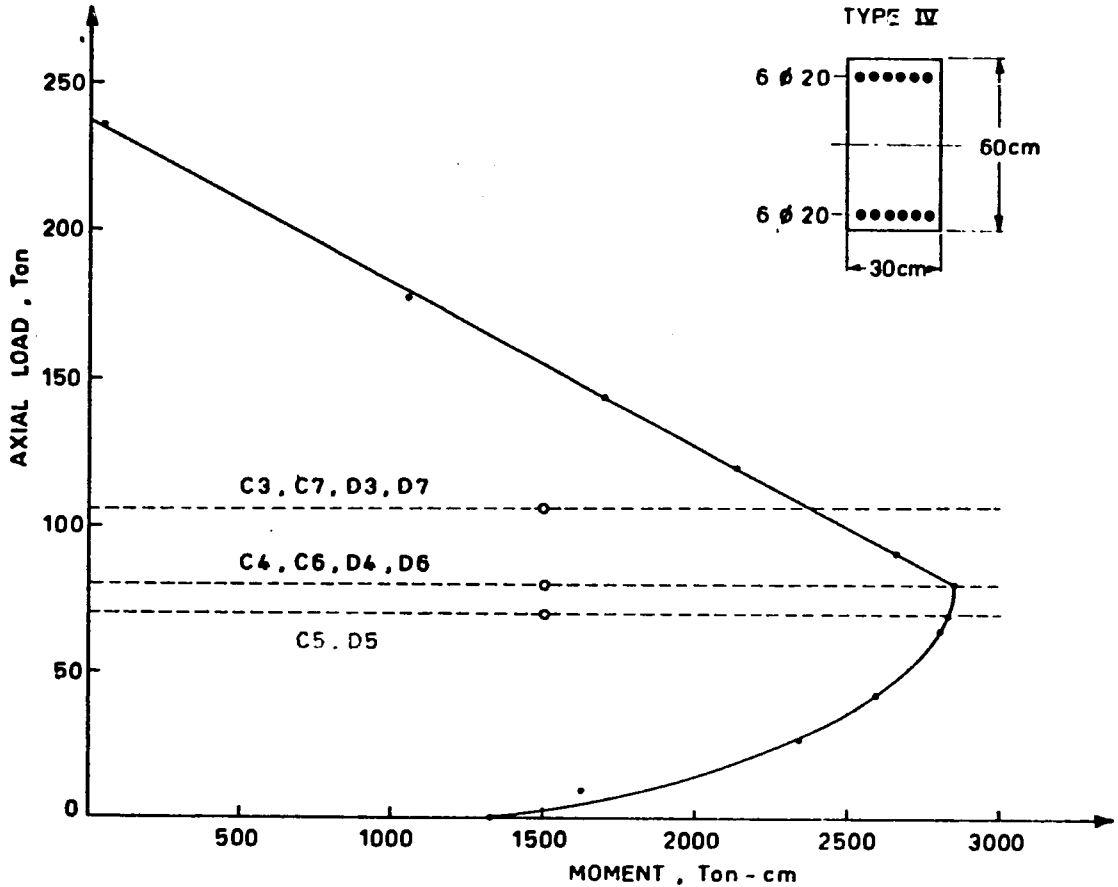

FIGURE 4c. INTERACTION DIAGRAMS OF GROUND LEVEL COLUMNS

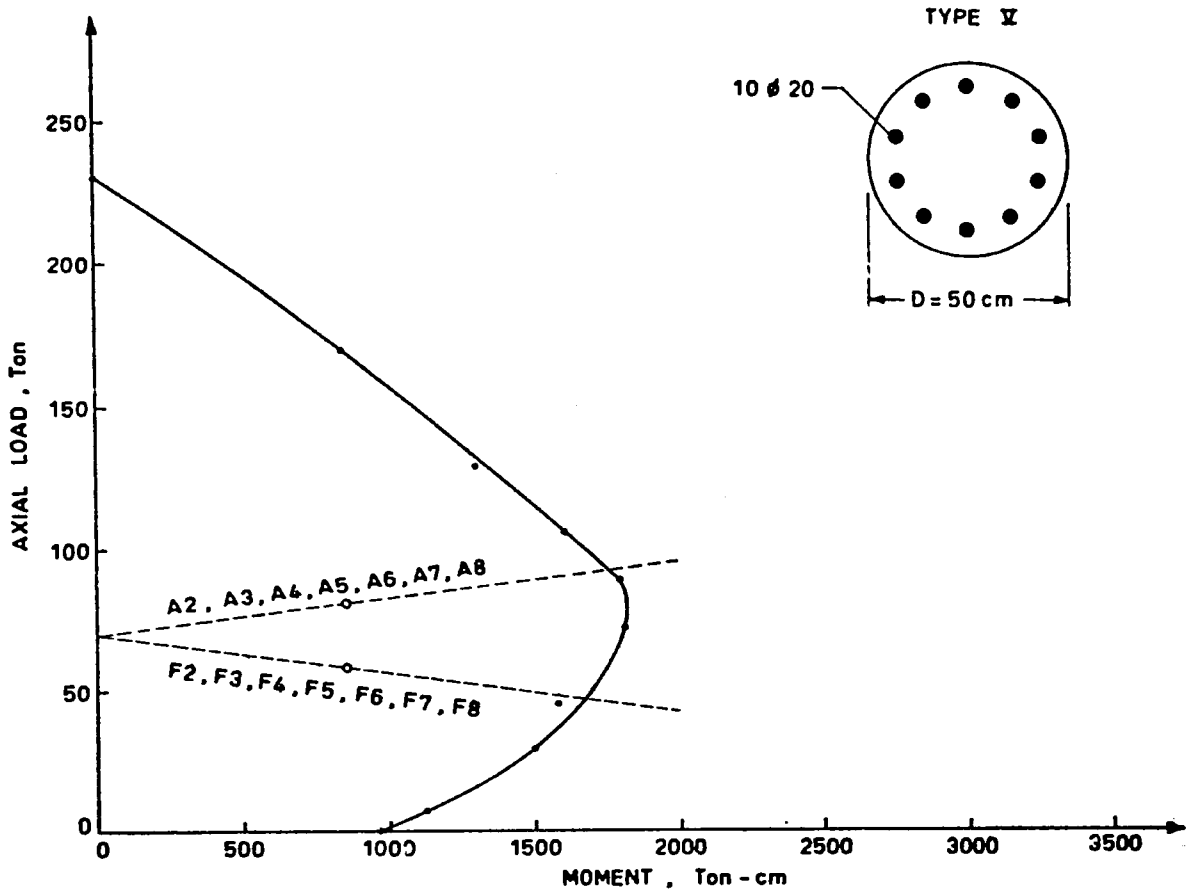

FIGURE 4d. INTERACTION DIAGRAMS OF GROUND LEVEL COLUMNS

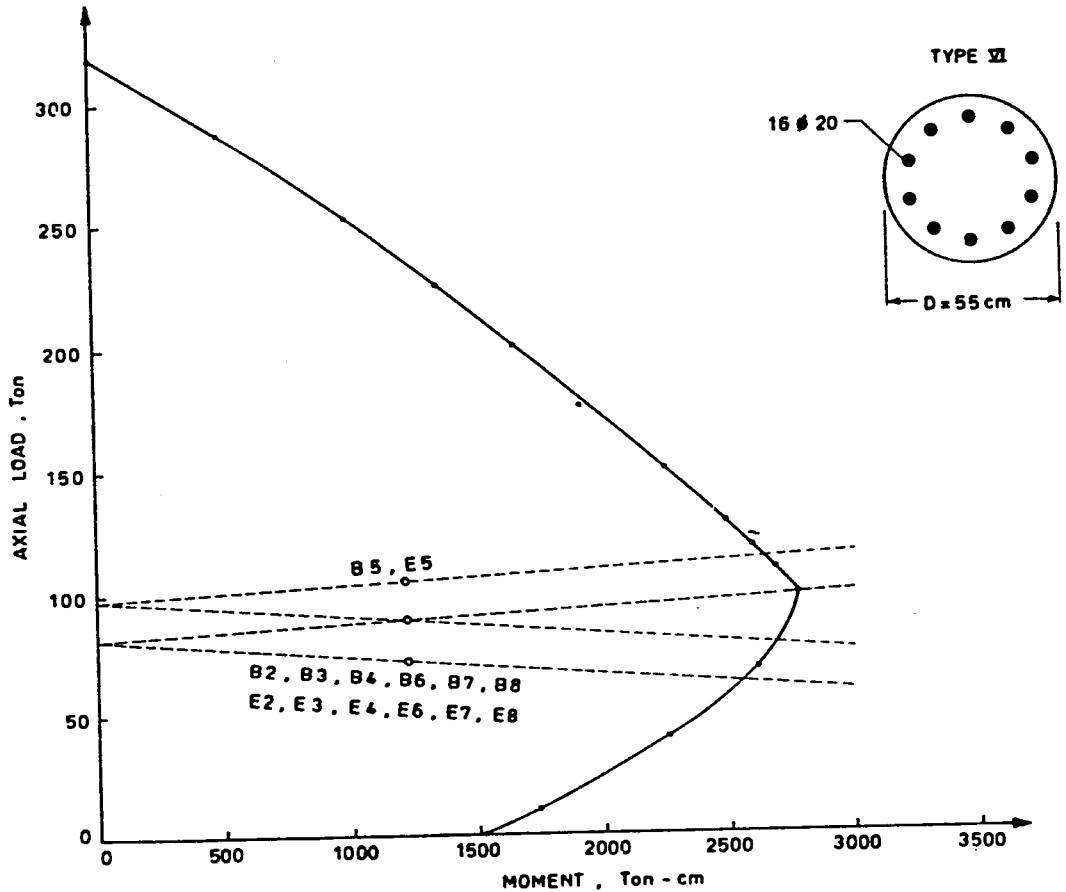

FIGURE 4e. INTERACTION DIAGRAMS OF GROUND LEVEL COLUMNS

TABLE 3. INFLUENCE OF LATERAL LOADS ON GROUND LEVEL COLUMNS, AKKUM BUILDING

Type	A m^2	y m	Ay^2	Number n	$I_{overturning}$ m^4	N (ton)	N_D ± (ton)	$I_{section}$ dm^4	$I/\Sigma I$	$Q=(I/\Sigma I)(417)$ (ton)	$M = 145Q$ (ton-cm)
I	0.15	12.5	23.44	4	93.75	55	8.72	45.0	0.0205	8.51	1234
II	0.21	7.5	11.81	4	47.25	54	7.33	63.0	0.0285	11.93	1730
III	0.21	2.5	1.31	8	10.50	67 106	2.44	21.4	0.0095	3.97	576
IV	0.18	2.5	1.125	10	11.25	106 80 69	2.09	54.0	0.0245	10.22	1482
V	0.196	12.50	30.63	14	428.75	70	11.40	30.7	0.0145	5.84	847
VI	0.238	7.50	13.39	14	187.43	82 97	8.30	44.9	0.0205	8.51	1234
			Σ	54	778.93						

$I_{overturning} = nAy^2$

Assuming that the resultant of the lateral load acts 10.15 m above the ground at the centre of the mass of the upper floors, the increase in axial load and bending moment for columns at the ground level can be found. For each column type, these increases are indicated in Figure 4 (see the preceding pages). Initial moments caused by gravity loads were neglected. The solid circles indicate the load-moment combination on the column for a lateral load of 417 tons, or 10% of the weight of the structure. For each column type two broken lines are given: these indicate whether the column is on the "tension" or "compression" side of the box girder. Computations on which these lines are based are summarized in Table 3. For columns on axes A, B, E and F an increase in moment is accompanied by a decrease in the axial load whereas for axes C and D lateral load produces only an increase in moment.

The results obtained from this simple analysis indicate that no column should be expected to fail in flexure on account of a 10% of g spectral acceleration (A). On the other hand, assuming that the shear strength (the nominal stress at which diagonal cracking occurs) of the columns is given by $0.5\sqrt{\sigma b}$, then columns of Type II and IV were likely to fail in shear given a lateral force of 10% of the weight of the building. Rectangular columns all had 8 mm diameter hoops at a spacing of 30 cm which contributed little to the shear strength. Circular columns were provided with spiral reinforcement at a pitch distance of 8 cm, and did not show shear distress. In fact columns B9, E1 and B1 (all of type II) exhibited diagonal cracking typical of shear failure. These columns must have failed in shear first and following a redistribution of lateral rigidity, damage must have progressively followed in the remaining columns.

In summary, the unusually low strength of concrete in columns at the ground level and the lack of adequate transverse reinforcement contributed towards the surprising extent of the damage observed in this building.

Intensity of the Ground Motion

There were no strong motion records of the earthquake motion, but the approximate order of the intensity can be estimated from the vibratory characteristics of the Akkum Building. Treating the structure as a simple oscillator anchored on fifty four columns, and using the gross sectional properties, the period may be determined as follows:

Weight of structure = 4168 tons

$$\text{Total lateral rigidity} = \frac{12E\ (\Sigma I)}{h^3}$$

where $E = (10)^6\ t/m^2$, $\Sigma I = 0.22\,(10)^4\ m^4$, $h = 2.90$ m (Table 3)

$$T = 2\pi \sqrt{\frac{W}{gh}} = 0.394 \text{ sec.}$$

This value compares reasonably well with that obtained from the modified UBC[2] equation.

Taking the height of the structure H = 17.4 m, and dimension parallel to the motion D = 25.0 m, Eq.2 gives T = 0.31 sec. A value of T = 0.35 sec. may therefore be reasonably assumed for the period of the building. As noted above a spectral acceleration of about 0.10 g may explain the damage observed. If one ascribes a damping

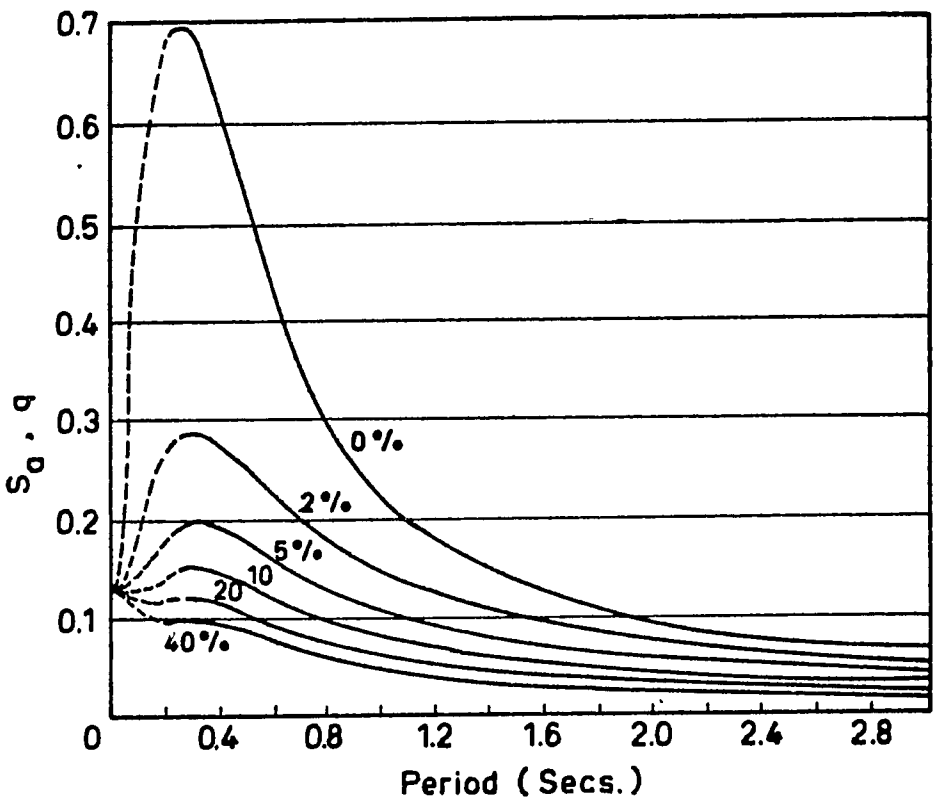

FIGURE 5. AVERAGE RESPONSE SPECTRA

of 5% of critical to the building, one would expect the building to have had a spectral acceleration (S_a) of 0.18 g. had it been subjected to the average strong motion acceleration.[3] Figure 5 shows the average strong motion acceleration spectra.

The ratio between the probable spectral acceleration A and S_a is 0.55; this means that in the N-S direction at the Akkum Building, the motion had an intensity 0.55 times as strong as indicated for the averaged strong motion spectra.[3] The latter equals 94.0 cm, so this indicates that the motion at the Akkum site had undamped spectral intensity of 53.0 cm.

REFERENCES

1. *US Geological Service, Nat. Earthq. Inf. Service (PDE), Feb. 1974.*

2. *Int. Conf. Building Officials, Sacramento, 1971. Uniform Building Code.*

3. *G.W. Housner, Proc. Amer. Soc. Civil Eng., 85, 109 (1959).*

DISCUSSION

In reply to Dr. Keightley, Dr. Gülkan said that some of the columns in the damaged building were circular and some were rectangular. All the rectangular columns had steel on two faces. Only the north-south motion was studied, and seismoscope records showed that this was the main component. Professor Nazır Ahmad asked if data were available about the soils, but Dr. Gülkan said that there was no information on the physical properties of the soils; only visual observations of the oscillations had been made.

FATIGUE CRACK PROPAGATION WITHIN THE EARTH CRUST DUE TO CYCLIC TIDAL LOADING AND EARTHQUAKE PREDICTION ALONG THE NORTH ANATOLIAN AND SAN ANDREAS FAULT SYSTEMS

Dr. Uğur Kuran

The application of three *in situ* field and four laboratory techniques to one specific case, namely, that of "Prediction of Earthquakes", were described in this research. The two *in situ* field techniques for determining Elastic Moduli and strain on rock bodies were reviewed. Two systems (Hydraulic jack and Extensometer) were described for the time dependence of the stress. Results of tests on different kinds of geologic formations (from different regions) which are subjected to repetitive loads, were reported. It was concluded that the presence of cyclic stress in the earth's crust due to tide generation force is responsible for earthquakes (or fatigue failures).

A review was given of the present state of knowledge of earthquake mechanism (or fatigue mechanism) that has been reached from studies on stress—deformation—time phenomena during Hydraulic jack tests, stress—strain—time phenomena within the earth's crust due to cyclic tidal loading, and fatigue crack propagation under repetitive loads.

An important secondary objective of this report was to describe a series of laboratory techniques for predicting fatigue life (or earthquake prediction) of rock samples. Results of tests on granite subjected to cyclic loading were reported. Both Reid's theory and the suggestion of Blake, which attribute the failure of rocks to stress levels exceeding the compressive strength of the rock structure, can be ruled out because the results of the present study indicate clearly that such failure can occur at stress levels well below the compressive strength of cultural material.

Therefore, fatigue failure (earthquake and rockburst) occurs when the cyclic tidal stresses in the earth's crust exceeds the endurance strength of the rocks.

Acoustic emission techniques, which have been widely used for non-destructive inspection purposes, have been used during this research programme to observe damage in fatigue rock specimens.

Both acoustic emission and continuous strain measurements on a centrally cracked cylindrical granite specimen indicate that strain-steps (or earthquakes) in high stress fatigue take place predominantly during crack propagation stage (CP). Each of the

strainstep mechanisms involved discontinuous crack extension (or jumps) which follows a path approximately parallel to the maximum shear zone.

The Kaiser effect occurs also in the cyclic loading of rocks at high stresses, that is if a rock is loaded to a given stress level and unloaded no emission will be observed during re-cycling until this level has been exceeded.

However, in the case of the rock experiments an exception was that low amplitude acoustic emission was observed at very low stress level.

A microscopical examination of a number of granite specimens in which cracking has occurred has shown that whenever a fatigue crack has subsequently developed in the shear zone it reveals an echelon pattern of exactly the same appearance as those experience in the field studies. The fatigue crack growth results which are based on micro-earthquake observations, have shown that at least three destructive earthquakes along the historic fault break in central California and two along the north Anatolian fault zone are likely candidates for near future large earthquakes.

It is believed that the earthquake mechanism described would not only reduce the intensive and unnecessary studies, but would accelerate geophysical engeneering and Rock Mechanics engineering studies, which would lead to a positive method of predicting earthquakes.

DISCUSSION

Professor Pınar thought that there were many kinds of cracks and their effects would be different.

EARTHQUAKE ANALYSIS OF GEOMETRICALLY NONLINEAR SYSTEMS

Dr. H. Faruk Karadoğan

To simplify the problem and keep computer time within reasonable limits some assumptions have been made in studies related to aseismic design. One of the con mon assumptions made was to neglect the effect of axial forces. Investigations

on models[1] and studies of the second order effect of axial forces have intensified during the last decade.[2] To clarify several aspects of the behaviour of certain structures, excited by real or artificial strong ground motions, mathematical models have been established and analysed by powerful computers. However, the results obtained from these studies can neither be generalized nor can they be easily put into practice by structural engineers.

The axial forces or lateral displacements in arches, radio-television towers, water tanks, silos, bunkers and in structures designed against buckling are relatively higher in comparison to those encountered in industrial and residental structure. Therefore, the second order effect of axial forces will be more pronounced in those systems. On the other hand, the structural engineer has to consider and limit the maximum amount of vibration and displacements which will occur during the life of the structure. Because of this, one can start to design any of the above structures by using the first order theory. In order to estimate the safety factor against buckling, the elastic buckling load of the system should be determined and then the necessity of the second order analysis should be decided. The design engineer may have to repeat the calculations several times. To avoid a quick method based on the results of the first order analysis and the safety factor against buckling is developed for materially linear, but geometrically nonlinear, systems, under dynamic loading conditions.

The assumptions made in this investigation are:

1 The system consists of straight bars in plane,

2 Bars are composed of linear elastic, homogeneous and isotropic material,

3 Displacements of the systems are relatively large but do not exceed the limitation of the second order theory, so the system has no geometrical linearity,

4 All external forces are conservative,

5 The axial forces are time-independent and axial deformations can be neglected in comparison with flexual deformations.

General Solution

When the displacements or axial forces are relatively great, as in slender structures (when the safety factor against buckling $N_b^{(1)}/N$ is relatively small), it is necessary to use the second order theory in which the deformed axes of the structure are taken into account only in the equilibrium conditions, but not considered in the

compatibility conditions. It is also known that one needs the axial forces which can be used in second order analysis to define the rigidity of the system as evaluated at the end of the first order analysis. On this basis the damped motion for lumped-mass multidegree freedom frame structures can be expressed as,

$$[M]\,[\ddot{\delta}]_{II} + [C]\,[\dot{\delta}]_{II} + [S]_{II}[\delta]_{II} = -[M]\,[U]\,\ddot{d}_x \qquad (1)$$

in which $[M]$ is the diagonal mass matrix; $[C]$, damping matrix; $[S]_{II}$, lateral stiffness matrix obtained according to the second order theory; $[\delta]_{II}$, a column matrix consisting of relative displacements according to the second order theory; $[U]$, a column matrix with its elements being 1 for horizontal earthquake excitations and $\ddot{d}_x$, the acceleration of the horizontal earthquake.

From the structural engineering point of view, it is more relevant to know the maximum values of $[\delta]_{II}$ than its variation with time during the whole earthquake excitation. In order to obtain reasonable results for practical purposes, the maximum displacements related to each mode, which do not occur at the same moment, can be added using a suitable procedure. To carry out an analysis like this, one has first to set up $[F]_{II}$ the lateral flexibility matrix, derived by using the second order theory and then find eigenvectors, eigenvalues and the participation factors according to the same theory, in addition to the corresponding values found previously by using the first order theory. It can be asked at this point to what degree will the changes in the dynamic characteristics of the system be, whose $\mathcal{N}_b^{(1)}/\mathcal{N}$ ratio is relatively small if the second order effect of axial forces is taken into account?

Dynamic Characteristics Dependent Upon Axial Forces

At a certain time "t", since the system considered is materially linear, the external forces are conservative and the stiffness of the system is constant for that moment, the relationship which expresses the interaction between the axial forces and the inertia forces can be stated by means of Betti's reciprocal theorem on each pair of the cases given as A-B and A-C:

Quantities \ Cases	$\mathcal{N} = 0$	$\mathcal{N}$	$\mathcal{N} = \mathcal{N}_b$
	A	B	C
Displacements	D_I	D_{II}	D_b
Slope	D'_I	D'_{II}	D'_b
Fictitious Distributed Moments	—	$\mathcal{N}\, n\, D'_{II}$	$\mathcal{N}_b\, n\, D'_b$
Distributed Inertia Forces	$m\,\omega_I^2 D_I$	$m\,\omega_{II}^2 D_{II}$	—

$$\text{A-B} \qquad \int m\,\omega_I^2 D_I D_{II}\cdot ds = \int m\,\omega_{II}^2 D_{II} D_I\cdot ds + \int \mathcal{N} n\, D_{II}' D_I'\cdot ds \tag{2a}$$

$$\text{B-C} \qquad \int m\,\omega_{II}^2 D_{II} D_b\cdot ds - \int \mathcal{N} n\, D_{II}' D_b'\cdot ds = \int \mathcal{N}_b n\, D_b' D_{II}'\cdot ds \tag{2b}$$

$$\text{A-C} \qquad \int m\,\omega_I^2 D_I D_b\cdot ds = \int \mathcal{N}_b n\, D_b' D_I'\cdot ds \tag{2c}$$

In these equations m is the intensity of the distributed mass; ω the circular frequency; $\mathcal{N}$ the axial force parameter; $\mathcal{N}_b^{(1)}$ the buckling value of $\mathcal{N}$; n the constant ratios between the axial forces; ($'$) the derivatives according to the displacement and I , II the subscripts of the first and second order theories. It must be noted that the integrals taking place in Eqs. 2a, 2b, 2c will be evaluated on the whole system. The following equations can be obtained by rearranging Eqs. 2a and 2b:

$$\frac{\omega_I^2 - \omega_{II}^2}{\mathcal{N}} = \frac{\int n\, D_{II}' D_I'\cdot ds}{\int m\, D_{II} D_b\cdot ds} \tag{3a}$$

$$\frac{\omega_{II}^2}{\mathcal{N}_b - \mathcal{N}} = \frac{\int n\, D_b' D_{II}'\cdot ds}{\int m\, D_{II} D_b\cdot ds} \tag{3b}$$

If there is any affinity between D_I and D_b , or if there is a similarity which can be accepted as an affinity, then

$$\frac{\omega_I^2 - \omega_{II}^2}{\mathcal{N}} = \frac{\omega_{II}^2}{\mathcal{N}_b - \mathcal{N}}$$

Hence, for a system in which the (i)the vibration mode is similar to (j)th buckling mode, i.e. $D_I^{(i)} \cong D_b^{(j)}$, we have

$$\frac{(\omega_{II}^{(i)})^2}{(\omega_I^{(i)})^2} + \frac{\mathcal{N}}{\mathcal{N}_b^{(j)}} = 1 \quad , \quad (\omega_{II}^{(i)})^2 = \frac{1}{\alpha^{(j)}}(\omega_I^{(i)})^2 \tag{4}$$

If Eq. 2c is rearranged

$$\frac{\omega_I^2}{\mathcal{N}_b} = \frac{\int n\, D_b' D_I'\cdot ds}{\int m\, D_I D_b\cdot ds} \tag{5}$$

and two sides of Eq. 4 is multiplied by $\omega_I^2 / \mathcal{N}$, then

$$\frac{\omega_I^2}{N_b} = \frac{\omega_I^2 - \omega_{II}^2}{N} \tag{6}$$

If the Eqs. 3a and 6 are compared

$$\frac{\omega_I^2}{N_b} = \frac{\int n\, D'_{II}\, D'_I \cdot ds}{\int m\, D_{II}\, D_b \cdot ds} \tag{7}$$

is found. Eqs. 5 and 7 together give the result

$$\frac{\int n\, D'_I\, D'_I \cdot ds}{\int m\, D_I\, D_I \cdot ds} = \frac{\int n\, D'_{II}\, D'_I \cdot ds}{\int m\, D_{II}\, D_I \cdot ds}$$

which will be correct if there is any affinity between $D_{II}^{(i)}$ and $D_I^{(i)}$, in addition to the affinity $D_I^{(i)} \equiv D_b^{(j)}$. The result just reached can be written as

$$[D]_I^{(i)} \cong [D]_{II}^{(i)} \tag{8}$$

for the first mode of any discrete system. Hence it is concluded that participation factors according to the first and second order theories are equal, i.e.

$$\Gamma_I^{(i)} \cong \Gamma_{II}^{(i)} \tag{9}$$

The accuracy of the equalities 4, 8 and 9 which depend on the affinity of $D_I^{(i)} \equiv D_b^{(j)}$ have been checked using two idealized cantilever beams with different shear and flexural deformation characteristics due to lateral forces, under two kinds of axial force distributions. And it is concluded that the formulae given above can be used for all structures consisting of frames and structural walls.

The Proposed Method

When the dynamic excitation is lateral, the ratio of (i) the modal displacements evaluated according to the first and second order theories can be obtained similar to the case of lateral static loads.[3] If Betti's reciprocal theorem is applied to the following cases A and B:

Quantities \ Cases	First Order Theory	Second Order Theory
	A	B
Displacements	$\delta_I^{(i)}$	$\delta_{II}^{(i)}$
Fictitious Dynamic Loads	$m S_{a,I}^{(i)}$	$m S_{a,II}^{(i)}$
Fictitious Forces Related with The Second Order Theory	—	P_F

$$(m S_{a,I}^{(i)}) \cdot \bar{\delta}_{II} = ((m S_{a,II}^{(i)}) + P_F) \cdot \bar{\delta}_I^{(i)}$$

$$\frac{\bar{\delta}_{II}^{(i)}}{\bar{\delta}_I^{(i)}} = \frac{((m S_{a,II}^{(i)}) + P_F)}{m S_{a,I}^{(i)}} \tag{10}$$

in which $(m S_{a,I}^{(i)})$, $\bar{\delta}_I^{(i)}$ and $(m S_{a,II}^{(i)})$, $\bar{\delta}_{II}^{(i)}$ are forces generated by dynamic excitation and modal displacements related to the (i)th mode of modal analysis respectively. P_F , the fictitious force which is used to keep the axis of the members in its original undeformed position in second order analysis is

$$P_F = m\, S_{a,II}^{(i)} (\alpha^{(i)} - 1) \tag{11}$$

If Eq. 10 is used together with Eq. 11

$$\frac{\bar{\delta}_{II}^{(i)}}{\bar{\delta}_I^{(i)}} = \alpha^{(i)} \cdot \frac{S_{a,II}^{(i)}}{S_{a,I}^{(i)}} \tag{12}$$

is obtained. One can easily reach the same conclusion for moments which are proportional to the displacements as

$$\frac{M_{II}^{(i)}}{M_I^{(i)}} = \alpha^{(i)} \cdot \frac{S_{a,II}^{(i)}}{S_{a,I}^{(i)}} \tag{13}$$

Eq. 12 can readily be written in more detail for the first few modes as follows:

$$\bar{\delta}_{II}^{(1)} = \bar{\delta}_{I}^{(1)} \cdot \frac{1}{1-\frac{N}{N_b^{(1)}}} \cdot \frac{S_a(T_{II}^{(1)})}{S_a(T_I^{(1)})}$$

$$\bar{\delta}_{II}^{(2)} = \bar{\delta}_{I}^{(2)} \cdot \frac{1}{1-\frac{N}{N_b^{(2)}}} \cdot \frac{S_a(T_{II}^{(2)})}{S_a(T_I^{(2)})} \tag{14}$$

$$\vdots \quad \vdots \quad \vdots \quad \vdots$$

because, $S_{a,II}^{(i)} = S_a(T_{II}^{(i)})$ is the acceleration spectrum ordinate according to the second order theory which will be found by using the eigenvalue given in Eq. 4. Since in structural systems, reciprocal of the buckling ratios related to the modes greater than the first mode can be considered as zero, i.e., $\frac{N}{N_b^{(2)}} \cong 0$, $\frac{N}{N_b^{(3)}} \cong 0$, . . ., Eqs. 4 and 14 can be rewritten as

$$T_{II}^{(1)} = T_I^{(1)} \cdot (1/(1-N/N_b^{(1)}))^{1/2}$$

$$T_{II}^{(2)} \cong T_I^{(2)} \tag{15}$$

$$T_{II}^{(3)} \cong T_I^{(3)}$$

$$\vdots \quad \vdots$$

$$\bar{\delta}_{II}^{(1)} \cong \bar{\delta}_{I}^{(1)} \cdot C$$

$$\bar{\delta}_{II}^{(2)} \cong \bar{\delta}_{I}^{(2)} \tag{16}$$

$$\bar{\delta}_{II}^{(3)} \cong \bar{\delta}_{I}^{(3)}$$

$$\vdots \quad \vdots$$

in which

$$C = \frac{1}{1-\frac{N}{N_b^{(1)}}} \cdot \frac{S_a(T_{II}^{1})}{S_a(T_I^{1})} = \alpha^{(1)} \cdot \frac{S_{a,II}^{(1)}}{S_{a,I}^{(1)}} \tag{17}$$

If both sides of the Eq. 16 are multiplied by the corresponding eigenvectors and participation factors which can be considered almost equal according to the Eqs. 8 and 9, the second order displacements related to modes can be found in terms of corresponding first order displacements and the coefficient C as

$$
\begin{aligned}
&[\delta]_{II}^{(1)} = [\delta]_{I}^{(1)} \cdot C \\
&[\delta]_{II}^{(2)} \cong [\delta]_{I}^{(2)} \\
&[\delta]_{II}^{(3)} \cong [\delta]_{I}^{(3)} \\
&\quad\vdots \qquad\qquad \vdots
\end{aligned}
\tag{18}
$$

To find the upper limits and probable values of the displacements, the displacements found using Eqs. 18 can be added as

$$
\begin{aligned}
&[\delta]_{II} = \left| [\delta]_{II}^{(1)} \right| + \left| [\delta]_{II}^{(2)} \right| + \left| [\delta]_{II}^{(3)} \right| + \cdots\cdots \\
&[\delta]_{II} = \left(([\delta]_{II}^{(1)})^2 + ([\delta]_{II}^{(2)})^2 + ([\delta]_{II}^{(3)})^2 + \cdots\cdots \right)^{1/2}
\end{aligned}
$$

respectively. Similar equalities for moment can be obtained as

$$
\begin{aligned}
&[M]_{II}^{(1)} = [M]_{I}^{(1)} \cdot C \\
&[M]_{II}^{(2)} \cong [M]_{I}^{(2)} \\
&[M]_{II}^{(3)} \cong [M]_{I}^{(3)}
\end{aligned}
\tag{19}
$$

and depending on the equilibrium of the member, storey shear forces at the ends of the thrusts can be found as

$$
\begin{aligned}
&[Q]_{II}^{(1)} = [Q]_{I}^{(1)} \cdot C - [N/h]\,[\Delta\delta]_{II}^{(1)} \\
&[Q]_{II}^{(2)} = [Q]_{I}^{(2)} - [N/h]\,[\Delta\delta]_{I}^{(2)} \\
&[Q]_{II}^{(3)} = [Q]_{I}^{(3)} - [N/h]\,[\Delta\delta]_{I}^{(3)}
\end{aligned}
\tag{20}
$$

where N is the axial force in columns; h, the height of the column; $[N/h]$, a diagonal

matrix; $\Delta\delta$, relative displacements between two ends of column, $(^{(i)})$ corresponding mode superscript, and subscripts $_{I}$ and $_{II}$ indicate the first and second order theories.

The coefficient C which has taken place at the right hand side of the Eqs. 18, 19 and 20 is the product of two parts, namely $\alpha^{(i)}$ and $S^{(i)}_{a,II}/S^{(i)}_{a,I}$ as can be seen from Eq. 17. Although the first part which is known as amplification factor for second order effects of axial forces, is only related with the ratio $N^{(i)}_{b}/N$ and is always greater than unity, the second part, $S^{(i)}_{a,II}/S^{(i)}_{a,I}$, can differ from unity depending on the excitation and dynamic characteristics of the structure such as the natural fundamental period and damping ratio. In order to illustrate what is said above, let the structures which have the same period be calculated according to the first order theory, but with different buckling loads, be considered. Because of the difference between the $N^{(i)}_{b}/N$ ratios, second order fundamental periods, $T^{(i)}_{II}$ will be different.

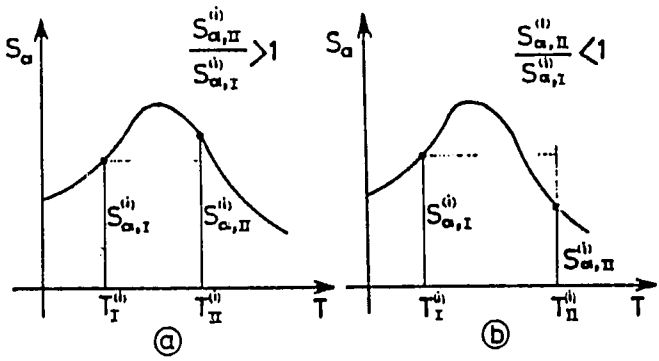

Figure 1

As it can be seen in Figure 1 while the ratio $S^{(i)}_{a,II}/S^{(i)}_{a,I}$ is greater than unity for the first structure, the same ratio will be less than unity for the second one. The product can also be less than unity even when α is taken into account.

The coefficient C described above will be used to understand easily the order of importance of the second order effect, to make a decision for second order dynamic analysis and to perform it by hand calculation, using Eqs. 18, 19 and 20 as well. In order to show how the coefficient C is changed by period, damping and the safety factor against buckling load, three diagrams are enclosed, depending on the sinusoidal ground motion as $P[f(\tau)] = P_1 \sin\Omega t$ with $\Omega=2\pi$ rd., for the El Centro California 1940 N-S (an example of an earthquake recorded on firm soil) and the N 81° W component of Latino Americana Tower Mexico (an example of ground motions resulting from filtering of earthquakes which are nearly white noise, through layers of soft soil within the range of linear or almost linear soil behaviour). Noting the diagrams given in Figures 2, 3, 4 and 5 it is roughly concluded that C can considerably differ from unity.

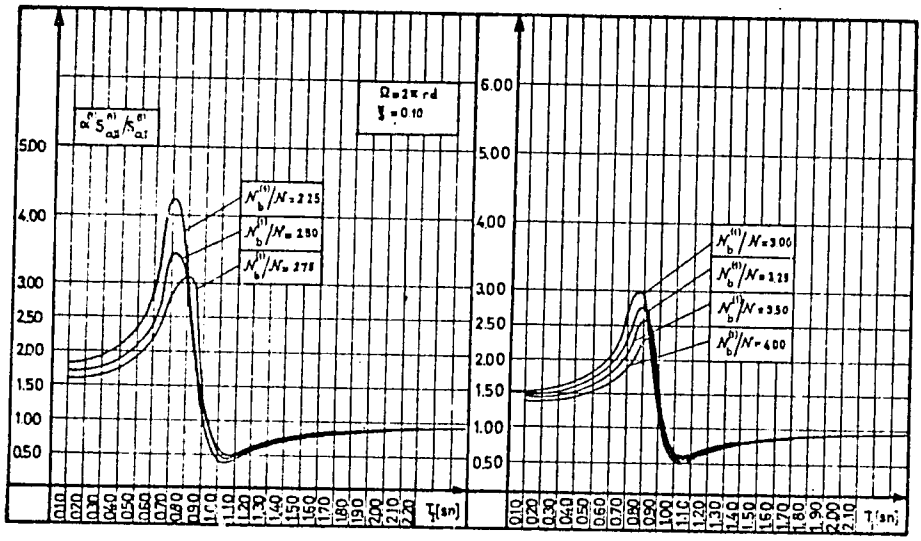

Figure 2

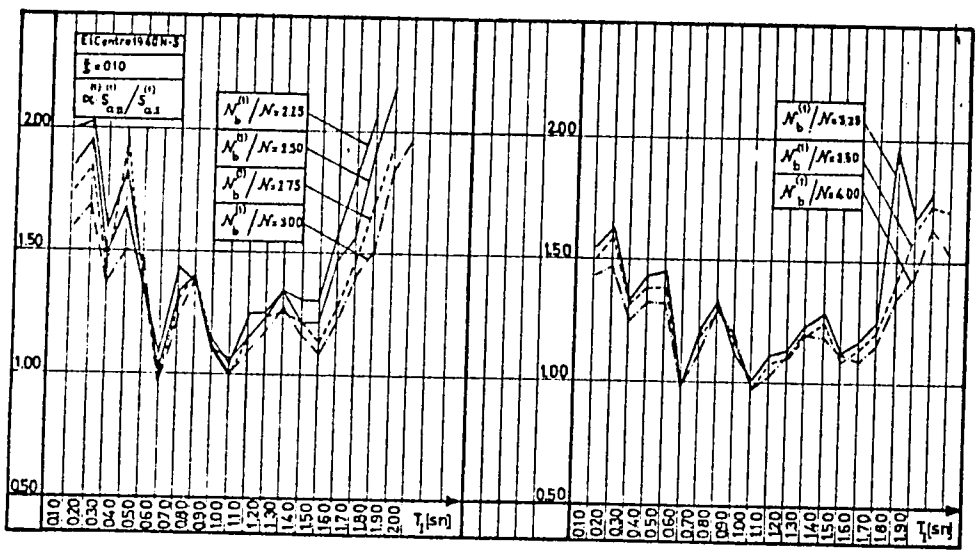

Figure 3

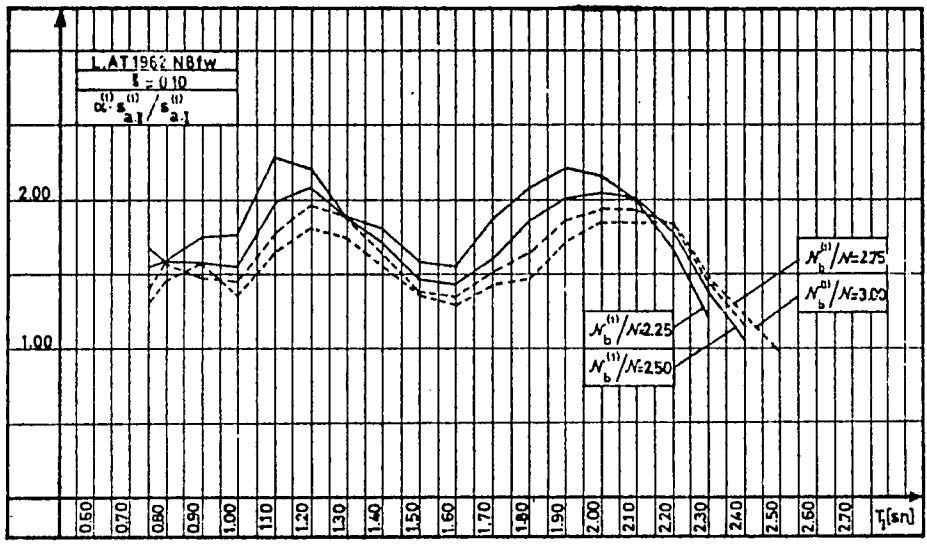

Figure 4

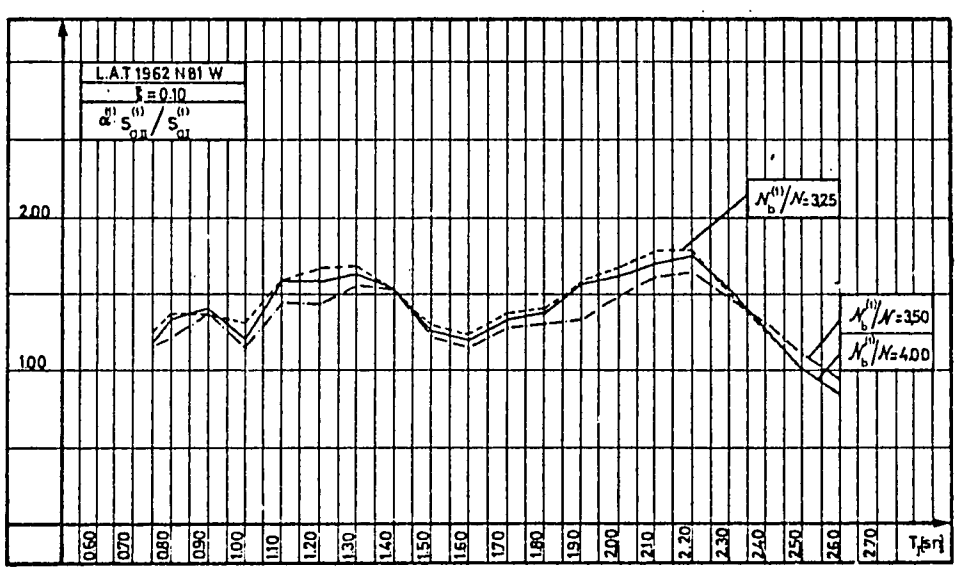

Figure 5

Numerical Examples

It was concluded at the end of two previous research studies (3) and (4) that the difference between the first and second order analysis is 10% and negligible respectively. And it was also concluded in (4) that the axial force effects on periods are not very important. The El Centro California 1940 N-S and some artificial earthquakes which can be compared with this famous one and the Taft California July 1952 N 21° E earthquake records have been used in these investigations. In order to criticize these results and to specify the accuracy of the proposed method, two examples are prepared by using the record of the Latino Americana Tow/ r 1962 N 81° W.

First Example:

The characteristics of the system for which the ratio $S^{(1)}_{a,II}/S^{(1)}_{a,I}$ is less than unity, are shown in Figure 6:

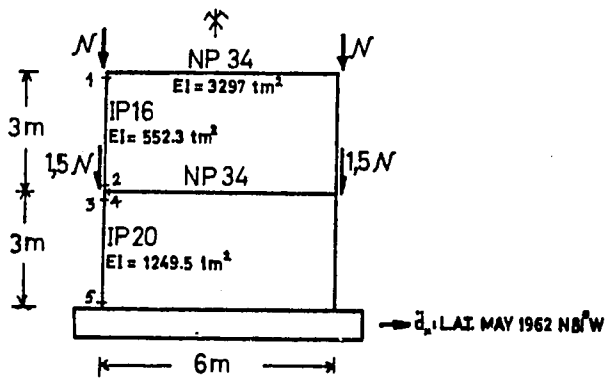

$$N_b^{(1)} = 401.48\ t \qquad N_b^{(1)}/N = 3.2814 \qquad \alpha^{(1)} = 1.483$$

$$C = \alpha^{(1)} \cdot \frac{S^{(1)}_{a,II}}{S^{(1)}_{a,I}} = 1.483 \times \frac{1.3015}{1.7235} = 1.086$$

Figure 6

The results of undamped earthquake analysis are outlined in the table below. In this table, columns marked with IE and IIE show the quantities calculated using the linear acceleration method IP and IIP show the results obtained by the spectrum analysis according to the first and second order theories respectively, and AIIP indicates the results reached by means of the proposed method. Studying this table it can be seen that weighted averages of differences between displacements $[\delta]$; storey shear forces, $[Q]$; and the moments at the cross sections numbered in Figure 6 according to the analysis IIE and AIIP are less than 1%.

QUANTITIES	FIRST ORDER ANALYSES		SECOND ORDER ANALYSES			DIFERANCES %		WEIGHTED AVARAGES of DIFERANCES %	
	IP	IE	IIP	AIIP	IIE	2 - 5	5 - 4	2 - 5	5 - 4
	1	2	3	4	5	6	7	8	9
[δ]	0.29976	0.30353	0.32365	0.32554	0.32364	6.63	0.59	6.79	0.56
	0.12425	0.13000	0.13664	0.13485	0.13933	7.18	-3.21		
[ΣQ]	56.088	60.682	42.373	45.160	44.869	-26.06	0.65	-26.35	-0.06
	90.575	96.809	68.872	70.765	71.128	-26.53	-0.51		
[M] 1	44.759	48.807	46.789	48.547	47.114	-1.86	3.04	3.68	0.46
2	39.390	43.013	41.190	42.682	41.459	-3.61	2.95		
3	56.122	60.718	62.106	60.838	64.157	5.66	-5.17		
4	94.242	94.143	102.117	102.350	101.859	8.20	0.48		
5	79.774	84.501	85.827	86.551	87.941	4.07	-1.58		

Second Example:

The characteristics of the system, for which the ratio, $S^{(1)}_{\alpha,II}/S^{(1)}_{\alpha,I}$ is greater than unity, are shown in Figure 7.

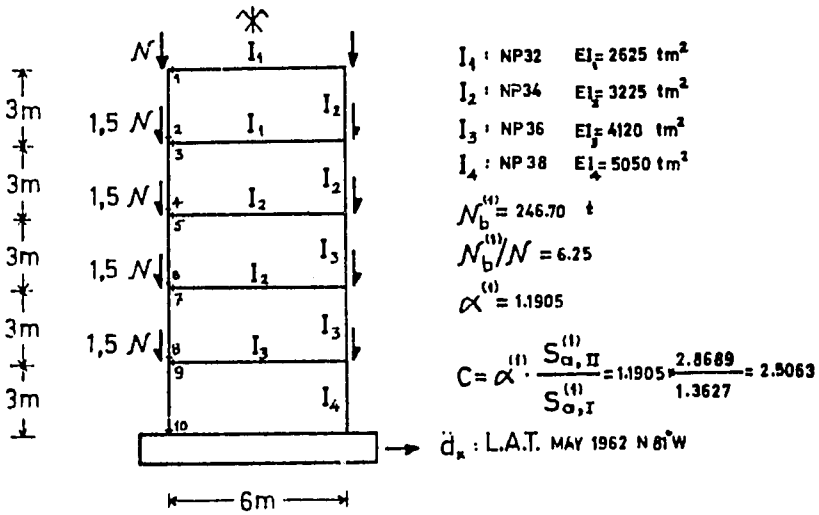

Figure 7

The results reached according to the above mentioned methods, IP, IE, IIP, IIE and AIIP are outlined in the table below. In this example weighted averages of differences between the displacements of the storey levels, storey shear forces and moments at the cross sections shown in Figure 7, calculated by means of IIE and AIIP are not much more than 2%.

Conclusions

A method has been developed herein for second order analysis of planar frames, excitated by horizontal dynamic forces. The conclusions reached are:

1. The fundamental periods and hence the response of structures can considerably effected by tne second order effects of axial forces and when it is desired these effects can be easily taken into account.

2. There is no significant discrepancy between the eigenvectors corresponding to the first and second order theories in frame structures wlth arbi-

QUANTITIES	FIRST ORDER ANALYSES		SECOND ORDER ANALYSES			DIFERANCES %		WEIGHTED AVARAGES of DIFERANCES %	
	IP	IE	IIP	AIIP	IIE	[2] - [5]	[5] - [4]	[2] - [5]	[5] - [4]
	[1]	[2]	[3]	[4]	[5]	[6]	[7]	[8]	[9]
[δ]	0.2733	0.2624	0.6742	0.6842	0.6804	159.30	0.56	169.71	-0.26
	0.2331	0.2203	0.5929	0.5968	0.5978	171.36	-0.17		
	0.1796	0.1600	0.4512	0.4500	0.4546	184.13	-1.01		
	0.1080	0.1002	0.2718	0.2706	0.2741	173.55	-1.28		
	0.0372	0.0358	0.0922	0.0932	0.0933	160.61	-0.11		
[ΣQ]	16.31	20.43	30.49	34.64	31.14	52.42	11.24	108.01	1.61
	34.57	39.65	69.92	74.29	70.92	78.87	4.75		
	47.74	43.76	100.30	100.15	100.54	129.75	-0.39		
	56.69	52.91	118.73	115.25	119.28	125.44	-3.38		
	60.21	58.79	124.84	131.23	126.46	115.10	3.77		
[M] 1	18.95	27.36	40.95	44.81	41.56	51.90	7.82	141.05	1.35
2	6.08	7.50	8.05	10.97	8.12	8.70	35.10		
3	35.74	40.54	81.70	86.78	82.80	104.24	4.80		
4	21.35	26.18	44.95	49.60	45.82	75.02	8.25		
5	59.11	60.10	144.83	147.37	146.02	142.92	0.92		
6	32.36	34.53	78.69	80.13	79.09	129.05	1.32		
7	67.40	60.05	170.57	168.84	171.51	185.61	-1.56		
8	48.88	43.95	125.08	122.23	125.57	185.71	-2.66		
9	66.63	62.31	166.09	165.77	167.63	169.03	-1.11		
10	72.35	69.55	171.12	179.05	173.39	149.30	3.26		

trary mass distribution and flexural or shear deformation. It can be accepted that there is an affinity between the eigenvectors calculated according to both theories. Therefore, the participation factors can be taken as equal in both analyses. The largest period corresponding to the second order theory can easily be obtained by using Eq. 4, while subsequent periods can be accepted as being approximately equal to the ones obtained by first order theory. Because of these reasons it is not necessary to make any calculations for free vibrations of the system according to the second order theory.

3. In order to make a decision about the order of importance and the necessity of using the second order analysis for dynamic horizontal loads

$$C = \frac{1}{1 - \frac{N}{N_b^{(1)}}} \cdot \frac{S_{a,II}^{(1)}}{S_{a,I}^{(1)}} = \alpha^{(1)} \cdot \frac{S_{a,II}^{(1)}}{S_{a,I}^{(1)}}$$

can be used as a criterion,

a— C may be either greater or less than unity. From the structural engineering point of view both cases are important, considering the safety and economy factors of the structure respectively.

b— Even $\alpha^{(1)}$ which is always greater than 1, is near to unity, C can significantly differ from unity due to the ratio $S_{a,II}^{(1)}/S_{a,I}^{(1)}$. Therefore, there can be cases in which second order analysis is not necessary in the case of static loads, but compulsory for dynamic loads.

4. Using the method developed, depending on the results outlined above, one can readily calculate the results of the modal analysis according to the second order theory multiplying only the quantities of the fundamental mode obtained by the first order theory by a factor C and using the same results for the other modes. Since it is not necessary to perform any kind of iteration either on axial forces or on displacements, the method is a direct procedure which does not necessitate the use of computers. The accuracy of the method does not diminish when the ratio, $N_b^{(1)}/N$, decreases. The method is applicable to any kind of lateral dynamic or static analysis as well as earthquake analysis. Considering the similarity of the buckling and free vibration mode shapes of

arches and space frames, it may be concluded that the proposed method may be applied to those systems by minor alterations.

REFERENCES

1. *A.C. Ruge, Bull. Seismol. Soc. Amer., 24, (1934).*

2. *J.J. Anderson and V.V. Bertero, Proc. 5th World Cong. Earthq. Eng., Rome, No. 369 (1973).*

3. *C.G. Subhash, Proc. Amer. Soc. Civil Eng., 95, ST8, Paper 6738 (1969).*

4. *R. Husid, Proc. 4th World Cong. Earthq. Eng., Santiago (1969).*

INFLUENCE OF EMBEDMENT ON VERTICAL FOUNDATION RESPONSE

Dr. Selçuk M. Erden and Professor Kenneth H. Stokoe

The behaviour of foundations under various types of dynamic loads has attracted considerable attention, especially within the last decade, and many analytical and experimental investigations have been conducted on dynamic soil-structure interaction problems. These have ranged from studies of the dynamic behaviour under high-amplitude loadings such as those generated by blasting and earthquakes to studies of the dynamic behaviour under low-amplitude leadings such as those generated by machine vibrations and vehicular traffic. The aim of these investigations has been to enable the designer to predict the response of soil-structure systems to dynamic loads, to avoid significant damage or failure in the case of high-amplitude loadings and to minimize vibrations in the case of low-amplitude loadings.

In most theories dealing with dynamic foundation response, the soil-foundation system is idealized as a rigid circular cylinder resting on an elastic half-space.[1] However, in reality the foundation is usually partially or totally embedded in the soil. The influence of this embedment on the response of the foundation is then needed properly to evaluate the total response of the soil-foundation-structure system.

Only within the last few years has attention been given to the analytical solution of the dynamic response of embedded foundations.(e.g. 2, 3, 4, 5) The results of analytical and experimental investigations have shown considerable quantitative variations, but these have all shown that for the soil-foundation system the natural frequency increases and the resonant amplitude decreases as embedment increases.

METHODS

Model Footing Test Facility. (MFTF). This is a circular bin about two meters in depth and about four meters in diameter. It contains moist sand surrounded by and underlain by a 0.3 m layer of wet sawdust, which is completely sealed in plastic to prevent migration of moisture out of it and to prevent migration of sand into it. The purpose of the MFTF is to model, in a controlled environment, an elastic half-space which can be used for low-amplitude dynamic testing. The sand in the MFTF represents this elastic half-space. The moist sawdust layer around the sand acts like an energy absorbing material so that much of the energy imparted to the sand during testing is absorbed in the sawdust and is not reflected back into the sand.

Properties of Sand in MFTF. Some properties of the sand in the top 0.5 m of the MFTF are given in Figure 1. The bottom meter of sand is loose as a result of both the filling procedure and the presence of the sawdust layer at the bottom of the bin

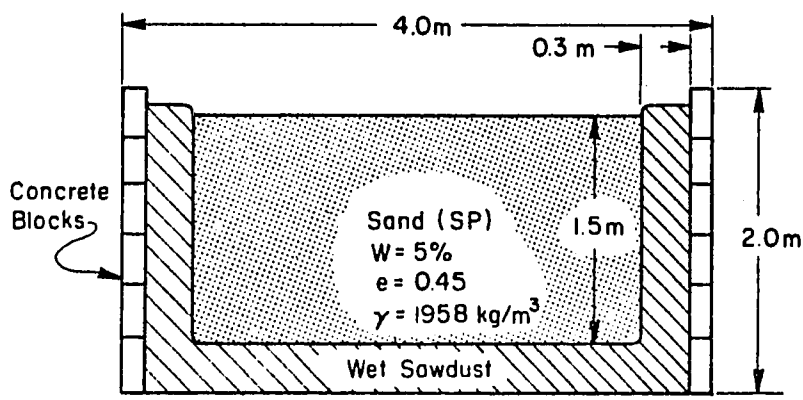

Figure 1
Cross-Section of Model Footing Test Facility, MFTF

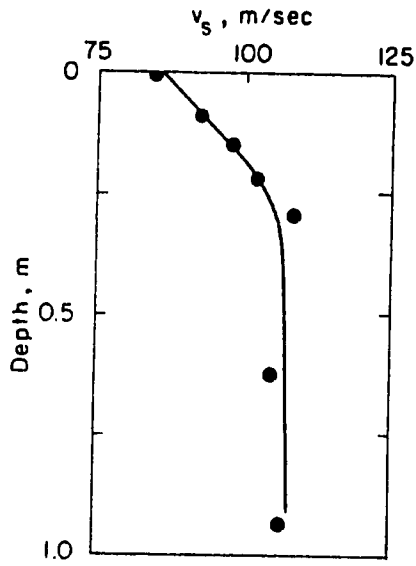

Figure 2. In-Situ v_s Profile in MFTF

which reduce the effects of compaction. The shear wave velocity profile of the sand in the MFTF was determined *in situ* by the cross-hole seismic method.[6] The resulting shear wave velocity profile is shown in Figure 2. Because of the decrease in density of the sand with depth after about 0.5 m, the measured shear wave velocity, v_s, does not continue to increase with depth as expected for a sand but becomes almost constant.

Model Footings. The basic shape of all model footings used in this study was a right circular cylinder. This shape was selected because it is the assumed shape of the foundation in most analytical solutions dealing with soil-structure interaction. Two basic types of model footings were used, surface and embedded. This distinction between the two types of footings was based on the location of the base of the footing relative to the sand surface. The base of the surface footing rested directly on the sand surface while the base of the embedded footings was founded at some depth beneath the sand surface.

All model footings were made of concrete, and each was cast-in-place. A cross-sectional view of a completed footings is shown in Figure 3. The embedded footings were constructed by first digging in the sand a hole with the same diameter as the footing. The hole was advanced to the depth required for the desired depth of embedment. Concrete was then poured into the hole until it was level with the soil surface. A sheet metal form of correct length for the exposed sides of the footing was

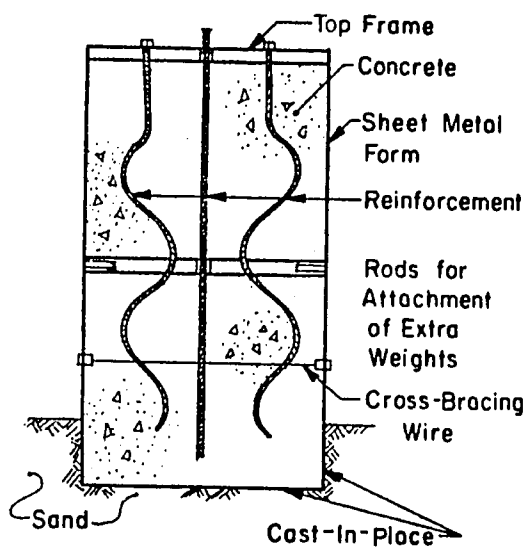

Fig. 3. Typical Cross-Section of embedded footing

placed directly over the concrete, and the casting was continued. In this manner, the concrete along the embedded depth as well as on the bottom of the footing was cast-in-place.

A total of two surface and three embedded footings were used. The surface footings acted as a reference with which the influence of embedment on the dynamic response of the embedded footings was evaluated. Also, two surface footings were used to determine the duplicability of test results. The average results of these surface footings were within one percent for natural frequency and within eleven percent for damping ratio.

Each embedded footing was tested at a different depth of embedment to evaluate the change in dynamic response with increasing embedment. The depths of embedment employed are given in Table 1. The embedment ratio, ζ , which is the depth of embedment divided by the radius of the footing, ranged from 0 to 1.2.

TABLE 1. BASIC FOOTING PROPERTIES

Footing Number	Average Radius cm	Average Height cm	Depth of Embedment cm	Embedment Ratio ζ	Weight Kg.	B_z
1	14.9	46.7	0.0	0.0	82.6 108 139	2.2 2.8 3.7
2	14.9	46.7	0.0	0.0	80.3 107 141	2.1 2.8 3.7
3	14.9	46.7	6.3	0.42	80.3 107 141	2.1 2.8 3.7
4	14.9	46.7	12.1	0.81	78.0 105 139	2.0 2.7 3.6
5	14.9	46.7	18.5	1.24	80.7 108 142	2.0 2.8 3.7

All footings were designed so that the base area, the height, and thus the weight were held constant. The exact dimensions of the model footings and corresponding basic properties are tabulated in Table 1. The mass ratio, B_z, was calculated using the lumped-parameter analysis[1] by:

$$B_z = (1 - \nu)\, m / (4 \rho r_o^3) \tag{1}$$

in which m is the mass of the footing, r_o is the radius of the footing, ν is Poisson's ratio (0.33 as determined by cross-hole tests), and ρ is the mass density of the soil. Because the radius and weights of the footings were held constant, B_z was essentially constant.

In addition to testing the footings at their initial weights, each footing was also tested at two other increased weights. (This allowed 15 footings to be tested). The footing weight was increased by adding lead weights to each footing. The weights were added symmetrically about the centre of gravity of the footing so as not to change the location of the centre of gravity.

Two sets of lead weights were used. Each set weighed about 27.2 kg and was specifically prepared for each footing by casting molten lead in moulds prepared according to the footing dimensions. The average thickness of each set was about 2.5 cm, and the average height was about 7.6 cm.

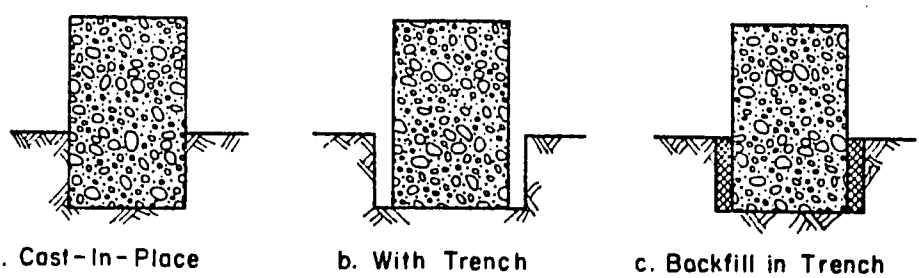

Figure 4. Embedment Conditions

Besides testing each embedded footing as a cast-in-place footing two other states of embedment were also investigated as shown in Figure 4: embedment with no soil contact along the embedded side trench around footing, and embedment in backfill with the backfill having the same density as the surrounding soil. Cast-in-place embedment and embedment with a trench around the footing should represent the two extremes of the influence of embedment while the influence of embedment in backfill should fall within these extremes and in fact should most closely represent the as-built condition.

Loading and Monitoring Equipment. The response of each footing was determined for transient-type loading. This loading was generated by the sudden release of an applied static tensile load. A hanging-weight system was used to apply the static load to the footing as shown in Figure 5.

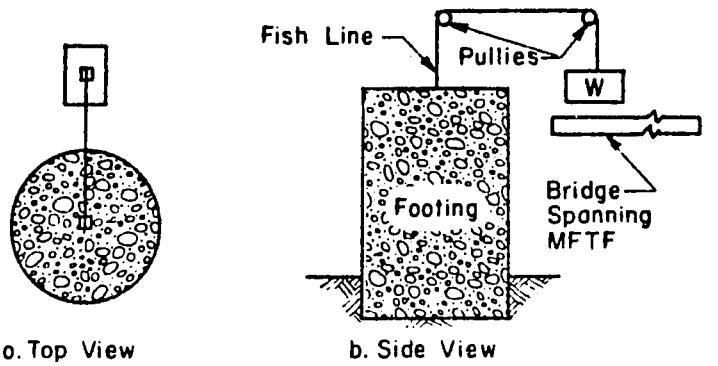

Figure 5. Loading Arrangement for Transient Vertical Excitation

The response of each footing was monitored with two vertical velocity transducers which were securely attached through the top frame to the top of the footing near its perimeter. A storage oscilloscope was used to view the output from the transducers.

Analysis of Data. Each model footing was tested in transient vertical motion as already explained. For each test condition, at least four records of the dynamic response of the footing were made. The damped natural frequency, f_d, and the damping ratio, D, were then determined from these records. The damped natural frequency was determined as shown in Figure 6 while the damping ratio was determined from the logarithmic decrement, δ, by:

$$\delta = 2\pi D/\sqrt{1-D^2} \tag{2}$$

With f_d and D determined, the natural frequency, f_n, is:

$$f_n = f_d/\sqrt{1-D^2} \tag{3}$$

With this approach the transient response of the footing is analyzed as if the system is a viscously damped single-degree-of-freedom system. This approach has been shown[1] to work well for transient vertical motion.

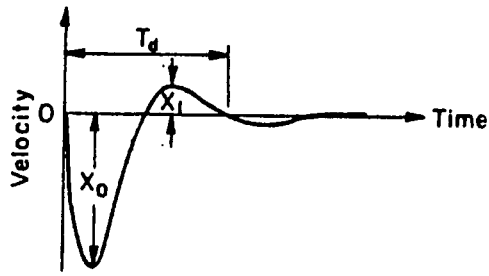

$f_d = 1/T_d$

$\delta = \ln(X_0/X_1)^2$

Figure 6. Analysis of Transient Response

RESULTS

Cast-In-Place Embedment. The influence of cast-in-place embedment on the natural frequencies of the soil-footing system is shown in Figure 7a (see the next page). The results show that the ratio of the natural frequency of a cast-in-place embedded footing, $f_{n(E)}$, to the natural frequency of a similar cast-in-place surface footing, $f_{n(S)}$, increased almost linearly with embedment ratio, ζ. In addition, this ratio, $f_{n(E)}/f_{n(S)}$, was essentially independent of mass ratio over the mass-ratio range (B_z = 2.1 to 3.7) used. For all practical purposes, the influence of cast-in-place embedment on the natural frequency can be expressed as:

$$f_{n(E)} = f_{n(S)}\,(1.00 + 0.20\zeta) \tag{4}$$

In Eq. 4, the response of the surface footing, $f_{n(S)}$, was actually measured. However, it can be calculated using the mass-spring-dashpot analogy. In this case the minimum vertical effective stress beneath the outside edge of the footing, $\bar{\sigma}_{v(min)}$, should be used to evaluate the effective shear modulus beneath the footing. The depth at which $\bar{\sigma}_{v(min)}$ occurs is approximately equal to the radius of the footing.

A portion of the increase in $f_{n(E)}$ with increasing embedment was a result of the shear modulus increase with depth. As can be seen from Figure 2, v_s or shear modulus did not increase with depth after about 0.3 m in the MFTF. Therefore, the measured natural frequencies for the embedded footings with ζ equal to 1.24 were multiplied by 1.08 to adjust $f_{n(E)}$ so that the results in Figure 7 would be representative of an increasing shear modulus with depth.

Many real situations do not show the shear modulus, G, increasing with

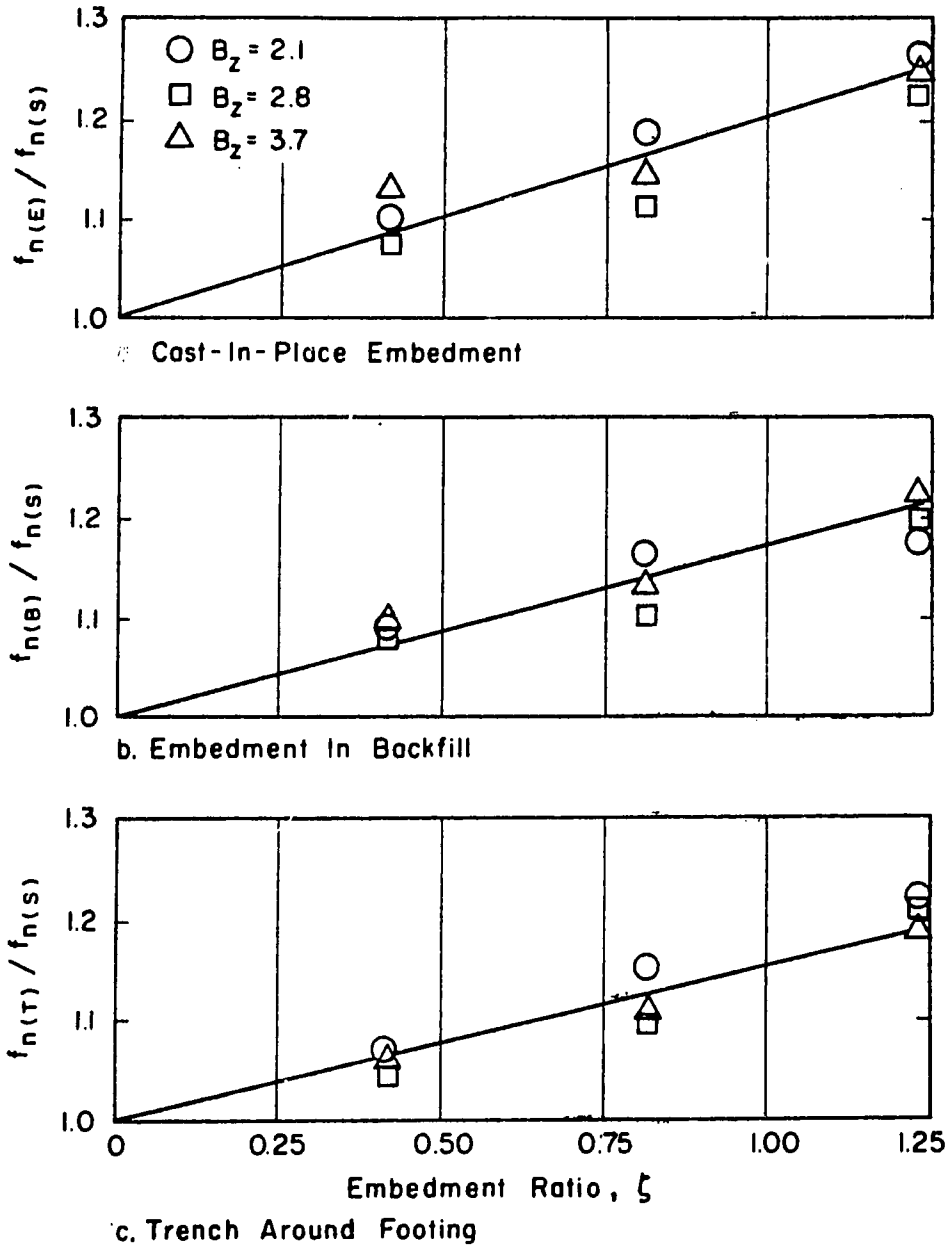

Figure 7. Influence of Embedment on Natural Frequency in Vertical Motion

depth. Therefore, an attempt was made to separate the influence on $f_{n(E)}$ of a changing shear modulus beneath the footing from the total influence of embedment. Shear modulus directly affects the spring constant which, in turn affects the natural frequency. Everything else being constant, the ratios of $f_{n(E)}/f_{n(S)}$ and G_E/G_S can be related by:

$$f_{n(E)}/f_{n(S)} = \sqrt{G_E/G_S} \tag{5}$$

where G_E and G_S refer to the effective shear moduli beneath an embedded and a surface footing, respectively and $f_{n(E)}$ refers to the increased natural frequency of an embedded footing caused only by an increase in G beneath the footing. The variation in shear modulus along the embedded sides of the footing is neglected in this analysis.

With the effective shear moduli for the sand in the MFTF, the influence of an increasing shear modulus with depth on the natural frequency of the embedded footings can be approximated as:

$$f_{n(E)} = f_{n(S)}\,(1.0 + 0.06\zeta) \tag{6}$$

for the embedment depths used. Based on above analysis, it is possible to express the influence of embedment alone, i.e., excluding the effect of shear modulus increase beneath the footing, on the natural frequency of cast-in-place footings. This expression is given by:

$$f_{n(E)} = f_{n(S)}\,(1.0 + 0.14\zeta) \tag{7}$$

where $f_{n(E)}$ refers to the embedded natural frequency independent of G.

If the shear modulus profile of a soil mass is known, then the effect of this profile on the natural frequency can be calculated separately. After this is done, Eq. 7 can be used to compute the further effect of embedment, and superimposing this to that caused by the shear modulus profile, the total influence of embedment on natural frequency can be calculated.

The influence of embedment on damping ratios was considerably different than the influence of embedment on natural frequencies. In Figure 8a, the ratio of the damping ratio of a cast-in-place embedded footing, D_E, to the damping ratio of a cast-in-place surface footing, D_S, is plotted versus the embedment ratio, ζ. As can be seen, the increase in damping ratio was not linearly related to an increase in embedment. Also, with increasing mass ratio of the footings, the effect of embedment on D_E was slightly reduced. For practical purposes this mass dependency could be disregarded within the range of mass ratios used in this study, and the influence of cast-in-place embedment on damping ratio can be expressed as:

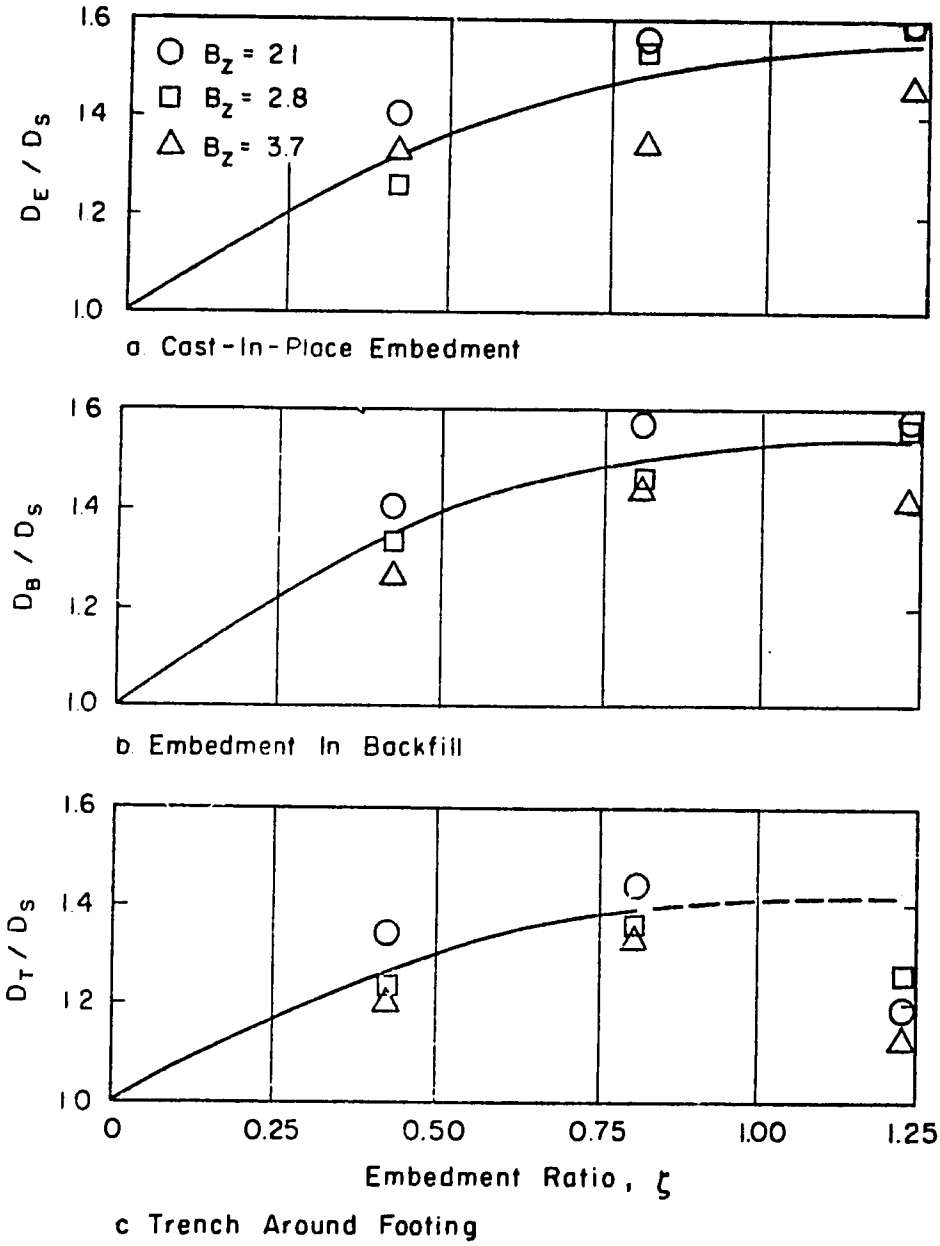

Figure 8. Influence of Embedment on Damping Ratio in Vertical Motion

$$D_E = D_S (1.00 + 0.90 \zeta - 0.37 \zeta^2) \quad (8)$$

In Eq. 8, D_S represents the combination of radiation and material damping.

Embedment in Backfill. The influence of embedment in backfill on the natural frequencies is shown in Figure 7b. The results show that the ratio of the natural frequency of a footing embedded in backfill, $f_{n(B)}$, to the natural frequency of a surface footing, $f_{n(S)}$, increased almost linearly with embedment ratio and was essentially independent of mass ratio. The increase in $f_{n(B)}$ with embedment ratio can be given as:

$$f_{n(B)} = f_{n(S)} (1.00 + 0.17 \zeta) \quad (9)$$

Included in Eq. 9 is the effect of an increasing shear modulus with embedment depth.

The influence on the natural frequency of embedment in backfill was similar to that found for cast-in-place embedment. However, embedment in backfill slightly reduced (about three percent at an embedment ratio of 1.0) the influence of embedment on the natural frequency relative to that found when the footing was cast-in-place.

The influence of embedment in backfill on the damping ratio was similar to that for cast-in-place embedment and is shown in Figure 8b. When the footings were cast-in-place, measured damping ratios, D_E, were essentially the same as measured damping ratios when the footings were embedded in backfill, D_B. As with cast-in-place embedment, some mass dependency was found. However, if this mass dependency is neglected, the influence of embedment in backfill on damping ratio can be given as:

$$D_B = D_S (1.00 + 0.99 \zeta - 0.45 \zeta^2) \quad (10)$$

In Eq. 10, D_S represents the combination of radiation and material damping.

Trench Around Footing. Each embedded model footing was also tested with no side contact along the embedded depth. The influence of this condition on the natural frequencies is shown in Figure 7c. The ratio of the natural frequency when the side contact was eliminated, $f_{n(T)}$, to the natural frequency when the footing was on the surface, $f_{n(S)}$, is plotted versus the embedment ratio, ζ. As can be seen in the figure, this effect was similar to but much smaller than the other two embedment conditions. The increase in $f_{n(T)}$ with embedment ratio can be expressed as:

$$f_{n(T)} = f_{n(S)} (1.00 + 0.15 \zeta) \quad (11)$$

Included in Eq. 11 is the influence of an increasing shear modulus with depth on the natural frequency. It is seen that, even with no side contact along the embedded sides

of the footing, the influence of embedment on vertical natural frequency is not caused solely by an increase in shear modulus (or else Eq. 11 would be the same as Eq. 6). In other words, when footings are embedded with no side contact, the soil around the footing is not acting merely as a surcharge. Other factors are causing an increase in the natural frequency of the embedded footings with no side contact.

The influence of embedment with no side contact on the damping ratio is shown in Figure 8c. The damping ratio, D_T, measured for these conditions was similar to but somewhat less than that measured for cast-in-place embedment. The increase in D_T with embedment ratio can be expressed as:

$$D_T = D_S (1.00 + 0.73 \zeta - 0.31 \zeta^2) \tag{12}$$

These results show that in terms of the damping ratio the presence of a continuous soil body around the sides of a footing (although not in contact with the footing) can not be explained in terms of a surcharge.

CONCLUSIONS

The following conclusions are based on this experimental investigation.

1. The natural frequency and damping ratio increased with increasing depth of embedment for all footings tested with the largest influence of embedment being exhibited by cast-in-place footings. Embedment in backfill slightly reduced the influence of embedment, and elimination of side contact between the soil and the footing further reduced the effects of embedment relative to cast-in-place footings.

2. The increase in natural frequency with embedment was practically independent of footing mass whereas the increase in damping ratio with embedment was slightly mass-dependent such that with increasing mass ratio, the influence of embedment on damping ratio decreased slightly.

3. Embedding a footing with no side contact resulted in a higher natural frequency and a higher damping ratio than that predicted for a similar surface footing with a surcharge applied to the soil around the footing equal to the embedment surcharge.

REFERENCES

1. *F.E. Richart, J.R. Hall, and R.D. Woods, "Vibrations of Soils and Foundations." Prentice-Hall, N.J., 1970.*

2. *M. Novak and Y.O. Beredugo, Proc. Amer. Soc. Civil Eng., 98, SM12, 1291 (1972).*

3. *Y.S. Chae, Highway Res. Rec., No. 323, 49 (1971).*

4. *M. Anandakrishnan and N.R. Krishnaswamy, Proc. Amer. Soc. Civil Eng., 99, SM10, 863 (1973).*

5. *B.N. Gupta, Geotechnique, 22, 129 (1972).*

6. *K.H. Stokoe and R.D. Woods, Proc. Amer. Soc. Civil Eng., 98, SM5, 443, (1972).*

DISCUSSION

Dr. Keightley asked if transducers were embedded in the sand to insure that there were no reflections back to the foundation. Dr. Erden said they were not used; the closest distance to the wall was about 4 ft and with the sawdust layer acting as an energy absorber, no reflections were observed for transient excitation. In reply to Professor Ambraseys, Dr. Erden said that the sand was compacted as much as possible, especially the top 2 ft; the moisture content was about 5-6% and the relative density about 95%; no tests were done with fully saturated sand as the object of the work was to study the influence of base shapes and embedments, not the soil properties. Dr. Gülkan asked what was the effect of moisture content in embedments. Dr. Erden said that little work had been done on saturated sand, but one study showed that the natural frequency and damping ratio in saturated conditions were about half the values for dry sand; generally the results would be proportional to the effective pressure in the soil. In reply to Dr. Keightley, Dr. Erden said that the range of strains observed was on the order of 10^{-5} to 10^{-6}. Dr. Erden agreed with Dr. Soydemir that since the testing performance was for low amplitude vibrations, the results were more relevant to machine foundations than to earthquake effects.

BEHAVIOUR OF DRY SAND SLOPES UNDER SEISMIC LOADING CONDITIONS

Professor Vahit Kumbasar and Dr. Ali Erguvanlı

It has been long recognized that vibrations have great effects on slopes composed of cohesionless soils. Ground vibrations caused by earthquakes, as well as vibrations from artificial sources, such as traffic and machinery, tend to change the mechanical properties and strength parameters of sands.

During the earthquakes that have occurred in the past 15 years, (Chile 1960, Alaska 1964, Niigata 1964) numerous failure cases in cohesionless soils have been reported due to ground settlements as a result of compaction; soil liquefaction at ground level in saturated loose sands; soil liquefaction in saturated cohesionless slopes; water front bulkhead failures due to backfill liquefaction; and slides caused by liquefaction of thin sand layers and due to the reduction of strength parameters. It is necessary to improve the design techniques and construction measures in cohesionless soils.

Many analytical and numerical techniques have been developed for stability analysis under dynamic loading conditions.[1] This study is confined to the application of pseudo-static forces on sand slopes, induced by ground vibrations. Accepting the conditions of an infinite dry sand slope, the safety factor against slope stability, with a horizontal force acting on the slope, has been derived in Figure 1.

Test Procedure

The soil used was coarse dry sand, originally brought from Podima (Yalıköy), with a grain size distribution of 0.63 to 1.00 mm. The composition was 99% quartz and 1% magnetic. The grain size characteristics were D_{60}, 0.78; D_{30}, 0.75; D_{10}, 0.70; C_c 1.1; Cu 0.97; e 0.75; γ_s 2.68 t/m^3.

During the tests, the sand was placed in loose condition in the plexiglass model test box (26 x 30 x 61 cm). The average void ratio before vibration was 0.75.

Two different kinds of model slopes were adopted during the tests due to the existence of different boundary conditions. Before the formation of model slopes, a layer of gravel was fixed to the base of the model test box to provide interaction between the table and the model. The infinite slope, as defined herein, has direct bound-

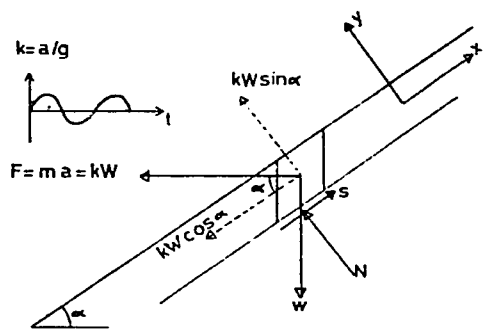

α = Initial slope angle.
ø = Angle of friction for dry sand

(1) $\Sigma F_x = 0$

$$S = W(\sin\alpha + k\cos\alpha) \quad \text{.....(1)}$$

(2) $\Sigma F_y = 0$

$$N = W(\cos\alpha - k\sin\alpha) \quad \text{.....(2)}$$

For Cohesionless soils.

$$\tau = N \tan \phi$$

$$\tau_f = W(\cos\alpha - k\sin\alpha)\tan\phi \quad \text{.....(3)}$$

Factor of safety against stability.

$$SF = \frac{\tau}{S} = \left\{\frac{\cos\alpha - k\sin\alpha}{\sin\alpha + k\cos\alpha}\right\}\tan\phi \quad \text{.....(4)}$$

k = 0 Static Conditions

$$SF = \frac{\tan\phi}{\tan\alpha} \quad \text{.....(5)}$$

k_c (Critical lateral load coefficient) SF = 1.0 $k_c = \tan(\phi - \alpha)$ .....(6)

Figure 1. Stability of an Infinite Slope with Horizontal Earthquake Force

aries with both the gravel base and the plexiglass side of the test box (Figure 2), whereas the finite slope has no direct boundary with either (Figure 3). The initial test slopes were straight planes, whose slope angles were measured at different locations and average values were taken.

The shaking table was based on an electric engine attached to a frequency varying disc. The rotation produced by the engine was adapted through a gear-box to three different frequencies. The rotation transferred to the amplitude variation disc by a rotating belt was given directly by a hinge rod to the aluminium table (1.5 cm thick and 120 cm in diameter). The aluminium shaking table is mounted on four rollers, thoroughly greased, to avoid Coulomp damping. This procedure results in vibrations which have a sinusoidal form. The frequency and amplitudes of sunisoidal vibrations corresponding to different stages were precisely measured and the velocities and accelerations were calculated.

The velocities and accelerations of the shaking table were calculated from the sinusoidal displacement function,

$$u = A \sin \omega t$$

where; u is the displacement, A is the maasured amplitude and ω is the angular frequency, $2\pi f$, calculated from the measured frequency, f. The velocity, corresponding to a certain amplitude and frequency thus varies,

$$v = \frac{du}{dt} = A\,\omega \cos \omega\, t$$

and the acceleration is

$$a = \frac{d^2u}{dt^2} = -A\,\omega^2 \sin \omega t$$

The maximum acceleration reached during sinusoidal shaking is when Sin $\omega t = 1.0$

$$a_{max} = -A\,\omega^2$$

The acceleration ratio k, was calculated as a/g. Results of these calculations

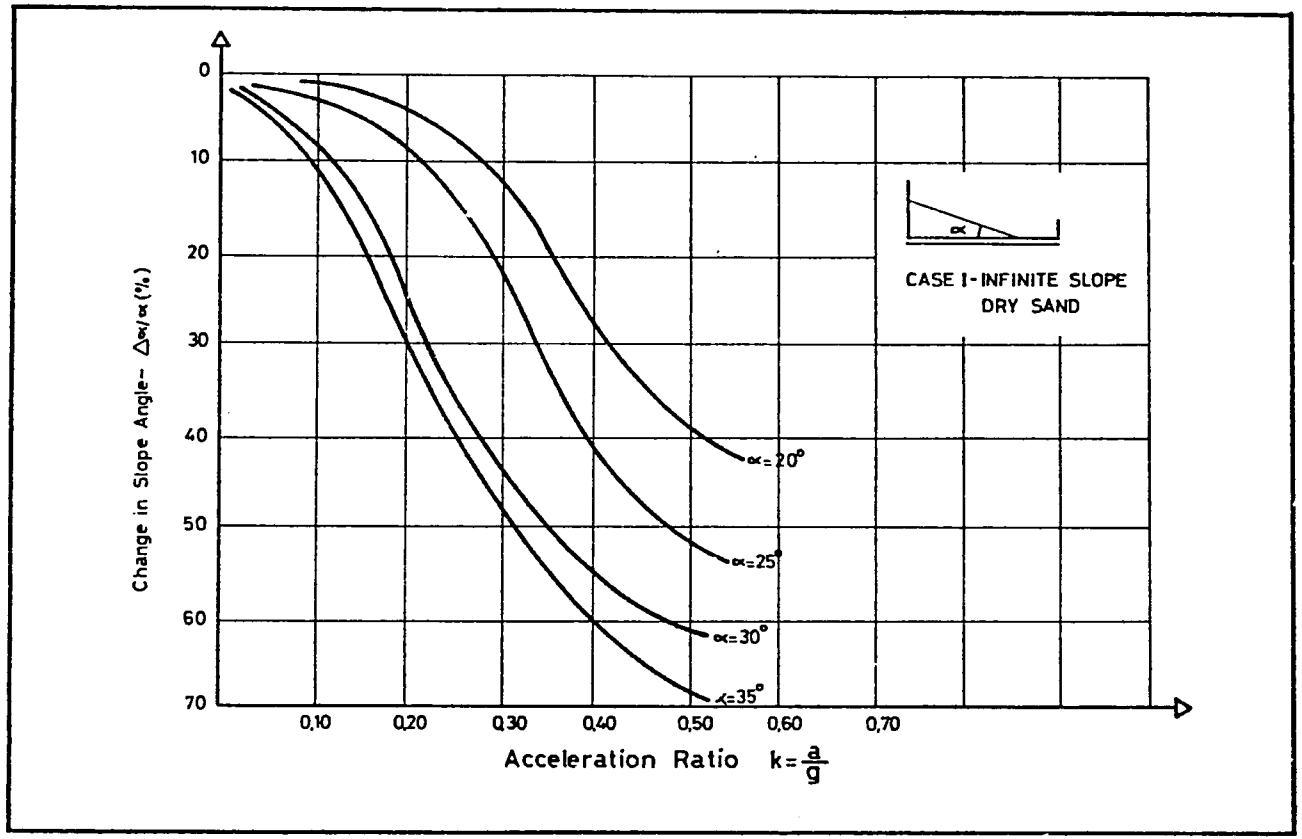

Figure 2. Variation in the Slope Angles with Applied Acceleration Ratios. (Case I)

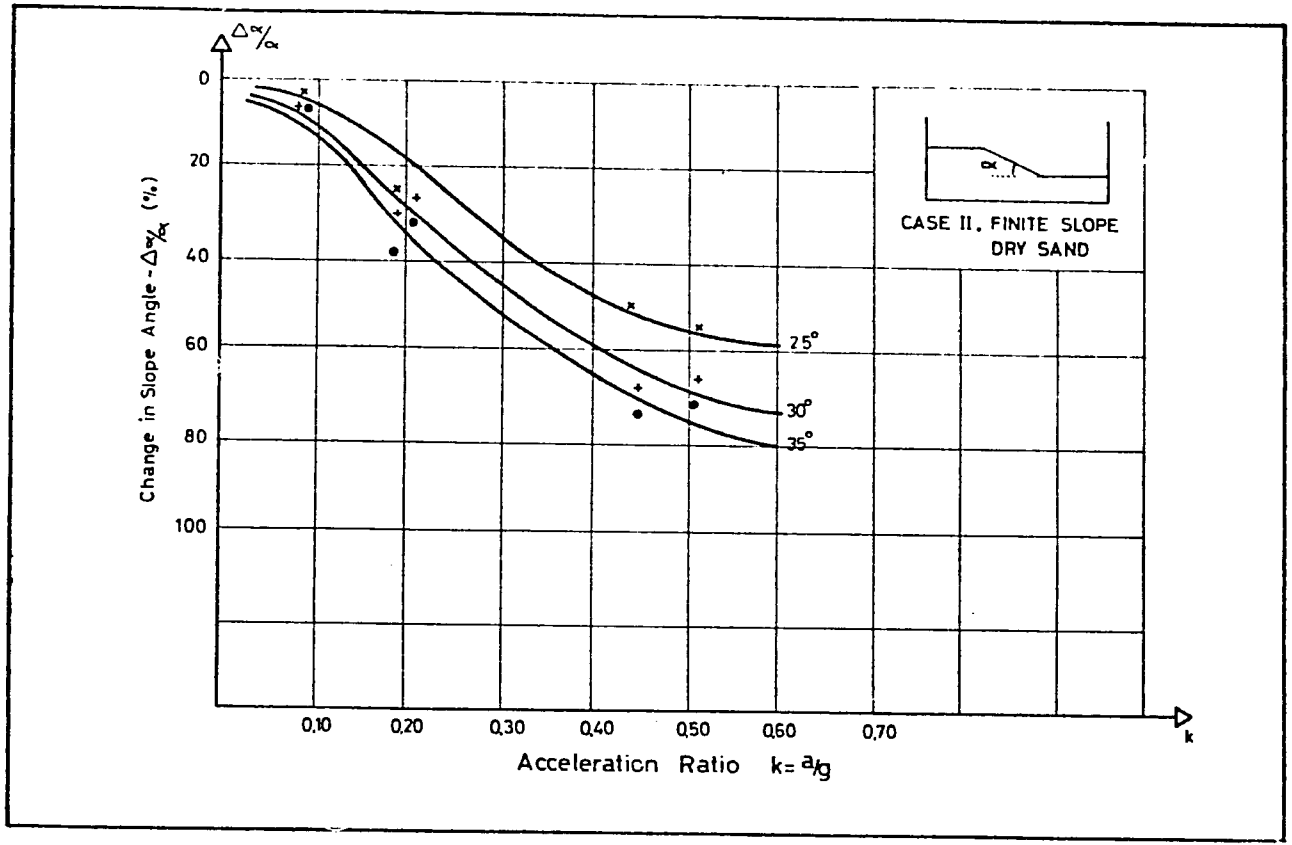

Figure 3. Variation in the Slope Angles with Applied Acceleration Ratios. (Case II)

are given in Figure 4 (see the next page).

Since relatively small model were used, the accelerations induced on the models were assumed to be the same as the dynamic characteristics of the table.

Test Results

The slope angle of dry sand slopes decreased as the acceleration ratios of the vibrations increased (Figures 5 and 6 on the next pages). For loose sand slopes, assuming the angle of repose at rest (initial α) is approximately equal to the friction angle in loose conditions, seismic shaking tends to decrease the strength parameters of dry sand.

Infinite slopes showed less change in their slope angles than the finite slopes (Figures 2, 3 and 7). For example, for an acceleration ratio of 0.20, an infinite slope with an initial slope angle of 30° registered a change of 24%, whereas for a finite slope the decrease was about 28%. This difference is probably due to the different boundary conditions.

At the end of the tests, the final dry sand slopes had planar surfaces. Other tests carried out on saturated sand slopes have demonstrated concave final test slopes.

The variation of the change in slope angle with acceleration ratio has the form

$$\frac{\Delta\alpha}{\alpha} = A.e^{-\frac{B}{k^2}}$$

where A was found to be 0.85 and B 0.16 after regression analysis for the infinite slope with initial slope angle of 25° (Figure 4).

Conclusions

It is known[2] that the angle of friction of cohesionless soils tends to decrease with acceleration ratio under dynamic stresses. Our work shows that a decrease in the strength parameter of dry sands occurs under seismic shaking. However, since our research was done on a small shaking table, with its limitations, further development is essential for comparisons to be made with analytical response and model similitude analysis.

Figure 4. Characteristics of the Shaking Table

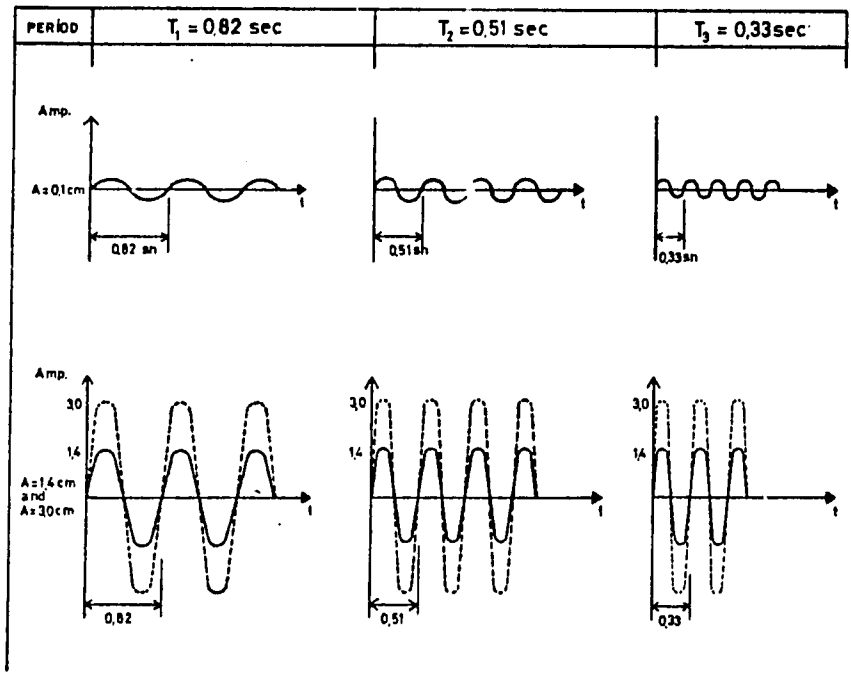

Period	Frequency	Angular Frequency	Vibration Amplitude	Maximum Acceleration	Maximum Velocity	$k=\frac{a_{max}}{g}$
T (s)	f (c/s)	ω (s)	A cm	a_{max} cm/s^2	V_{max} cm/s	–
0,82	1,22	1,65	0,1	5,85	0,77	0,006
			1,4	81,90	17,20	0,0083
			3,0	175,50	22,90	0,179
0,51	1,95	12,25	0,1	14,98	1,23	0,015
			1,4	209,86	17,16	0,213
			3,0	449,90	26,80	0,458
0,33	3,00	18,84	0,1	35,34	1,88	0,046
			1,4	494,81	26,40	0,505
			3,0	1060,3	56,60	1,08

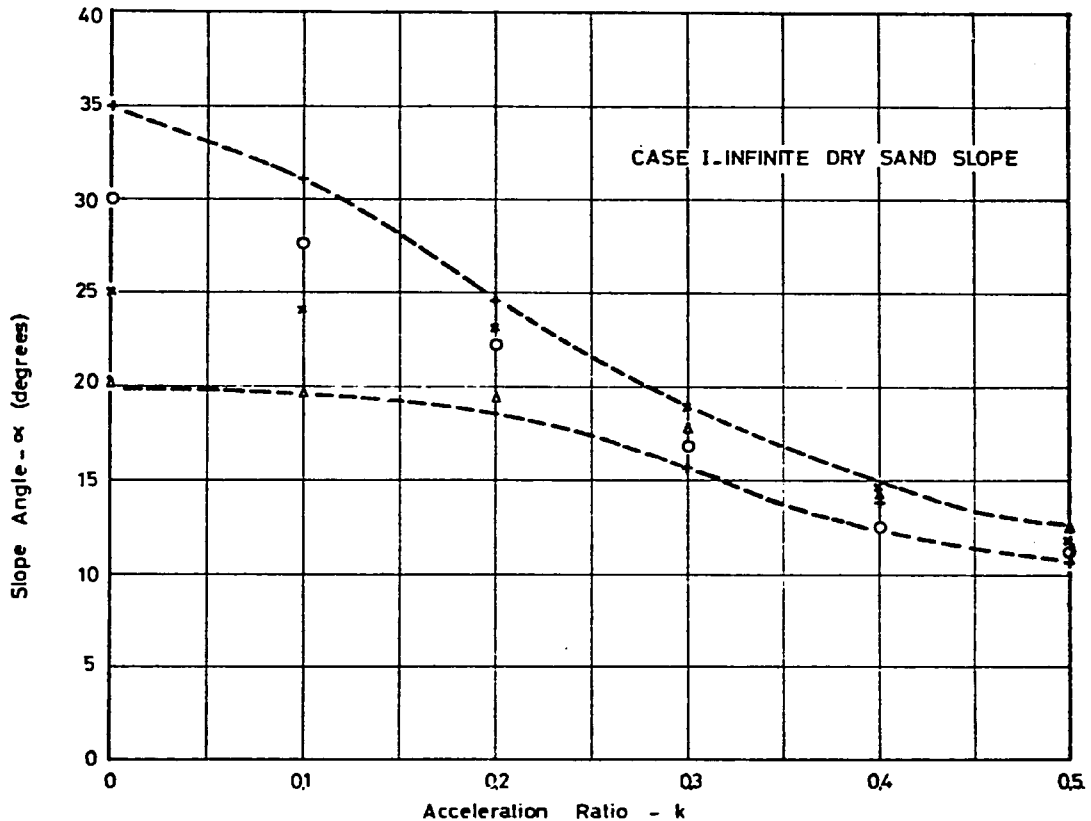

Figure 5. Variation of Final Stable Slope Angle with Acceleration Ratio

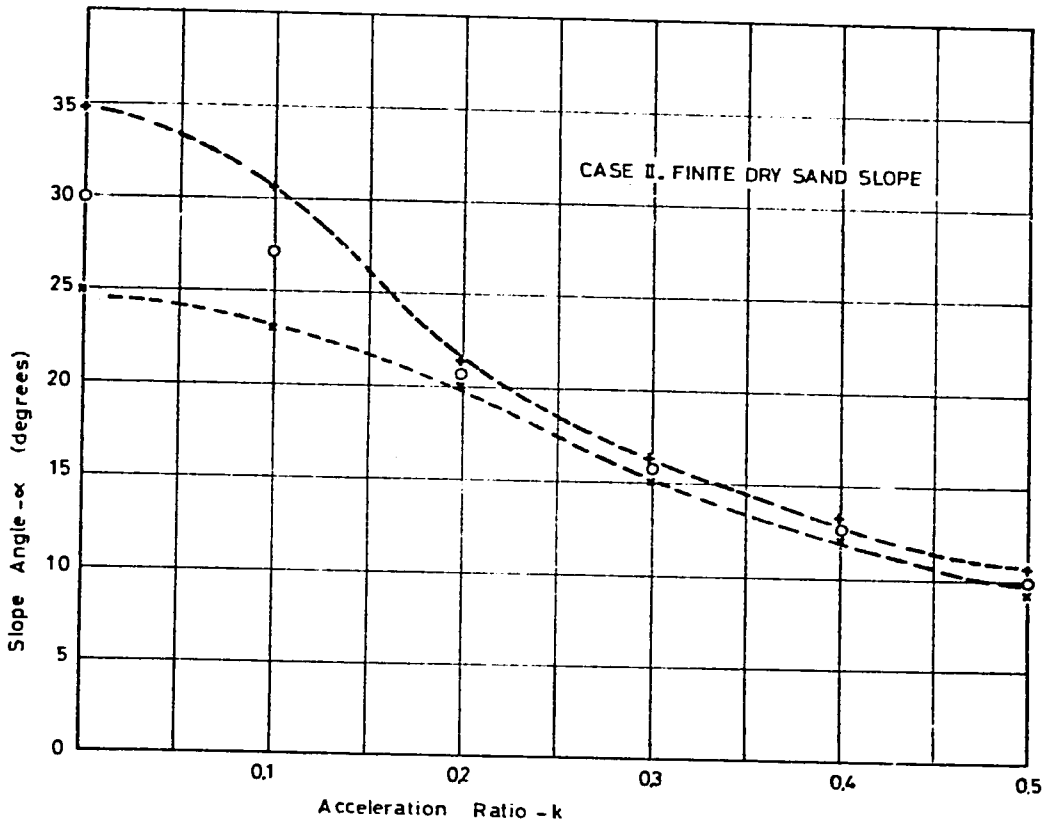

Figure 6. Variation of Final Stable Slope Angle with Acceleration Ratio

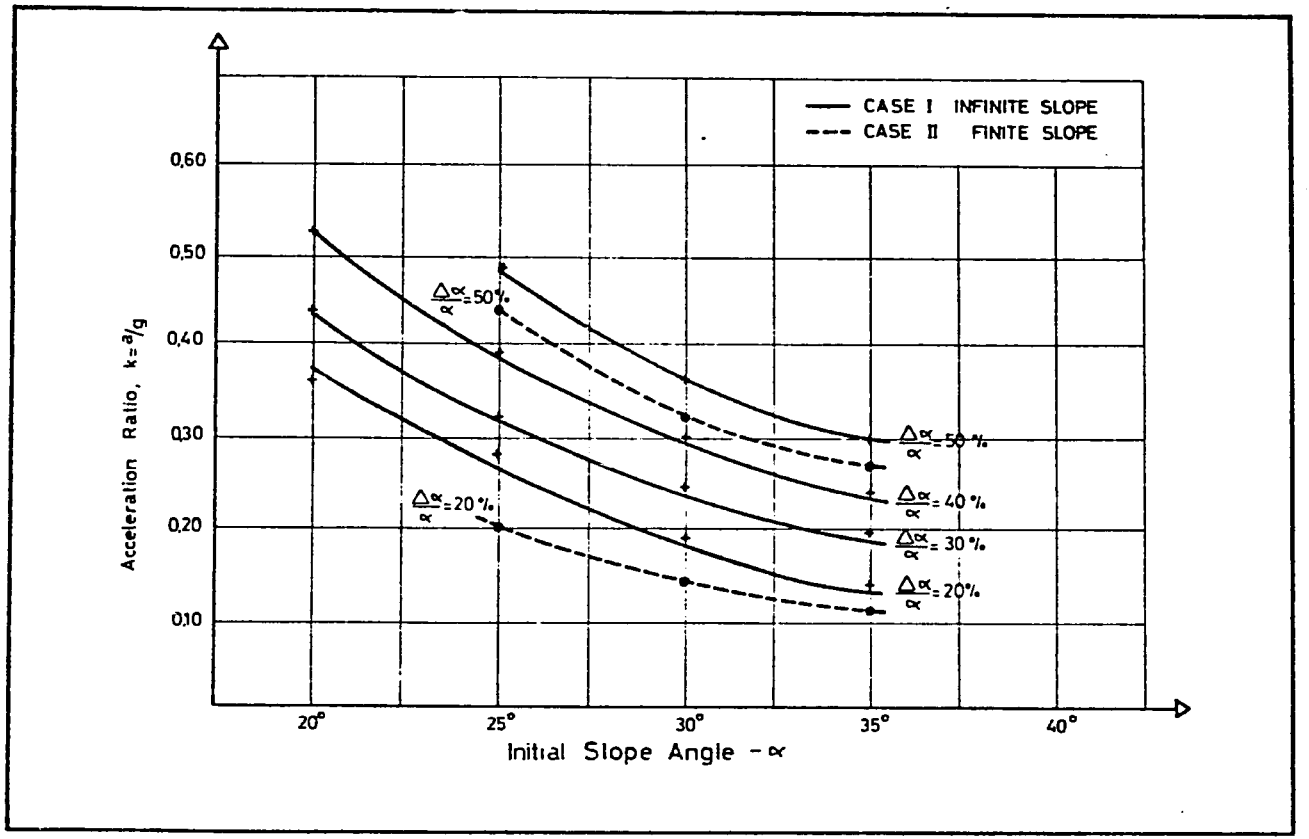

Figure 7. The Effects of Initial Slope Angle and Acceleration Ratio on Failure Criteria

REFERENCES

1. O. Okamoto, "Earthquake Engineering". University of Tokyo Press, 1973.

2. D.D. Barkan, "Dynamics of Bases and Foundations". McGraw Hill, 1962.

DISCUSSION

Professor Ambraseys commented that the behaviour of granular materials was different at very low confining pressures, up to about $10 g/cm^2$; these pressures were not often studied but they did affect behaviour in models such as those described.

PLANE–STRAIN ANALYSIS IN SOIL–STRUCTURE INTERACTION PROBLEMS

Professor W.D. Liam Finn, Dr. E. Varoğlu and Mr. T. Nogami

In soil-structure systems, soil is frequently idealized as a linear elastic half-space or a layer of infinite extent and finite depth. The foundation of the structure may be a single rigid rectangular slab, a combination of such slabs. This approach is limited principally by the availability of analytical solution for the elastic dynamic response of the half-space (or layer) under a time-varying loading which is applied the foundation-soil interface. Because of the mathematical complexities involved, soil-structure interaction problems are frequently simplified by assuming are that structure is idealized as a single mass structure; ground is simulated as a lumped mass; an equivalent mass-spring system is employed for structure and soil; or that foundation of the structure is taken as a circular slab. An alternative approach would be to us the readily available finite element techniques for static and dynamic plane-strain analysis.[1,2]

Lateral Static Soil-Structure Interaction

A structure with a rigid rectangular slab foundation of length 2c and width 2a which rests upon a homogeneous elastic soil layer of depth h which in turn rests upon a rigid base, is subject to static lateral loading. The lateral displacement of the foundation which is obtained from plane-strain analysis of a cross-section will differ

from the actual lateral displacement of the foundation. This difference is due to the difference between the shear stiffnesses of the soil layer used in plane-strain analysis and in the three-dimensional analysis of the problem.

2-D shear stiffnesses of a soil layer is defined as the required lateral force per unit length of an infinitely long rectangular area on the surface of an elastic layer to cause unit lateral displacement of the rectangular area (K_{2-D}). Similarly, the average lateral force per unit length of a rectangular area on the surface of an elastic-layer required to cause a unit lateral displacement of the rectangular area will be referred to as 3—D shear stiffnes of the elastic layer (K_{3-D}).

A modified Young's modulus is obtained by multiplying the Young's modulus of the soil by the factor K_{3-D}/K_{2-D} in the plane-strain analysis. The lateral displacements of the three-dimensional model can then be obtained accurately. A numerical method has been developed to compute 3—D shear stiffness of a soil layer for a given laterally loaded rectangular area over the soil layer employing Cerruti's formula.[3] 2—D shear stiffness of the soil layer has been computed numerically for uniform lateral displacement of a strip area.

The shear stiffness ratio K_{3-D}/K_{2-D} is compared with the ratios c/a and 2c/h in Figures 1 and 2 for several values of h/a. It is evident that the use of plane-strain analysis instead of a three-dimensional analysis will involve an error in the lateral displace-

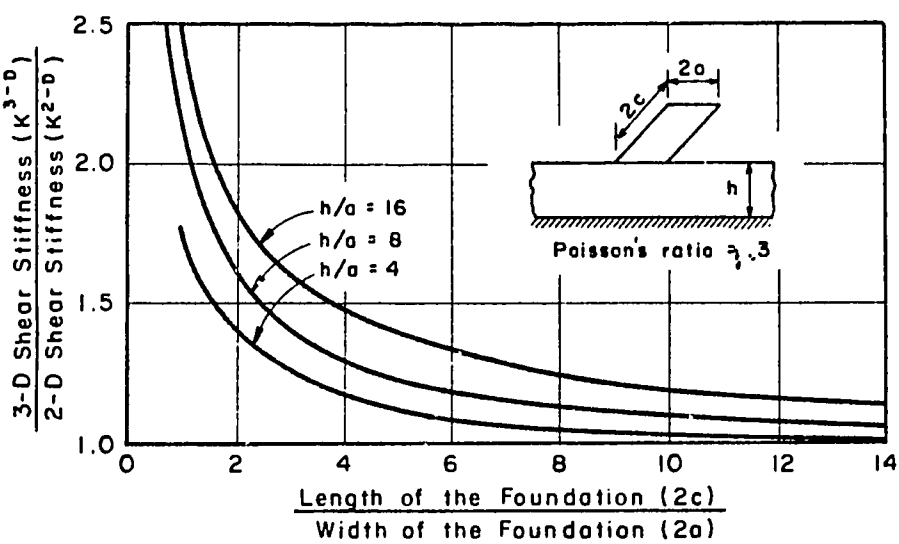

Figure 1. Shear Stiffness Ratio of the Soil Layer Versus c/a.

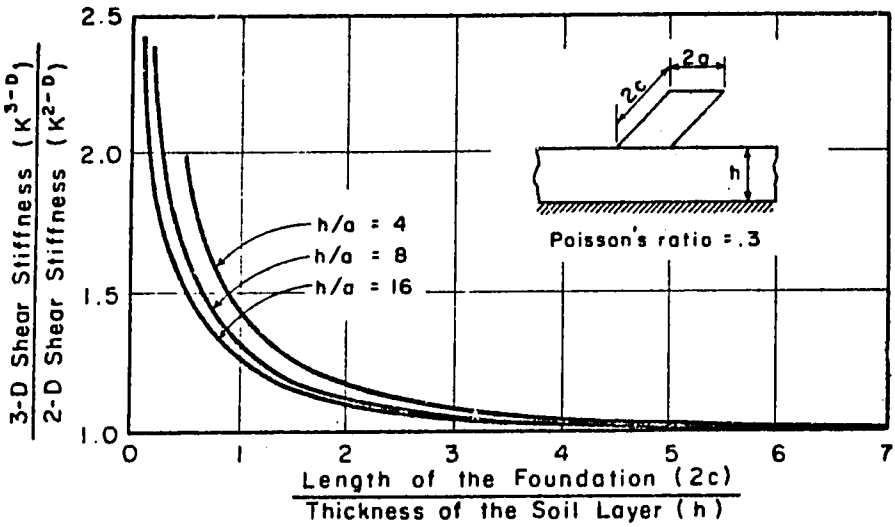

Figure 2. Shear Stiffness Ratio of the Soil Layer Versus 2c/h.

ments of the model which increases with increasing h/a and decreasing c/a. For example, the 3—D shear stiffness of the soil layer is 22.5% larger than the 2—D shear stiffness of the soil layer when c/a = 8. Figure 1 also shows that the use of plane-strain analysis will result in an error in the calculated lateral displacement of the model of less than 10%, if c/a $\geqslant$ 10 and h/a $\leqslant$ 8.

Lateral Dynamic Soil-Structure Interaction

In this problem, it is important to determine the lateral force F(t) exerted on the foundation by the soil-layer and the lateral displacement u(t) of foundation soil-layer interface. After the function u(t) is determined, the structure can be separately analysed to determine the displacement and/or the stresses at any point. This soil-structure interaction problem may be reduced to two sub-problems which will yield two relationships between the two unknown functions F(t) and u(t).

The first relationship between u(t) and F(t) can be obtained by analysing the lateral motion of the structure alone, prescribing the lateral displacement of the foundation as u(t) and denoting the required lateral force exerted on the foundation by the soil layer as F(t).

The second relation may be obtained by analysing the motion of the soil-layer. Here the soil-layer is subject to a lateral excitation on its fixed interface with a rigid base and to a lateral force of $-F(t)$ acting on the area of the interface with the foundation of the structure, with a resultant displacement $u(t)$ of this area. The solution of this problem can be obtained by combining the solutions for a soil-layer with free surface subject to a lateral excitation on its fixed interface with a rigid base; and a soil-layer resting on a rigid base subject to a total lateral force $-F(t)$ exerted by the structure on a surface area of the soil-layer.

The plane-strain analysis of system where the foundation is a rectangular slab amounts to the simplification of the relation between $F(t)$ and $u(t)$ obtained from the soil-layer problem.

The dynamical problem of an elastic layer subject to a uniform lateral load is now considered. The relationship between the amplitude of the lateral displacement $u \exp(i\,\omega\, t)$ at the centre of the loaded area and the amplitude of the lateral load $q \exp(i\,\omega\, t)$ per unit length of this area can be expressed as:

$$\frac{u^{3-D}}{q} Ga = 2c\,(f_1^{3-D} + i f_2^{3-D}) \qquad \text{Rectangular Area Loading} \qquad (1)$$

$$\frac{u^{2-D}}{q} Ga = f_1^{2-D} + i f_2^{2-D}) \qquad \text{Strip Area Loading} \qquad (2)$$

Here, f_1^{3-D} and f_2^{3-D} are the real and imaginary parts of the 3—D lateral compliance; f_1^{2-D} and f_2^{2-D} are the real and imaginary parts of the 2—D lateral compliance. The shear modulus, mass density and the Poisson's ratio of the layer are denoted by G, ρ and ν respectively. The rectangular area is of length 2c and width 2a; the width of the strip is 2a.

3—D lateral compliance of an elastic layer has been reported earlier[4] and 2—D compliance has now been determined. These are both functions of dimensionless excitation frequency $a_0 = \omega a / \sqrt{G/\rho}$, the Poisson's ratio and the ratio of the width of the loaded area to the depth of the layer. The 3—D compliance is also dependent on the ratio of the width to the length of the rectangular area. For excitation frequencies smaller than the fundamental frequency $\pi \sqrt{G/\rho}$ 2h of the layer in shear, the functions f_2^{3-D} and f_2^{2-D} vanish: it is then possible to modify the material properties of the

elastic layer in a strip area loading problem so that the lateral dynamic displacement $u^{2-D} \exp(i\omega t)$ of the centre line of the strip is equal to the lateral displacement $u^{3-D} \exp(i\omega t)$ of the centre of the rectangular area in the rectangular area loading problem. The width of the strip should be equal to that of the rectangle and the loads per unit length of the loaded areas should be identical. The modification of the material properties should be such that the shear wave velocity and Poisson's ratio of the elastic layer has not been changed after modification. Then, this modification becomes:

$$G^{2-D} = G \frac{f_1^{2-D}(a_o)}{2c\, f_1^{3-D}(a_o)} \qquad \text{for } a_o < \frac{\pi}{2}\frac{a}{h} \tag{3}$$

$$\rho^{2-D} = \rho \frac{f_1^{2-D}(a_o)}{2c\, f_1^{3-D}(a_o)}$$

Here, G^{2-D} and ρ^{2-D} are modified values of the shear modulus and the mass density of the elastic layer to be used in the plane-strain analysis.

The functions f_1^{2-D}/a and f_1^{3-D} are illustrated in Figures 3 and 4 (see the next pages), and from these, the modification factor $f_1^{2-D}/(2c\, f_1^{3-D})$ is evaluated. The modification factor as a function of a_o is illustrated in Figure 5 (see page 79) for $c/a = 2$ and $c/a = 1$.

The above modification of the shear modulus and the mass density of the elastic layer is dependent on the excitation frequency. In some finite element techniques, the response of the system to be an arbitrary excitation is evaluated directly by a modal analysis without first computing the response of the system to a harmonic excitation and using Fourier integral techniques. Therefore, a frequency dependent modification of the material properties of the layer cannot be incorporated into such finite element techniques. Instead a modification of the shear modulus and the mass density of the layer, which amounts to the multiplication of both by a constant factor, is proposed. Then the statical lateral displacements of the rectangular area and the corresponding strip area are identical. Also, shear wave velocity of the layer is kept unchanged after modification.

The factor necessary to modify the shear modulus and the mass density of the soil layer can be taken from Figures 1 or 2 for several values of c/a and h/a. This approach has the advantage it is not necessary to evaluate the dynamical lateral compliance of the soil layer to determine the modification factor; it is sufficient to make a

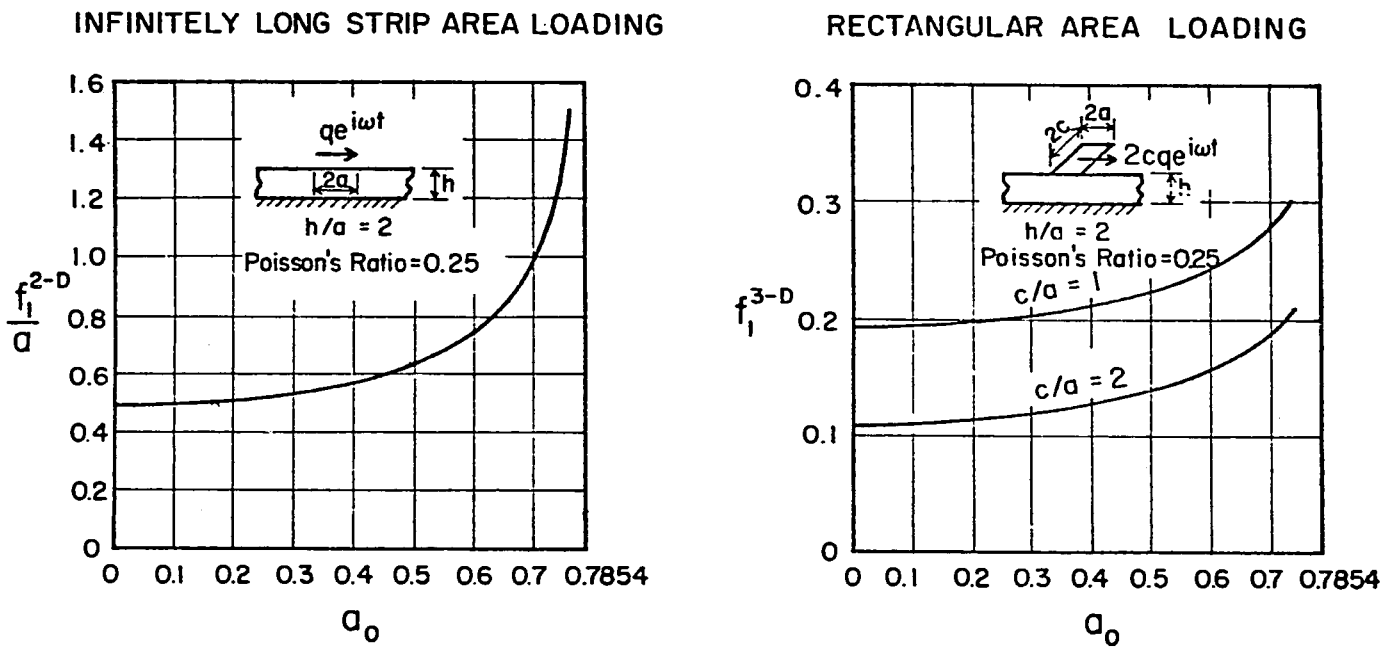

Figure 3. Lateral Compliance of the Soil Layer for h/a = 2.

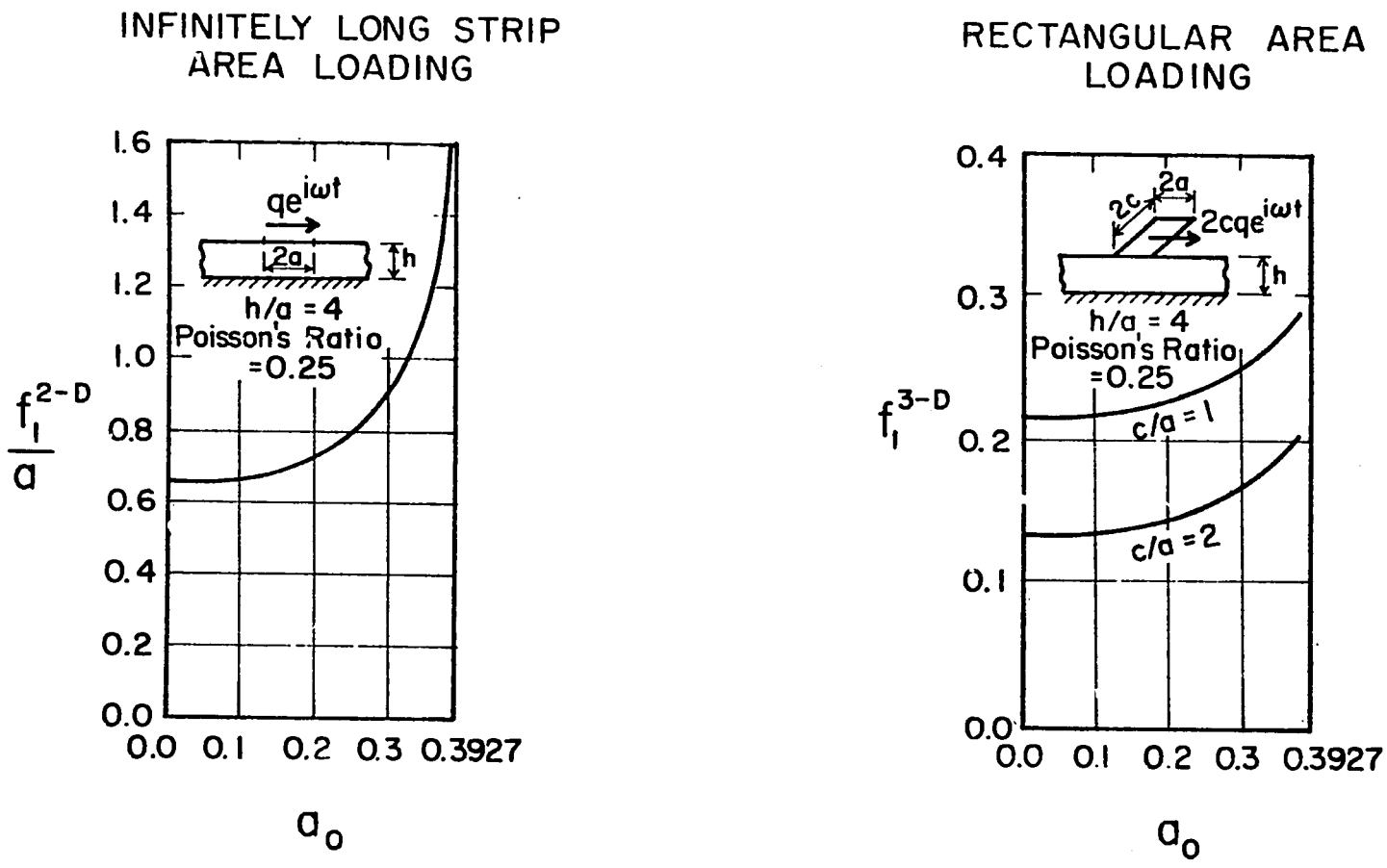

Figure 4. Lateral Compliance of the Soil Layer for h/a = 4

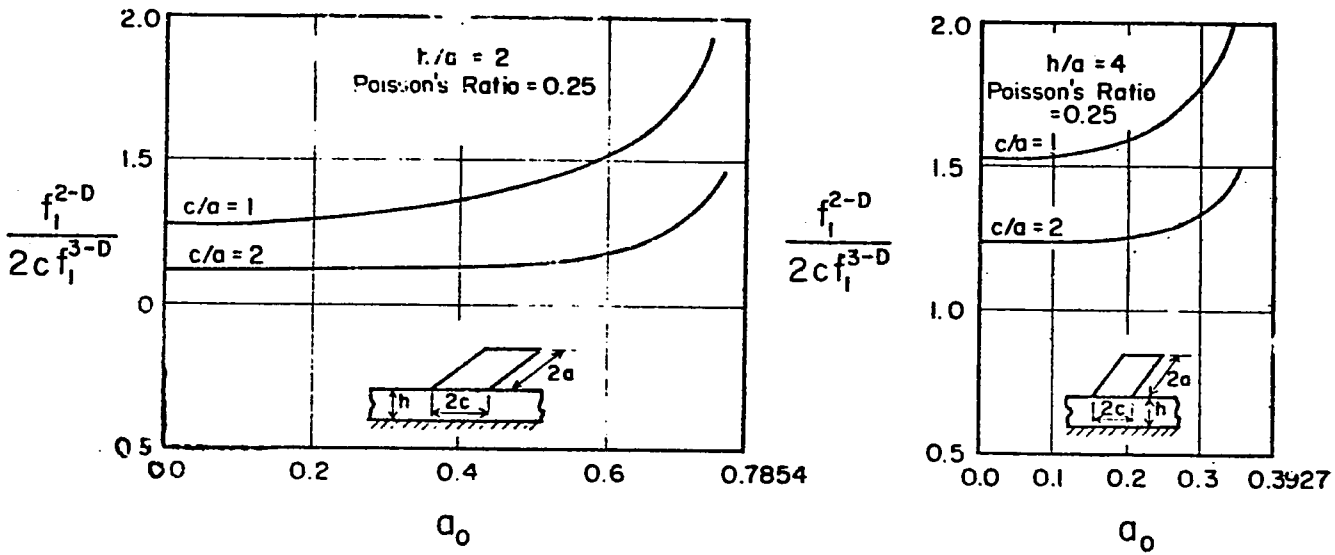

Figure 5. Frequency Dependent Modification Factor

statical analysis of a soil layer. Hence, this type of modification is quite practical and can be efficiently incorporated into plane strain finite element analysis to account approximately for the influence of the aspect ratio of the rectangular foundation of the structure.

To illustrate the proposed equivalent 2—D analysis, the fundamental frequency of a soil-structure system will be evaluated. This system consists of a rigid rectangular block of width 2a and length 2c which rests upon a homogeneous elastic soil layer of depth h. The lateral input motion at the base of the soil layer is exp ($i\omega t$). The mass of the rigid block is denoted by M. It is assumed that the rigid block is flat enough and experiences no rocking motion.

The dimensionless fundamental frequency $(a_o)_F^{3-D}$ of this system is given by:

$$(a_o)_F^{3-D} = \frac{1}{\sqrt{b\, f_1^{3-D}}} \tag{4}$$

where the dimensionless mass ratio b is defined as:

$$b = \frac{M}{\rho a^3} \tag{5}$$

Similarly, the fundamental frequency of this system obtained from plane-strain analysis is given by:

$$(a_o)_F^{2-D} = \frac{1}{\sqrt{b'\, f_1^{2-D}}} \tag{6}$$

where

$$b = \frac{m}{\rho a^2}, \text{ and } m = \frac{M}{2c} \tag{7}$$

The fundamental frequency of this system obtained from the three-dimensional analysis, modified and unmodified plane-strain analysis (analytical and finite element solutions) are illustrated in Figures 6 and 7 for c/a = 1 and c/a = 2.

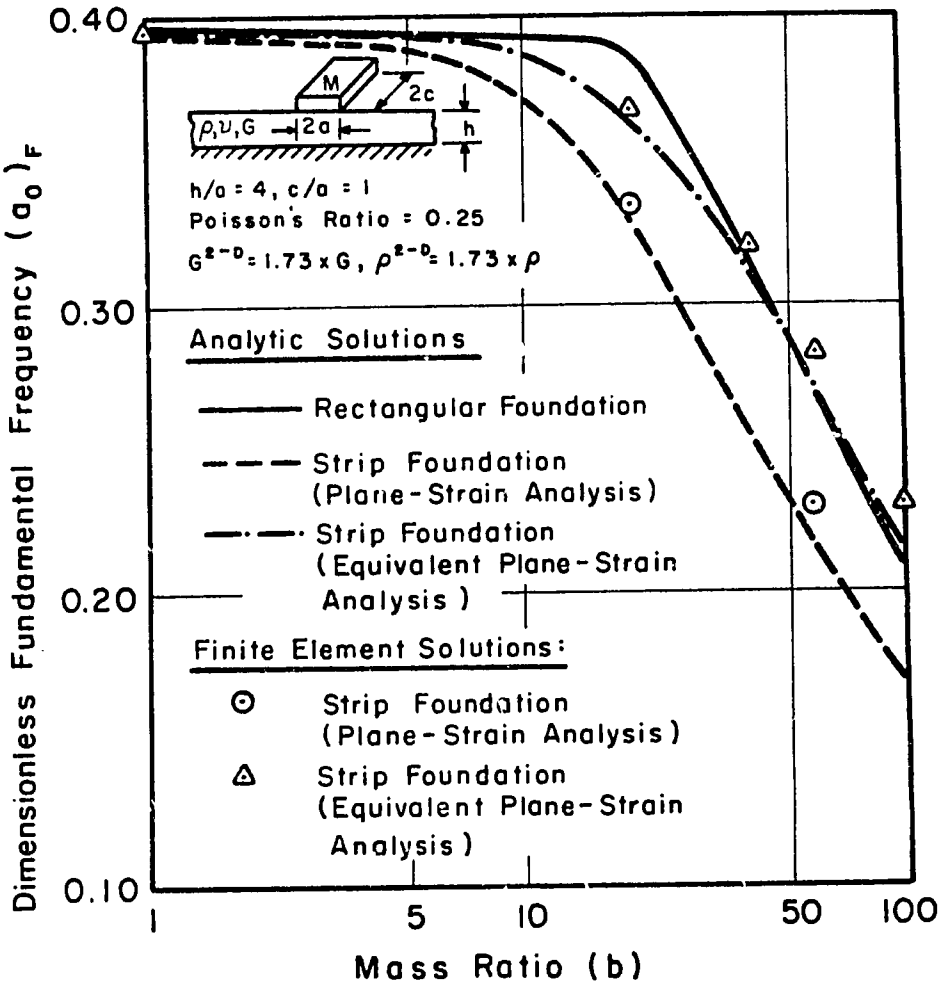

Figure 6

Fundamental Frequency of the Foundation-Soil System, c/a 1.

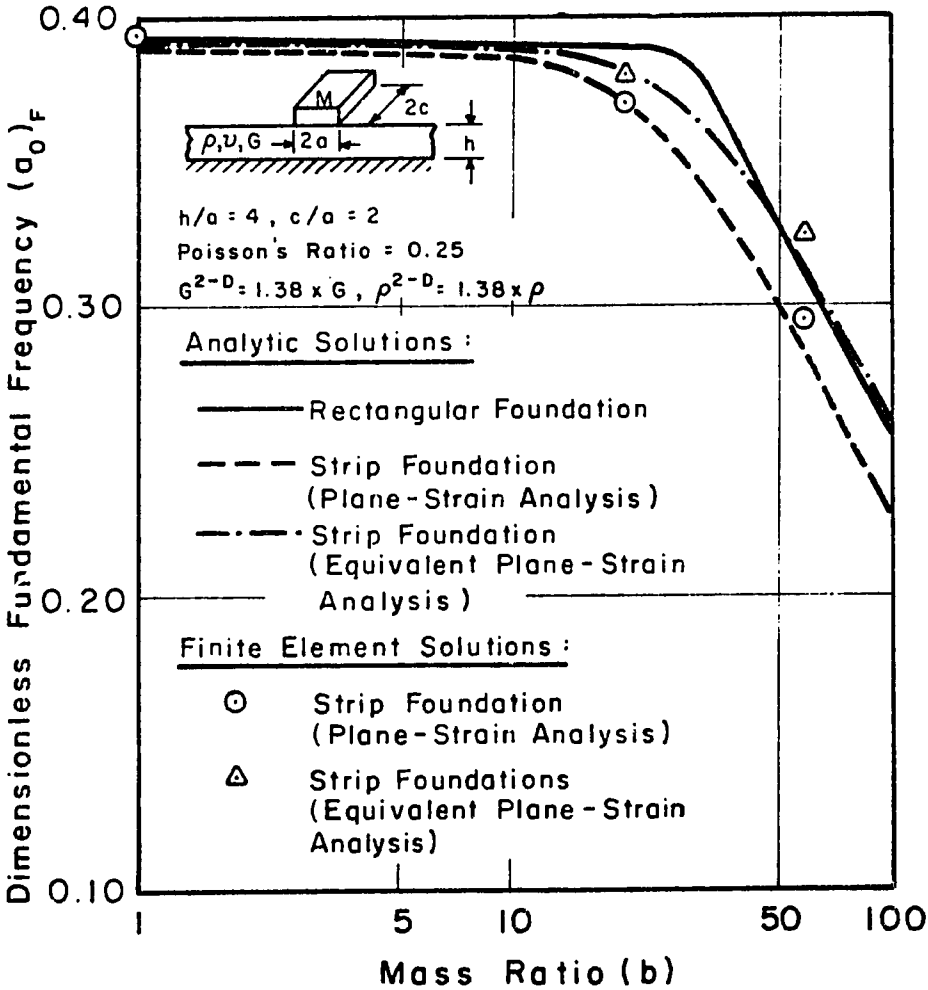

Figure 7

Fundamental Frequency of the Foundation-Soil System, c/a 2.

Conclusion

It is shown that an equivalent plane-strain analysis of the system where the shear modulus and the mass density of the soil-layer are modified depending on the excitation frequency may take into account the three-dimensional effects of the rectangular foundation. However, the computation of a frequency-dependent modification factor requires the evaluation of the lateral dynamic compliances of an elastic layer for a rectangular area loading and a strip area loading. The frequency dependency of the modification prohibits its incorporation into some finite element techniques (plane-strain analysis) which employ modal analysis to evaluate the response of the system to an arbitrary excitation.

A modification which is independent of the excitation frequency, for the material properties of the soil-layer has been proposed to account approximately for the three-dimensional effects of the foundation. This modification requires the evaluation of the shear stiffnesses of an elastic layer for a rectangular area loading and a strip area loading. The proposed modification has the advantage that it can be easily incorporated into any finite element techniques (plane-strain) and a statical analysis of the elastic layer will suffice to determine the modification factor.

As an example, the fundamental frequency of a rigid rectangular foundation-soil layer system has been investigated. From the results illustrated in Figures 6 and 7, we may conclude that an equivalent plane-strain analysis which employs a constant modification factor may be a useful approach when the mathematical difficulties prohibit the three-dimensional dynamical analysis of the system.

REFERENCES

1. *W.D. Liam Finn and J. Khanna, Proc. 3rd Earthq. Symp., Roorke, India, 1966, p. 315.*

2. *R.W. Clough and A.K. Chopra, Proc. Amer. Soc. Civil Eng., 92 EM2, 197 (1966).*

3. *E.H. Davis and H. Taylor, Proc. 5th Int. Conf. Soil Mech. Foundn. Eng., 1, (1961).*

4. *T. Kobori, R. Minai and T. Suzuki, Ann. Rep. Res. Inst. Prev. Nat. Disaster, Kyoto Univ., 11, (1968).*

DISCUSSION

In reply to Dr. Keightley, Dr. Varoğlu said that for the simple system the exact solution could be obtained, as described by Whitman.

SOME SOIL ENGINEERING ASPECTS FOR CONSTRUCTION WORKS IN EARTHQUAKE ZONES

Professor S. Nazir Ahmad

Foundation soils play an important role in construction work in earthquake zones. From the seismic point of view, rock and well-consolidated rocky soils which are unaffected by weathering, and dense soils with low moisture content, are the most suitable types of foundation soils, but there will be sites having water saturated gravels, sands, porous clays, plastic and non-porous clays which are seismically unfavourable. Soil engineering studies and applications will be required to make these as favourable as possible within economic considerations. The design of construction works in such zones is dependent on the soil engineering studies.

The various aspects to be studied include first the examination of the foundation soils and then applying the techniques of drainage, reduction in Ground Water Table, compaction, soil injection, improvement in grading, stabilizing of land slides, etc.

If the above factors are not applied measures must be taken to render the buildings and structures earthquake resistant by means of special planning and special construction measures in seismically unfavourable soils.

The design rating in various zones depends on the type of buildings and also the nature of the foundation soil. In the zone of maximum intensity the construction of buildings and structures is generally not recommended if the soil characteristics are unfavourable. If construction in this zone is necessary, the soils of the foundation could be made comparatively favourable by proper drainage, soil injection and improvement in the grading. This will minimize the special earthquake resistivity measures needed for the construction. The more seismically unfavourable a soil is, the more special earthquake resistivity measures are required. These measures also depend on the type of structures: for large civic buildings, radio stations, etc. special measures will be needed. For buildings of secondary importance like single storey houses, light duty buildings, etc., improved site conditions with reasonable measures of earthquake resistivity could be sufficient.

In planning towns and industrial areas a study of engineering geology, ground water conditions and seismology must be made to find the seismic adequacy of the area. Swampy regions, areas of high water table, areas where flood and erosion is expected, sliding areas of open pit mining, regions endangered by cave-ins, and avalanches

must be avoided. If it is necessary to build in these areas, soil and site conditions must be improved to reduce the earthquake damage.

In planning heavy construction areas, central sections of cities and industrial areas should be located in areas with seismically favourable soils. It is desirable to separate large construction zones by planted areas and city squares.

In engineering design it is necessary to estimate the strength of structure or its behaviour where it is subjected to earthquake ground motion. The method of analysis commonly used to resist dynamic loading assumes the structure to be attached to a rigid foundation, consequently the design techniques disregard any influence of local properties of the ground. However, it is now realised that the dynamic interrelationship between behaviour response of a structure and the characteristics of its foundation medium, the interaction effect, is very important. Studies on soil-structure interaction effects should correspond to the actual behaviour of the structure when subjected to earthquakes. The variable nature of the soil-structure interaction and needs detailed study.

DISCUSSION

Dr. Keightley asked what was intended by the suggestion of separating central sections of cities and industrial zones by planted areas and squares. Dr. Nazir Ahmad said that if large structures were too close, earthquake damage was likely to be much greater; he considered that even for separate structures there was interaction between them.

THE PREDICTION OF EARTHQUAKES BY AN ELECTRICAL METHOD

Mr. Fikret Kaftanoğlu and Dr. Bilgin Kaftanoğlu

During the Second World War, a noticeable increase in earthquakes and floods in Turkey was observed. One of the authors, as an amateur investigator, looked into the possibility of a correlation between these events considering the explosions taking place during the War. He thought that these events might have an effect on the earth's electromagnetic field, or the reverse might be true that the changes in earth's electro-

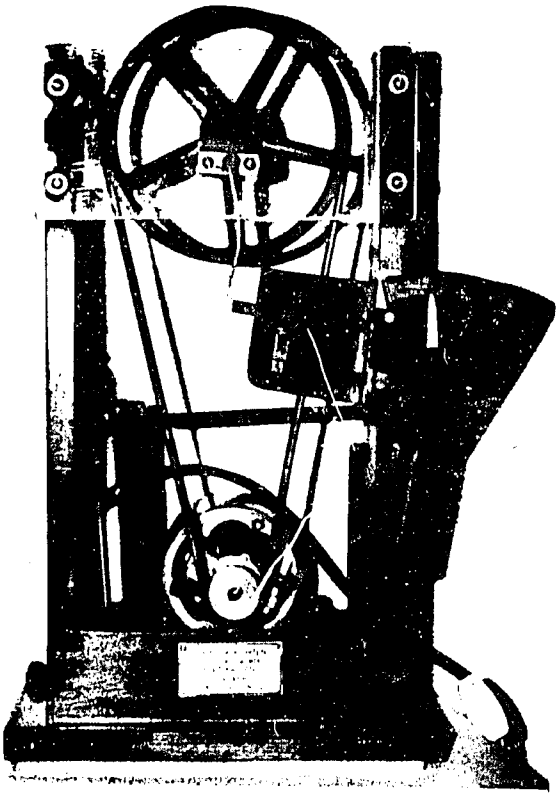

Figure 1
Apparatus for measuring atmospheric electrical charge

magnetic field might influence the occurrence of such natural events. With this basic idea, he set out to construct a device[1] which could measure the electrical charge in the atmosphere.predicted by this method. Recently Nersesov[2] has described the prediction of earthquakes by the measurements of electrical conductivity of rocks and the radioactive gases in waters from wells.

The apparatus developed to measure the electrical charge in the atmosphere (Figure 1) consists of a series a.c. electromotor mounted on a wooden platform. A brass pulley on the shaft of the motor drives an upper pulley with a larger diameter by means of a leather belt. The belt tension is adjusted by a tensioning device. The upper pulley is mounted on two roller bearings. The roller bearing housings are mounted on glass plates to provide electrical insulation. The glass plates are in turn fixed on the wooden frame of the apparatus.

An electrical cable is attached to the bearing housing, and the other end of the cable is plugged into the stationary electrode of the measuring device. The other grounded electrode can be moved by means of a screw drive. A pointer is attached to the screw drive to indicate the gap between the electrodes.

When the motor is started, depending on the atmospheric charge, a spark may jump across the gap between the two electrodes. The gap is increased to the limit until no spark is seen. The maximum spark length is obviously proportional to the spark potential in volts.

It is observed that the electrical charge, as measured, changes as a function of time. When it rises and subsequently falls, experimental results indicate that an earthquake may be expected within the next few days. The magnitude of the earthquake

depends on the amount of the decrease in the electrical charge.

In some cases, when the charge reaches a maximum and starts to fall, and i the atmospheric conditions are such that thenderstorms and rain are present, then th possibility of an earthquake occurring in the next few days is reduced. It is felt that th electrical energy discharged by other means such as thunderstorms, reduces the possibilit of earthquakes taking place.

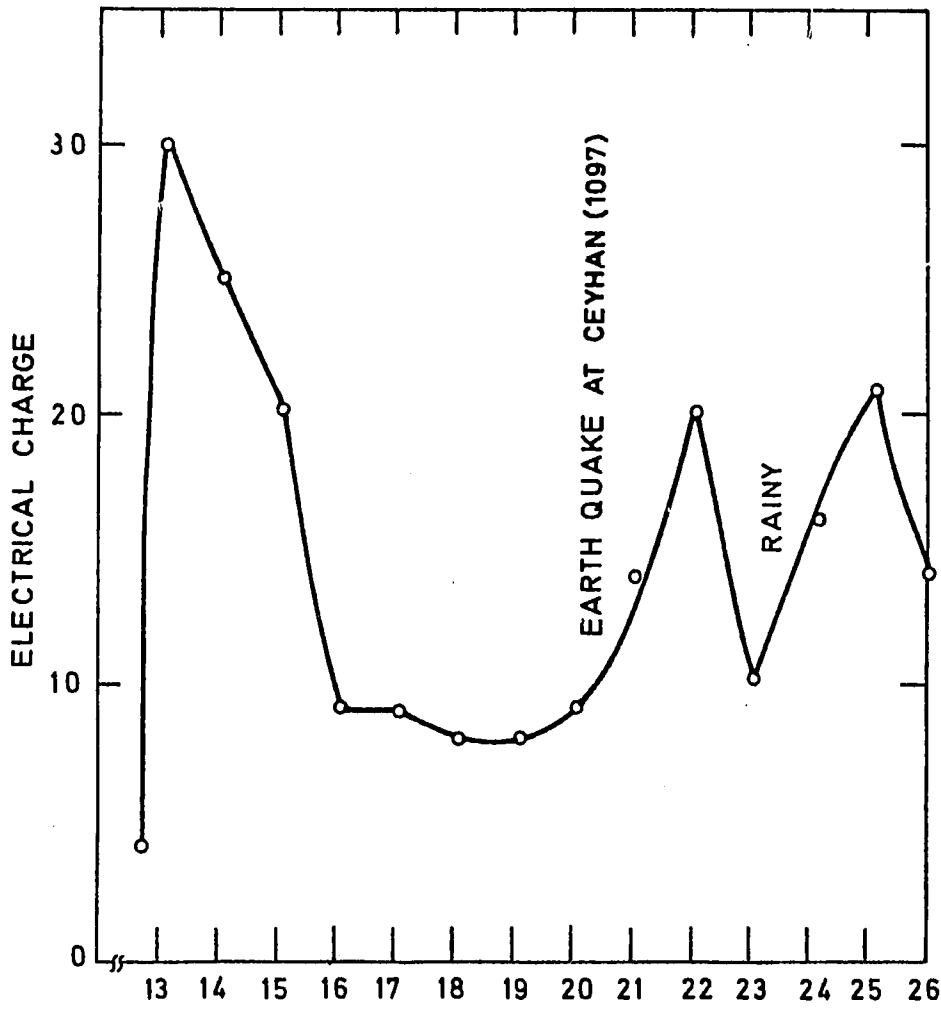

Figure 2. DAYS OF MARCH 1945

The location of the occurrence of an earthquake cannot be predicted using a single apparatus. If a network of such devices could be used, the relative magnitude as well as the location of earthquakes could perhaps be predicted.

Experiments were started in March 1945. Figure 2 (see the preceding page) shows the results of the first series of experiments. There is a peak in the electrical charge on March 13th, 1945: On the same day, a possibility of an earthquake occurring within the next few days was reported to the Ministry of Construction. Three days later the charge was reduced from 30 to 10 units. On the fourth day following this decrease, there was a devastating earthquake in Ceyhan, No. 1097 in the Turkish Earthquake Catalogue.[3]

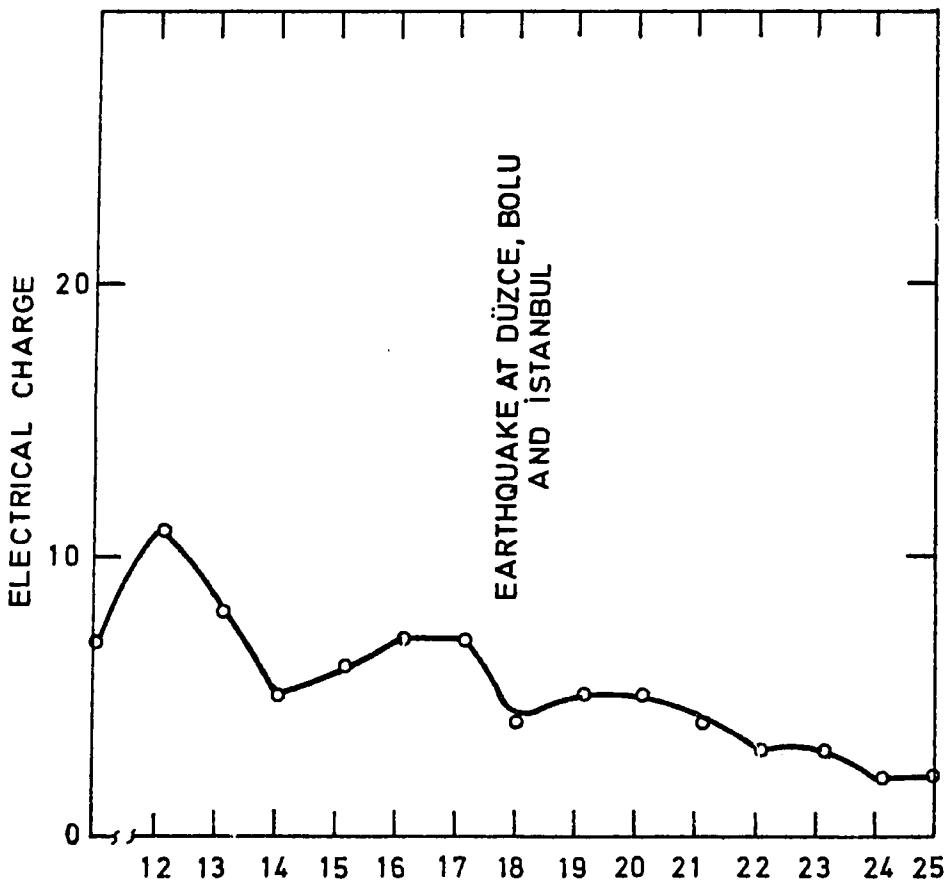

Figure 3. DAYS OF MAY 1945

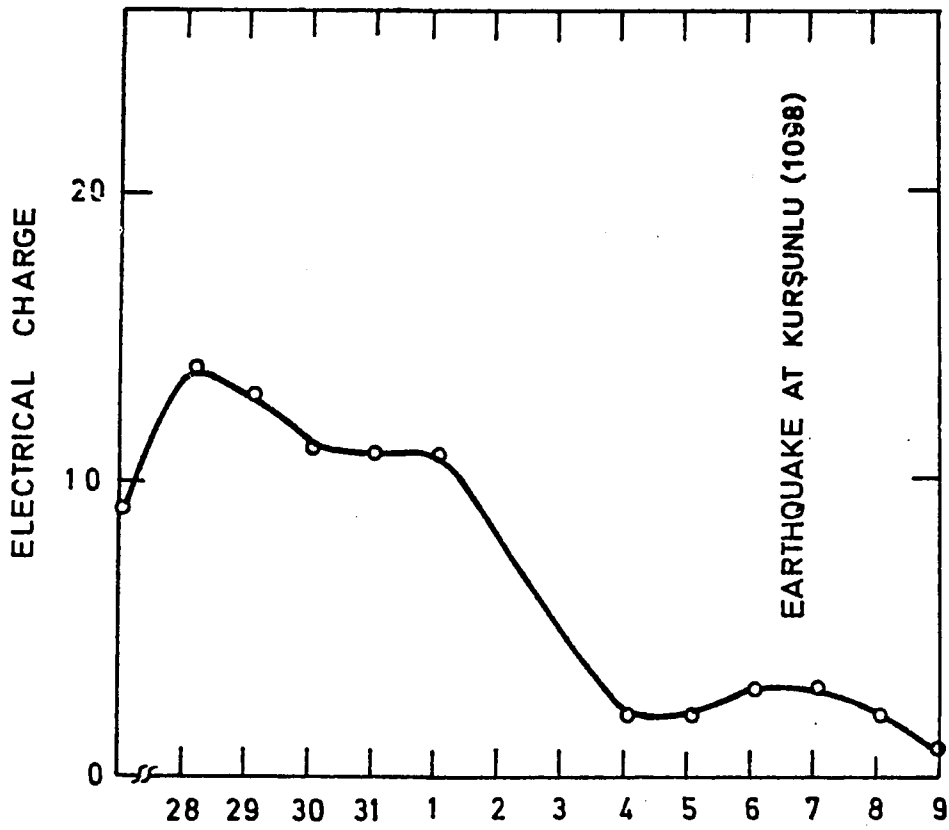

Figure 4. DAYS OF MAY AND JUNE 1945

On the 23rd of March 1945 a second dip (Figure 2) was noticed. No earthquake was reported in the following days. It was felt that this was due to the rainy and thundery weather, and electrical charge in the atmosphere was discharged by such a mechanism.

Figure 3 shows the variation of the electrical charge in May 1945. On the 13th May 1945 an earthquake was predicted and University of Istanbul was informed. Four days after the minimum charge, an earthquake was reported in Düzce, Bolu and İstanbul. [Ulus Newspaper, 17th May 1945; these earthquakes are not included in the Catalogue (3)].

Figure 4 shows another curve in which decrease in the electrical charge was

followed by an earthquake at Kurşunlu (No. 1098, Ref. 3). The time lag between the minimum charge point and the time of earthquake is around three days. The prediction of this earthquake was also reported to the University of İstanbul.

Figure 5 shows another example where the minimum electrical charge point was followed by an earthquake in Muğla after three days (Ulus Newspaper, 1st July 1945). Since all of the above predictions were reported to the Science Faculty of the University of İstanbul, and the predictions came true, the senior author was invited for

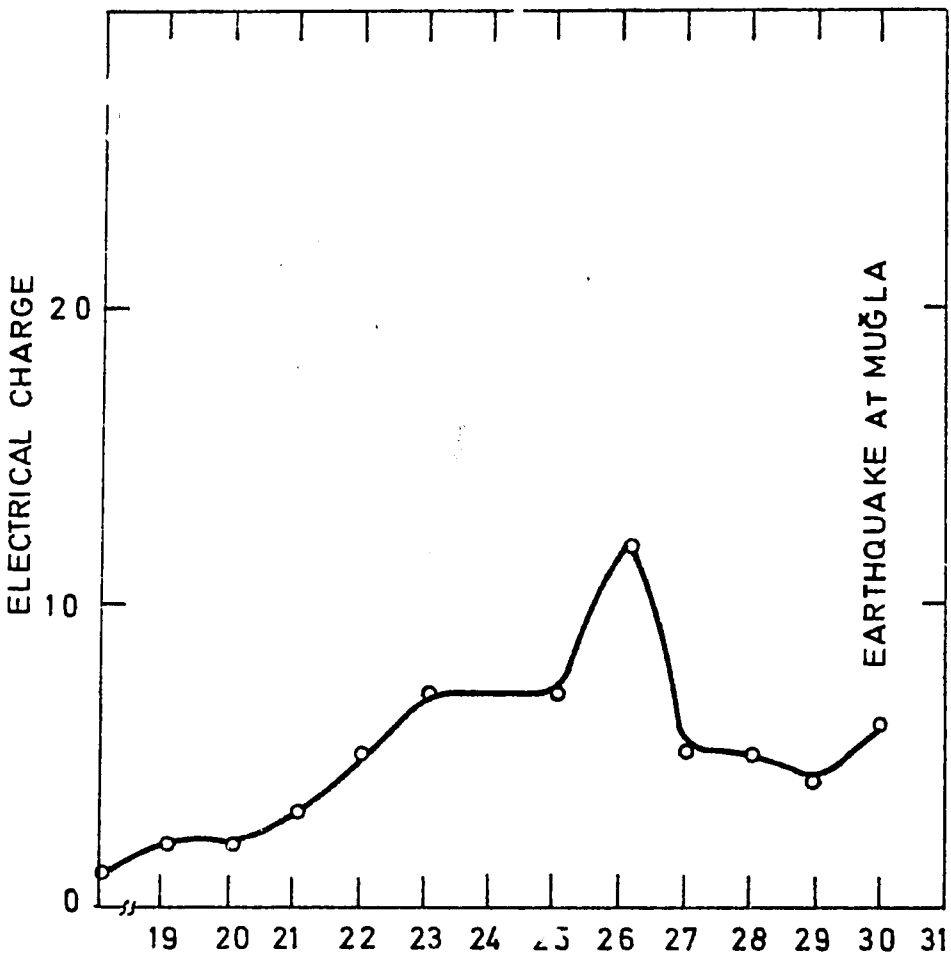

Figure 5. DAYS OF JUNE 1945

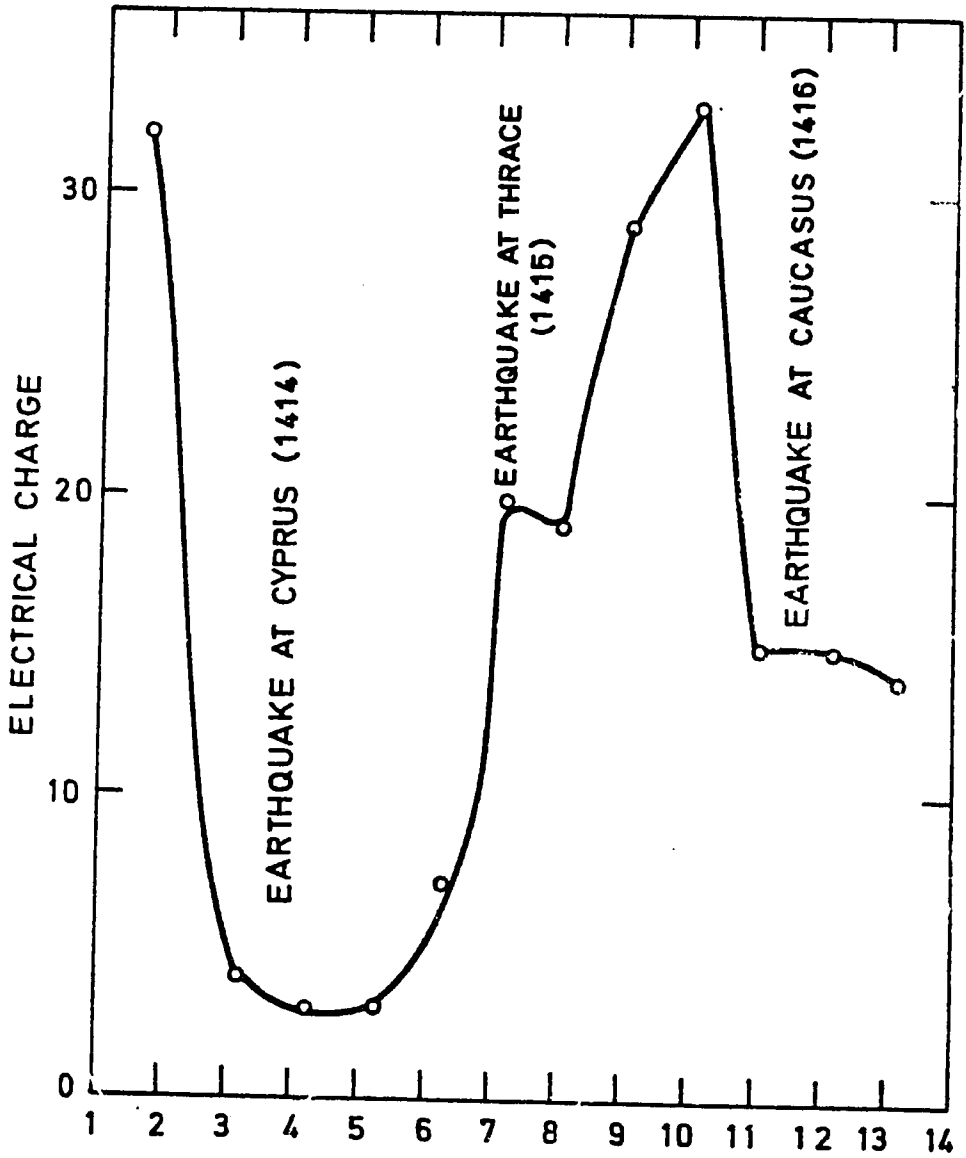

Figure 6. DAYS OF JUNE 1945

discussions and demonstrations to the University. The University was given an apparatus for experimentation. However. after a number of years, the University expressed that they were unable to conduct experiments and no qualified opinion was given.

Further experiments were carried out and predictions continued to be quite successful.

Table 1 shows the investigation of a continuous 4-month period in 1953-4. A number of earthquakes were predicted and reported to the Seismology Institute of the İstanbul Technical University. There is documentary evidence on the dates of reporting of the predictions. Here, again not all the earthquakes could be found in the Catalogue (3). For these earthquakes, the drops in the electrical charge were upto 35 units.

TABLE 1. EARTHQUAKE PREDICTIONS REPORTED TO İSTANBUL TECHNICAL UNIVERSITY, 1953.

Date of Prediction	Date of Earthquake	Location	Reference
21/11/53	24/11/53	Palu	Anadolu News Agency
	28/11/53	Urfa, Elazığ, Diyarbakır	State Meteorological Office
5/12/53	5/12/53	Dodecanese	Ref. 3, No. 1400
	10/12/53	Ayvalık	Anadolu New Agency
	10/12/53	Göynük	Anadolu News Agency
13/12/53	13/12/53	N. Turkey	Ref. 3, No. 1401
	15/12/53	E. Turkey	Ref. 3, No. 1402
27/12/53	28/12/53	Greece	Ref. 3, No. 1403
	2/ 1/54	Dodecanese	Anadolu News Agency
8/ 1/54	11/ 1/54	Erzurum	Anadolu News Agency
15/ 1/54	18/ 1/54	N. Turkey	Anadolu News Agency
27/ 1/54	2/ 2/54	N. Turkey	Anadolu News Agency
11/ 2/54	15/ 2/54	Van	Anadolu News Agency
	20/ 2/54	İzmir	Anadolu News Agency
	22/ 2/54	Crete	Ref. 3, No. 1404
1/ 3/54	4/ 3/54	Germencik	Anadolu News Agency

Figure 6 shows the month of June 1954; again earthquakes (Nos. 1414, 1415, 1416, Ref. 3) took place soon after a minimum is reached in the electrical charge. On the 10th June 1954 the prediction of an earthquake had been reported to the Seismology Institute of the Technical University of İstanbul, and later, two apparatus were given to this Institute, but it was learned that proper investigations could not be carried out.

The results presented above are typical of many found by the authors. Figure 7 shows the most recent record of the variation of the electrical charge: a few days after a drop in the electrical charge, an earthquake in Erzurum—Pülümür was reported by the Turkish News Agency (25th October 1974).

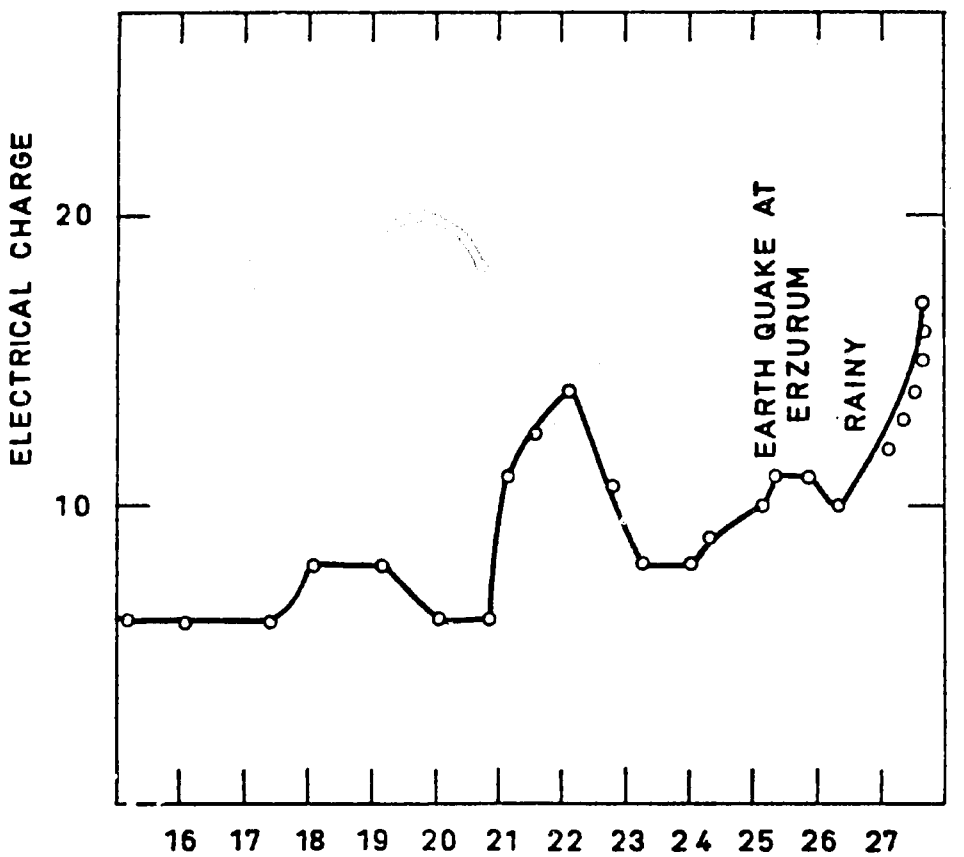

Figure 7. DAYS OF OCTOBER 1974

The investigations are still continuing, and programme of research will be undertaken at the Middle East Technical University.

REFERENCES

1. *Turkish Patent 4109, 1945.*

2. *I. Nersesov, Conf. on Prediction of Earthquakes, Menlo Park, California, 1973.*

3. *K. Ergin, U. Güçlü, and Z. Uz, Geophysics Inst., İstanbul Tech. Univ., Publ. 24, 1967.*

DISCUSSION

Several of the participants expressed considerable scepticism about the validity of the work described.

NON–LINEAR WAVE PROPAGATION IN SOILS

Dr. A. Askar and Dr. A.S. Çakmak

Although earthquakes occur with large deformations and high stresses and are non-linear phenomena, most studies in engineering seismology and soil dynamics have been based on linear analyses. Problems such as the shifts in frequency and dispersion due to the amplitude, generation of harmonics and the coupling of shear and volumetric waves are essentially non-linear and cannot be accounted for by a linear theory.

This paper considers the propagation of non-linear waves in an unbounded medium showing the effect of amplitude on the frequency shift and the coupling of the various shear modes, and also the problem standing waves (thickness-shear modes) in a single layer. The non-linear equation used is the Korteweg-de Vries Equation[1,2] which in one dimension with no dissipation can be written as

$$\frac{\partial \gamma}{\partial t} = \gamma \frac{\partial \gamma}{\partial x} + \varepsilon \frac{\partial^3}{\partial x^3}$$

corresponding to a non-lienar stress-strain relation for the soil of the form:

$$\delta = G\gamma + \frac{1}{2} \varepsilon \gamma^2$$

where G is the shear modulus, γ the shear strain ε is the non-linearity coefficient. If dissipation is included, this becomes

$$\delta = G\gamma + \frac{1}{2} \varepsilon \gamma^2 + \eta \frac{\partial \gamma}{\partial t}$$

where η is the coefficient of internal friction. Then

$$\frac{\partial \gamma}{\partial t} = \gamma \frac{\partial \gamma}{\partial x} + \eta \frac{\partial^2 \gamma}{\partial x \partial t} + \varepsilon \frac{\partial^3 \gamma}{\partial x^3}$$

Non-Linear Stress-Strain Relations

Consider the kinetic and potential energies T and V for an elastic continuum

$$T = \int_L \frac{1}{2} q \left(\frac{\partial v}{\partial x}\right)^2 dx \qquad V = \int_L U\, dx$$

Here v(x,t) is the shear displacement perpendicular to the wave propagation along x, q is the mass density and U is the internal energy density. In the classical linear elasticity theory

$$U = \frac{1}{2} G \left(\frac{\partial v}{\partial x}\right)^2$$

with G as the shear modulus. To accomodate nonlinearity, for similar behaviour in compression and extension, let

$$U = \frac{1}{2} G_0 \left(\frac{\partial v}{\partial x}\right)^2 + \frac{1}{4} G_1 \left(\frac{\partial v}{\partial x}\right)^4 \qquad (1)$$

where G_1/G_o is a measure of the non-linearity. The field equations in this case can be obtained as the Euler equations corresponding to the variational equation

$$\delta \int_{t_o}^{t_1} \int_L \left[\frac{1}{2}\rho \left(\frac{\partial v}{\partial t}\right)^2 + \frac{1}{2} G_o \left(\frac{\partial v}{\partial x}\right)^2 + \frac{1}{4} G_1 \left(\frac{\partial v}{\partial x}\right)^4 \right] dx\, dt = 0$$

Then the field equations are obtained as:

$$\rho \frac{\partial^2 v}{\partial t^2} = G_o \frac{\partial^2 v}{\partial x^2} + G_1 \left(\frac{\partial v}{\partial x}\right)^2 \frac{\partial^2 v}{\partial x^2} \tag{2}$$

Introducing the semi-characteristic coordinate stretching, for $c^2 = (G_o/\rho)$ as the wave velocity in the linear approximation

$$\xi = x - ct \qquad\qquad \tau = \frac{G_1}{2G_o} ct \tag{3}$$

and assuming $G_1/G_o \ll 1$, one obtains

$$\frac{\partial \gamma}{\partial \tau} = \gamma^2 \frac{\partial \gamma}{\partial \xi}$$

where $\gamma = \partial v / \partial x$ is the shear strain. This equation bears close relationship to the Burger

$$\frac{\partial \gamma}{\partial \tau} = \gamma^p \frac{\partial \gamma}{\partial \xi} + \nu \frac{\partial^2 \gamma}{\partial \xi^2} \qquad \nu = \text{cons.}$$

and Korteweg-de Vries equation

$$\frac{\partial \gamma}{\partial \tau} = \gamma^q \frac{\partial \gamma}{\partial \xi} + \mu \frac{\partial^3 \gamma}{\partial \xi^3} \qquad \mu = \text{cons.}$$

For the internal energy density U, rather than assuming it to depend on only $\partial v / \partial x$ as in (1), we assume it to depend on the gradient of the strain as well, i.e. $\partial^2 v / \partial x^2$ it is also possible to obtain the Korteweg-de Vries equation. Thus for,

$$U = \frac{1}{2} G_o \left(\frac{\partial v}{\partial x}\right)^2 + \frac{1}{2} G_1 \left(\frac{\partial v}{\partial x}\right)^4 + \frac{1}{2} G_2 \left(\frac{\partial^2 v}{\partial x^2}\right)^2$$

and by the procedure outlined above of taking the variational equation and performing the coordinate transformation in (3), one finds the Korteweg-de Vries equation with $\mu = G_2/G_o$. The interesting aspect of the Korteweg-de Vries equation is that it predicts non-dispersive solitary waves as:

$$\delta = a\,\mathrm{sech}^2 \left[\sqrt{\frac{a}{2\mu}} \left(\xi - \frac{a}{3}\tau\right)\right]$$

where a is the amplitude of the solitary wave.

A Solution for Non-Linear Waves Based on Poincare's Perturbation

We now seek a solution of (2) that is periodic in time for small yet finite amplitudes. To apply a perturbation scheme to (2), let

$$w = \lambda^{1/2} v \qquad w(x.t) = W(t) \exp(iqx)$$

where λ will eventually be set equal to 1.

Then (2) becomes

$$\rho \frac{d^2 W}{dt^2} + G_o q^2 W - \lambda G_1 q^4 e^{2iqx} W^3 = 0 \tag{4}$$

The classical perturbation scheme based on expanding W in the form

$$W(t:\lambda) = W_o(t) + \lambda W_1(t) + \lambda^2 W_2(t) + \ldots$$

is known to give divergent results because of secular terms such as t cos t (3). To avoid this, Poincare considered an expansion of the angular frequency of the periodic solution as

$$\Omega(\lambda) = \Omega_o + \lambda \Omega_1 + \lambda^2 \Omega_2 + \ldots \tag{5}$$

where

$$\Omega_o = (G_o/\rho)^{1/2} q \tag{6}$$

is the angular frequency for the linear case. Let us introduce another new time scale s by writing

$$s = \Omega t$$

and consider W (t) as a function of s :

$$W(t:\lambda \equiv \eta(s:\lambda) = \eta_o(s) + \lambda\eta_1(s) + \lambda^2\eta_2(s) + \ldots$$

Using the fact that

$$\frac{d^2}{dt^2} = \Omega^2 \frac{d^2}{ds^2}$$

(4) becomes

$$\Omega^2 \frac{d^2\eta}{ds^2} + \Omega_o^2\eta - \lambda \left(\frac{G_1}{G_o} \Omega_o^2 q^2 e^{2iqx}\right) \eta^3 = 0 \tag{7}$$

Introducing the expansions for Ω and η into (4) and grouping the coefficients of the various powers of λ , we obtain

$$\frac{d^2 \eta_o}{ds^2} + \eta_o = 0$$

$$\frac{d^2 \eta_1}{ds^2} + \eta_1 = -2\frac{\Omega_1}{\Omega_o} \frac{d^2 \eta_o}{ds^2} + \alpha \eta_o^3 \tag{8}$$

$$\frac{d^2 \eta_2}{ds^2} + \eta_2 = -\left[2\frac{\Omega_2}{\Omega_o} + \left(\frac{\Omega_1}{\Omega_o}\right)^2\right] \frac{d^2 \eta_o}{ds^2} - 2\frac{\Omega_1}{\Omega_o} \frac{d^2 \eta_1}{ds^2} + 3\alpha\eta_o^3\eta_1$$

where

$$\alpha = \frac{G_1}{G_o} q^2 \exp(iqx)$$

To make the problem definite, let us also use the initial conditions

$$W(o) = A \qquad \frac{dW}{dt}\Big|_{t=o} = 0 \tag{9}$$

In terms of the η, (9) implies

$$\eta_o|_{s=o} = A \qquad \eta_i|_{s=o} = 0 \qquad (i = 1, 2, \ldots)$$

$$\frac{d\eta_i}{ds}\Big|_{s=o} = 0 \qquad (i = 0, 1, 2, \ldots) \tag{10}$$

From (8) and the boundary conditions in (10), the solution of order zero is found to be

$$\eta_o = A \cos(s)$$

Notice that even though η_o has the same form as the solution for the linear case, the angular frequency Ω is different from that of the linear case.

Inserting η_o into the second equation of (8), we find

$$\frac{d^2\eta_1}{ds^2} + \eta_1 = 2\frac{\Omega_1}{\Omega_o} A\cos(s) + \frac{1}{4}\alpha A^3 [3\cos(s) + \cos(3s)]$$

where use is made of the identity $\cos^3(s) = \frac{1}{4}[3\cos(s) + \cos(3s)]$. Since cos s is a solution of the homogeneous part, the term with cos s on the right-hand side is a secular term leading to divergence through a term of the form s cos s. In order to preserve the periodicity and prevent divergence, we must have

$$\Omega_1 = -\left(\frac{3}{8}\frac{G_1}{G_o} q^2 e^{2iqx} A^2\right) \Omega_o \tag{11}$$

The remaining part has a solution

$$\eta_1 = \frac{1}{32} \frac{G_1}{G_o} q^2 e^{2iqx} A^3 (\cos s - \cos 3s)$$

which satisfies the initial conditions

$$\eta_1 |_{s=o} = 0 \qquad \frac{d\eta_1}{ds} |_{s=o} = 0$$

To proceed, one can then insert Ω_1 and η_o, η_1 into the third equation of the perturbation scheme.

Collecting these results, working to the second order of approximation, and returning to the physical variables V and t, we have

$$V = Ae^{iqx} \cos \Omega t + \frac{1}{32} \frac{G_1}{G_o} q^2 A^3 e^{iqx} (\cos \Omega t - \cos 3 \Omega t)$$

If we insert Ω_o and Ω_1 from (6) and (11) into (5) the explicit form of the dispersion relation becomes

$$\Omega = \sqrt{\frac{G_o}{\mu}} q \left[1 - \frac{3}{8} \frac{G_1}{G_o} q^2 e^{2iqx} A^2 \right] + 0(A^4) \tag{12}$$

This solution for the displacements is a standing wave which preserves its shape and has several harmonics present with frequencies which are integer multiples of a fundamental frequency (—2).

Notice that the above solution in (12) is valid for unbounded medium. However, as is seen in the next section, the same idea can also be applied to finite domains with slight modifications.

Spectrum of a Forced Non-Linear Single Layer

Consider a layer of thickness d which is forced sinusoidally with frequency Ω at $x = d$ and is traction free at $x = 0$. The problem is thus defined by the differential equation and boundary conditions below:

$$G_o \frac{\partial^2 v}{\partial x^2} + G_1 \left(\frac{\partial v}{\partial x}\right)^2 \frac{\partial^2 v}{\partial x^2} = \rho \frac{\partial^2 v}{\partial t^2} \tag{13}$$

$$\frac{\partial v}{\partial x}\Big|_{x=o} = 0 \qquad V\big|_{x=d} = d\,A\cos\Omega t$$

where A is the non-dimensional displacement at $x = d$. Introducing the dimensionless displacement $\eta = \lambda^{1/2} V/d$ spatial coordinate $y = x/d$ and the stretched time variable $s = \Omega t$. In terms of these variables, the system in (13) becomes:

$$d^2 \frac{\Omega^2}{c^2} \frac{\partial^2 \eta}{\partial s^2} - \frac{\partial^2 \eta}{\partial y^2} = \lambda \frac{G_1}{G_o} \left(\frac{\partial \eta}{\partial y}\right)^2 \frac{\partial^2 \eta}{\partial y^2} \tag{14}$$

$$\frac{\partial \eta}{\partial}\Big|_{y=o} = 0 \qquad \eta\big|_{y=1} = A\cos(s)$$

To solve this non-linear boundary value problem, let

$$\eta(y, s{:}\lambda) = \eta_o(y, s) + \lambda\,\eta_1(y, s) + \ldots \tag{15}$$

$$\Omega(\lambda) = \Omega_o + \lambda\,\Omega_1$$

Introducing (15) into (14) and separating terms with the various powers of λ, one finds for the first two orders, the following equations:

$$q^2 \frac{\partial^2 \eta_o}{\partial s^2} - \frac{\partial^2 \eta_o}{\partial y^2} = 0$$

$$\frac{\partial \eta_o}{\partial y}\Big|_{y=o} = 0 \qquad \eta_o\big|_{y=1} = A\cos(s) \tag{16}$$

$$q^2 \frac{\partial^2 \eta_1}{\partial s^2} - \frac{\partial^2 \eta_1}{\partial y^2} = -2d\,\Omega_o\Omega_1 \frac{\partial^2 \eta_o}{\partial s^2} + \frac{G_1}{G_o}\left(\frac{\partial \eta_o}{\partial y}\right)^2 \frac{\partial^2 \eta_o}{\partial y^2}$$

$$\frac{\partial \eta_1}{\partial y}\Big|_{y=o} = 0 \qquad\qquad \eta_1\big|_{y=1} = 0$$

where

$$q^2 = \frac{\Omega_o^2\, d^2}{c^2} \qquad\qquad c^2 = G_o/\rho$$

The steady solution for the zeroeth order is easily found to be

$$\eta_o = A\,\frac{\cos\,(qy)}{\cos q}\,\cos\,(s) \tag{17}$$

For the first order, let us substitute (17) into the right hand side in (16):

$$q^2\,\frac{\partial^2 \eta_1}{\partial s^2} - \frac{\partial^2 \eta_1}{\partial y^2} = 2d\,\Omega_o\Omega_1\,\frac{\cos\,(qy)}{\cos q}\,A\cos\,(s)$$

$$- \frac{G_1}{G_o}\,q^4\,\frac{\sin^2 qy\,\cos qy}{\cos^3 q}\,A^3\cos^3(s) \tag{18}$$

$$\frac{\partial \eta_1}{\partial y}\Big|_{y=o} = 0 \qquad\qquad \eta_1\big|_{y=1} = 0$$

The general solution for η_1, that satisfies the boundary conditions is of the form

$$\eta_1\,(y, s) = \Big[\sum_{h=1,3,5\ldots} C_n\,\cos\Big(\frac{h\,\pi\,y}{2}\Big)\Big]\quad S\,(s) \tag{19}$$

Substituting (19) into (18) and rearranging the various terms by making use of the trigonometric identities

$$\sin^2(qy)\cos(qy) = \frac{1}{4}[\cos(qy) - \cos(3qy)]$$

$$\cos^3(s) = \frac{1}{4}[3\cos(s) - \cos(3s)]$$

one finds

$$\eta_1 = A^3 \left\{ [\sum_{h=1,3,5\ldots} \frac{F_h}{(\frac{h^2\pi^2}{4} - q^2)} \cos\frac{h\pi}{2} y] \operatorname{Cos}(s) + [\sum_{h=1,3,5\ldots} \frac{G_h}{(\frac{h^2\pi^2}{4} - 9q^2)} \cos\frac{h\pi}{2} y] \cos 3s \right\}$$

where

$$F_n = [\frac{2\Omega_o\,\Omega_1}{A^2}\frac{d^2}{\cos q} - \frac{3}{16}\frac{G_1}{G_o}\frac{q^4}{\cos^3 q}]\alpha_n + \frac{3}{16}\frac{G_1}{G_o}\frac{q^4}{\cos^3 q}\beta_n$$

$$G_n = \frac{1}{16}\frac{G_1}{G_o}\frac{q^4}{\cos^3 q}(\alpha_n - \beta_n)$$

$$\alpha_n = \frac{\sin(\frac{n\pi}{2} + q)}{\frac{n\pi}{2} + q} + \frac{\sin(\frac{n\pi}{2} - q)}{\frac{n\pi}{2} - q}$$

$$\beta_n = \frac{\sin(\frac{n\pi}{2} + 3q)}{\frac{n\pi}{2} + 3q} + \frac{\sin(\frac{n\pi}{2} - 3q)}{\frac{n\pi}{2} - 3q}$$

One can continue to solve for the higher order terms in the perturbation scheme. However, at this stage of the calculations the frequency Ω_1, is yet unknown. To determine it, let us consider the expression for the total energy (4).

$$E = \int_o^d \left[\frac{1}{2} G_o \left(\frac{\partial v}{\partial x}\right)^2 + \frac{1}{4} G_1 \left(\frac{\partial v}{\partial x}\right)^4 + \frac{1}{2} \rho \left(\frac{\partial v}{\partial t}\right)^2 \right] dx$$

Since this quantity is conserved, we can take, for simplification in the calculations its value at $t = 0$. In terms of the dimensionless variables η, y and Ω of the perturbation scheme, one finds:

$$E = \lambda^2 d\, G_o \int_o^1 \left[\frac{1}{2} \left(\frac{\partial \eta}{\partial y}\right)^2 + \frac{1}{2} \frac{\Omega^2}{c^2} \left(\frac{\partial \eta}{\partial s}\right)^2 + \lambda \frac{1}{4} \frac{G_1}{G_o} \left(\frac{\partial \eta}{\partial y}\right)^4 \right] dy \qquad (20)$$

Introducing the perturbation expansions in (20) for η and Ω and separating the various order terms, one finds:

$$\frac{E}{G_o d} = \frac{1}{2} \int_o^1 \left[\left(\frac{\partial \eta_o}{\partial y}\right)^2 + q^2 \left(\frac{\partial \eta_o}{\partial s}\right)^2 \right]_{s=o} dy \qquad (21)$$

$$O = \int_o^1 \left[\frac{\partial \eta_o}{\partial y} \frac{\partial \eta_1}{\partial y} + q^2 \frac{\partial \eta_o}{\partial s} \frac{\partial \eta_1}{\partial s} + q^2 \frac{\Omega_1}{\Omega_o} \left(\frac{\partial \eta_o}{\partial s}\right)^2 + \frac{1}{4} \frac{G_1}{G_o} \left(\frac{\partial \eta_o}{\partial y}\right)^4 \right]_{s=o} dy$$

With similar terms for the higher orders. This procedure keeps the energy bounded and is Equivalent to the extraction of the secular terms in the Poincare procedure. Ω_1, is calculated from the second of (21) as:

$$\frac{\Omega_1}{\Omega_o} = \frac{-\int_o^1 \left[\left(\frac{\partial \eta_o}{\partial y}\right)\left(\frac{\partial \eta_1}{\partial y}\right) + q^2 \left(\frac{\partial \eta_o}{\partial s}\right)\left(\frac{\partial \eta_1}{\partial s}\right) + \frac{1}{4} \frac{G_1}{G_o} \left(\frac{\partial \eta_o}{\partial y}\right)^4 \right]_{s=o} dy}{q^2 \int_o^1 \left(\frac{\partial \eta_o}{\partial s}\right)_{s=o} dy}$$

Conclusion

The results of the calculations for a linear and non-linear analysis of a single layer are compared schematically in Figure 1 by displaying the magnification factor $M = [\, \eta\,(o) \,/\, \eta\,(1)\,]$. It is seen that the singularities of $1/\cos q$ at $q = \pi/2, 3\pi/2, \ldots\ldots,$

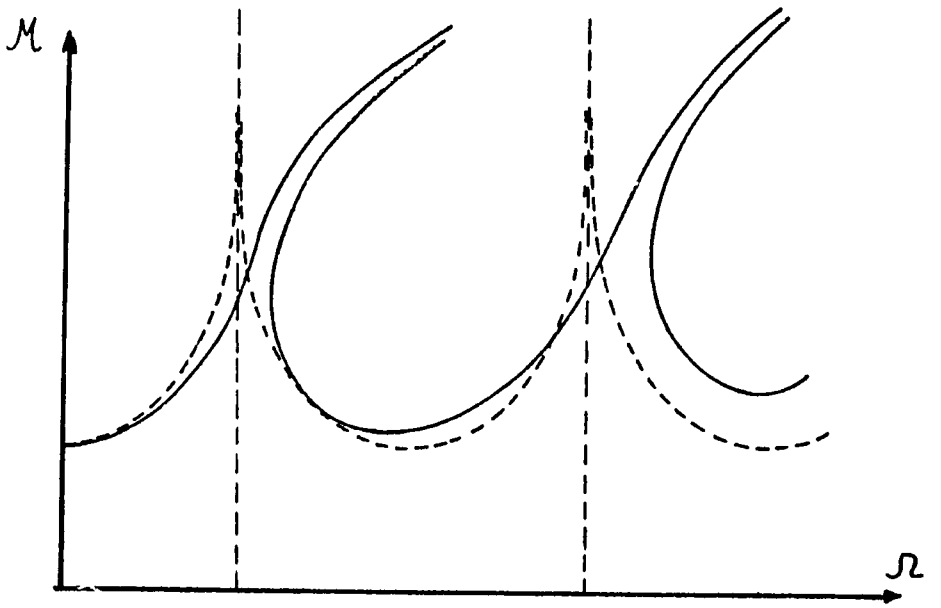

Figure 1

according to the linear analysis disappear due to the non-linearity. Furthermore, the non-linearity shifts the frequencies causing the highest magnification. This consideration may have importance in determining the dominant earthquake frequency at a location. The calculations presented here may be extended within the same formalism to multilayered systems along with introducing damping.

REFERENCES

1. *A. Jeffrey and T. Kakutany, SIAM Review, 14, 669 (1971).*

2. *A. Askar, Proc. Roy. Soc. Lond., A 334, 83 (1974).*

3. *J.D. Cole, "Perturbation Methods in Applied Mathematics". Blaisdell, New York, 1968.*

4. *M. H. Millman and J.B. Keller, J. Math. Phys., 10, 342 (1969).*

DISCUSSION

In reply to Professor Ambraseys, Dr. Askar said that it was possible to satisfy the boundary conditions at the lower limit by the Poincare method. Dr. Keightley commented that the variations in motions on the surface were attributed to non-linear transmission by the medium, and pointed out that the nature of the sources could also vary. Dr. Askar said that the variation in the sources would also be non-linear. Dr. Kumbasar said that it had been assumed that the same stress relationship applied to loading and unloading, and asked if it was possible to generalise for different relations between loading and unloading curves. Dr. Askar said that the work was originally concerned with wave propagation in crystals in electronics, where the loading/unloading effect did not arise; the object of the paper was to point out the relevance to earthquake studies. However, the method would be applicable to nonsymmetrical cases.

General view of Lice. The old town was centred round the cleft in the foothills in the centre, on the steep hillside, beneath rock outcrops. Note the large scar on the hillside at the extreme right, where a large avalanche fell just clear of the town.

Looking towards the centre of the old town. In this area, not a single wall was left standing.

Near the centre of the town: note the wood beams from collapsed roofs.

While this report was being prepared , a serious earthquake occurred at Lice in South-Eastern Turkey. The CENTO Scientific Secretary visited the area about two weeks after the disaster, and the following photographs record some of his impressions.

Attempting to recover household belongings.

A house substantially intact, in the worst area of devastation.

The main mosque, "built with Faith", was largely undamaged, except for the collapse of the minaret.

This building, apparently a small generating plant, was partly built in traditional style: this part remained intact. The other part of "reinforced concrete" has completely collapsed.

The same building: note that the concrete has crumbled and peeled off from the reinforcing.

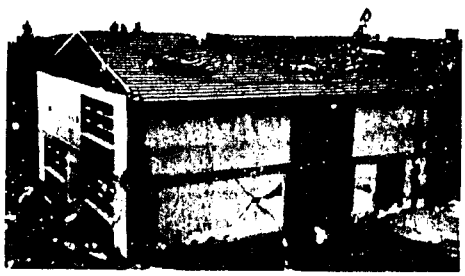

A school near the centre of the old town. Note that the chimneys and gable wall have separated from the main structure.

The Lycee, at the foot of the hill.

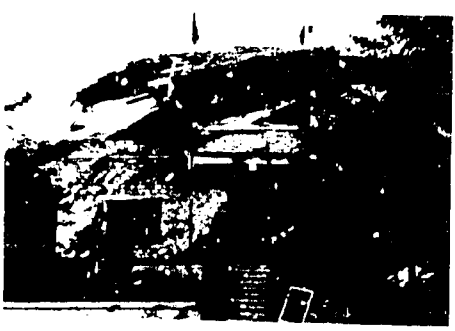

A new building which was nearly completed, at the foot of the hill.

A new building which was nearly completed, at the foot of the hill.

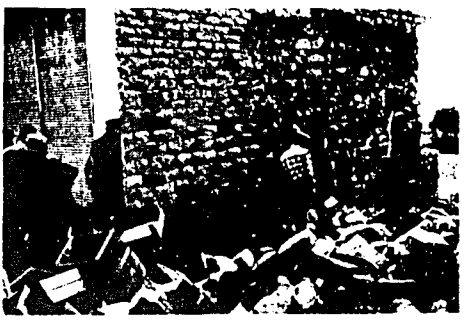

Rebuilding a shop: the outer wall had collapsed but the inner wall had held up.

Houses built in the 1960s, well away from the hillside, but only a few of the townspeople agreed to move to them. These buildings had only superficial damage.

A large new building which was nearly completed, about 3 km from the town. The roof collapsed and slid about 2 m outwards, part of it falling to the ground.

SEISMIC ANALYSIS OF THE SITE OF SOMA–II THERMOELECTRIC PLANT

Professor Semih S. Tezcan and Dr. H. Turan Durgunoğlu

The Turkish Electric Power Authority, TEK, is planning to build a new thermoelectric power plant of 300 MW capacity, at the north eastern side of the existing plant at Soma, Manisa, in the western Turkey. This paper describes a study of the geotechnical and seismic parameters of the soil.

Thirty-seven bore holes were drilled to depths of 15 m to 40 m at various locations on the site (Figure 1 —see the next page). Laboratory tests gave a series of soil parameters, void ratio, water content, effective angle of shear strength, overconsolidation ratio, plasticity index. The geometric and physical properties of the soil layers underlying the site, previously had been determined by another power authority by means of field measurements using resistivity and seismic refraction. A nonlinear shear wave propagation analysis has been performed to give the soil amplification parameters and the soil predominant periods.

Soil Data

Four Soil cross sections are given in Figures 2, 3, 4 and 5 (see the next pages). It was extremely difficult to extract undisturbed soil samples due to the presence of granular and silty materials, so the shear strength values of most soil samples in the laboratory tests were unexpectedly small compared to the very high values of standard penetration test blow counts. Consequently, three plate loading tests are to be performed at the site of heavy structural units using a minimum base plate 70 cm square, to give a more accurate assessment of soil allowable pressure.

Microtremor Analysis

Microtremors were recorded in two mutually perpendicular horizontal directions (NS and EW), at each of the four stations shown in Figure 1 to determine the predominant period of the soil during very small elastic vibrations. A Geotech S13 model seismometer was used with an on-line Servagor ink pencil recording unit. The speed of the paper was about 12 mm/sec. All records were taken after midnight of October 26/27, 1974 for a duration of more than one minute. A portion of these records corresponding to about a period of 35 seconds was digitized visual inspection.

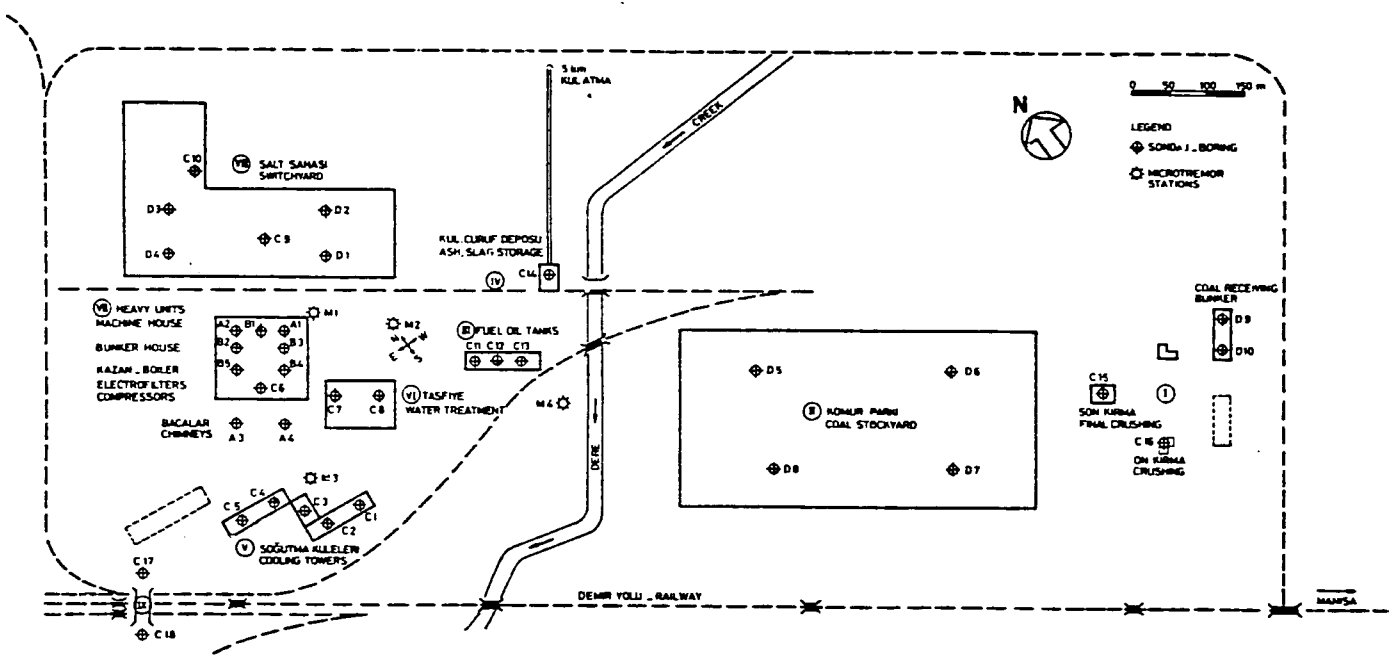

FIGURE 1. SOMA—II THERMOELECTRIC POWER PLANT GENERAL LAYOUT

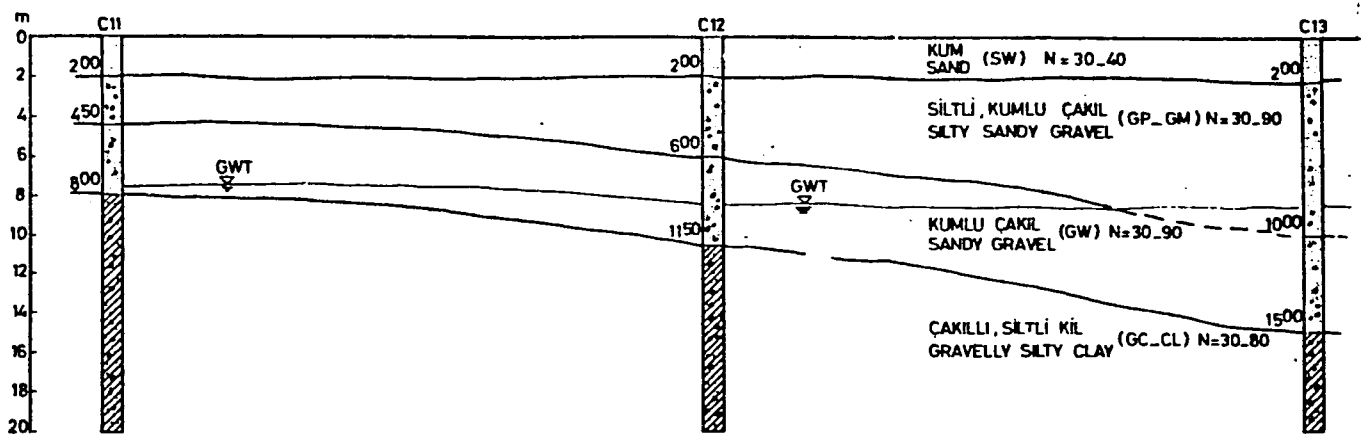

FIGURE 2. SECTION C11 — C13

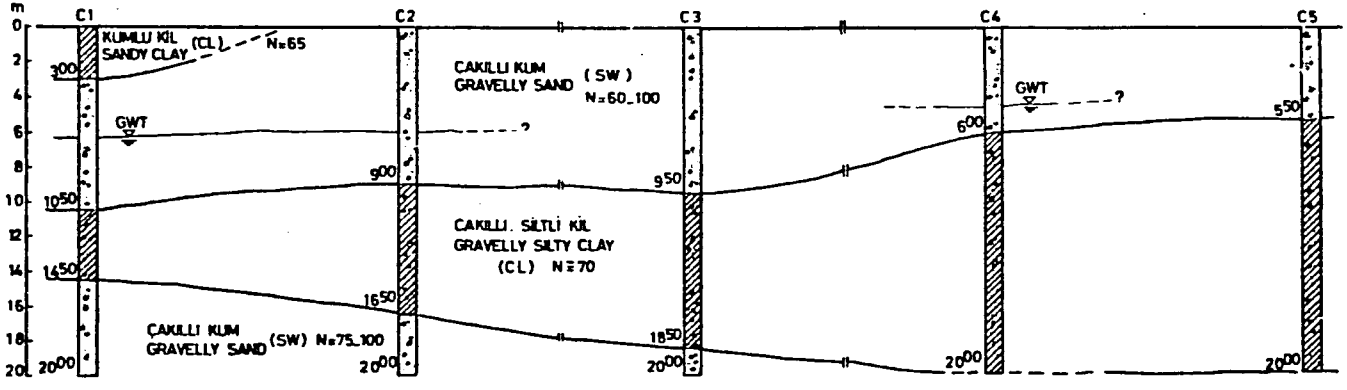

FIGURE 3. SECTION C1 — C5

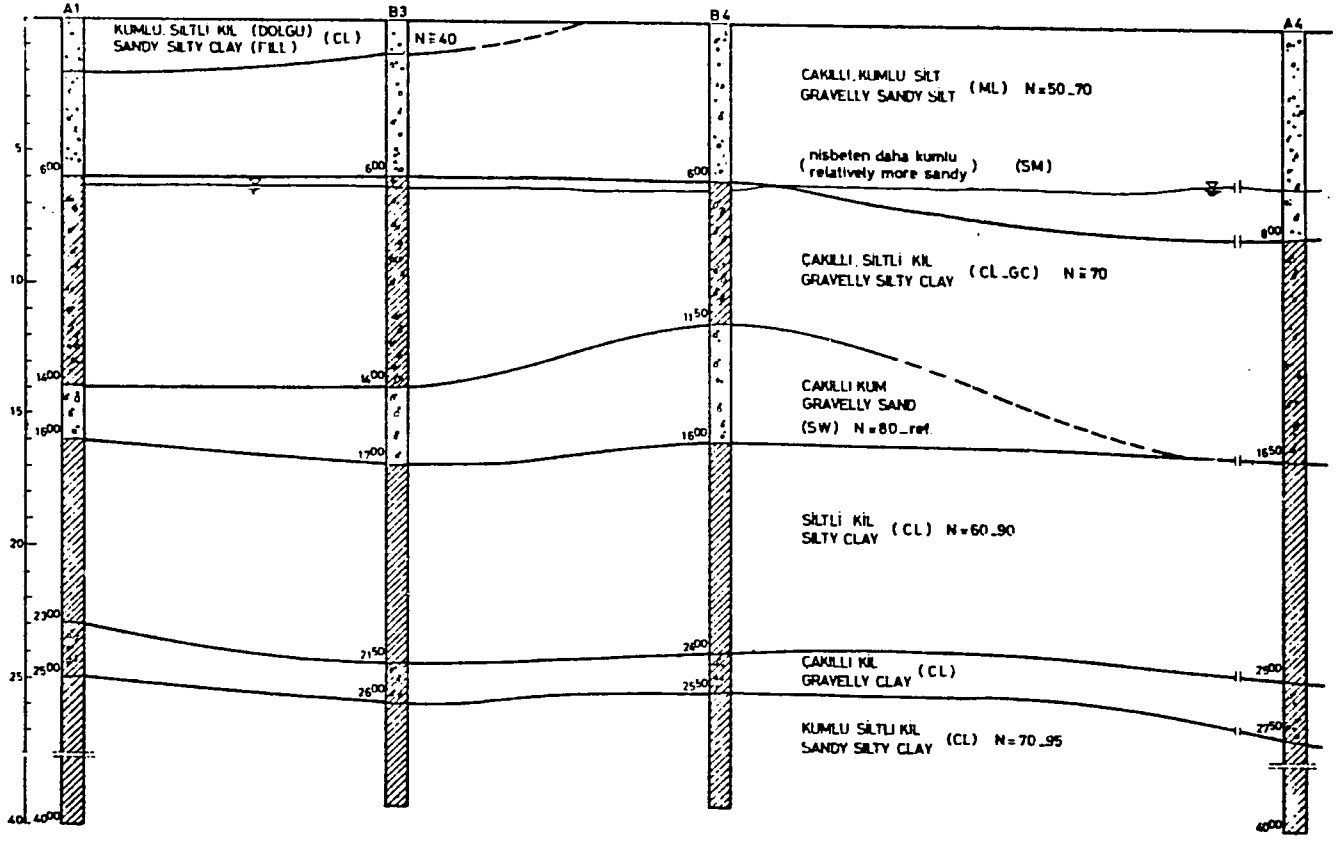

FIGURE 4. SECTION A1 — A4

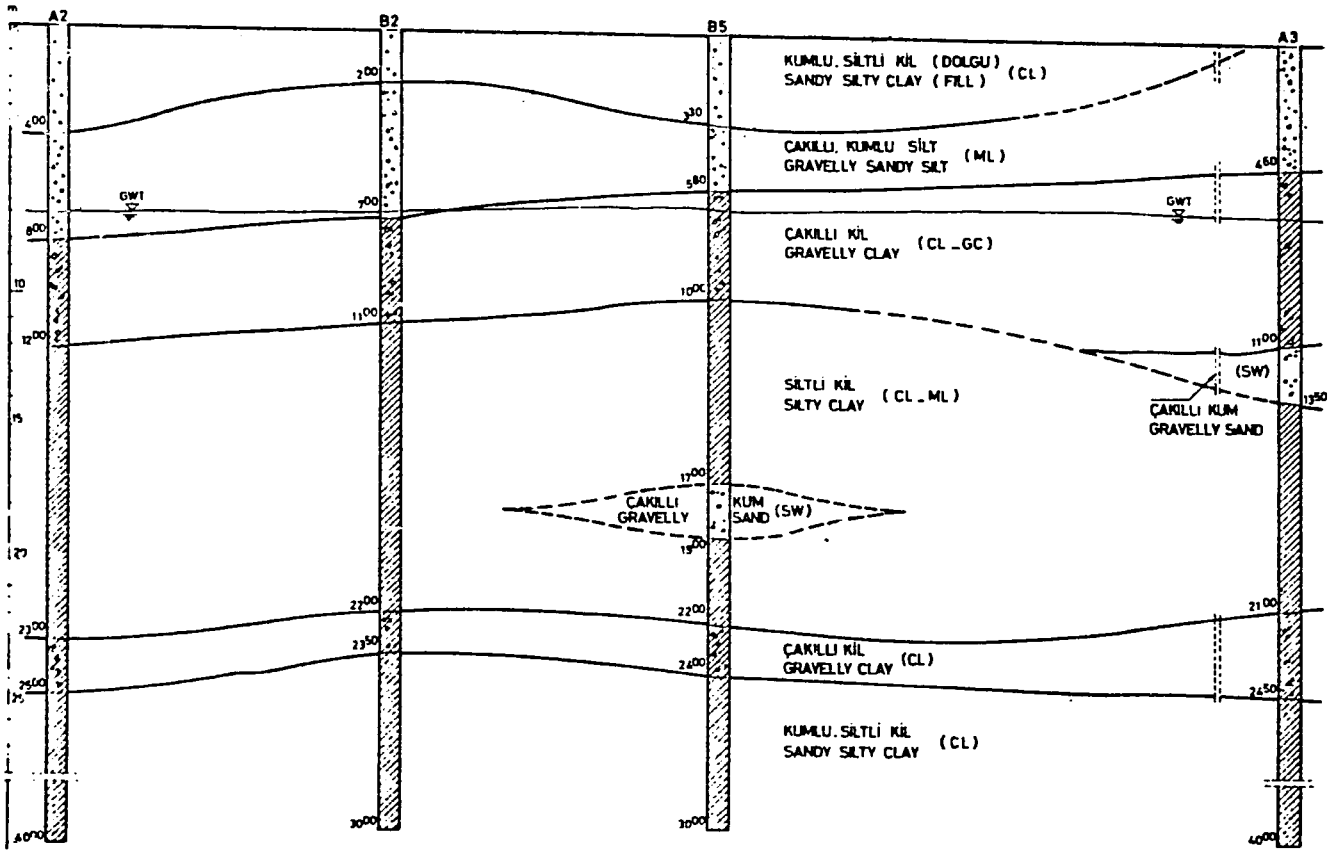

FIGURE 5. SECTION A2 — A3

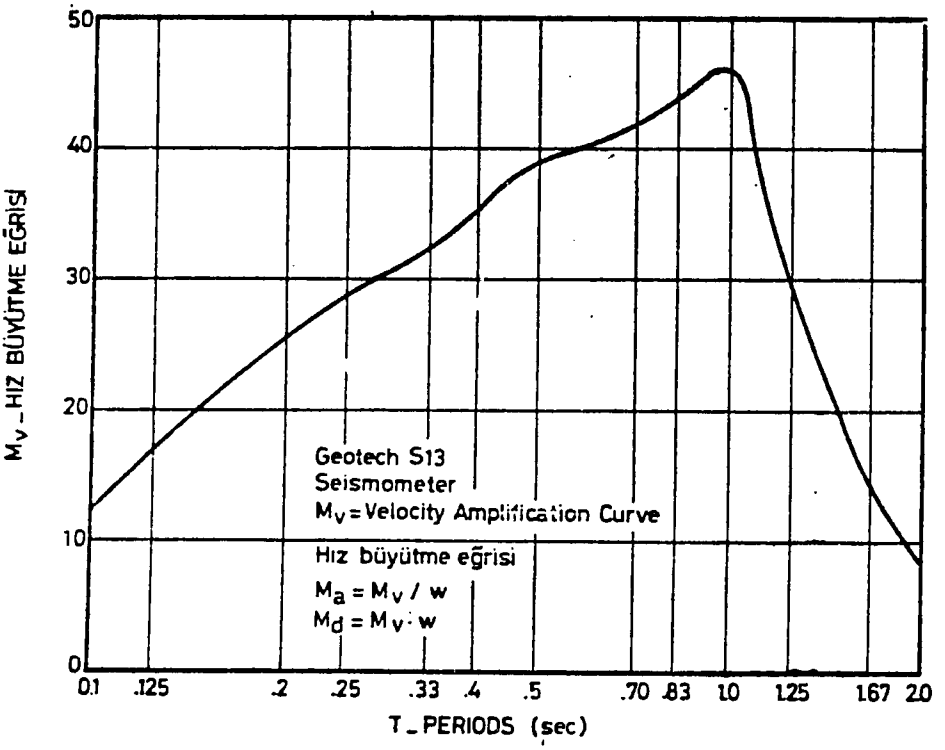

FIGURE 6

400 data points were considered at each record. The velocity amplification sensitivity of the seismometer is shown in Figure 6. The velocity spectra of all the records were determined by the fourier amplitude spectrum technique and are shown in Figures 7 to 10.

There is a distinct predominant period of the soil at about T = 0.46 seconds. Peaks at larger periods above 2 seconds may be attributed to the very small sensitivities of the seismometer at this range.

Typical Soil Profile

The typical soil profile is shown on the left of Figure 11 (see page 121). The profile on the right is based on the geophysical survey referred to above. In calculating the shear moduli of each soil layer, the Hardin-Drnevich design formulae[1] were employed

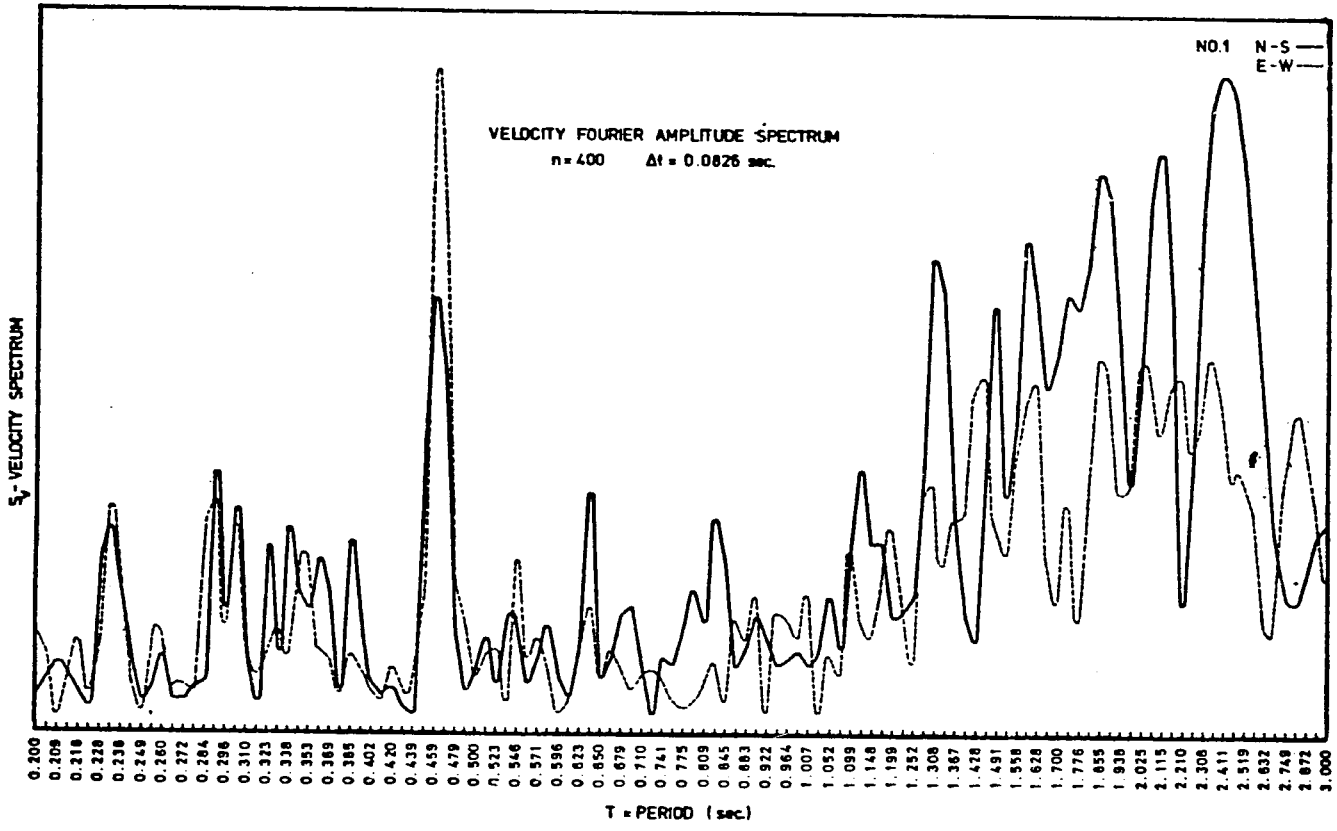

FIGURE 7. VELOCITY SPECTRUM

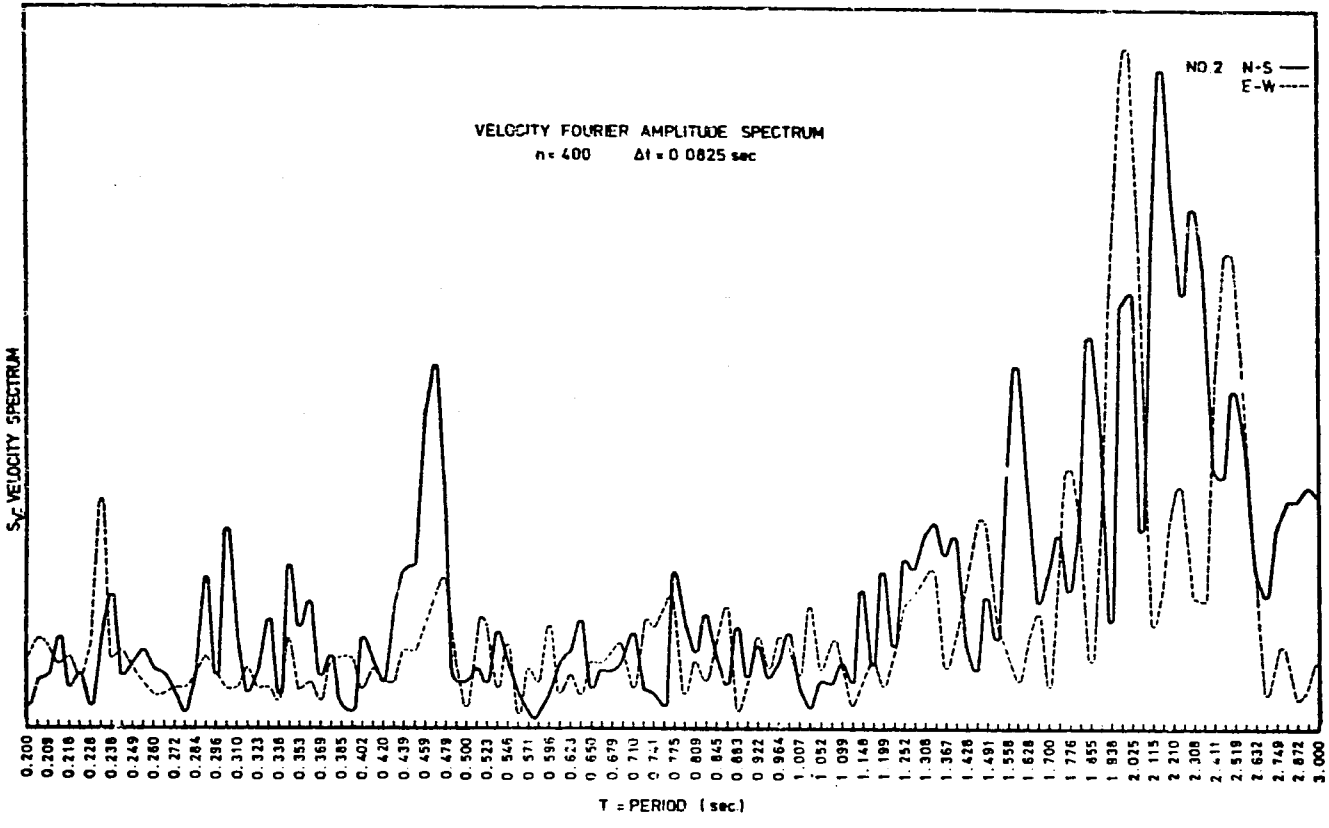

FIGURE 8. VELOCITY SPECTRUM

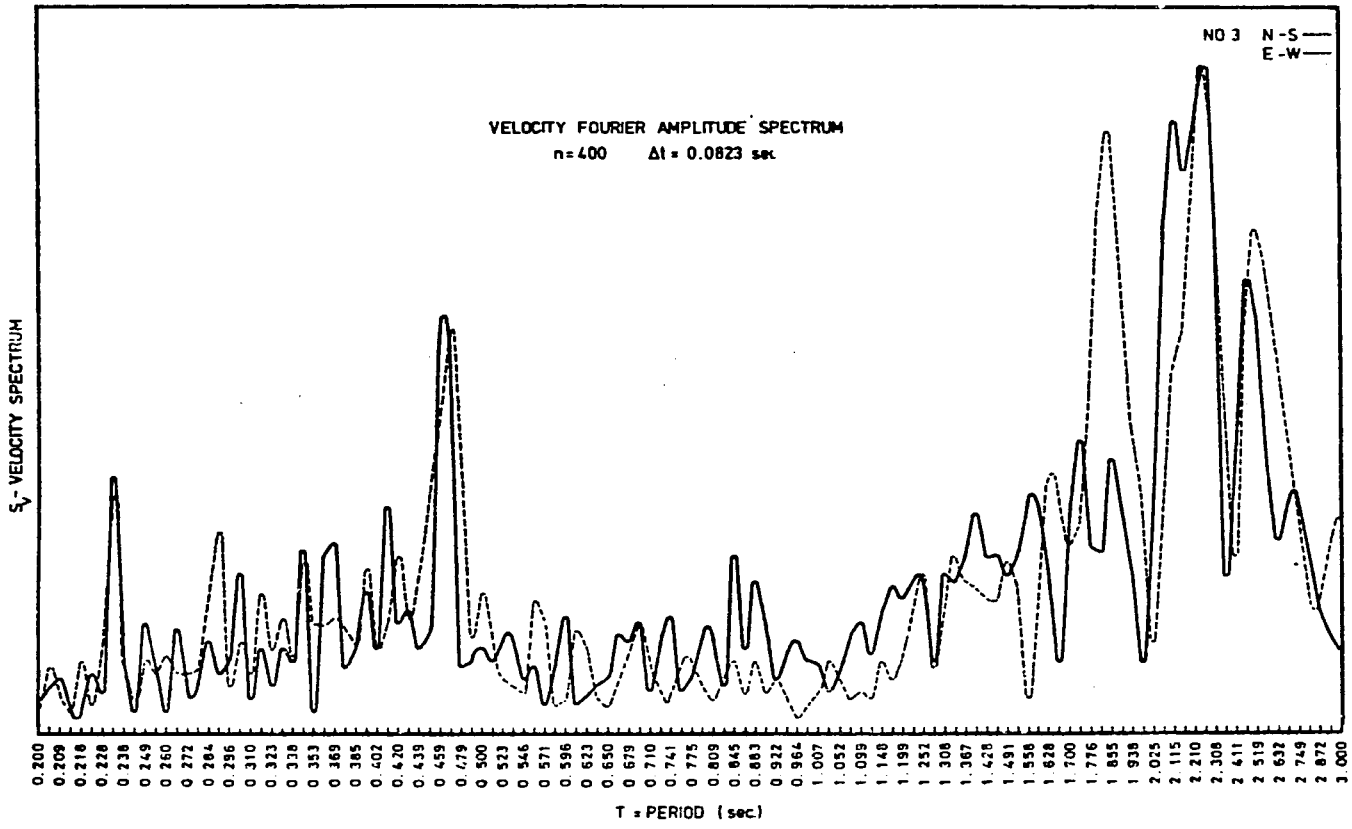

FIGURE 9. VELOCITY SPECTRUM

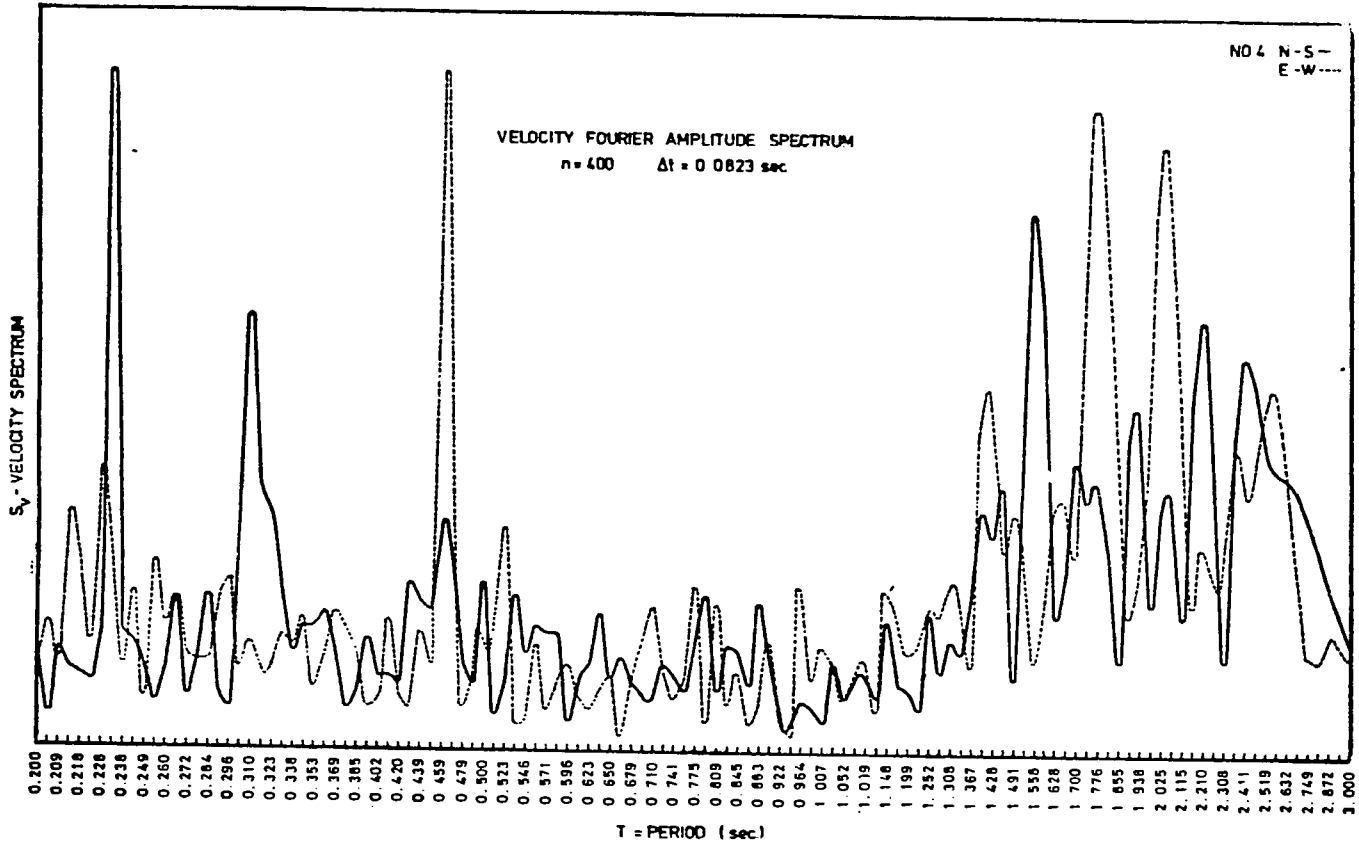

FIGURE 10. VELOCITY SPECTRUM

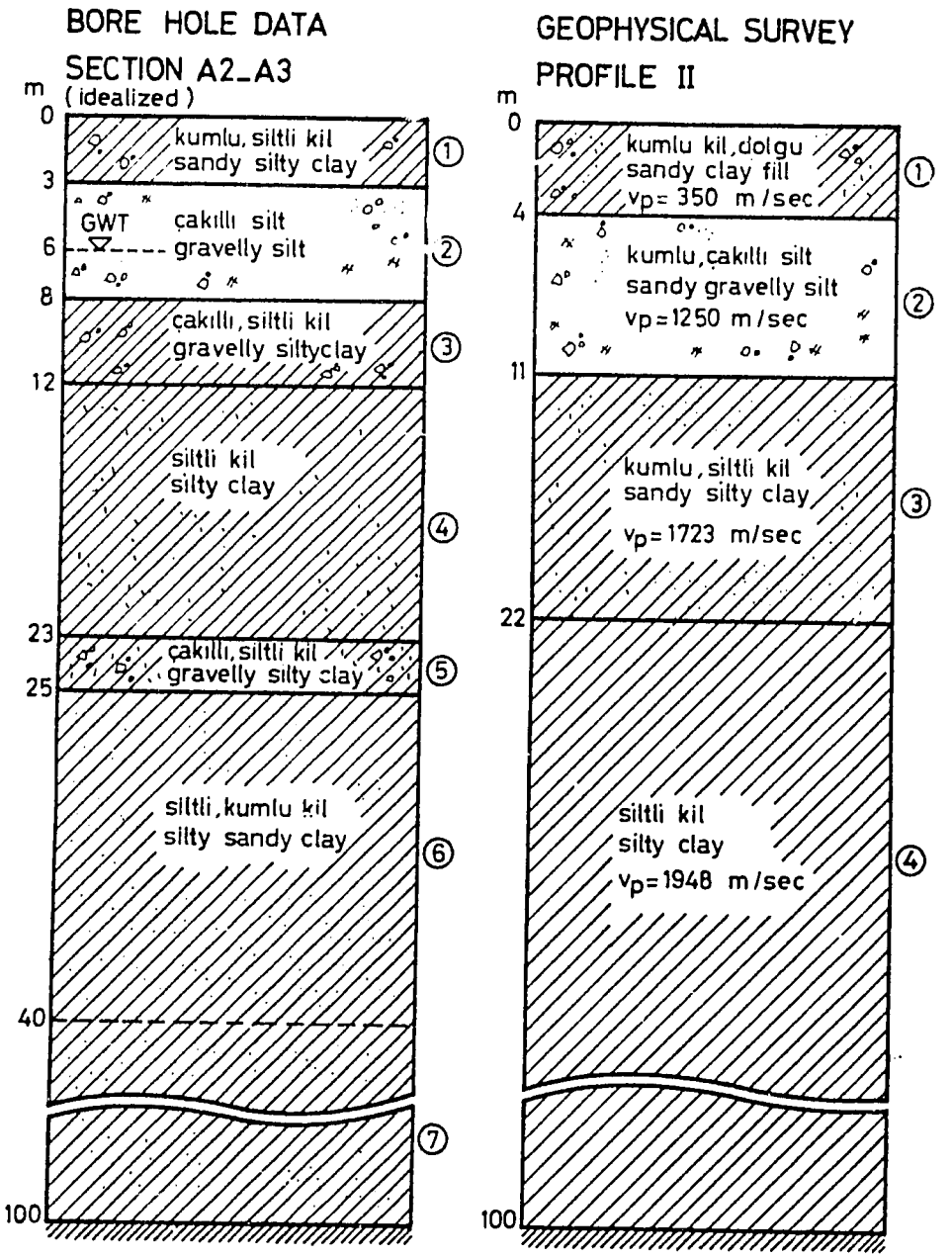

FIGURE 11. COMPARISON OF BORE HOLE AND GEOPHYSICAL DATA

to account for the disturbance of the samples, a constant disturbance factor of 2.5 was used. Shear wave velocities at each soil layer are in good agreement with those determined from the geophysical survey.

Seismicity of the Region

Soma is listed as a second degree earthquake risk zone in the 1974 Earthquake Zone Map, but a strong earthquake of magnitude M = 7.51 and intensity $I_0 = 10$ occurred in the northern region at Yenice-Gönen on 18 March 1953. It is therefore strongly recommended that the Power Plant be designed on the basis of a first degree earthquake zone.

Soil Amplification Analysis

Assuming a sinusoidal shear wave input at the base rock level, with varying frequencies and amplitudes, it is possible to determine the amplitudes and frequency contents of the surface motion, taking into account the nonlinearity of the shear modulus with varying values of shear strain.[2] For the idealized soil profile given in Figure 11, a shear wave propagation analysis has been performed using the Hardin-Drnevich design equations as described above and also using the compressional wave velocities of the seismic refraction studies with the assumed values of Poisson's ratio. Results (Figures 12 and 13) show that the predominant period of the soil is approximately at T = 0.56 seconds for very small amplitude motions. For large amplitude motions the predominant period gradually moves to the right to higher period ranges of T = 1.2 seconds. For very large amplitude motions in the order of 0.12g input base rock acceleration no predominant period is observed.

Natural periods of the structures in this power plant should, therefore, be outside the critical period zone of T = 0.5 and T = 1.2 seconds.

REFERENCES

1. *B.O. Hardin and V.P. Drnevich, Proc. Amer. Soc. Civil Eng., 98, SM7 (1972).*

2. *P.B. Schnabel, J. Lysmer, J. and H.B. Seed, Earthq. Eng. Res. Centre, Calif., Berkeley, Report 72-12 (1972).*

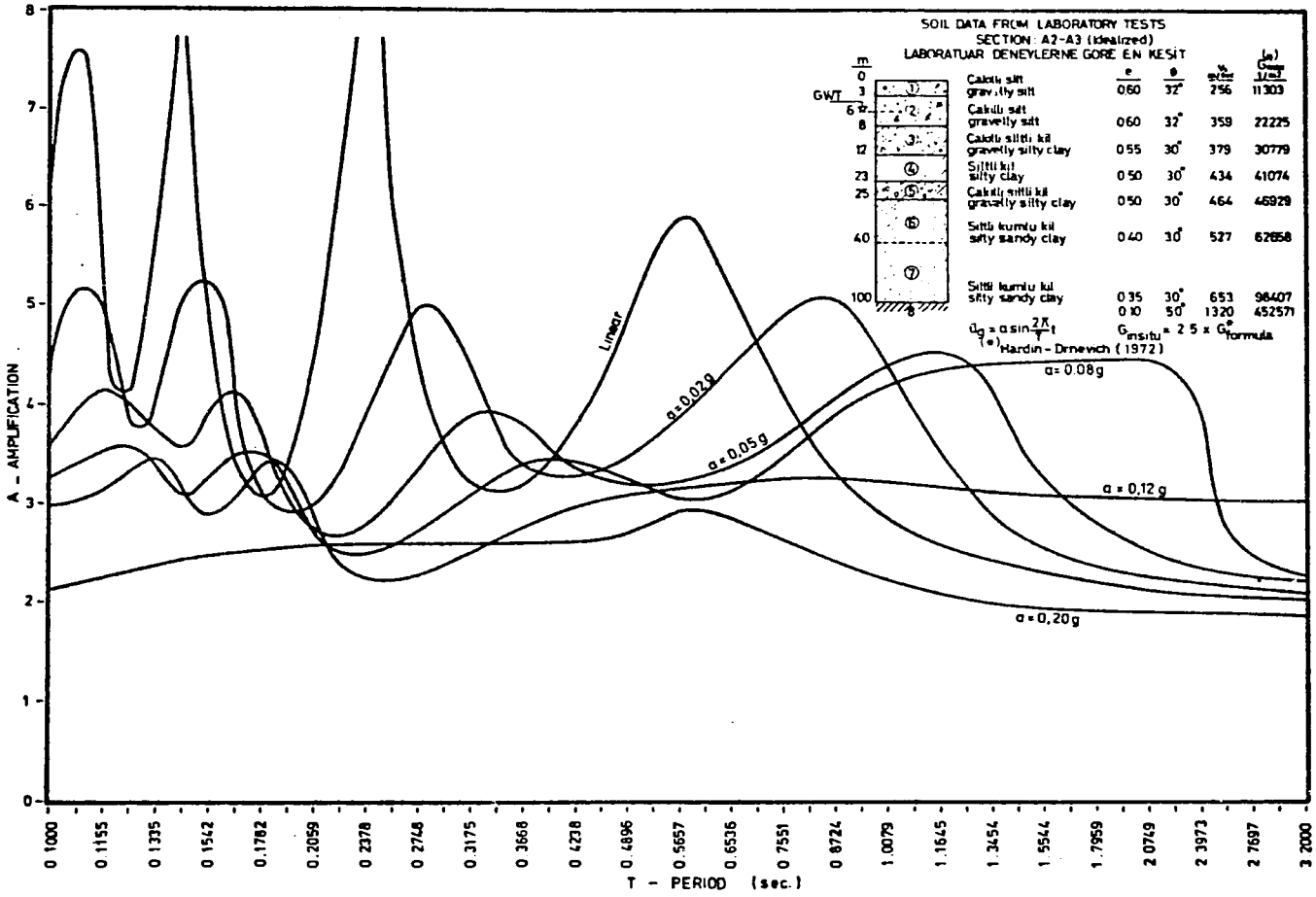

FIGURE 12. SOIL AMPLIFICATION

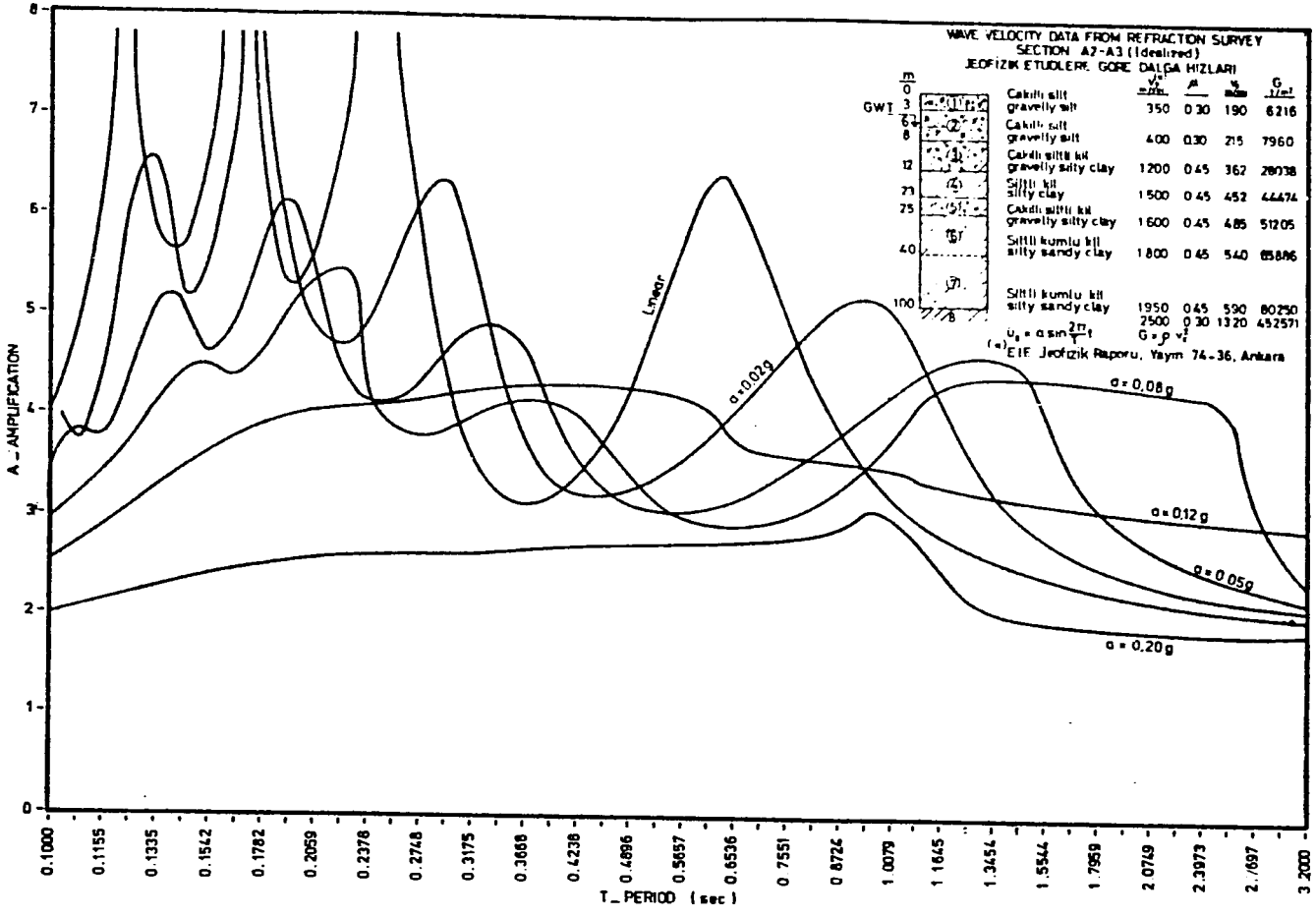

FIGURE 13. SOIL AMPLIFICATION

DISCUSSION

Dr. Askar asked what was the value of the ratio expressing non linear property of elastic to linear systems: Dr. Tezcan said that since the shear modulus was related to shear strength the shear modulus was known. Professor Ambraseys referred to the need for care when using formulae and graphs relating damping and strain: these were obtained from laboratory experiments and the observed effects were characteristic of the model and did not necessarily apply to the natural situation.

A GEODYNAMICAL STUDY FOR THE CENTRAL ANKARA REGION

Dr. Çetin Soydemir, Dr. Aybars Gürpınar and Mr. Yener Özkan

Local soil conditions are a key parameter to be considered in a seismic susceptibility analysis and the basic theory explaining and predicting their effect on seismic response is the so-called 'one-dimensional amplification theory'.[1, 2, 3] In this simulation the soil is considered to be replaced by horizontal elastic (or viscoelastic) layers on a rock half-space. Shear waves travelling vertically strike the lower boundary and produce horizontal oscillations of the deposit. The spectral density function of the earthquake motion is simulated using the elastic parameters of the assumed horizontal soil layers. The two dimensional model makes use of the theory of random wave propagation in elastic layered media. In this way both P and S waves are considered and the solution is obtained as a function of the angle of incidence of the assumed wavefront on the interface of the bedrock and soil layers, which can be estimated from considerations of possible epicentral distances and focal depths.

The site under consideration is Kızılay square in Ankara. At present it is occupied by the headquarters of the Turkish Red Crescent General Directorate (TRCGD). It is the intention of TRCGD that the present three storey building be replaced by a modern social-business complex, with three major units, namely theatre, hotel and office blocks which are approximately ten, twenty and thirty stories in height respectively. The lay-out also includes underground recreational and shopping areas, a swimming pool, a major garage and other units in a six storey deep basement.

Local Geology

The Ankara basin has a considerable depth of graywacke which has been subjected to severe folding and faulting. With these tectonic movements, the lower diorite magma has flowed upwards through a system of dykes in the thick graywacke and formed superficial andesities and dacites. The weathered and eroded graywacke and lime stone on the highlands surrounding the basin has been carried onto the central region round Kızılay probably during the Quaternary Period. The thickness of the sediments is about 30 m – 40 m. around Kızılay, slightly increasing in the direction of Sıhhiye.

The surface of the site is flat, at 862 m above sea level.

Subsoil Profile

Fifteen borings varying from 30 m to 60 m in depth were performed, with Standard Penetration Tests (SPT) and groundwater observations. Disturbed and undisturbed samples from the subsoil and core samples from the bed-rock were taken. The geological section is shown in Figure 1 and 'idealized characteristic average geological section' in Figure 2. There are three main layers:

a) from the ground surface to a depth of 18-22 m, there is a rather heterogeneous layer of fine gravel-coarse sand-clay. The upper 8-10 m section is largely 'artificial fill' material. The observed SPT values vary between 10 and 50 in an erratic manner, which is not unusual for such a formation. The ground water table is at depth of about 8 m.

The average total unit weight of the formation is 2 ton/m^3. The granular formation, loose to medium dense in consistency, exists in a clay matrix. The clay constituency of the mixture is of CL-CH type according to the Unified Soil Classification (see Figure 3 on page 129).

Figure 4 (on page 130) shows the results of confined and unconfined compression and unconsolidated-undrained triaxial tests performed on undisturbed samples taken from the lower half of the layer.

b) between 18-20 m to 38-42 m there is a very stiff-hard, red-brown clay of the type usually referred to as 'Ankara Clay'. This is quite homogeneous except that it contains intermittent concretions and concentrations of gravel-coarse sand. The SPT values mostly exceed 50. It is extremely difficult to obtain undisturbed samples from a formation of such consistency with a piston type sampler, so a limited number of samples were obtained with a special Dennison type rotary sampler.

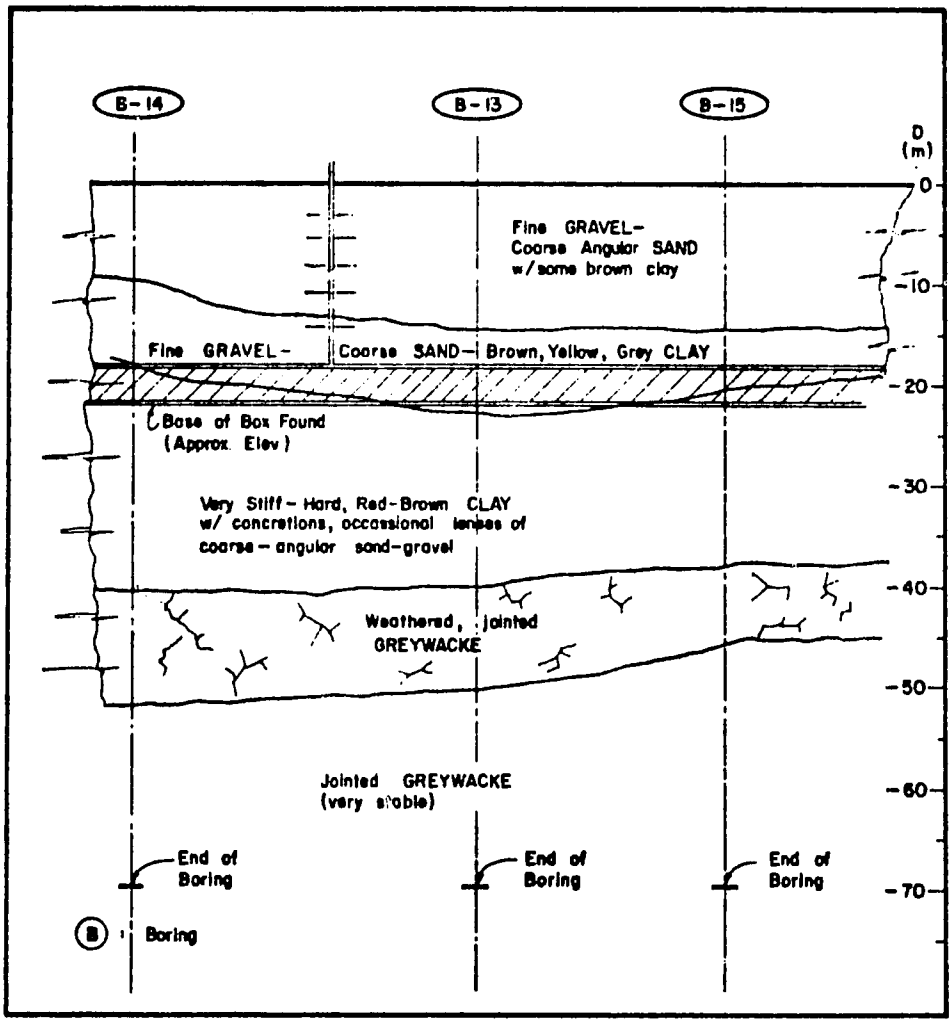

FIGURE 1. GEOLOGICAL SECTION AT THE SITE

The clay medium is of (CH) type (Figure 3) with water content between 25 and 40%, which is about the plastic limit.

The consolidation test data have yielded a virgin compression index $C_c = 0.14 - 0.24$, and a swelling index; $C_s = 0.02 - 0.04$.

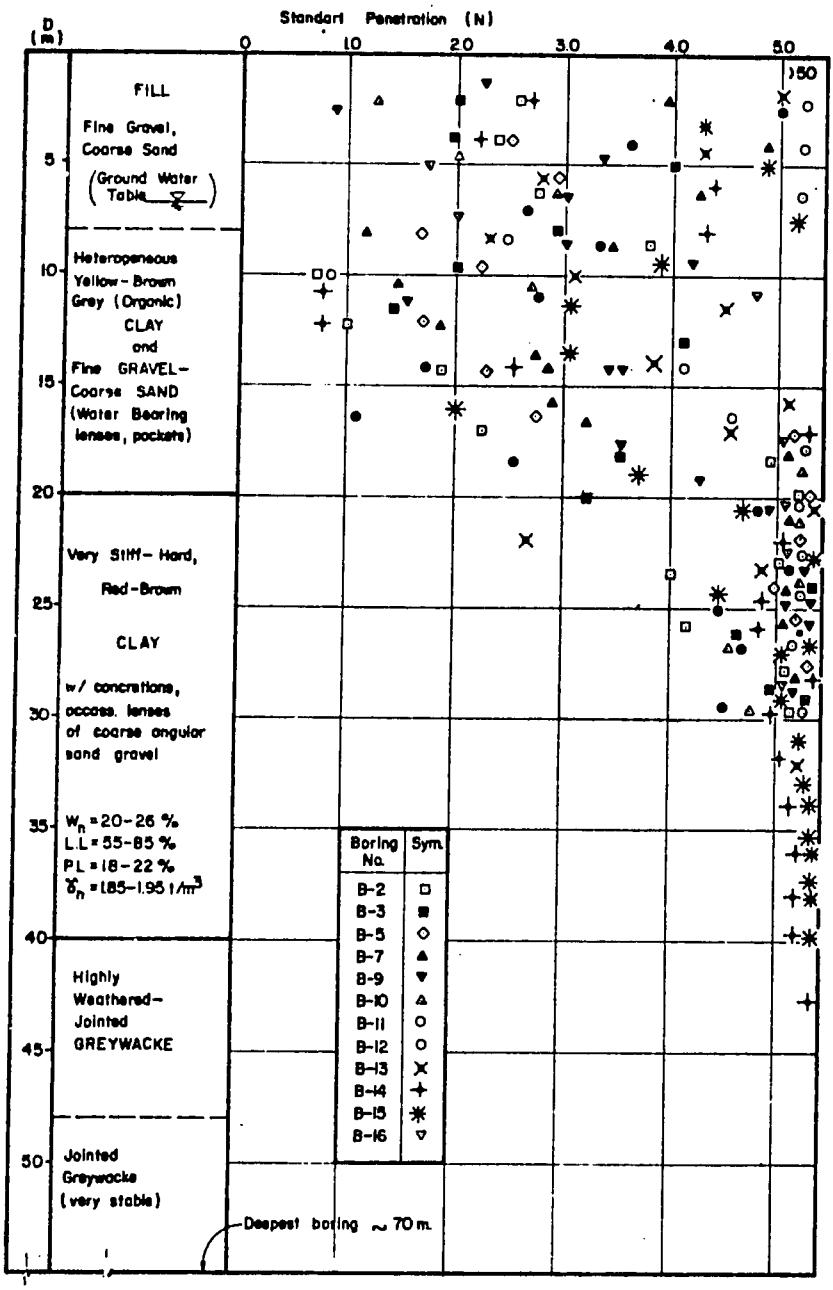

FIGURE 2. IDEALIZED GEOLOGICAL—SUBSOIL PROFILE AT THE SITE

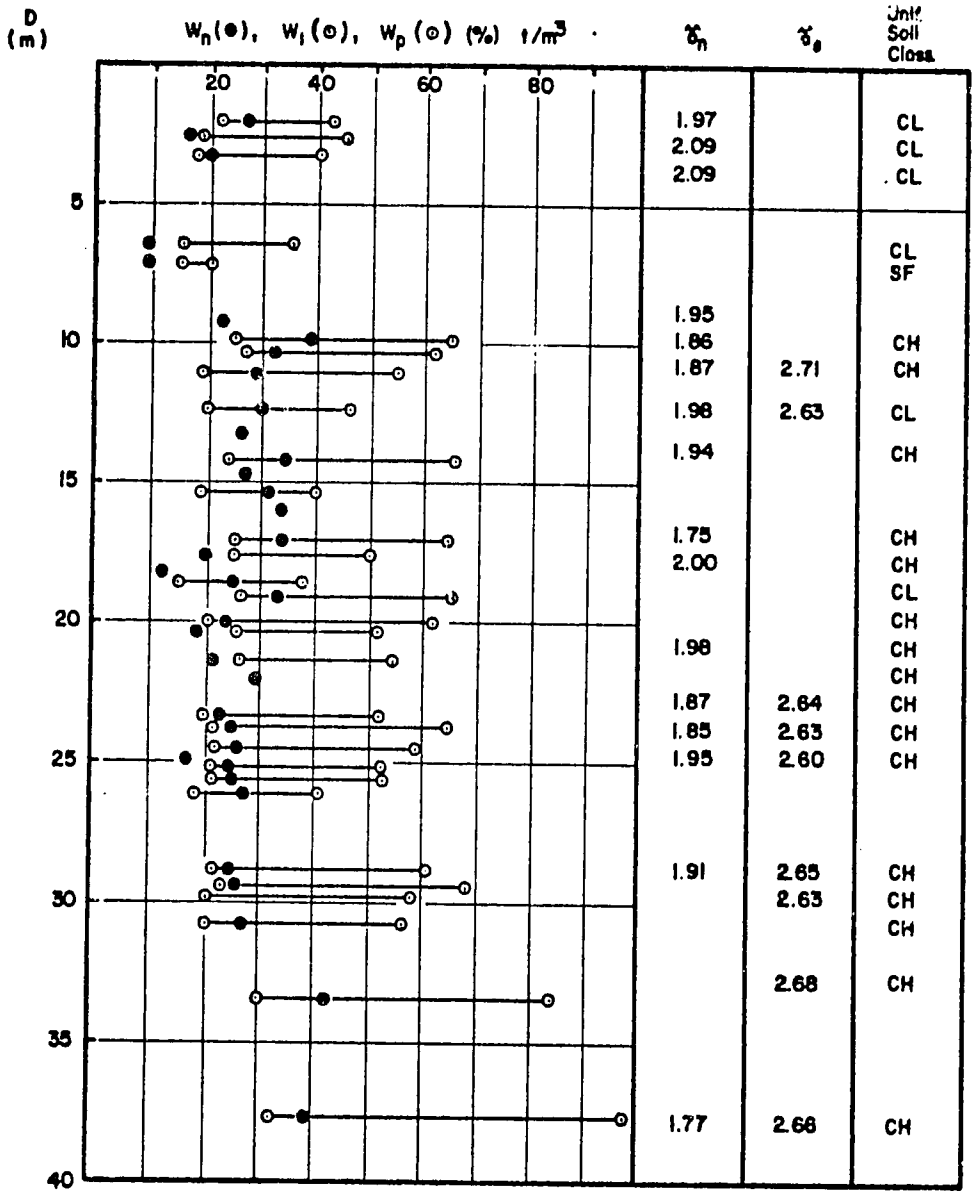

FIGURE 3. INDEX PROPERTIES OF SUBSOIL

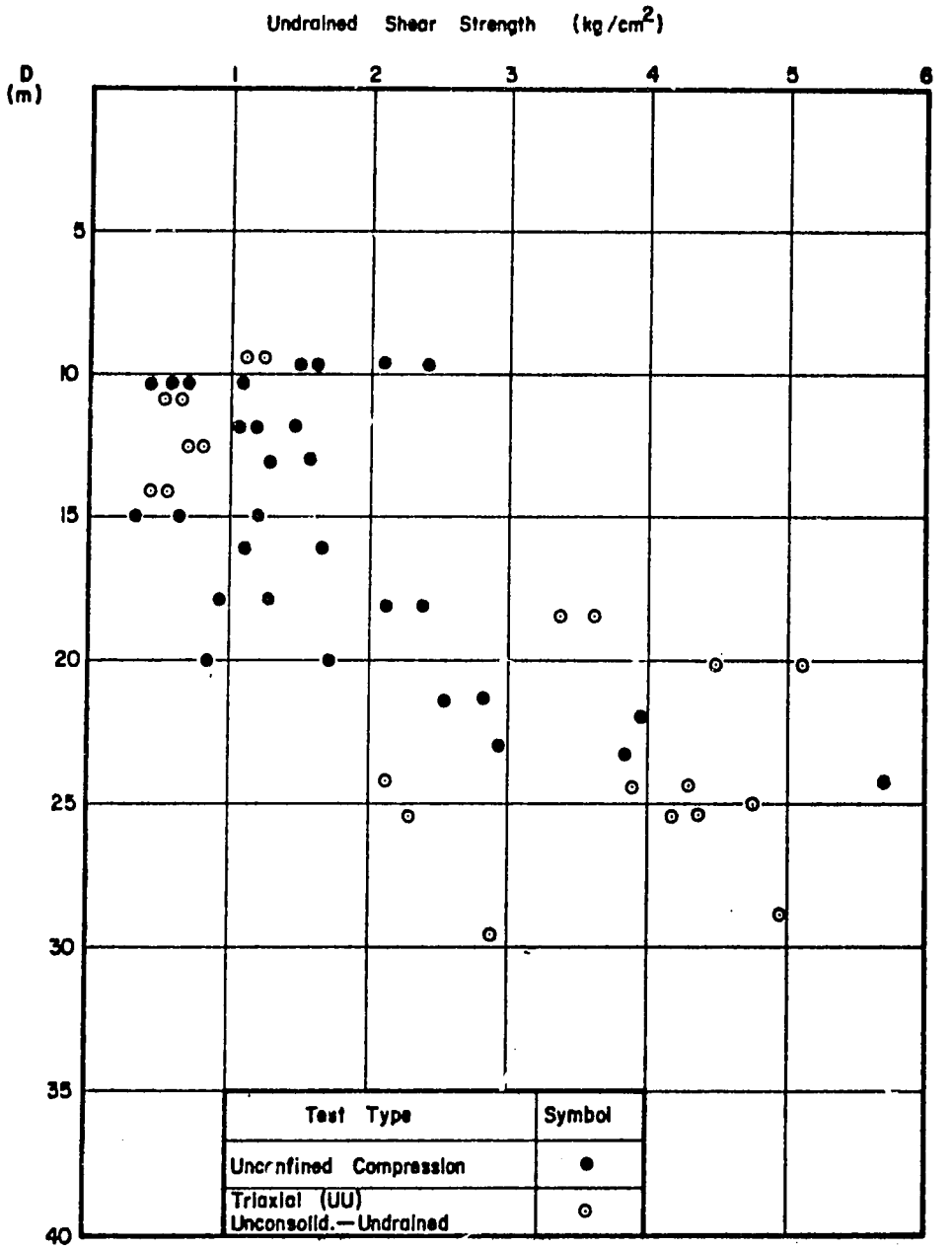

FIGURE 4. STRENGTH DATA FOR THE SUBSOIL

c) the graywacke (bedrock) formation consists of an upper 6 m – 10 m of highly weathered-jointed segment which has very distinct sets of joints. Below an average depth of 48 m. the jointing becomes less distinct and the graywacke presents a relatively more stable structure. It is assumed that below 80 m the graywacke becomes very stable with little jointing.

Geodynamical Evaluation

Since 1900, two earthquakes with magnitude greater than 5.75 (Richter scale) have occurred in the Ankara region, the 1943 Çankırı (M = 7.50) and 1944 Bolu (M = 7.50) earthquakes, 114 km and 152 km from Ankara respectively. Thus, no earthquake with magnitude over 5.75 has occurred within 100 km of Ankara in the last four centuries.

In contrast to the relativity settled (static) geological structure of the Ankara region, the highly active North Anatolian Fault Zone is located about 100 km north of the city. If an earthquake of magnitude of 8.0 occurred with an epicentral distance of 100 km and at a focal depth of 25 km, then the angle of incidence would be 75°, and the predominant wave periods[4] would be between 0.5 and 1.0 sec.

Micro-regional simulation may be achieved in two steps: first the spectral characteristics of the earthquake motion at the bedrock level have to be determined.[5] (See Figure 5 on the next page).

$$S_1 = 10^{0.61M-1.73R-0.67}\left\{1+\frac{1}{\sqrt{[(1+\alpha)/(1-\alpha)]^2\,[1-(T/Tg)^2]^2+[0.3/\sqrt{Tg}]^2(T/Tg)^2}}\right\}$$

Where,

M = Magnitude on Richter's scale (taken as 8.0 in this case)
R = epicentral distance (taken as 100 km in this case)

$$\alpha = \frac{\rho_1 v_1}{\rho_2 v_2}$$

ρ_1, ρ_2 = densities of the materials of the layer and of the subjacent medium, respectively

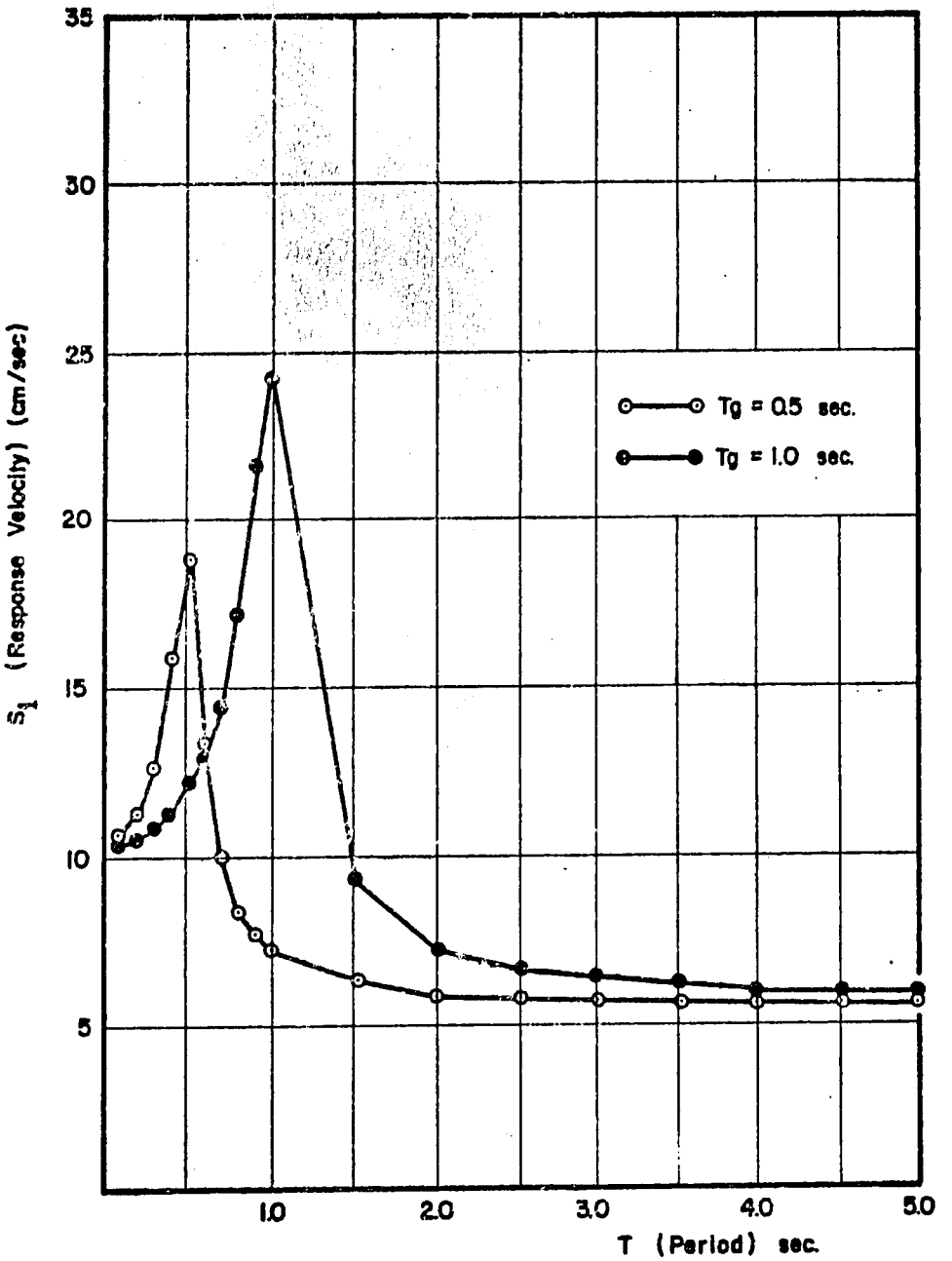

FIGURE 5. VELOCITY RESPONSE SPECTRUM AT BEDROCK (Microseismic—Kanai Approach)

v_1, v_2 = wave velocities in the layer and in the subjacent medium, respectively

T = natural period

T_g = predominant period of waves (taken from 0.5—1.0 sec. in this case)

Making use of S_1, the parameters of the soil layers presented in Figure 6 (see the next page) and with an angle of incidence of 75°, the velocity spectral density function of the motion on the ground surface can be obtained by using theoretical spectrum simulation technique.[6] (See Figure 7 on page 135).

Displacement and acceleration spectral density functions S (ω) caneasily be obtained by multiplying the ordinates of the velocity spectral density function by $\frac{1}{\omega^2}$ and ω^2 respectively, where $\omega = \frac{2\pi}{T}$. Using these three spectral density functions, root mean square values E (x^2) for these random processes can be determined from the following relation:

$$E(x^2) = \int_{-\infty}^{\infty} S(\omega) \, . \, d\omega$$

The root mean square values of the displacement, velocity and acceleration processes in this case at hand are:

$$\gamma_{rms} = 1.82 \text{ cm}$$

$$\dot{\gamma}_{rms} = 21.7 \text{ cm/sec}$$

$$\ddot{\gamma}_{rms} = 51.7 \text{ cm/sec}^2$$

Predominant period of vibration T_o has been determined as 0.85 sec. employing the following relations:

$$\omega_o^2 = \frac{\int_{-\infty}^{\infty} \omega^2 S(\omega) \, d\omega}{\int_{-\infty}^{\infty} S(\omega) \, d\omega}$$

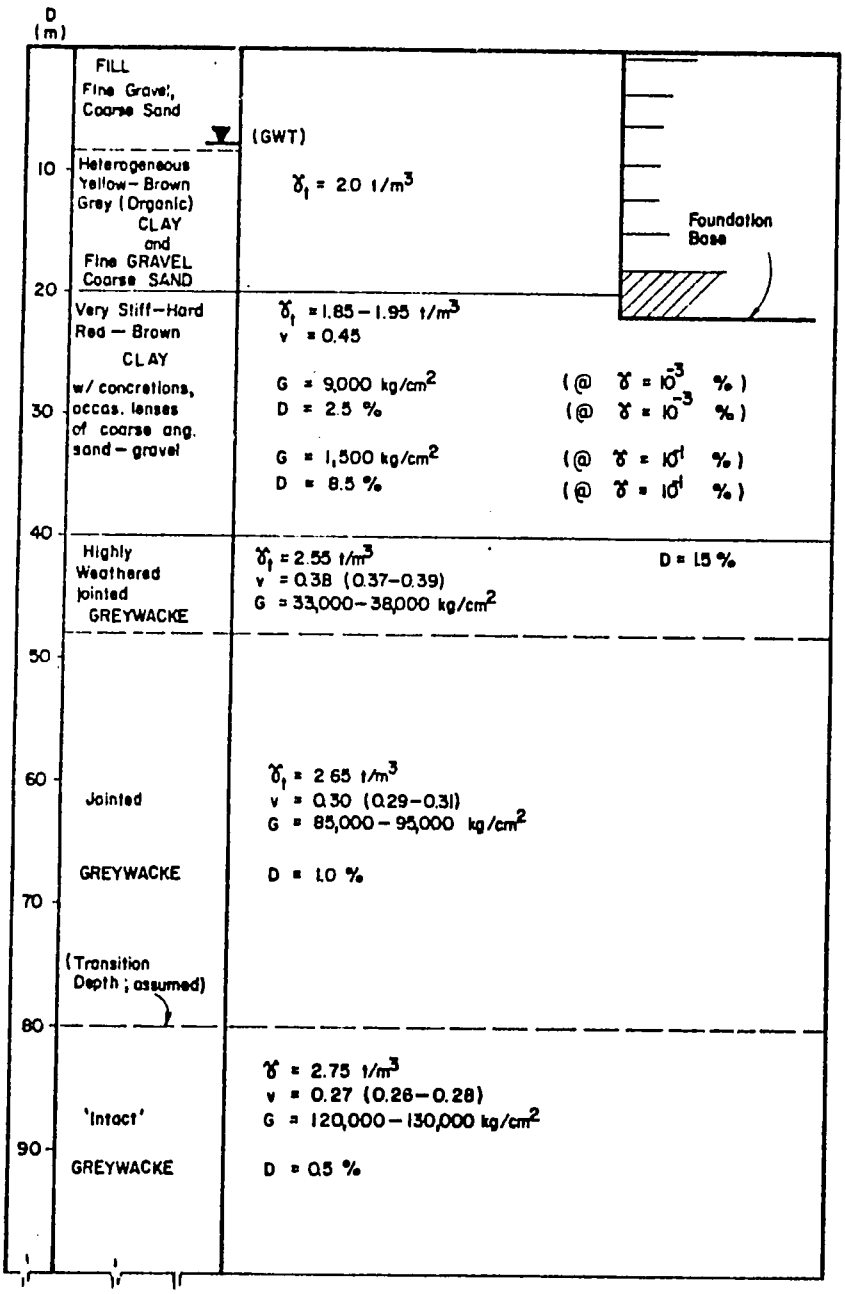

FIGURE 6. ASSIGNED SUBSOIL PARAMETERS FOR GEODYNAMIC EVALUATION

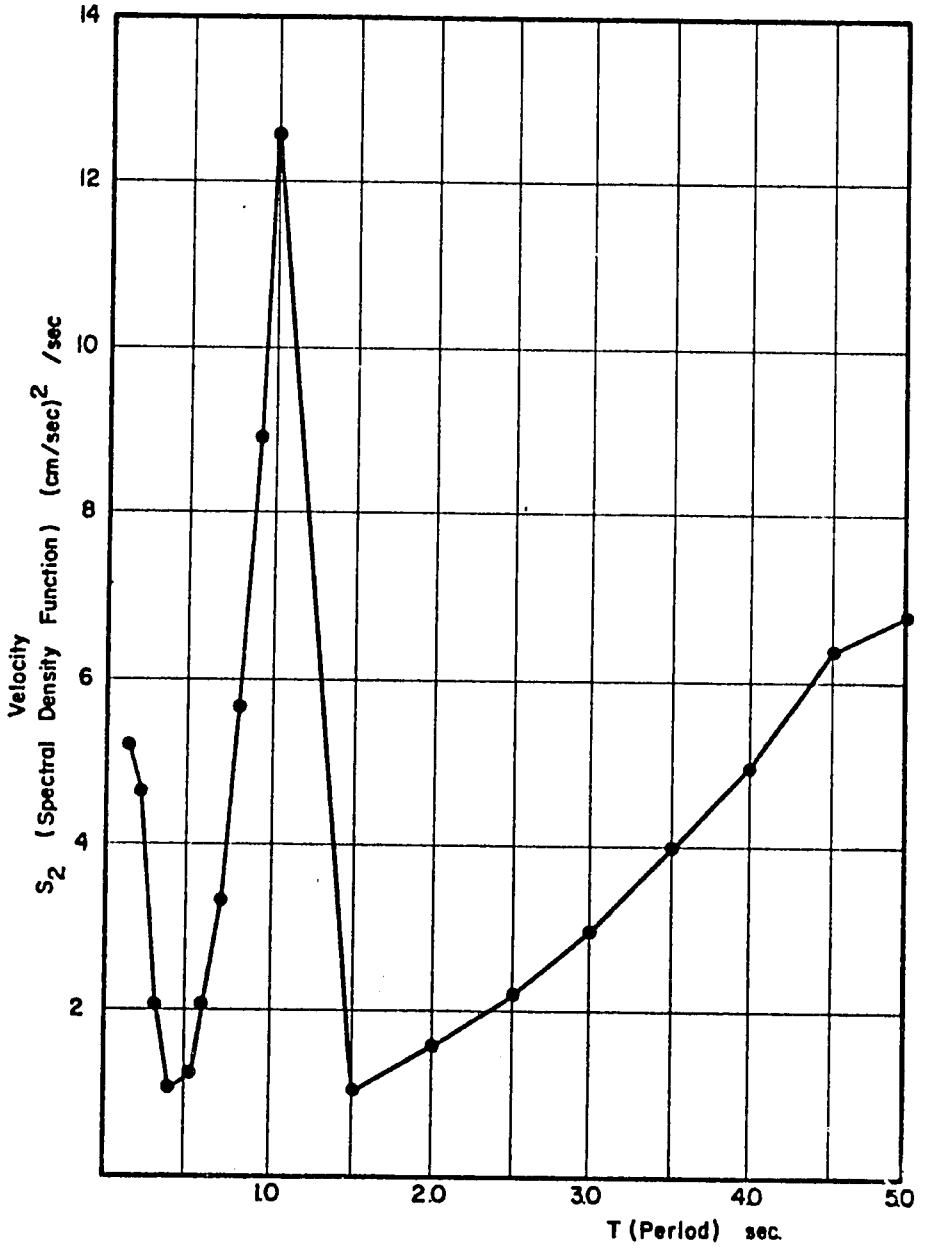

FIGURE 7. SPECTRAL DENSITY FUNCTION (Continuous Medium; Özgür-Gürpınar Approach) on the ground surface.

$$T_o = \frac{2\pi}{\omega_o}$$

The expected fractions of time ν_a^+ velocity, acceleration and displacement processes above or below an arbitrary level a are plotted in Figures 8, 9 and 10 respectively. Kobayashi and Nagahashi[7] have established correlation coefficients showing the relationship of each of these modes of excitation to response acceleration, deflection and base shear coefficient as a function of the natural period T of structure (See Figure 11 on page 140). T will be different for each of the three structural units under consideration; an appropriate choice may be made for the critical mode of excitation. Then, by using ν_a^+ for the critical mode (i.e. Figures 8, 9 or 10) consistent risk criteria can be determined.

REFERENCES

1. *K. Kanai, Bull. Earthq. Res. Inst., Tokyo, 28 (1950).*

2. *K. Kanai, Bull. Earthq. Res. Inst., Tokyo, 29 (1951).*

3. *H.B. Seed, Proc. Soil Dynamics Spec. Sess., 7th Int. Conf. Soil Mech. and Found. Eng., Mexico City, 1969.*

4. *H.B. Seed, I.M. Idriss and F.W. Kiefer, Proc. Amer. Soc. Civil Eng., JSMFE, Sept. 1969.*

5. *N.M. Newmark and E. Rosenblueth, "Fundamentals of Earthquake Engineering". Prentice Hall, 1971.*

6. *D. Özgür and A. Gürpınar, 5th World Conf. Earthq. Eng., Rome (1973).*

7. *H. Kobayashi and S. Nagahashi, Conf. on Seismicity of Balkan Region, Ankara (1974).*

DISCUSSION

Dr. Gürpınar agreed with Dr. Tezcan that in large magnitude earthquakes the predominant period may not be a good parameter, but the spectral density function was commonly used. Dr. Goudarzi asked if the proposed building would withstand a magnitude 7 earthquake. Dr. Gürpınar said that Ankara was seismically inactive, and the

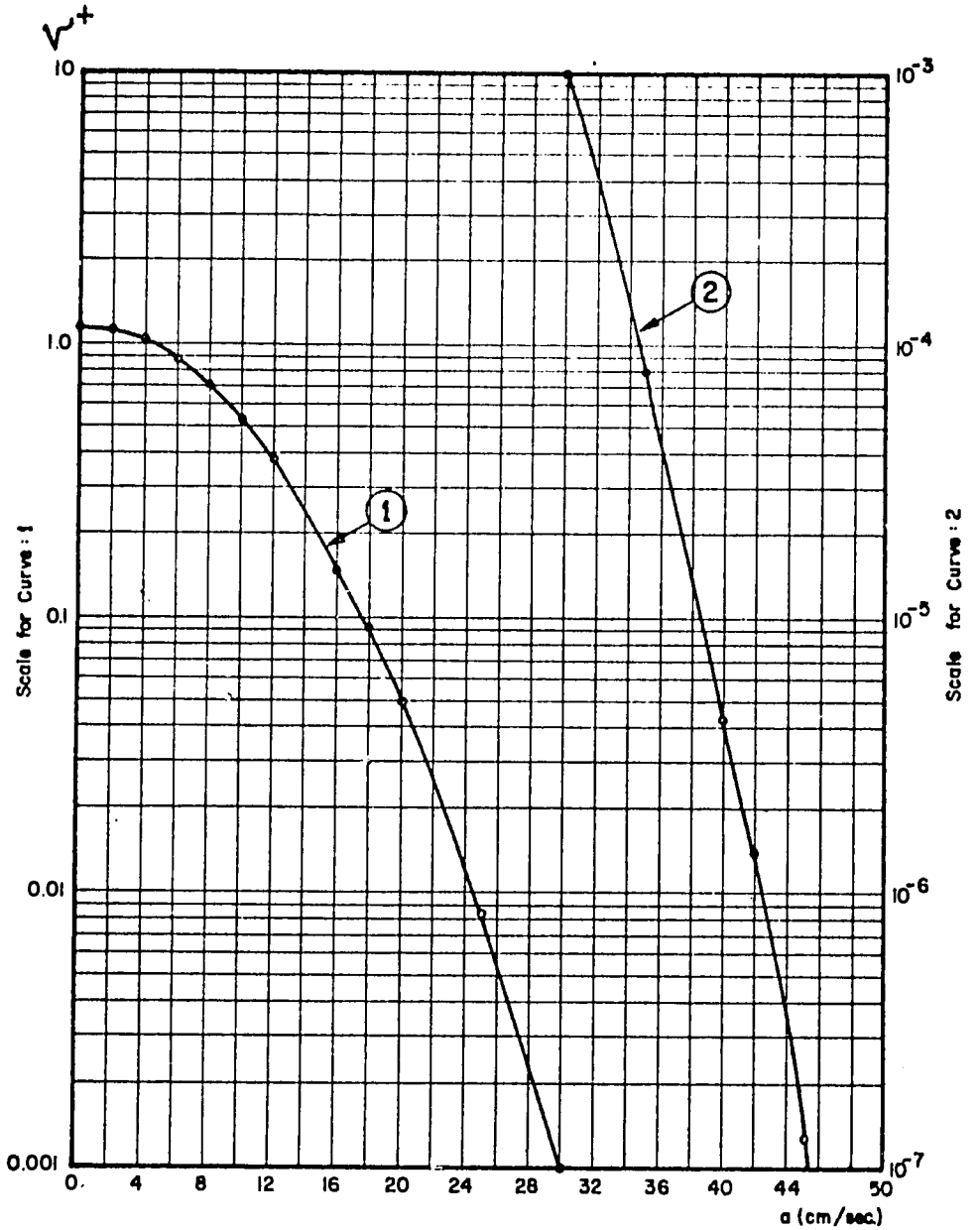

FIGURE 8. EXPECTED FRACTION OF TIME THAT GROUND VELOCITY EXCEEDS "a"

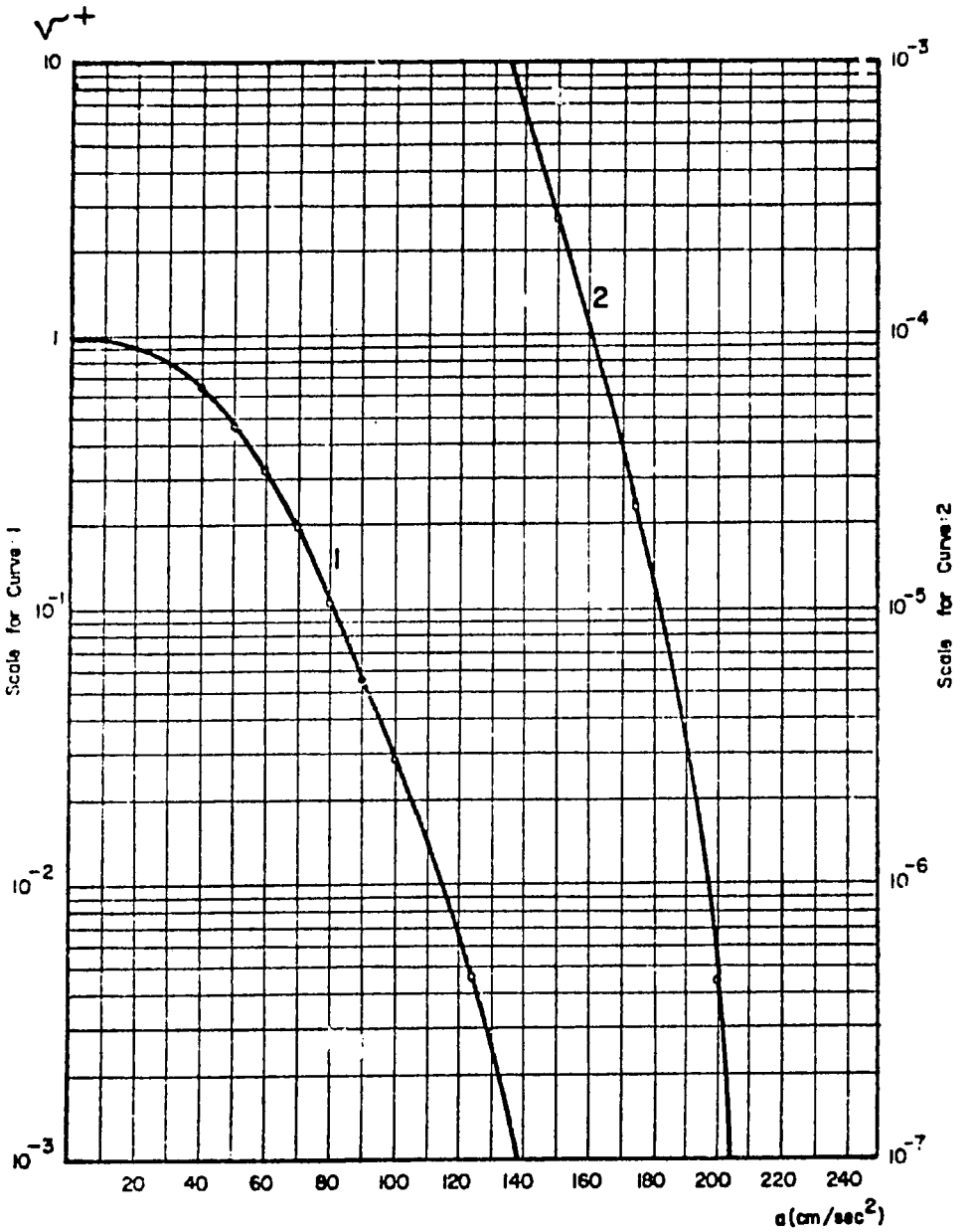

FIGURE 9. EXPECTED FRACTION OF TIME THAT GROUND ACCELERATION EXCEEDS "a

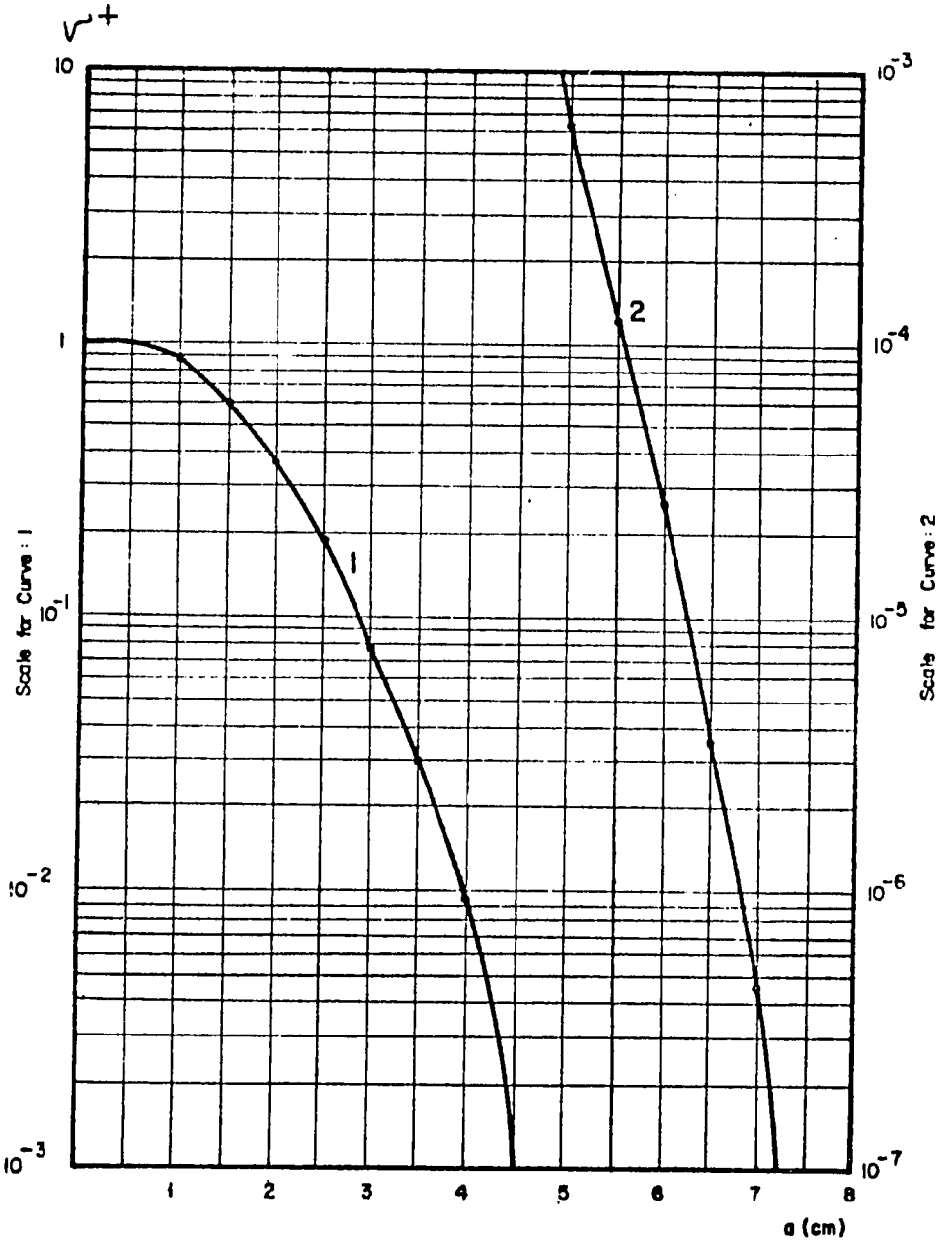

FIGURE 10. EXPECTED FRACTION OF TIME THAT GROUND DISPLACEMENT EXCEEDS "a"

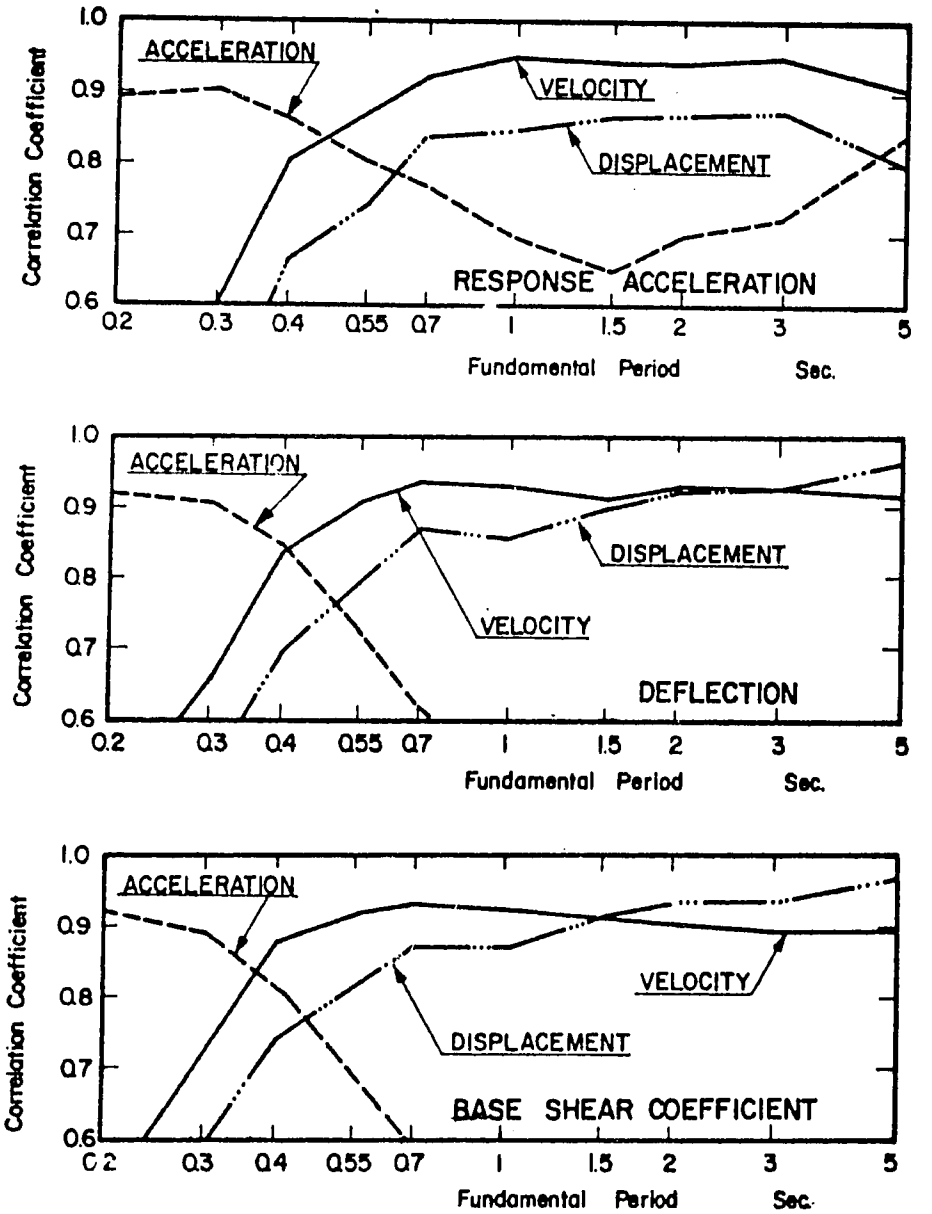

FIGURE 11. VARIATION OF CORRELATION COEFFICIENT BETWEEN GROUND MOTION AMPLITUDE AND RESPONSE OF STRUCTURE AGAINST FUNDAMENTAL PERIOD OF STRUCTURE. (After Kobayashi et. al. ; Ref. 7)

North Anatolian fault was more than 100 km away; in designing the building it had been assumed that no earthquake stronger than 5.5 would occur within the life of the building within 100 km. In reply to Dr. Askar, Dr. Gürpınar said that the calculations had been based on a two dimensional model.

THE STIFFNESS OF AN INFILLED PORTAL FRAME UNDER HORIZONTAL LOAD

Dr. S. Tanvir Wasti and Dr. Polat Gülkan

The influence of infill walls on the structural behaviour of building frames has often been stdudied for lateral loads such as those created by earthquakes. It has always been found that an infill wall of brick and mortar or similar materials increases the structural stiffness of the system. However, little is known about infilled frames, although the large increase of shear forces due to the "short column" effect in partially infilled frames has been mentioned.[1,2]

The presence of a partial or total infill wall affects the behaviour of a frame under horizontal load by increasing both its stiffness and its ultimate capacity. The dynamic structural characteristics of the building frame of which the wall is a part also change significantly. We now propose a method for assessing the increase in the stiffness of infilled frames.

Proposed Analytical Model

An attempt[3] to incorporate infill walls of variable height into an analysis of a portal frame-wall system under a single horizontal load, based on a Rayleigh-Ritz approximation of the deformed shape of the infilled frame shows good agreement with experimental work.[4] The same assumptions[3] are now made for the frame-wall system shown in Figure 1 (see the next page), as follows:

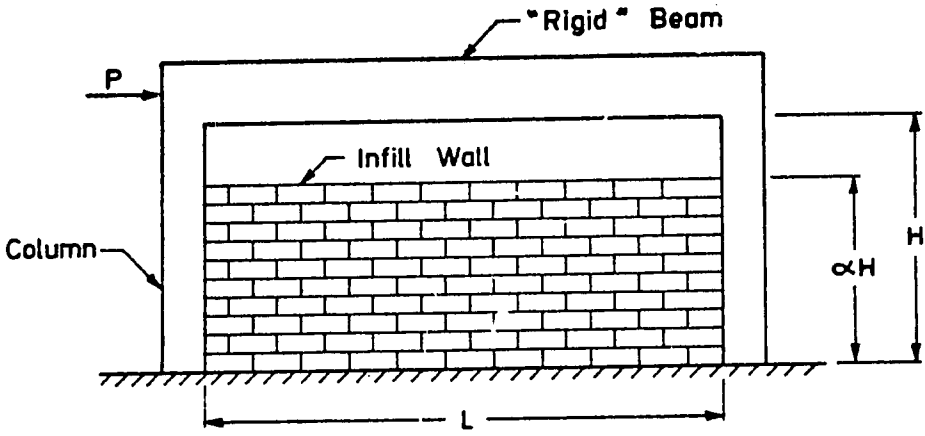

Figure 1. Frame—Infill Wall System

(1) The infill wall inhibits the bending of the column on the top of which the horizontal load P acts and does not affect or hinder the structural action of the right hand column in any way.

(2) The action of the infill wall is represented by an elastic foundation αH where the coefficient α, indicating the extent of infill, is between 0 and 1.

(3) The beam of the portal frame is treated as rigid compared to the two columns and thus the columns can be considered as built-in at both ends. Both columns are taken to possess the same flexural rigidity EI.

Neglecting column axial deformations, the frame-wall system can now be considered as a compound of two parallel beam-like columns, each taking a different share of the horizontal load P but subject by conditions of compatibility to the same lateral deflection Δ. For the subsequent derivation the frame will also be taken as fully infilled; the reduction to partial infilling shall follow in a straightforward manner. The elastic foundation replacing the infill wall is assumed to be made up of n springs spaced equdistantly along the distance H. In general, the stiffnesses of the springs are designated as $k_1, k_2, \ldots k_n$. The free body diagram of the analytical model for the frame-infill wall system is shown in Figure 2. The spring reactions are denoted by $R_1, R_2, \ldots R_n$; M_1, M_2 represent the unknown moments at the top of the frame columns; P_1 and P_2 indicate the division of the applied concentrated load P.

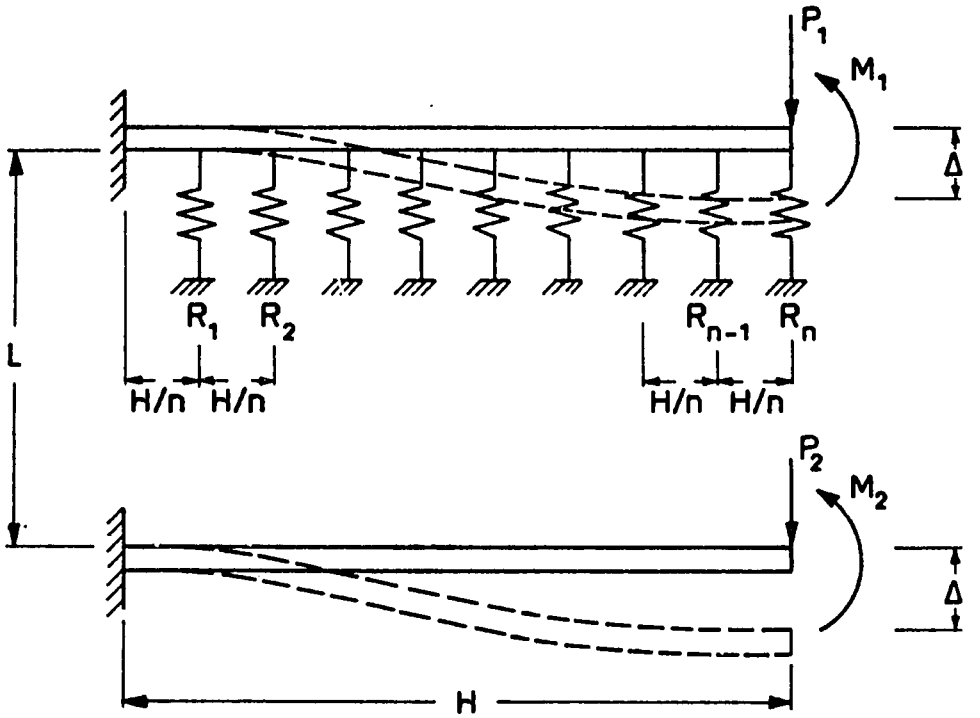

Figure 2. Free Body Diagram of Equivalent System

Solution by Complementary Energy[5]

Considering the "beam" with load P_2, the expression for the complementary energy C_2 can be written as

$$C_2 = \int_0^H \frac{M^2\,dx}{2EI} = \int_0^H \frac{(M_2 - P_2 x)^2\,dx}{2EI} \tag{1}$$

where x is measured from the right hand end in Figure 2. Using the relations

$$\frac{\partial C_2}{\partial M_2} = 0 \tag{2}$$

Agency for International Development
Library
Room 1656 NS
Washington, D.C. 20523

$$\text{and} \quad \frac{\partial C_2}{\partial P_2} = \Delta \tag{3}$$

the following results are obtained·

$$M_2 = \frac{P_2 H}{2} \tag{4}$$

$$\text{and} \qquad \Delta = \frac{P_2 H^3}{12EI} \tag{5}$$

The complementary energy expression for the "beam" with n springs can now be written as:

$$C_1 = \frac{1}{2EI} \int_0^{H/n} [M_1 + (R_n - P_1)x]^2 \, dx + \int_{H/n}^{2H/n} [M_1 + (R_n - P_1)x +$$

$$(R_n - P_1)x + R_{n-1}(x - \text{——})]^2 \, dx + \ldots\ldots + \int_{\frac{(n-1)H}{n}}^{H}$$

$$[M_1 + (R_n - P_1)x + R_{n-1}(x - \frac{H}{n}) + \ldots\ldots$$

$$R_1 (x - \frac{(n-1)H}{n})]^2 \, dx$$

$$+ \frac{1}{2} \left(\frac{R_1^2}{k_1} + \frac{R_2^2}{k_2} + \ldots\ldots \frac{R_n^2}{k_n} \right) \tag{6}$$

where x is again measured from the right hand end in Figure 2.

The relations $\dfrac{\partial C_1}{\partial M_1} = 0$ and $\dfrac{\partial C_1}{\partial P_1} = \Delta$ now yield the equations:

$$\int_0^{H/n} [M_1 + (Rn - P_1)x]\,dx + \int_{H/n}^{2H/n} [M_1 + (R_n - P_1)x +$$

$$+ R_{n-1}(x - \frac{H}{n})]\,dx + \ldots\ldots\ldots + \int_{\frac{(n-1)H}{n}}^{H} [M_1 + (R_n - P_1)x$$

$$+ R_{n-1}(x - \frac{H}{n}) \ldots + R_1(x - \frac{(n-1)H}{n})]\,dx = 0 \qquad (7)$$

$$\int_0^{H/n} [M_1 + (R_n - P_1)x]\,x\,dx + \int_{H/n}^{2H/n} [M_1 + (R_n - P_1)x$$

$$+ R_{n-1}(x - \frac{H}{n})]\,x\,dx + \ldots\ldots + \int_{\frac{(n-1)H}{n}}^{H} [M_1 + (R_n - P_1)x$$

$$+ R_{n-1}(x - \frac{H}{n}) + \ldots R_1(x - \frac{(n-1)H}{n})]\,x\,dx = -EI\Delta \qquad (8)$$

The complementary energy for the "beam" must also be minimized with respect to each spring reaction, so the following n supplementary equations are obtained:

$$\frac{\partial C_1}{\partial R_i} = \frac{1}{EI}\left\{\int_{\frac{(n-1)H}{n}}^{H} [M_1 + (R_n - P_1)x + R_{n-1}(x - \frac{H}{n}) + \right.$$

$$\left. \ldots\ldots R_1(x - \frac{(n-1)H}{n})]\,.\,(x - \frac{(n-1)H}{n})\,dx\right\} + \frac{R_1}{k_1} = 0 \qquad (9)$$

$$\frac{\partial C_1}{\partial R_2} = \frac{1}{EI} \int_{\frac{(n-2)H}{n}}^{\frac{(n-1)H}{n}} [\, M_1 + (R_n - P_1)\, x + R_{n-1} (x - \frac{H}{n}) +$$

$$\ldots\, R_2 (x - \frac{(n-2)H}{n})\,] \,.\, (x - \frac{(n-2)H}{n})\, dx +$$

$$\int_{\frac{(n-1)H}{n}}^{H} [\, M_1 + (R_n - P_1)\, x + \ldots\, R_1 (x - \frac{(n-1)H}{n})\,]$$

$$(x - \frac{(n-2)H}{n})\, dx \quad + \frac{R_2}{k_2} = 0 \tag{10}$$

$$\frac{\partial C_1}{\partial R_n} = \frac{1}{EI} \int_0^{H/n} [\, M_1 + (R_n - P_1)\, x\,] \,.\, x\, dx +$$

$$\int_{H/n}^{2H/n} [\, M_1 + (R_n - P)\, x + R_{n-1} (x - \frac{H}{n})\,]\, x\, dx + \ldots$$

$$\int_{\frac{(n-1)H}{n}}^{H} [\, M_1 + (R_n - P_1)\, x \ldots + R_1 (x - \frac{(n-1)H}{n})\,]\, x\, dx$$

$$+ \frac{R_n}{k_n} = 0 \tag{11}$$

Equating the values of Δ in Equations (5) and (8) and recalling the relation:

$$P_1 + P_2 = P \tag{12}$$

where P is the known external concentrated load, a system of n + 3 equations is obtained in the n + 3 unknowns $R_1, R_2, \ldots R_n, M_1, P_1, P_2$. Equation (4) provides for separate evaluation of the moment M_2. As the integrals repeat themselves, the calculation of the matrix coefficients for the unknowns is not difficult even when done manually for $n \leqslant 6$.

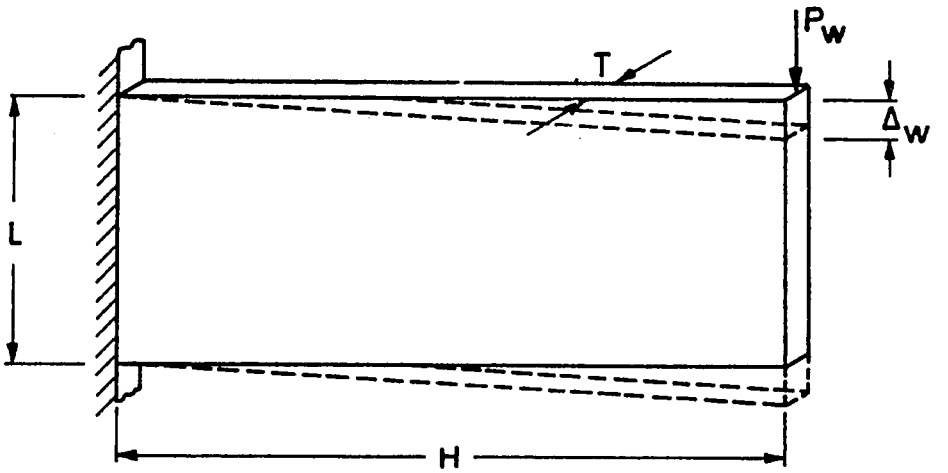

Figure 3. Shear Deformation of Infill Wall

Assessment of Spring Stiffness

Hitherto it has been assumed that the values of the spring stiffnesses k_1, $k_2, \ldots k_n$ are known. For the purposes of comparison with experimental values, a simple method of assessing the spring stiffnesses is now proposed.

The infill wall, of thickness T, and material elastic modulus E_W, is idealized as a deep beam subjected to shearing action as shown in Figure 3.

The deflection Δ_W is given by

$$\Delta_W = \frac{P_W H}{A_W G_W} \tag{13}$$

where $A_W = LT$ and $G_W = \dfrac{E_W}{2(1+\nu)}$

The total stiffness of the wall K_W is the value of P_W when Δ_W is unity, i.e.

$$K_W = \frac{E_W LT}{2H(1+\nu)} \tag{14}$$

If the infill wall in the analytical model is replaced by n springs, then, as a first approximation, if all spring stiffnesses are taken as equal,

$$k = k_1 = k_2 = \ldots . k_n = \frac{K_W}{n} \tag{15}$$

infilled frames of wall height αH the value for K_W is $\frac{E_W LT}{2\alpha H(1+\nu)}$. Since $\alpha < 1$, K_W increases rapidly as the infill height decreases. The lateral deflection Δ of the system, however, increases with the decrease in infill height, because as $\alpha \to 0$ the structural action of the column supersedes that of the wall. Presumably as α falls below a certain value, say $\frac{1}{3}$, the action of the infill wall may be replaced by just one spring of stiffness K_W at a height $\frac{\alpha H}{2}$ from the base.

Determining the spring stiffness K_W is much more complex for the actual case of a wall made up of two different materials, brick and mortar. If either the brick or the mortar is highly deformable the stiffness of an infill comprising both must approach zero. One way of expressing this result is to substitute for E_W in Eq. (14) an "equivalent" elastic modulus given by

$$(E_W)\,eq = \frac{E_{brick} \cdot E_{mortar}}{E_{brick} + E_{mortar}} \tag{16}$$

This simplification does not take into account the degree of bond between the two materials which affects the behaviour more intimately than the strength of the individual materials.

Comparison of Analytical and Experimental Results

A computer program allowing for the replacement of the infill wall by an

arbitrary number n of equidistant springs was prepared. The accuracy of the program was checked by the explicit derivation and solution of the equations (6–12) for the cases n = 1,2,3 and 6. The stability of the analytical results was checked by inserting successive values of n equal to 3, 6 and 12 into the computer program, keeping the total stiffness constant. The total change in the analytical deflection for a given load was influenced by less than 5%.

The load-deflection relationship obtained from the program was next compared with the work of Fiorato. Sozen and Gamble.[4] Although openings for windows and narrow slits in the walls are considered, no partially infilled frames have been tested. As a result, direct comparisons with only a few of the tested frame models are possible. Fiorato treats the infill wall of brick and mortar as a "monolithic" material and have carried out extensive tests to evaluate the elastic properties of the infill.

For the analytical model, n was taken as 6 for the portal frames: as shown in Figure 4 (see the next page). Good agreement was obtained. Similar agreement was also obtained when comparison was made between the results of experiment 0-0 (completely infilled frame without shear connectors) from the work of Mallick and Garg,[6] and the analytical model with n = 6.

REFERENCES

1. *J.L. Stratta and J. Feldman, Bull. Seism. Soc. Amer., 61, 609 (1971).*

2. *S.Z. Uzsoy and E. Çıtıpıtıoğlu, Bull. Seism. Soc. Amer., 62, 1113 (1972).*

3. *P. Gülkan and S.T. Wasti, Bull. Earthq. Inst. (Turkey), 4 (1974).*

4. *A.E. Fiorato, M.A. Sozen and W.L. Gamble, Univ. Illinois Civil Eng. Studies, Struct. Res. Series No. 370 (1970).*

5. *T.M. Charlton, "Energy Principles in Applied Statics". Blackie, London, 1959.*

6. *D.V. Mallick and R.P. Garg, Proc. Inst. Civil Eng., 49, 193 (1971).*

DISCUSSION

In reply to Dr. Lashkari, Dr. Wasti said that the left-hand column of the infilled frame abuts onto the wall while the right-hand column is completely uninhibited. In reply to Dr. Ambraseys, Dr. Wasti said that the model did not apply to a cracked wall,

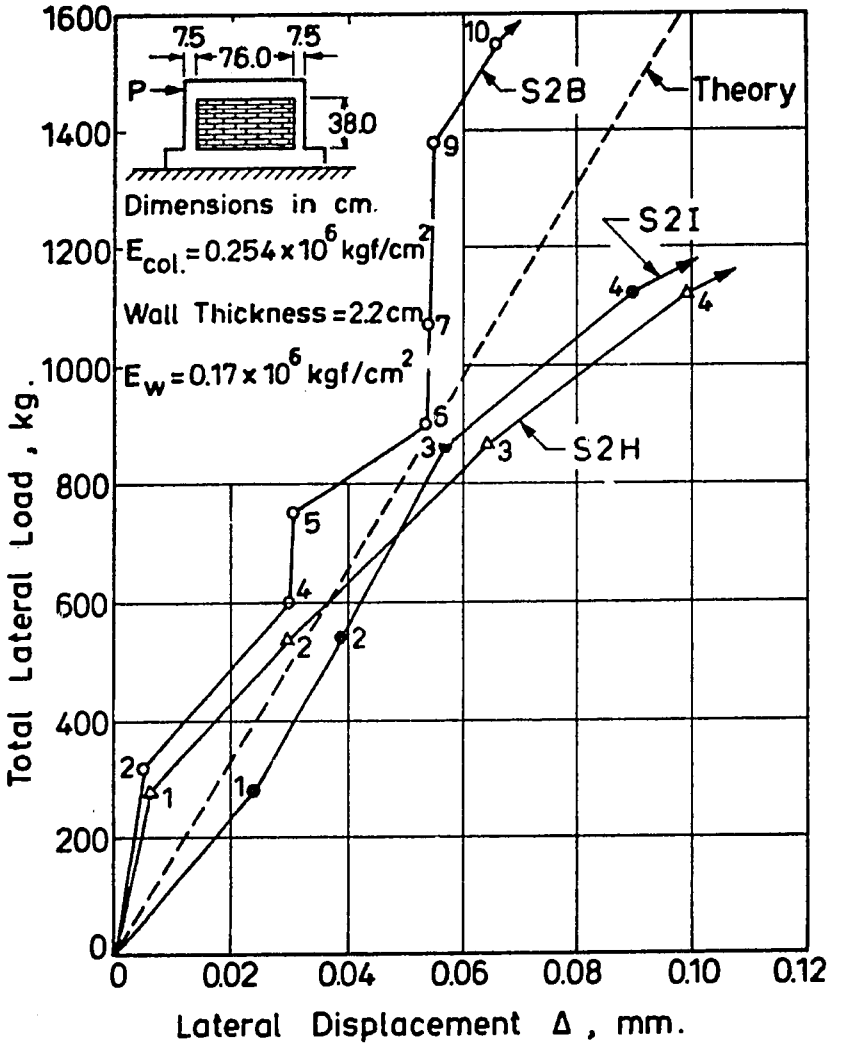

Figure 4. Comparison of Experimental Results (Florato et al.) with Theoretical Relationship

but only to elastic structures, and added that it would be interesting to study the effect of cracks. Dr. Çelebi asked what would happen if an axial load was applied: Dr. Wasti said that this was not considered. In reply to a further question, Dr. Wasti agreed that the work needs to be extended to cover damping; quasi-dynamic tests on models in which the column and infilled wall interact would also be useful. Mr. Lloyd commented that the materials used in the infilled panel were important; in general the consistency of the bricks was good, but the mortar was very variable.

FREE VIBRATION ANALYSES OF THE BOSPHORUS SUSPENSION BRIDGE

Professor Semih Tezcan and Dr. Muzaffer İpek

A general plan of the Bridge is given in Figure 1 (see the next page). A theoretical analysis has been carried out on the dynamic properties of the bridge to supplement the experimental survey. First, one half of the bridge was idealized into three different mathematical models composed of planar flexural and axial force members, as shown in Figure 2. The mathematical model for torsional vibration is the same as that for vertical vibration except that the flexural rigidities of the deck are replaced by the corresponding stiffness of a pure shear beam. Consequently, no rotational degree of freedom was necessary to define at the joints.

In the vertical vibrations, a total of 144 cable and deck members interconnected at 86 joints are assumed to represent one half of the bridge. The weight of the bridge is considered to be focussed at 23 discrete points. The focussed masses at the tower and the suspended deck are assumed to vibrate in horizontal and vertical directions respectively. Those on the cable are assumed to vibrate both in the vertical and longitudinal directions. Physical and geometric properties of the structural members have been taken from the Bosphorus Bridge Calculations, prepared by Freeman, Fox and Partners in 1968 (the dead load geometry of the main cable and the suspended deck was undefined in these calculations, so parabolic variations have been assumed for the centerline of main cable and the suspended deck for purposes of analytical investigations).

Vertical Vibrations

The equation of free vibration for an undamped multi-degree freedom structural system is

$$\begin{bmatrix} K_{11} & K_{12} \\ K_{12}^{T} & K_{22} \end{bmatrix} \begin{Bmatrix} X_s \\ X_p \end{Bmatrix} + \begin{bmatrix} 0 & 0 \\ 0 & M \end{bmatrix} \begin{Bmatrix} \ddot{X}_s \\ \ddot{X}_p \end{Bmatrix} = 0$$

in which $\{X_s\}$ = column vector of secondary degrees of freedom in which no vibration is assumed to take place, $\{X_p\}$ = column vector of primary degrees of freedom in which the actual vibration takes place, $[M]$ = diagonal mass matrix containing the lumped mass values corresponding to the primary vibrating directions. Taking advantage

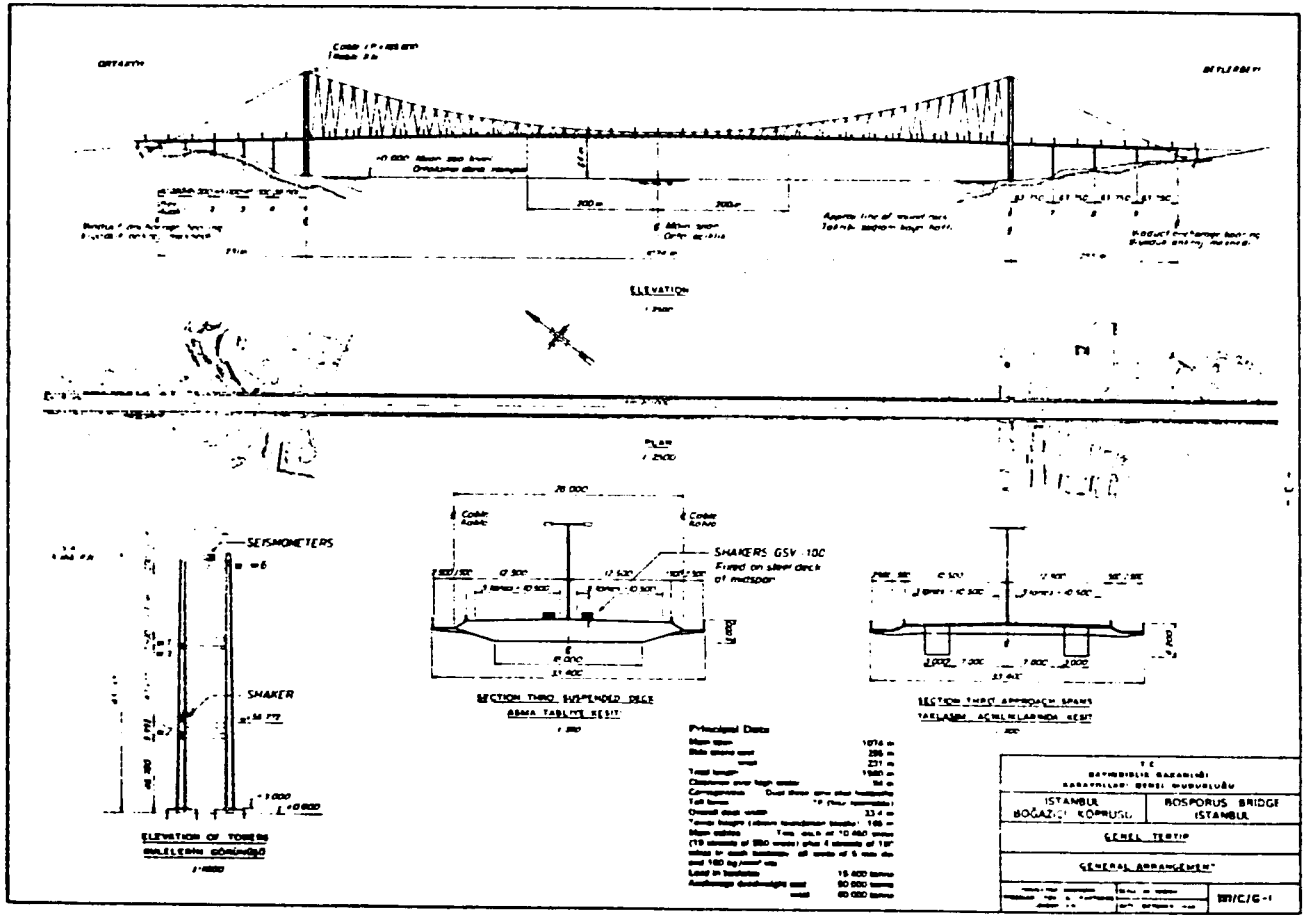
ELEVATION
PLAN
SEISMOMETERS
SHAKER
ELEVATION OF TOWERS
SHAKERS GSV 100
Fixed on steel deck at midspan
SECTION THRU SUSPENDED DECK
SECTION THRU APPROACH SPANS
Principal Data
ISTANBUL BOĞAZI KÖPRÜSÜ
BOSPORUS BRIDGE ISTANBUL
GENERAL ARRANGEMENT

FIGURE 1.

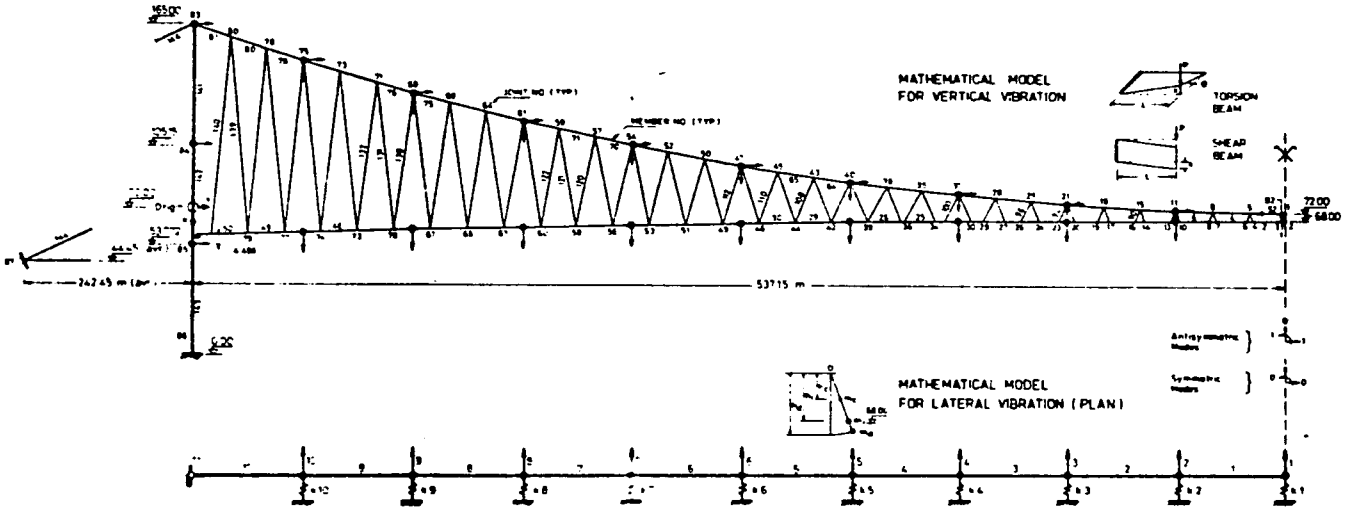
MATHEMATICAL MODEL
FOR VERTICAL VIBRATION
TORSION BEAM
SHEAR BEAM
53715 m
MATHEMATICAL MODEL
FOR LATERAL VIBRATION (PLAN)

FIGURE 2.

of the zero mass values along the secondary degrees of freedom, the above set of equations may be reduced to the size of primary degrees of freedom as follows:

$$[K^*]\{X_p\} + [M]\{\ddot{X}_p\} = 0$$

in which, the reduced stiffness matrix $[K^*]$ is

$$[K^*] = [K_{22}] - (K_{12})[K_{11}]^{-1} (K_{12})$$

In order to avoid the matrix inversion process, for large structures, the reduced stiffness matrix may be obtained by Gaussian elimination procedure which is more conaenient and simpler for computer application purposes.[1]

After the reduced stiffness matrix is obtained, the Jacobi method of diagonilization is applied to determine the eigenvalues and eigenvectors. The nonlinear stiffness matrix of the cable system, however, corresponds to the tangent stiffness condition at the dead load equilibrium geometry.

Mathematical Model for Torsional Vibrations

Normally, the torsional vibrations of a suspension bridge require a three dimensional analysis. It is possible, however, to reduce the three dimensional system into a planar form by making an analogy between the torsional and shear beam. In this analogy it is assumed that the bridge longitudinal centreline is undeflected. Shear distortion x of a cantilever shear beam is

$$x = \frac{PL}{GA}$$

in which L = cantilever length, P = acting load, G = shear modulus, A = cross sectional area. On the other hand, the vertical displacement x, at the extreme corner of a horizontal cantilever plate, subjected to a torsional motion by means of a point load P, is

$$x = \theta b = (PLb/GJ)\, b$$

Equating the above two deflections, a fictitious cross-sectional area A is obtained for the shear beam as follows:

$$A = \frac{J}{b^2}$$

A similar analogy may be established between the equations of motion of a cantilever shear beam and torsional beam as follows:

$$\text{Shear beam} \quad : \quad m\ddot{x} + \frac{GA}{L} x = 0$$

$$\text{Torsion beam} : \quad I_m\ddot{\theta} + \frac{GJ}{L} \theta = 0$$

in which m = mass per unit length of shear beam, I_m = unit length mass moment of inertia of torsion beam. When the coefficients of the second terms in the above equations, after dividing by the mass values, are equated

$$\frac{GA}{mL} = \frac{GJ}{I_m L}$$

the fictitious mass value for the analogous shear beam is obtained as

$$m = \frac{I_m}{b^2}$$

It is, therefore, possible to replace the suspended deck in torsional vibrations by a fictitious shear beam with a cross-sectional area of $A = J/b^2$ and unit length mass density of $m = I_m/b^2$. No flexural rigidity is assigned to the fictitious shear beam. After the suspended deck is idealized into a shear beam the rest of the mathematical model is identical to that of vertical vibrations, and hence, all calculations may be performed by the same computer program applicable to the vibrations of planar structures.

Mathematical Model for Lateral Vibrations

The focussed weights of the main cable and the suspended deck are transferred onto a fictitious straight horizontal beam passing through the elevation of the suspended deck at midspan. It is assumed that the weights of the main cable and the suspended deck vibrate about a constant center of rotation located in the longitudinal plane of symmetry. The motion of the bridge at any particular vertical section, therefore, is similar to that of a pendulum.

Tne fictitious weights m_i at the i'th mass point along the horizontal fictitious beam are obtained from

$$h_i m_i = h_c m_c + h_d m_d$$

in which h_i, h_c and h_d = distance from the centre of rotation of the pendulum and the lumped mass at the i'th point on the fictitious horizontal beam, the lumped mass on the main cable and the lumped mass on the deck, respectively. The spring constant k_i representing the stiffness of the bridge against horizontal motion, from the natural period expression of a simpler linear pendulum of height h_i, is

$$k_i = \frac{w_i}{h_i}$$

After the fictitious mas values m_i and also the fictitious spring constants k_i are evaluated, the dynamic analysis of a straight beam resting on elastic foundations yields the required dynamic properties of the bridge.

TABLE 1 NATURAL PERIODS (SECONDS)

HORIZONTAL		VERTICAL		TORSIONAL	
a	b	a	b	a	b
15.48 S	14.15	6.83 S	6.24	3.07 S	3.16
5.77 A	6.10	4.64 A	5.02	2.09 A	2.49
2.65 S	3.44	3.51 S	3.50	1.57 S	1.43
1.50 A	2.01	3.10 A	2.86	1.23 A	1.34
0.96 S	1.66	2.39 S	2.23	1.02 S	1.14
0.67 A	1.26	2.05 A	1.83	0.85 A	0.92
0.49 S	—	1.67 S	1.57	0.79 A	—
0.38 A	—	1.45 A	1.34	0.78 S	—
—	—	1.22 S	1.22	0.74 S	—
—	—	1.09 A	1.08	—	—
—	—	0.97 S	0.95	—	—
—	—	0.89 A	—	—	—

Analytical Study

Experimental Study

S = Symmetrical Modes

A = Anti-symmetrical Modes

Nonlinearity of the System

The nonlinearity of the bridge structure is included in the dynamic analysis by making use of the concept of tangent stiffness matrices.[2,3] Only geometric nonlinearities are included. The presence of axial forces corresponding to dead load conditions, tension positive, are included in the stiffness matrices of all the structural members. In order to reduce the amount of computational efforts, only one half of the bridge is investigated. Average of the two side span dimensions and cable tensions are used in the calculations. Degrees of freedom of the nodes at midspan are appropriately selected to suit to the conditions of symmetrical and anti-symmetrical modes, as shown in Figure 3 (see the next page). Results of analytical investigations are summarized in Table 1 and also in Figures 3 to 8. The ambient vibration study which we have also carried out (unpublished) gives results (Table 1) which are in good agreement with the analytical results.

REFERENCES

1. *S.S. Teżcan and M. İpek, Proc. Int. Symp. Digital Computer Appl. in Eng., Tech. Univ., İstanbul, 1970.*

2. *S.S. Tezcan, Proc. Int. Symp. on Suspension Bridges, Lab. Nac. Eng. Civil, Lisbon, 1966.*

3. *S.S. Tezcan and S. Cherry, Proc. 4th World Cont. Earthq. Eng., Santiago (1969).*

DISCUSSION

Dr. Çelebi asked what lateral load was allowed for in the design, to cover earthquake forces: Dr. İpek said that no special provision was made for seismic activity, but the dynamic calculations allowed for 10% static force. In reply to further questions, Dr. İpek said that the vertical models automatically made combined allowance for the cables and decks; in the horizontal model mean values for the cables and deck were used, and the idealised cable and deck system was regarded as a pendulum. In reply to Dr. Gülkan, Dr. İpek said that force vibration tests and ambient vibration tests under strong winds were conducted before the bridge was open to traffic.

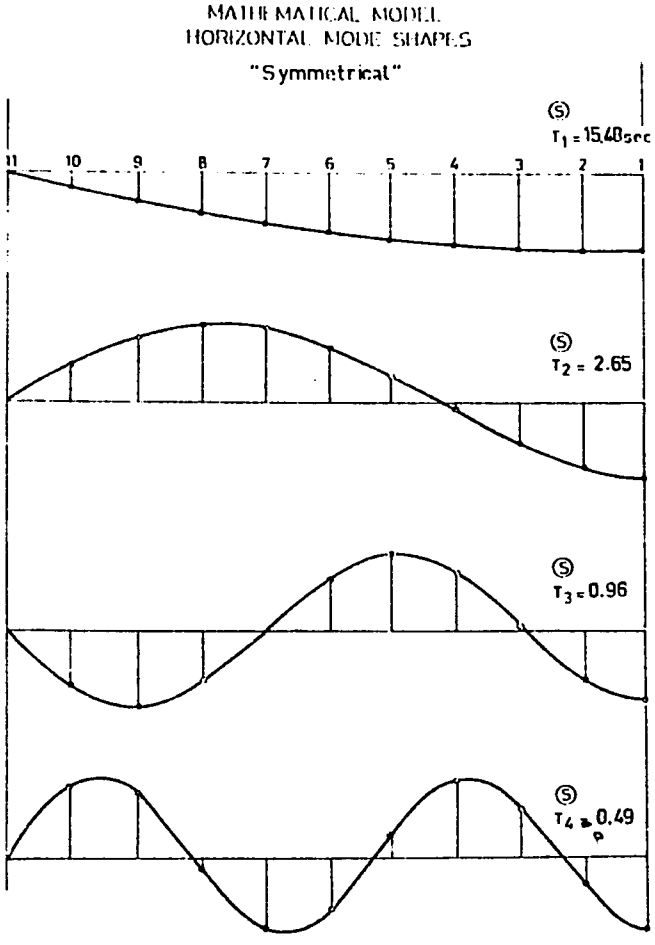

FIGURE 3

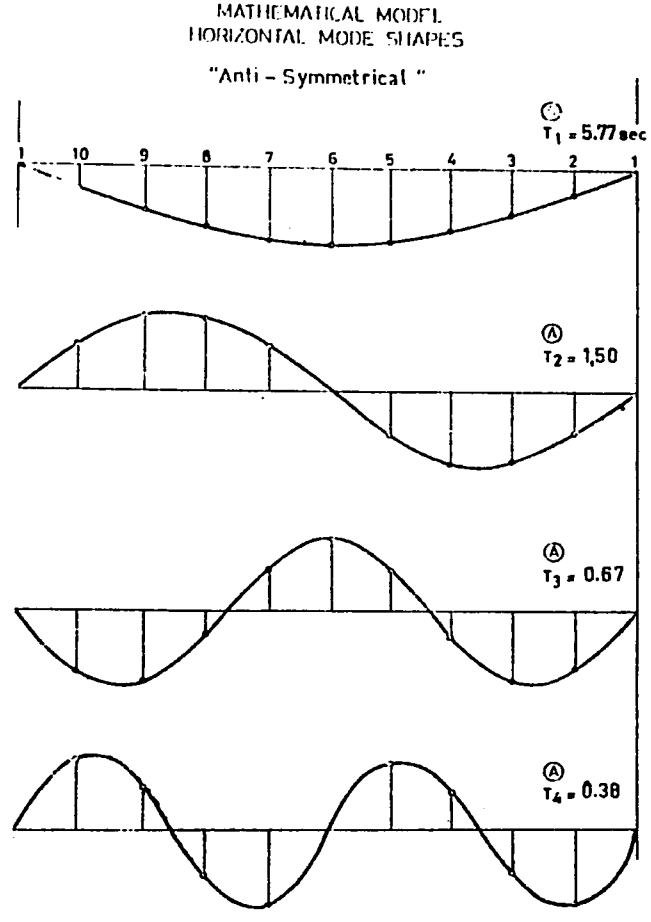

FIGURE 4

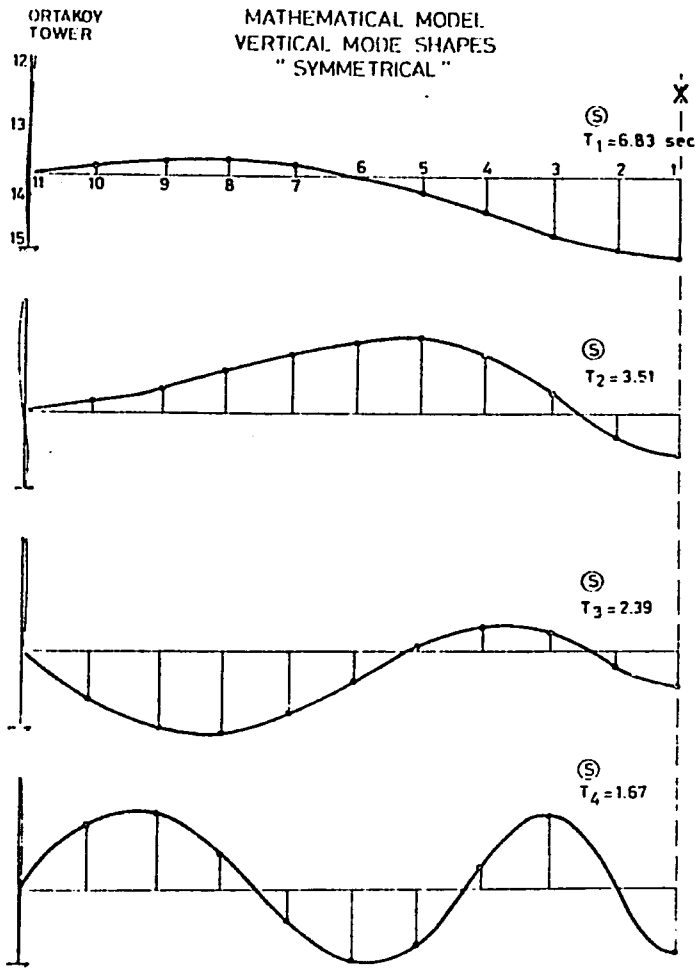

FIGURE 5

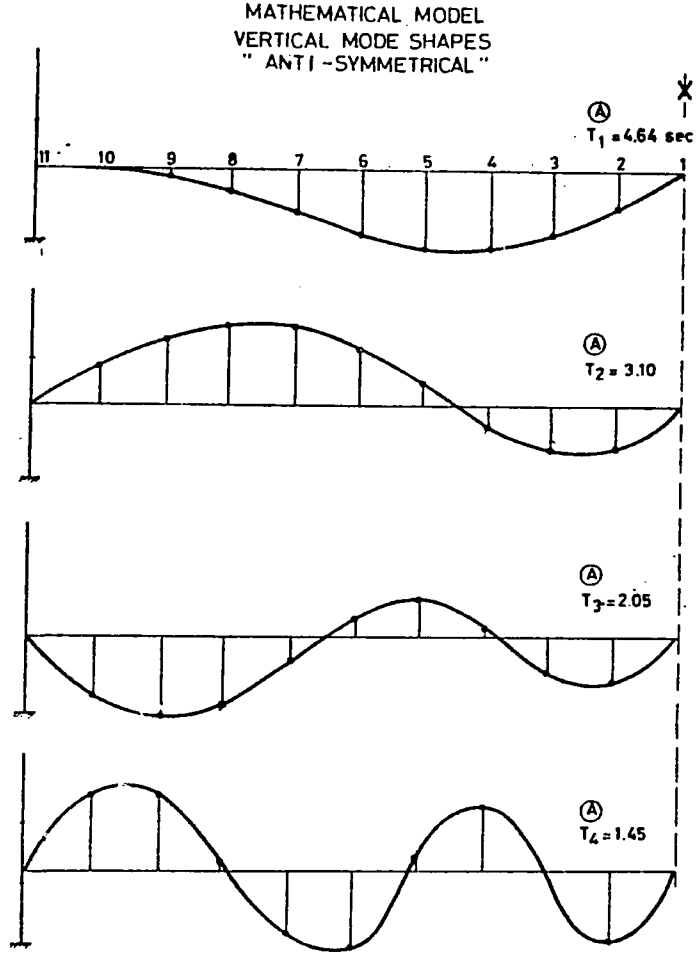

FIGURE 6

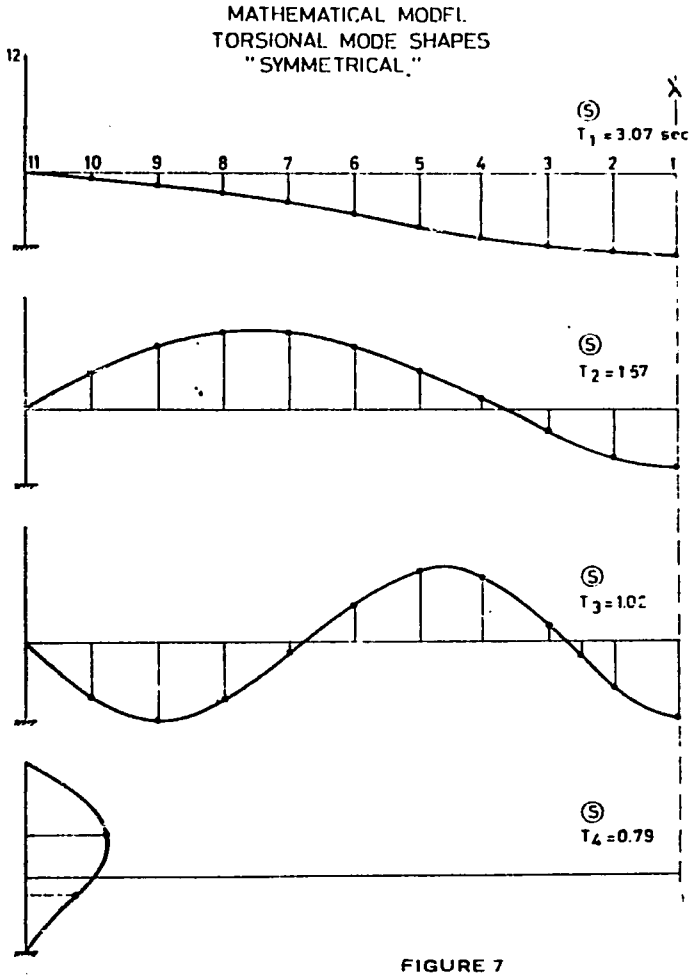

FIGURE 7

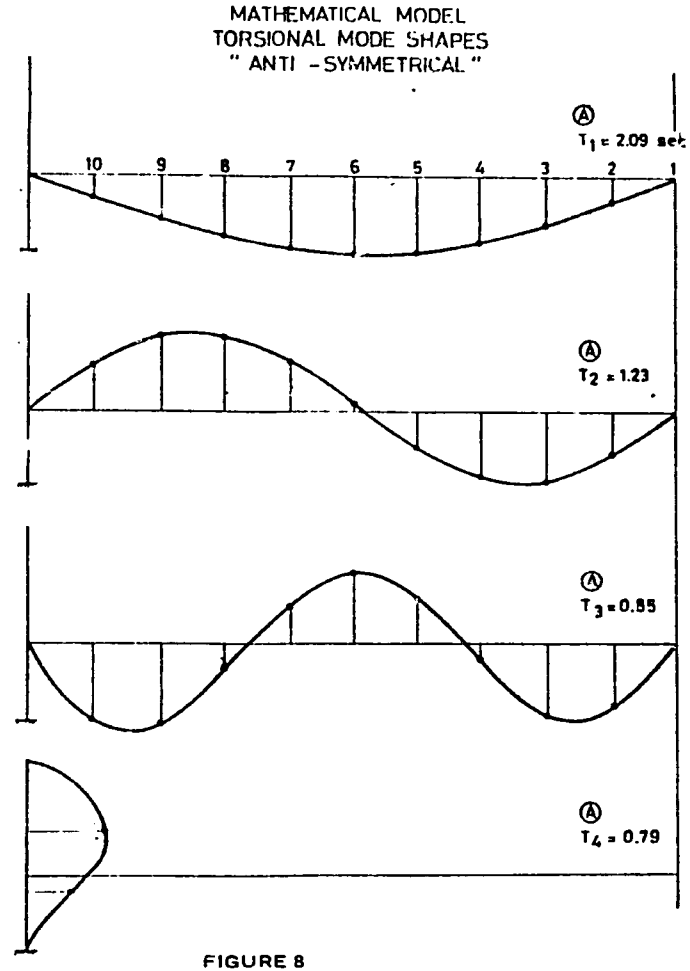

FIGURE 8

A MODEL FOR SHEAR PINCHED HYSTERESIS LOOPS

Dr. M. Çelebi

The hysteretic behaviour of reinforced concrete framed structures during earthquakes varies under different conditions. The normal shape of hysteresis loop expected as a result of reversed loading and, therefore, change of sign of curvatures in a shear span can be represented by a Ramberg-Osgood model. Other mathematical representations of hysteretic behaviour have been adopted: one is that of an elastoplastic behaviour, but a more realistic one is the degraded stiffness hysteresis loop.[1] Park, Kent and Sampson[2] theoretically formulated the hysteretic behaviour by using material characteristics and finite element approach.

One variation from the Ramberg-Osgood is due to the presence of high nominal shear stresses v_u in the reinforced concrete beams. The nominal shear stress is dependent on the shear span to depth ratio, and the percentage of longitudinal steel. Due to the presence of the nominal shear stresses, the shape of the hysteresis loops change, resulting in a decrease of area of the hysteresis loop and a change in the instantaneous stiffness represented by the slope of the hysteresis curve.

Various laboratory tests[1,3] have shown the conditions under which shear pinching takes place.

Importance of Shear Pinching

This occurs due to the type of cracking that develops as a result of the presence of nominal shear stresses. First diagonal cracking takes place in the shear spans under reversed loading. At unloading, a more or less constant stiffness is observed, but at the moment the load reaches zero, the stiffness of the cracked portion is decreased due to the opening of cracks; at a very slight increase of load in the opposite direction the displacement is greater. Therefore, the stiffness is decreased in the new loading case when the load is increasing from zero. This also results in a decrease of the area of the hysteresis loop.

The change in stiffness is important because of its influence on non-linear analyses. The decrease in the area of the hysteresis loop is important because it means a decrease in the equivalent damping fraction ξ as formulated by Jacobsen[4] and Hudson.[5]

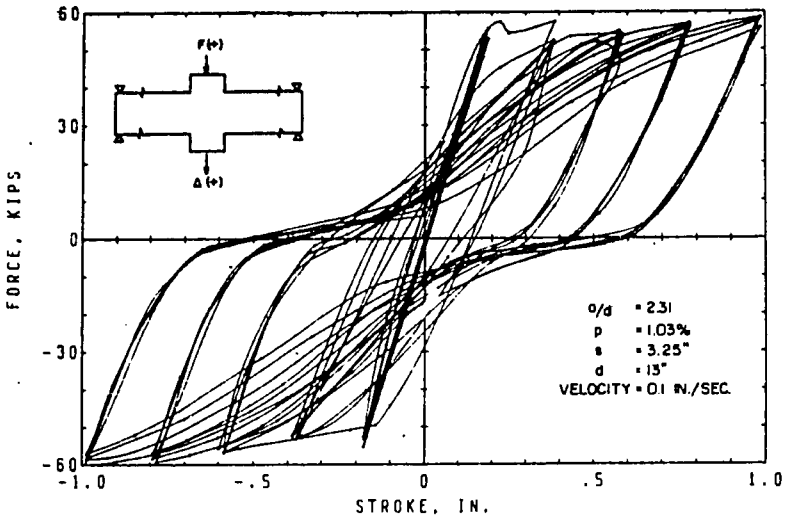

FIGURE 1
Shear Pinched Hysteresis Loop (Experimental)

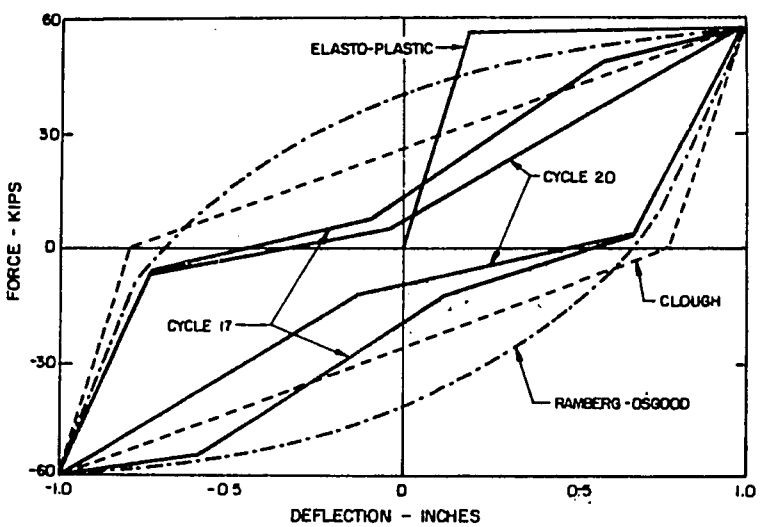

FIGURE 2
Comparison of Shear Pinched Loop

Accordingly, in the equation

$$\xi = \frac{1}{4\pi} \frac{\Delta W}{W_i}$$

it is seen that ξ is directly proportional to ΔW which is the area of the hysteresis loop. W_i is the energy defined by the area under triangle formed by the yielding slope at a particular value of displacement (or ductility) for which ΔW is considered. In other words, due to shear pinching, energy absorption capability of shear spans are decreased.

Test Results

Figure 1 shows the hysteresis loops of a component with two shear spans and a/d ratio of 2.31 and p = 1%.[3] This emphasizes the occurrence of shear pinching at different displacements (or ductilities), and also the variation of shear pinched hysteresis loops from the mathematical models used previously. Figure 2 shows a comparison of two hysteresis loops with the Ramberg-Osgood, the degraded stiffness and the elasto-plastic models.

Figure 3 (see the next pages) summarizes the results of a series of tests conducted in Japan by Umemura, Aoyama and Ito. The solid lines are traced from the actual hysteresis loops and the broken lines have been added to show the actual hysteresis loop being completed to Ramberg-Osgood hysteresis loops.

The change of loop stiffness against ductility and the a/d ratio as a parameter are shown in Figure 4[3] (see page 167). The hysteresis loops in Figure 1 are part of these series. It is seen that for the same p of 1%, when a/d ratio is smaller (that is, when the nominal shear stresses are higher), the rate of decrease of stiffness is faster.

Proposed Model

A new mathematical model (Figure 5 on page 168) can be derived from Figure 1 and 3 and other shear pinched hysteresis loops, by subtraction of two small Ramberg-Osgood hysteresis loops from a larger Ramberg-Osgood hysteresis loop. The larger loop can always be defined in terms of P_y, the load at yielding, and Δ_y, the displacement at yielding. Both P_y and Δ_y can be estimated for a given shear span and section properties. The two smaller Ramberg-Osgood models can be defined byparameters of the larger loop such as P_o, x_o, P_y, Δ_y, α and r. The shaded area then will more realistically represent the shear pinched hysteresis loops.

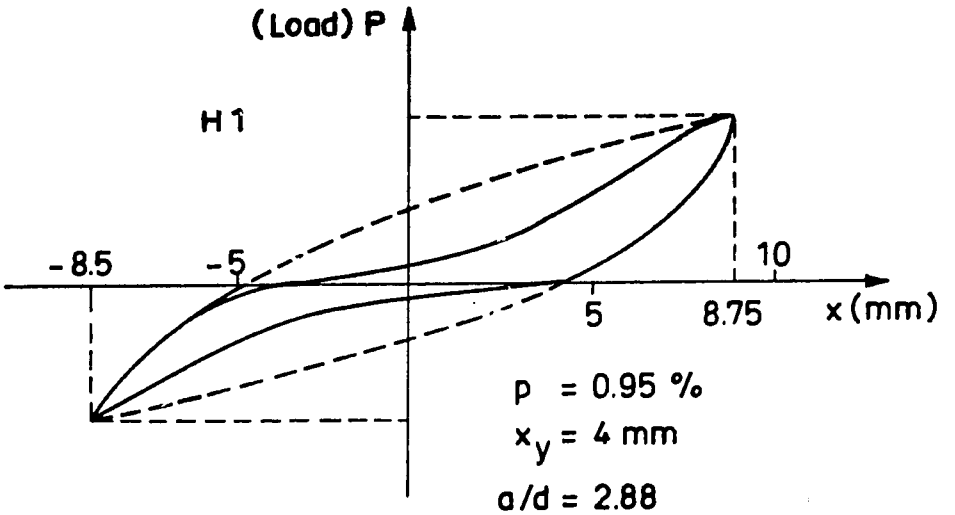

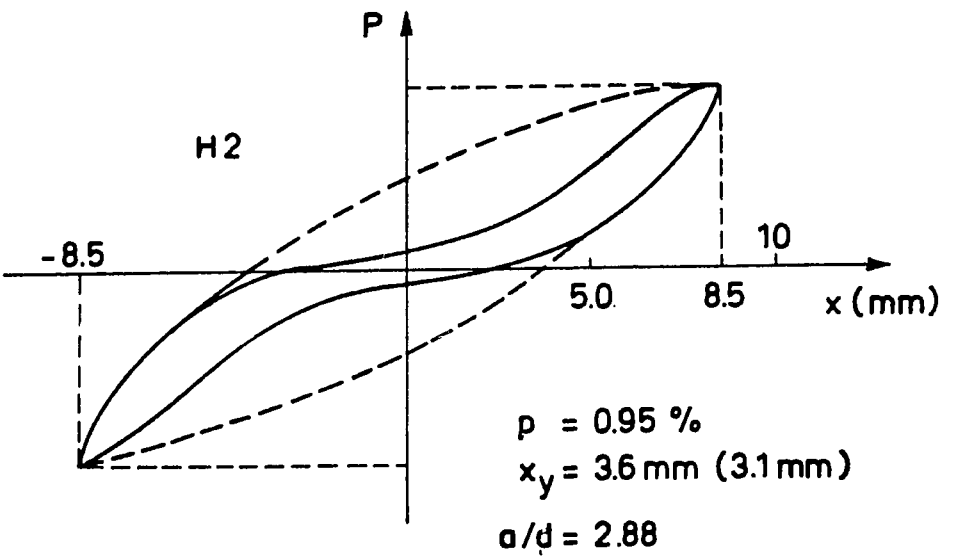

FIGURE 3a. HYSTERESIS LOOPS OF JAPANESE TESTS

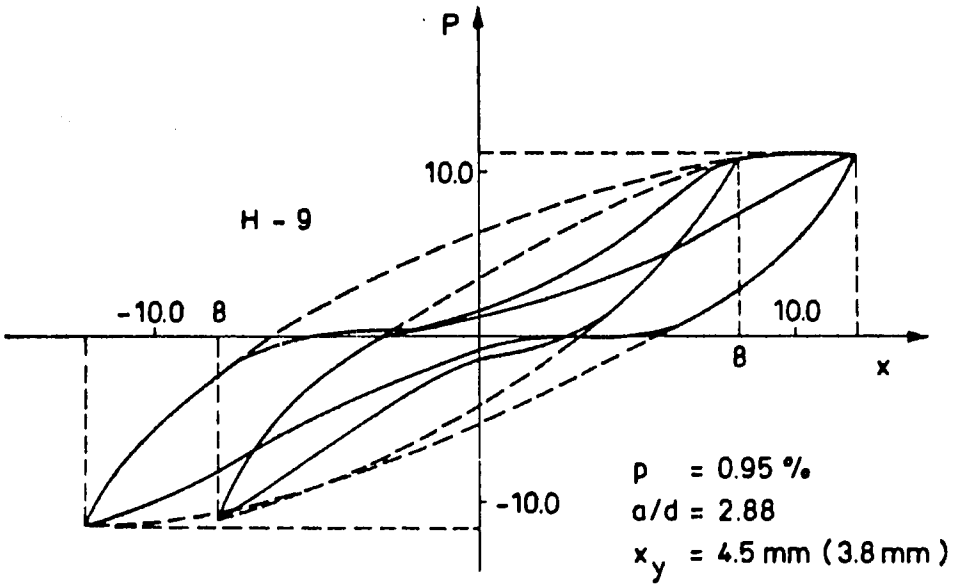

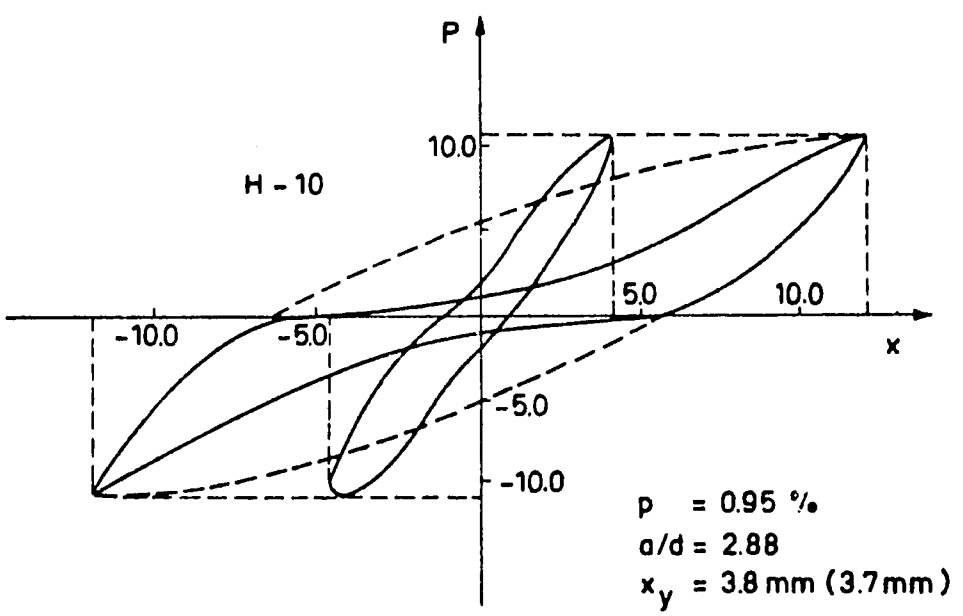

FIGURE 3b. HYSTERESIS LOOPS OF JAPANESE TESTS

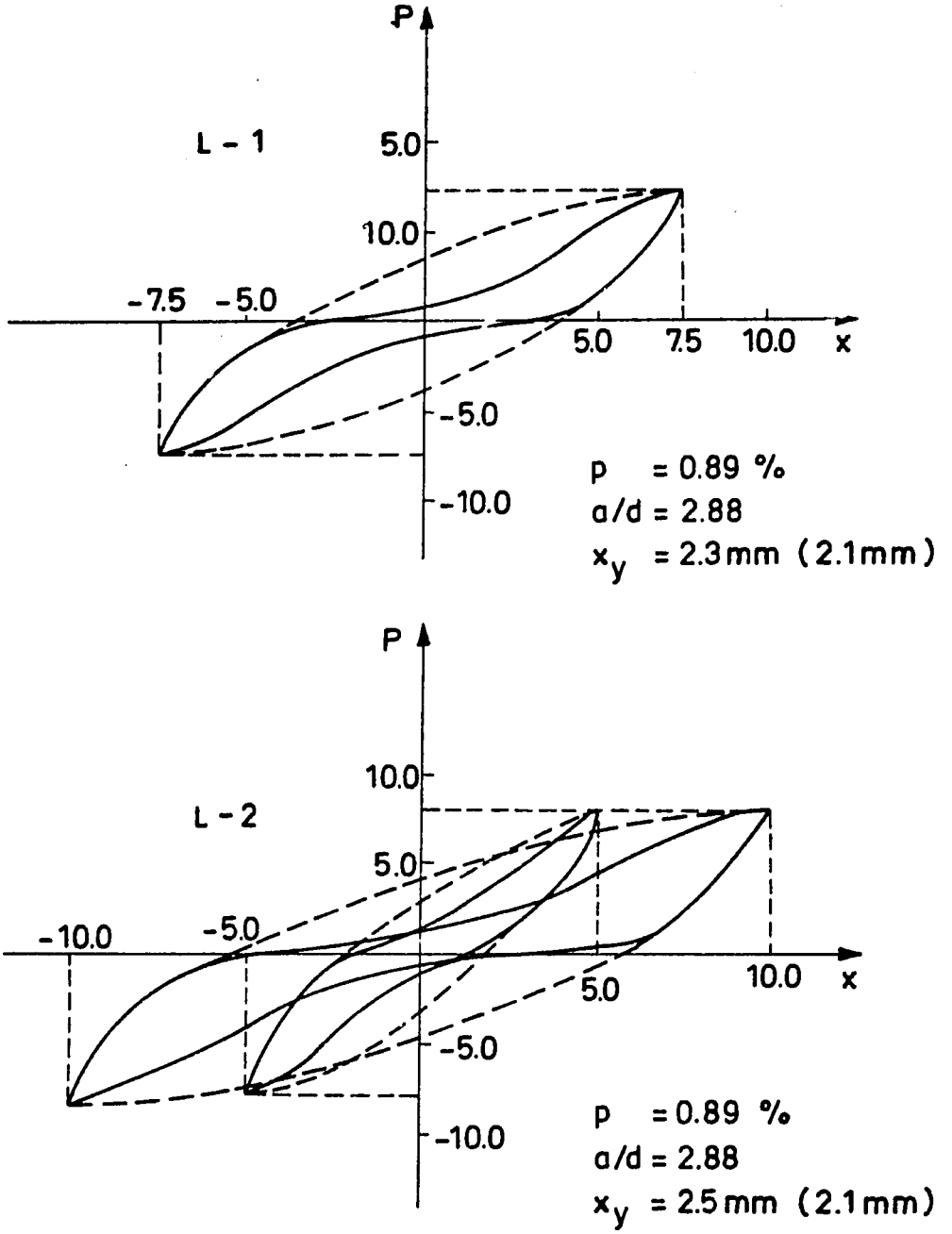

FIGURE 3c. HYSTERESIS LOOPS OF JAPANESE TESTS

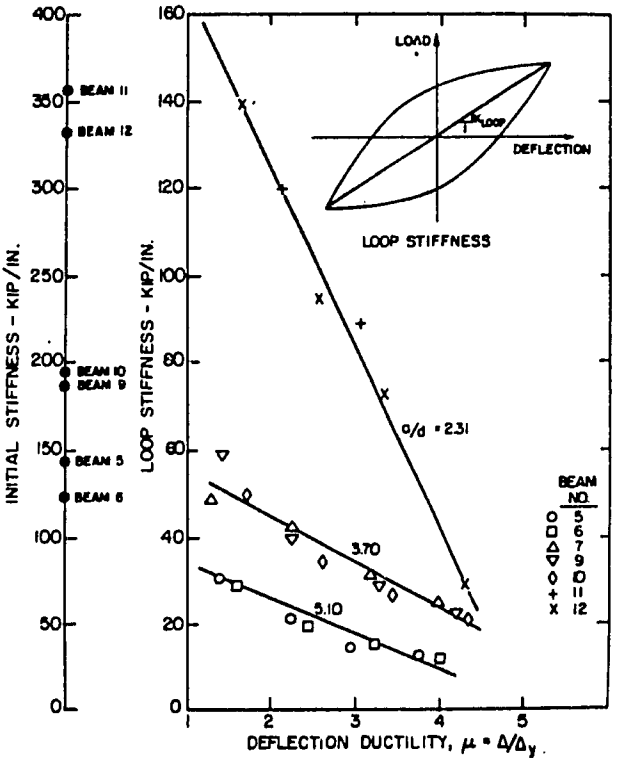

FIGURE 4. CHANGE OF STIFFNESS

REFERENCES

1. *R.W. Clough, Struct. Eng. Lab. Rep. 66-16. Univ. Calif., Berkeley, 1966.*

2. *R. Park, D.C. Kent and R.A. Sampson, Proc. Amer. Soc. Civil Eng., ST7 (1972).*

3. *M. Çelebi and J. Penzien, Earthq. Eng. Res. Centre Rep. 73-4. Univ. Calif., Berkeley, 1973.*

4. *L.S. Jacobsen, Proc. 2nd World Cong. Earthq. Eng., Tokyo, 1960.*

5. *D.E. Hudson, Proc. 3rd World Cong. Earthq. Eng., Auckland, 1965.*

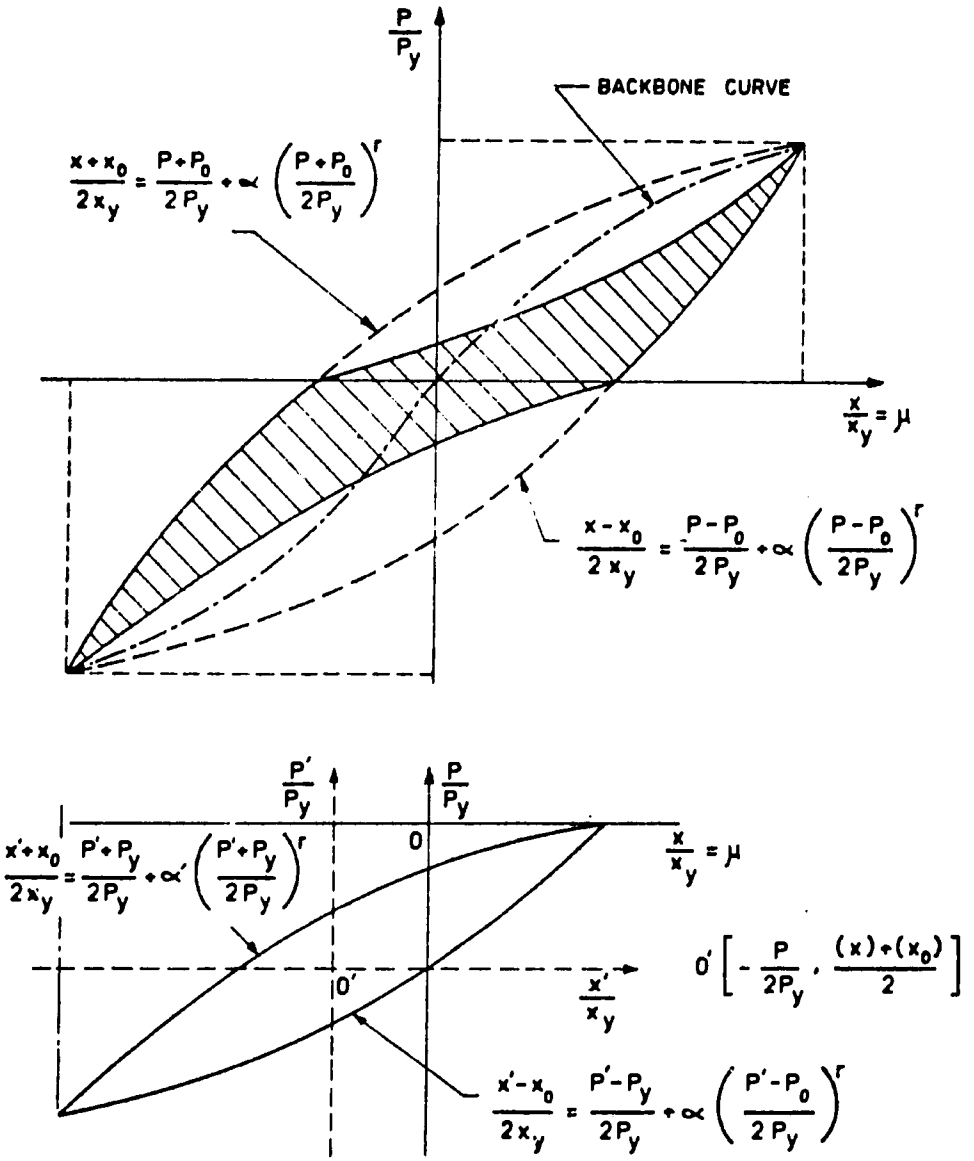

FIGURE 5. PROPOSED PINCHED HYSTERESIS LOOP

DISCUSSION

Dr. Keightley asked why the loop had reverse curvature. Dr. Çelebi said that as unloading proceeded towards zero load the diagonal cracks open so there is very little resistance: the first increment of load in the reverse direction causes a greater displacement than before; changing the shape, stiffness, etc. Dr. Gülkan commented that the effect of shear pinching makes the curves extremely unstable; he added that the model described considered only equal displacement in either direction, whereas in an earthquake symmetrical displacement never occurred. Dr. Çelebi said that some tests with uneven displacement had been done, but the results were not yet available.

ANALYSIS OF A HOSPITAL DAMAGED BY THE BURDUR EARTHQUAKE

Mr. Alkut Aytun and Mr. Nejat Bayülke

The Burdur earthquake of May 12, 1971 had a magnitude 6.2 (PAS) and the epicentral coordinates were 37.°6 N, 29.°8 E (NOAA) The loss of life was 57; 150 people injured, 1524 houses were damaged beyond repair or collapsed, and 4878 houses had moderate to light damage. The isoseismal map of the earthquake is given in Figure 1 (see the next page). From the past earthquake records, the observed maximum intensity for this region was VIII MM.

The hospital in Burdur was completed in 1968: it was a five-storey reinforced concrete frame building with hollow concrete block filler walls. Furnace slag was used as aggregate for the blocks.

The building has a rectangular plan (Figure 2) and the bearing of the axis along the longer dimension of the building was W-31-S. It seems that the design calculations of the building were not in accordance with the acceptable practice for earthquake zones. For columns, beams and slabs, the minimum requirements of the building code had been adopted, without going into calculation. There had been no consideration of earthquake forces, though the city was in the earthquake zone of the first degree.

ISOSEISMAL MAP OF BURDUR, TURKEY, OF MAY 12,1974

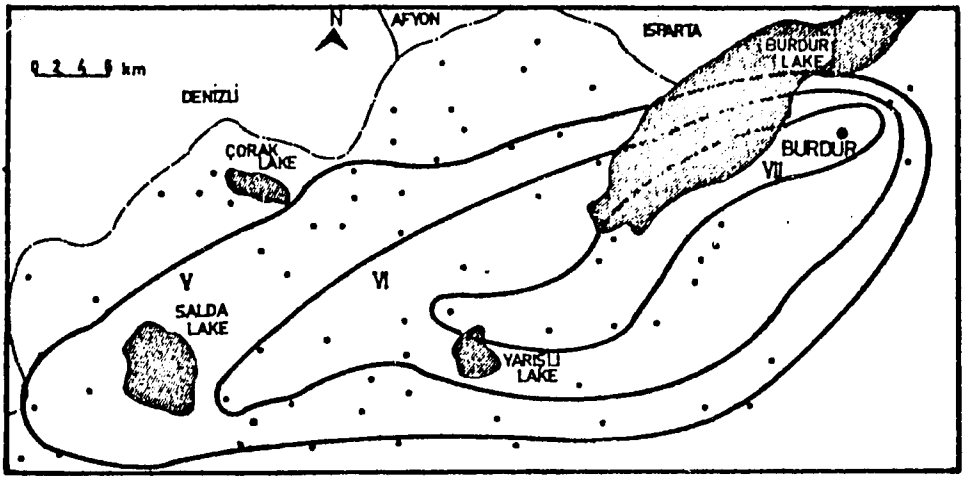

Figure 1.

PLAN OF THE HOSPITAL BUILDING (UNSCALED)

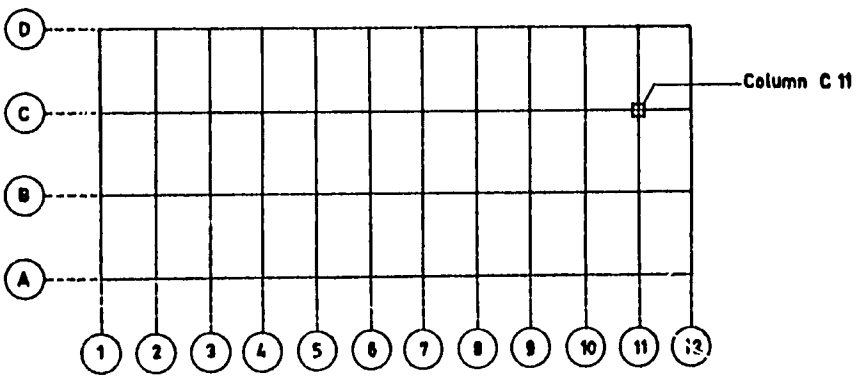

Figure 2.

On the front and back of the building, the window lintels had been cast together with the columns. The window sills had been made from highly rigid and strong concrete of compressive strength about 500 kg/sq cm. The columns had been laterally restrained both at the top and bottom levels of windows. In this way, the free length

of the outer columns of the ground floor had been reduced from 2.70 m to 1.40 m, which is the height of the window opening. Thus, the relative rigidities of the outer columns were extremely increased, considering deflections along the longer dimension of the building.

The D-Method of Professor Muto has been used in the calculation of the rigidities of the structure. The length of the outer columns were assumed as 1.40 m, while the length of the inner columns were taken as 2.70 m. The contribution of the filler walls to rigidity is neglected: it is believed that this is realistic, as the hollow concrete blocks can easily be broken under lateral loads. The first mode vibration period of the building in the longer direction, was thus found to be 0.53 sec.

Damage Caused by the Earthquake

All the columns of the ground floor were damaged, and the filler walls had large shear cracks and several of them had collapsed. On the upper floors the columns

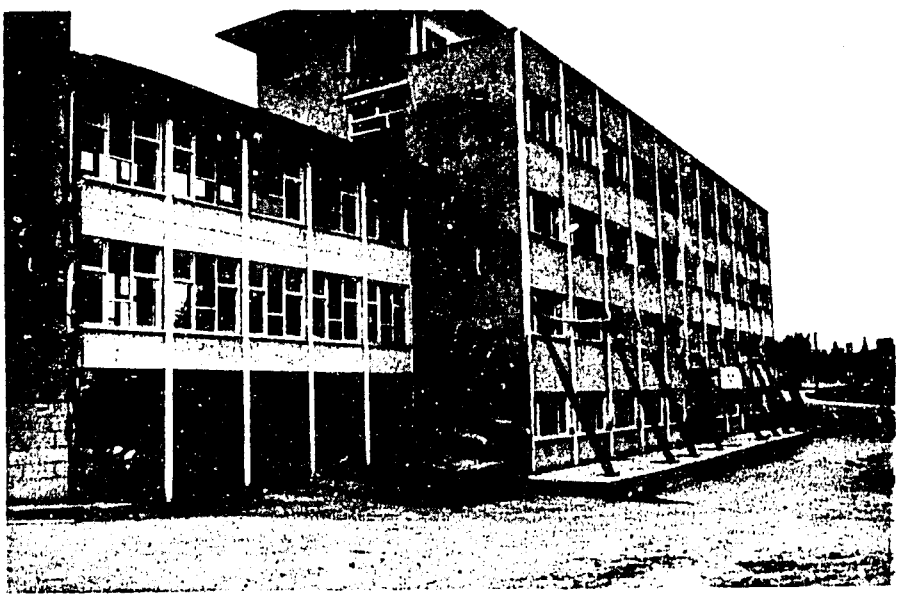

Figure 3. View of hospital building after the earthquake.

had no damage, while the extent of the damage in the filler walls decreased gradually. This fact is seen in Figures 4 to 7 which also point out to the fact that the upper stories

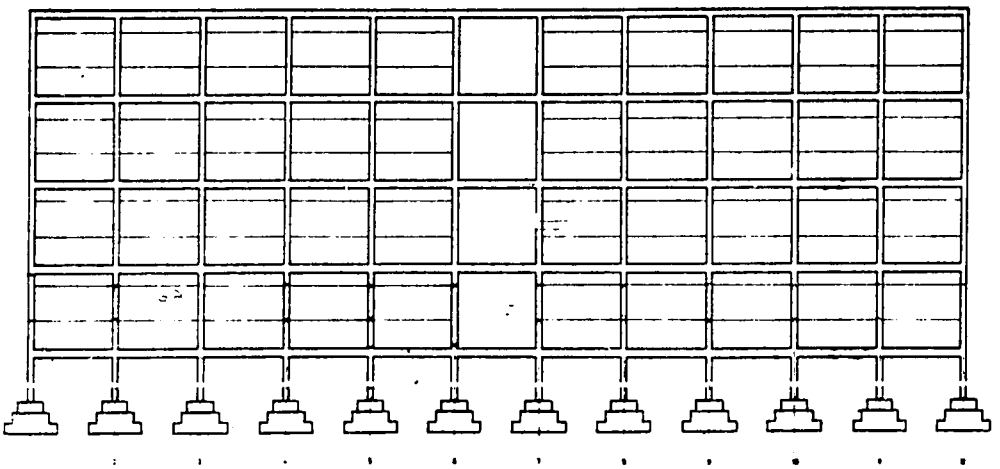

Figure 4. Cracking Pattern on A-Frame

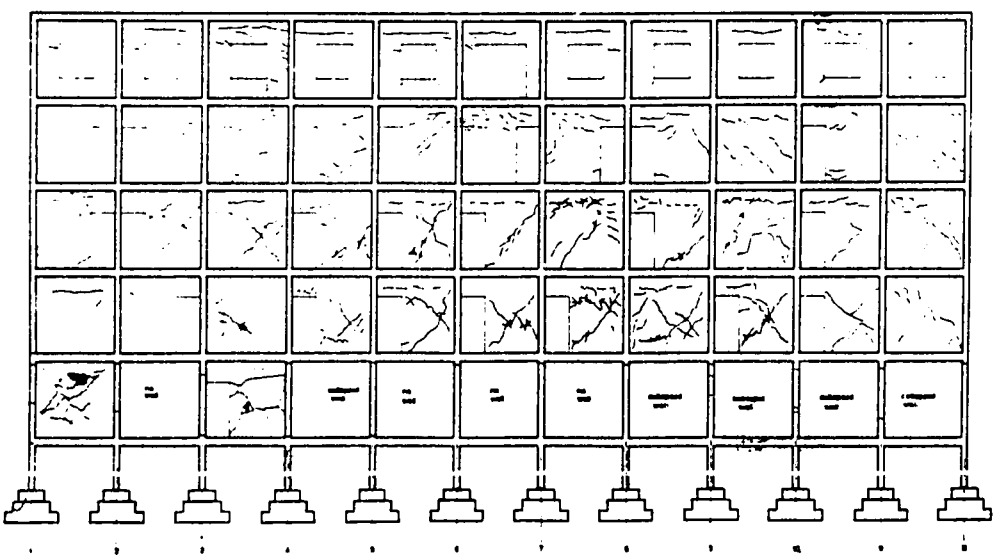

Figure 5. Cracking Pattern on B-Frame

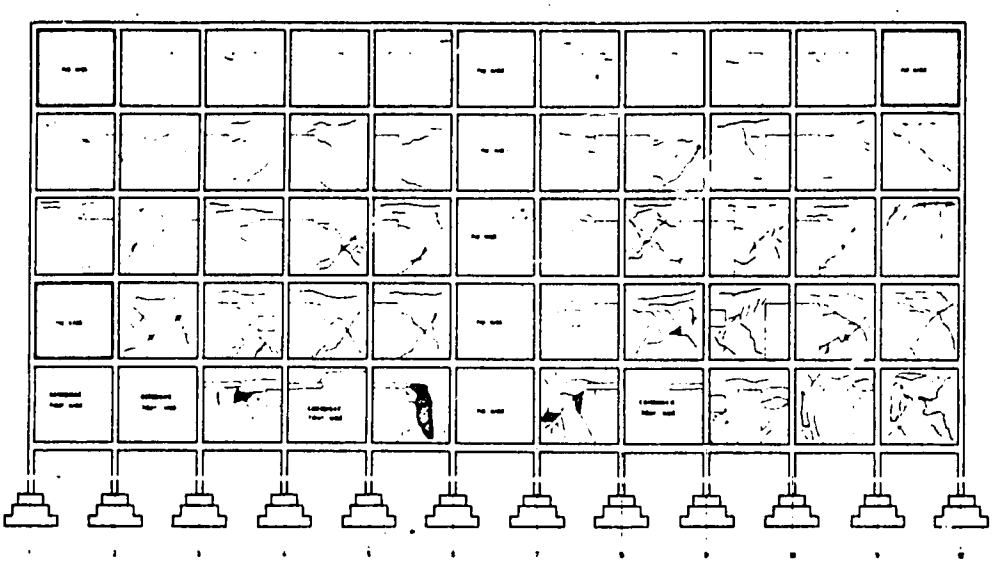

Figure 6. Cracking Pattern on C-Frame

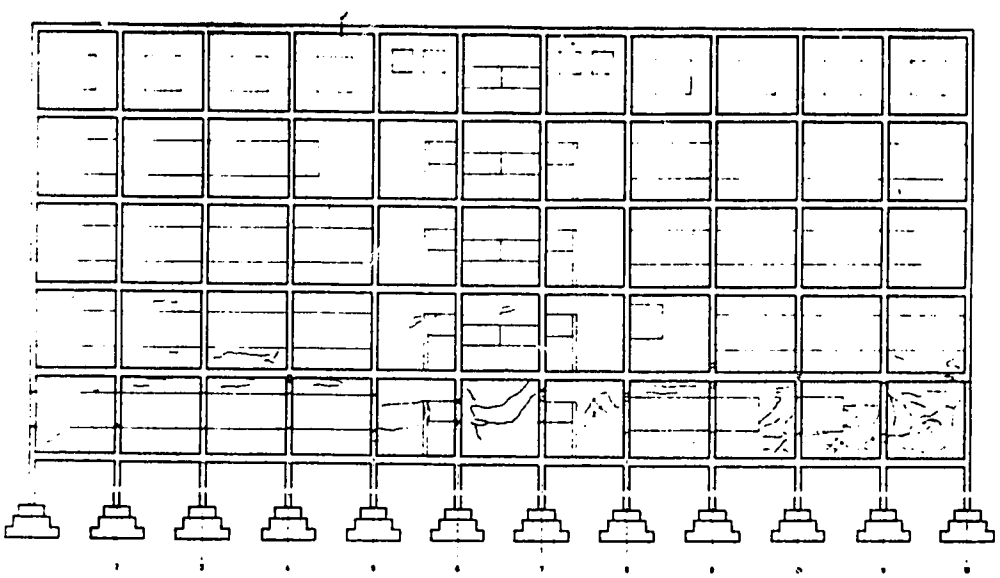

Figure 7. Cracking Pattern on D-Frame

too, had experienced considerable amount of relative displacement in decreasing rate with storey number. On the whole, the building had displaced laterally only in the ground floor. There was no permanent relative displacement between any of the upper floors. The building behaved as if it were a single degree of freedom system, resting on the columns of the ground floor. Finally, the whole mass had a permanent displacement towards W-31°-S direction. The permanent horizontal displacements of the ground floor column-tops were measured. There were large variations between the individual measurements. As there were no permanent deformations in floor slabs, it was concluded that a certain part of the differences were actually due to building errors. An average value of 2.8 cm was taken as the actual permanent displacement for all ground floor column-tops.

All the ground floor columns along A and D axes had bending failure in the longer direction of the building, at the top and bottom level of the window openings (Figures 8 and 9). As mentioned before, the reinforced concrete window lintels and high-strength-concrete window sills reduced the effective length of the columns along the A and D axes. The other ground floor columns were not subjected to this kind of shortening. In some of the columns of the inner axes, compression failure due to bending were observed, while the rest of them failed in tension mode due to bending (see bending moment-axial force interaction diagrams in Figure 10 on page 176).

Analysis of the Damage

A lateral force distribution, as shown in Figure 11 (on page 177), is assumed. From this distribution, the total lateral force coming to the ground floor columns is calculated. Since there was no column or other structural damage in the upper stories, it was assumed that the upper structure behaved as a single degree of freedom system, and only the ground floor columns were analysed. This was believed to be sufficiently realistic, considering only large deformations. Cracking in the filler walls along the shorter dimension of the building indicate that the structure was forced in that direction too, but a comparison of the extent of the non-structural damage leads to the conclusion that the structure was mainly affected along its longer dimension. Another report on this earthquake[2] concludes that the direction of the destructive shocks was not much different from damage to other structure. Furthermore, this building is more sensitive to lateral forces in its longer dimension.

The axial load coming to each column is calculated, taking into account the changes due to lateral loads. The concrete compressive strength was assumed as 100 kg/sq cm and the steel strength as 2200 kg/sq cm in the calculation of bending moment-axial force interaction curves of the ground floor columns. The moment affecting each column due to vertical and lateral forces is calculated along with axial force, and using

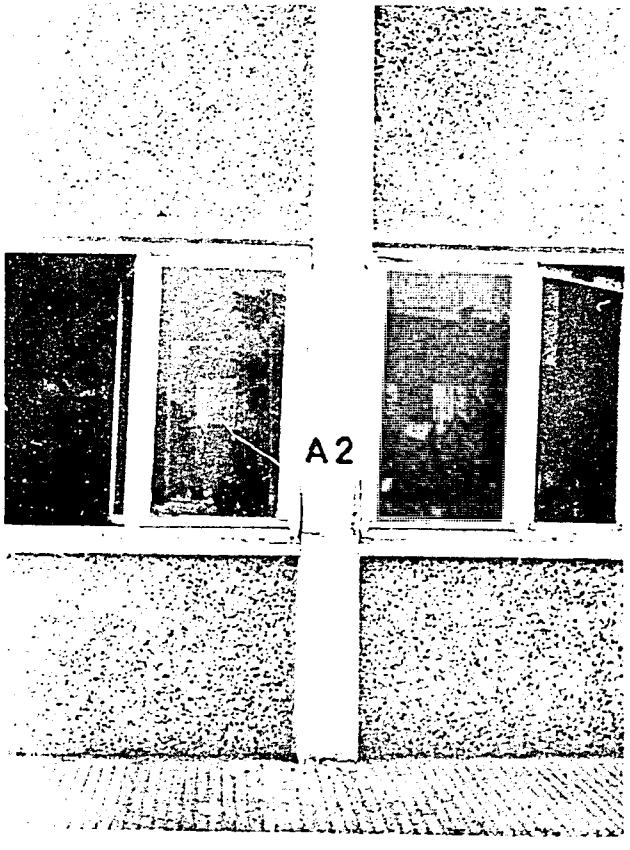

Figure 8. Damage of A2 Column, ground floor

Figure 9. Damage of B6 and B6 Columns in ground floor

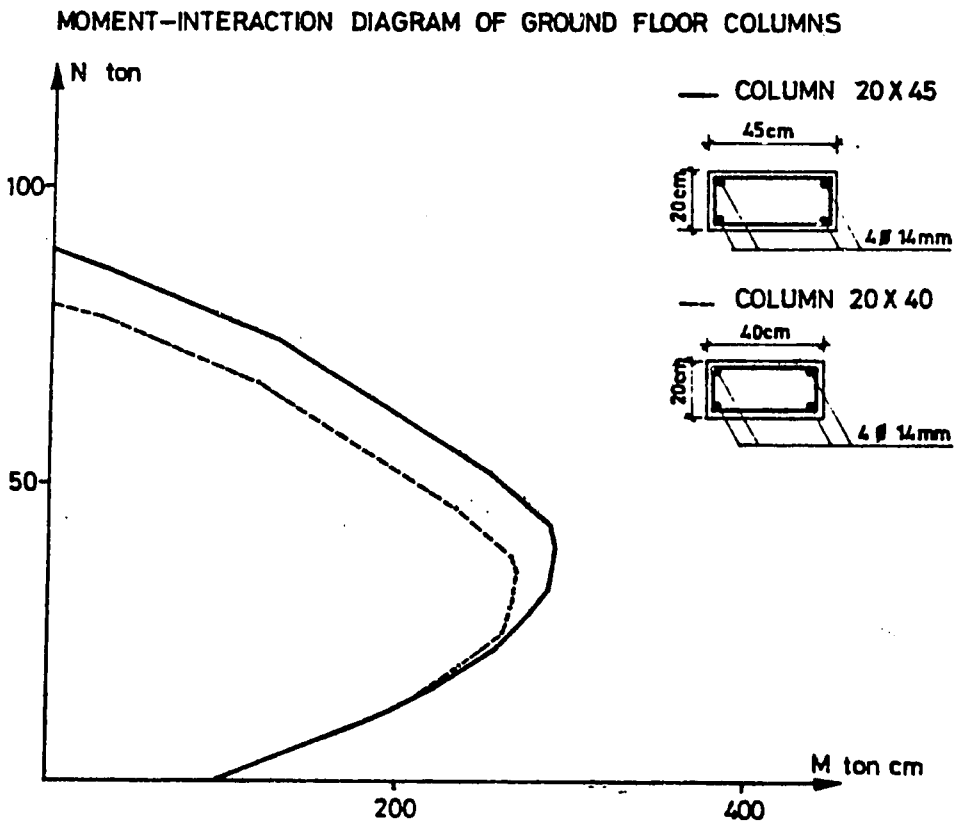

Figure 10.

the interaction curves, the moment that the section can take is compared with that actually present. If the former is less than the latter, than the column is safe. The lateral force is then increased until the first column failed. In the analysis, first the effect of torsion due to unsymmetry of the weight (top floor) has been considered, but it was found to be of minor effect, and later on, was neglected in the calculations. When a column reached its capacity, it was assumed that it sustained no greater shear force afterwards. The remaining lateral force is then distributed in proportion with the rigidities of the elastic columns. The outer columns failed first, because they were extremely rigid com-

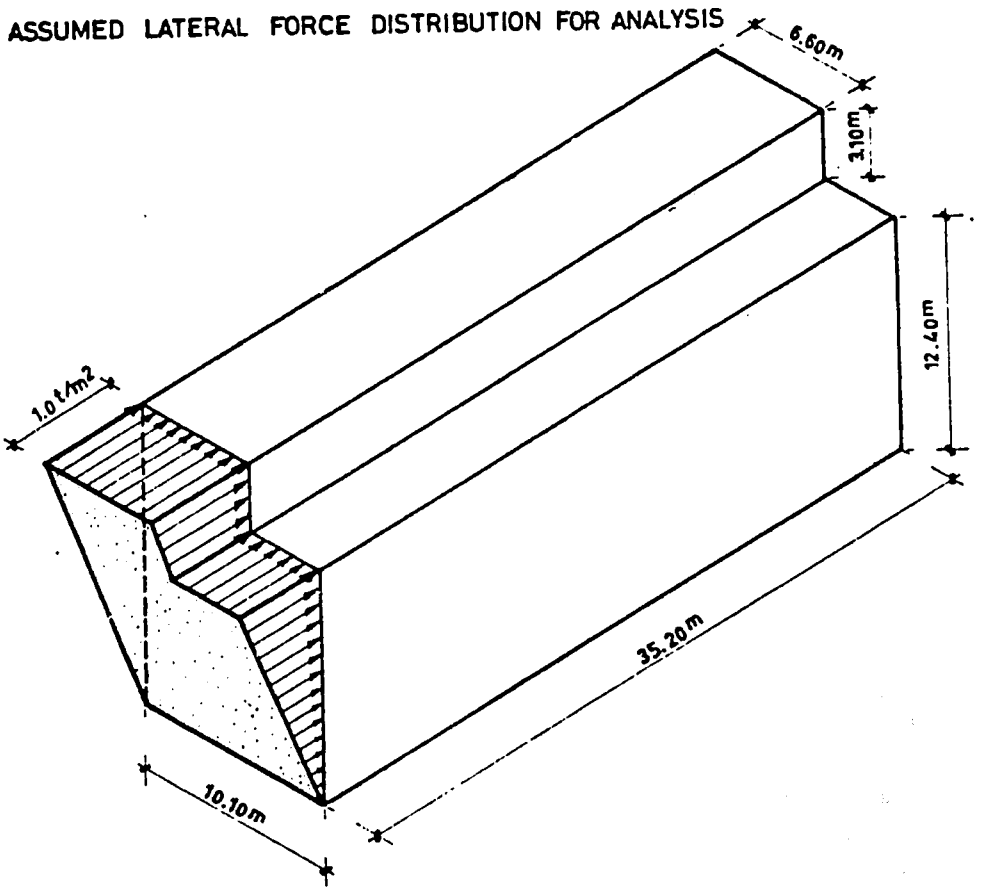

Figure 11

pared to the inner columns and, before the failure of outer columns, the inner columns received only a very small portion of the base shear force.

Columns A-1 and A-12 failed first when an equivalent static force coefficient C = 0.056g was applied. At 0.058g, columns D-1 and D-12 failed, and at 0.060g the rest of the columns of the A-axis and columns D-6 and D-7 failed. At C = 0.061g the remaining columns of the D-axis failed. After the failure of all outer columns B-1, B-12, C-1 and at 0.084g columns C-12, B-3, B-10, B-11 failed. The rest of the ground floor columns failed at a lateral static equivalent force coefficient C = 0.085g. Most of the columns failed in tension mode, but there were also some bending-compression failures (e.g. B-12, B-3, B-10 and B-11).

The actual first mode vibration period of the damaged structure was measured by a periodmeter developed by one of the authors, with human force as excitation. The first mode period of the structure in the longer direction was found to be 0.56 sec. as compared to 0.53 sec. found by analytical calculations. It should be mentioned that, after the earthquake, the ground floor of the building had been braced by 40 cm. diameter timber logs both in the longer and shorter dimensions (Figure 3). Therefore, the actual period of the damaged structure was certainly larger than 0.56 sec. The measured period in the shorter dimension was 0.45 sec.

The yield displacement of the first failed column A-1, has been calculated as 1.11 cm. The average max. displacement of the columns of the ground floor was obtained as 2.8 cm. This gives a ductility ratio of 2.55. Since the column A-1 failed at C = 0.056g, the minimum static equivalent lateral force coefficient is about 0.11g. Even though the length of the columns were reduced considerably, still they were slender in the general sense, and bending failures occurred well before the shearing stresses reached a critical level. This has also been checked numerically.

REFERENCES

1. *K. Ergin, U. Güçlü and Z. Uz, Geophysics Inst., İstanbul Tech. Univ., Publ. 24 (1967).*

2. *S. Tezcan, M. İpek and A. Altınok, İstanbul Chamber Civil. Eng., Publ. 6 (1971).*

DISCUSSION

In reply to Dr. Keightley, Mr. Aytun said that the building was subsequently demolished. Mr. Dülgeroğlu asked why the central columns on the D-axis failed before the intermediate columns: Mr. Aytun said that the corner columns failed first and then the central columns failed because of differing heights, causing differences in rigidity. Dr. Tezcan asked how the damage to the building should have been avoided: Mr. Aytun said that the design made no allowance for the effect of the non-structural elements, which were very rigid; the design engineer designed only the frame and subsequently the architect put in the rigid elements.

SIMPLE ZONING OF NORTH–EAST OF IRAN

Dr. K. Moazami Goudarzi and Dr. J. Hossein Javaheri

This paper considers the seismic activity of the North East of Iran, between 34° and 38°N and 56.5° and 60°E. The available macroseismic information of this region before 1904 is as follows:

643	Khorasan. A destructive earthquake, aftershocks continuing for 70 days.
765	Khorasan. There was an exceedingly severe earthquake in Khorasan and a mountain in Bishak (Zavah) moved about 5 km.
816	Khorasan. A damaging earthquake, aftershocks continuing for 70 days.
818	Khorasan. Aftershocks continuing for 70 days. Many buildings were destroyed.
840 July	Zavah in Khorasan was overturned by an earthquake, burying its inhabitants and becoming mound of dust.
856	Fars, Khorasan, Qum, Damghan. Mountains were ruptured and fractures appeared on the ground.
856 Dec.	This earthquake destroyed many towns in Khorasan from Nishapur in the north to Qayen in the south where 45,000 people perished. It is very likely that there was, in fact, a series of earthquakes which affected Khorasan in 856, and one of them was very near to Qayen.
859–860	Khorasan. Many people were killed.
1052	Khorasan. The intensity of the earthquake was greatest in Bayhagh and Bayhagh castle was destroyed.
1065 (1066)	Khorasan. A number of villages subsided into the earth and people fled to the plains. A number of mountains were ruptured.

1123–1124 Khorasan. Many towns were ruined and 8,000 people were killed. The damage extended to Hireh and Ghaznah.

1208 Nishapur. A strong earthquake with 10 days of continuous aftershocks.

1389 Nishapur. A destructive earthquake occurred after a strong storm.

1549 Khorasan. Qayen was destroyed and 3,000 people killed in the region.

1611 Dec. 9 Khorasan. In Asfand, particularly in Dughabad, a series of earthquakes caused heavy damage. In Goulabad 800 people were killed.

1646 Shirvan. The town was destroyed.

1667 Shirvan. 12,000 people were killed.

1673 Khorasan. 4,000 people were killed in Mashad and 1,600 were killed in Nishapur.

In August 1673 another earthquake caused severe damage to south of Torbat. Between this date and the beginning of twentieth century, there is a big gap in the seismic history of Khorasan.

1687 April Kashmar. A destructive earthquake in Kashmar caused damage in Mashhad.

1852 Feb.22 Khabushan was almost totally destroyed and about 2,000 people were killed in the district.

1871 Dec.23 Khabushan was heavily damaged and 2,000 people were killed in the Quchan region.

1871 Aug.10 Mashhad. An earthquake occurred but no damage was reported.

1872 Jan.6 Bojnurd-Quchan. A destructive earthquake in this region, more than 4,000 people were killed in the district of Quchan.

1872 Feb.1 Mashhad, Cheneran, Quchan. A strong earthquake was felt in Mashhad and caused some damage ih Cheneran and Quchan. One person was killed. Four shocks were felt.

1879 Apr.2 Bojnurd. A local destructive shock killed 700 people at Bojnurd.

1893 Nov.17 Quchan. A large earthquake in the Ouchan region killed 5,000 people.

1894 Jan.17 Quchan. A strong aftershock added to the damage at Quchan where 700 people were killed.

1895 Jan.19 Quchan. Another destructive earthquake happened, killing many people and destroying many old and newly built houses. After the previous earthquakes people had been adviced not to rebuild the town on the same place, but they did not heed this warning.

1897 Feb.8 Khorasan. Four shocks were recorded, one was very strong. No damage at all to the new town of Quchan.

1900 Feb.18 Shirvan. A strong earthquake occurred, but no damage or casualty was reported.

1903 Sep.25 Kashmar (Old Torshiz). This town and twenty-five villages were heavily damaged and about 200 people were killed. This earthquake, which had numerous strong aftershocks, extended to the west of Kashmar in a very thinly populated and partly deserted area from which no macroseismic information is available.

Earthquakes from 1923 were as follows:

Date	Time (GMT)	Latitude	Longitude	Magnitude	Depth (km)
4th Feb., 1923		Bojnurd. 200 houses collapsed.			
17th Sept., 1923	00.09	37.4N	57.7E	6.5	14
		Bojnurd. Destructive in the upper Atrek. Nine villages around Bojnurd were totally destroyed and 22 villages damaged. The earthquake killed 157 people and the shock was felt in Mashhad and Eshkhabad.			
10th Dec., 1925	05.59	37.2N	57.8E	5.0	13
		Shirvan. The town was damaged and 2 people were killed and two villages in the vicinity were destroyed. The shock was felt in Mashhad.			

Date	Time (GMT)	Latitude	Longitude	Magnitude	Depth (km)
7th Sept., 1928	—	36.2N	59.4E	—	—
		Mashhad. Some damage was caused and two people were killed.			
1st May, 1929	16.00	36.3N	59.0E	—	—
		Nishapur. More than 2000 people were killed and 300 villages damaged. It was felt in Khorasan and Esghabad. A fault 35 km in length was observed.			
1st May, 1929	15.37	38.0N	56.8E	7.1	15
		A major earthquake associated with faulting in the upper reaches of the River Atrak. The earthquake affected both Iran and part of Soviet Turkestan. In Iran 3253 people were killed and 1150 wounded, of whom 2553 were killed in the region of Shirvan. The shock destroyed 88 villages killing 6542 cattle. In Turkestan the damage was heavy in the Garmab area where 20 people were killed. Deaths elsewhere were 600 in Gifan, 300 Zerdau, 320 Kheyrabad, 250 Rabat, 18 Jafarabad, 80 Arsanob. In Bojnurd 400 houses collapsed and the villages of Serani, Kulun-Kaleh, Kurkulab and Kheyrabad in Turkestan were totally destroyed. The earthquake destroyed 500 houses around Bojnurd, and caused considerable damage as far as Ashkhabad where 26 people were wounded. The damage was also considerable in Firyuza, Gaudak and Quchan. Minor damage occurred in Jajarm and Bandargaz. 12 strong aftershocks were felt within 24 hours at widely separated points, from Bandargaz to Kalat. More than 400 aftershocks were felt in the region during the following two years.				
3rd May, 1929	16.20	37.8N	57.8E	5.0	13
		Destructive at Gifan, Rabat, Jafarabad and Sarani where 850 people were killed; the villages were totally destroyed.			
4th May, 1929	06.31	37.5N	58.2E	5.0	12
		Destructive aftershock in the region of Shirvan and Bojnurd in which 70 houses were destroyed and 2000 people were killed; Quchan was also damaged.			
9th May, 1929	01.34	37.5N	57.3E	—	—
		Bojnurd. Some damage.			

Date	Time (GMT)	Latitude	Longitude	Magnitude	Depth (km)
24th June, 1943	—	36.2N	57.8E	—	—
	Sabzevar. Many people were killed and injured; several aftershocks were felt.				
5th Oct., 1948	20.30	34.38N	54.61E	—	—
	Khorasan. 352 people were killed and 540 were injured. It was felt all over Khorasan.				
5th Oct., 1962	—	25.6N	59.3E	—	—
	Ahmadabad; many people were injured.				
6th Oct., 1962	20.00	35.2N	59.1E	—	—
	Torbat-e-Heidari; five people were killed.				
31st March, 1963	02.27	36.9N	57.9E	4.5	33
	Hendujan. It was also felt in Bam and Sabzevar. At Dehnehadjagh 76 houses were destroyed and 4 people were killed and 2 wounded. Both Bam and Dehneh were shaken twice by aftershocks on 2nd and 3rd April.				
31st Sept., 1968	10.47	34.0N	59.0E	7.3	13
	Khezri (Gonabad). 14,000 people were killed. This destructive earthquake has been studied by many groups of seismologists (see for example refs. 1—5).				
3rd Jan., 1969	03.16	37.1N	57.9E	5.6	11
	Destructive in the region of Reshtehiye Alla-Dagh. The villages of Dahneh Hodjagh, Bam and those in the District of Shirvan and Bojnurd were heavily damaged. In this region 50 people were killed and 300 injured. The damage extended to Nishapur, Bojnurd, Quchan, Shirvan, Sabzevar and Isfarayen making 2000 homeless.				

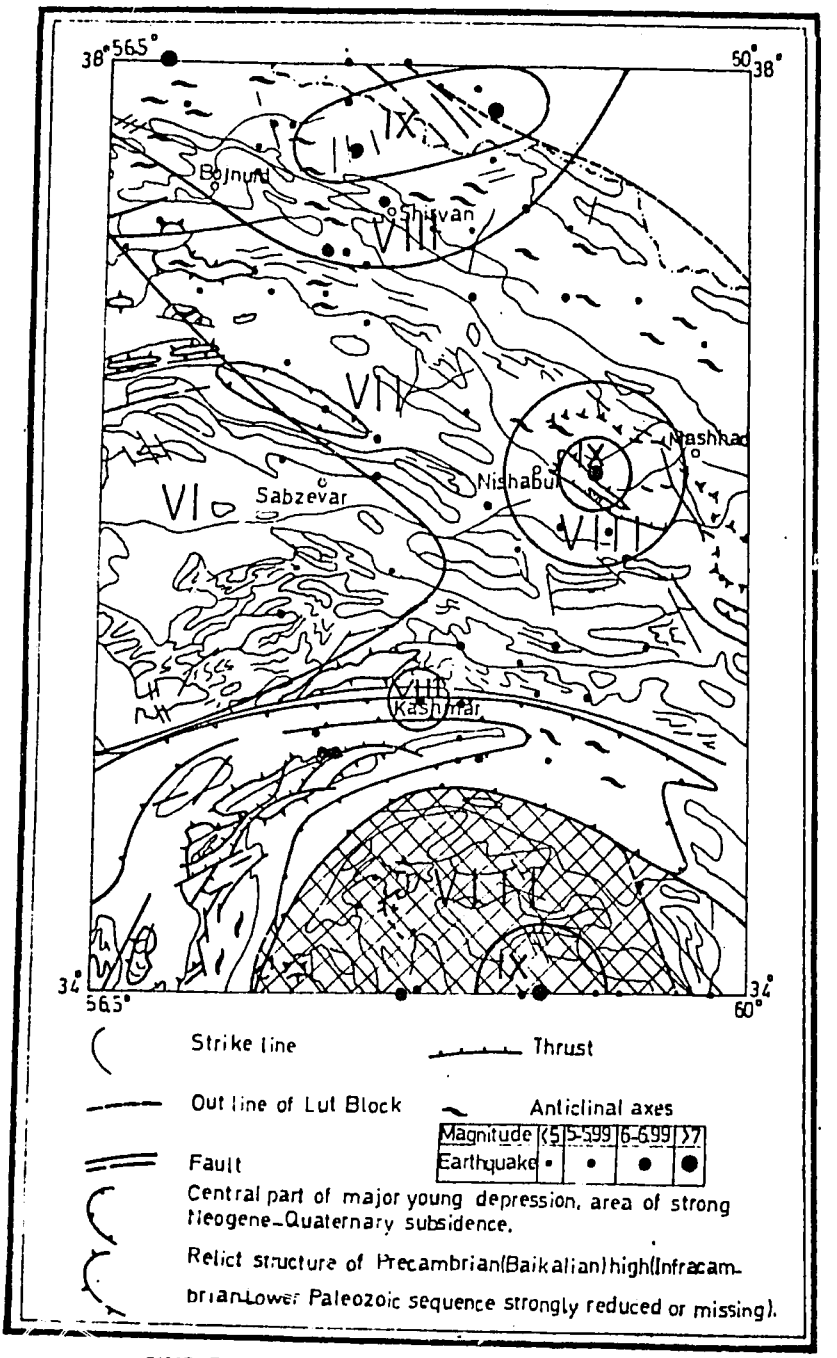

SIMPLE ZONING MAP OF NORTH EAST OF IRAN

Data for earthquakes since 1904 can be summarised as follows:

Earthquakes Magnitudes	Number in Eshghabad 36-38°N 556.5-60°E	Number in Torbat-e-Heidari 34-36°N 56.5-60°N
Greater than		
7	3	1
6–7	2	4
5–6	20	13
3.5–5	95	14

A previous study[6] by one of the authors shows that in the Eshghabad region at least one earthquake with magnitude greater than 4, 5 and 6 is expected to occur every 1, 8 and 42 years respectively. In the Torbat-e-Heidari region at least one earthquake with magnitude greater than4, 5 and 6 is expected to occur every 9, 13 and 34 years respectively.

From the past records, the region can be divided[7] into different zones, in which earthquakes of maximum intensity X and minimum intensity VI are expected during this century (Figure 1).

REFERENCES

1. *K.C. Bayer, Bull. Seism. Soc. Amer., No. 5 (1968).*

2. *UNESCO Report, 1214/BMS.RD/SCE.*

3. *M. Niazi, Bull. Seism. Soc. Amer., No. 5 (1969).*

4. *S. Crampin, Bull. Seism. Soc. Amer., No. 5 (1969).*

5. *J.S. Tchalenko and N.N. Ambraseys, Geol. Soc., Amer. Bull., 81, 41 (1969).*

6. *K. Moazami-Goudarzi, Bull. Fac. Sci. Tehran University, 3 (1971).*

7. *K. Moazami-Goudarzi, Seismology, (Min. of Sci., Iran), No. 1 (1972).*

DISCUSSION

In reply to Dr. Gürpınar, Dr. Goudarzi said that microseismic data were being used and the results would be comparable with those obtained in the USSR.

THE CLASSIFICATION OF HAZARD ZONES IN PAKISTAN

Mr. M. Anwaruddin Ahmad

Pakistan falls within the orogenic belt which is known for its seismic instability. The most active regions are the northern Hindu Kush, north-western Himalaya, Quetta-Sibi re-entrant region and adjoining areas. More than 700 earthquakes of magnitudes 4 and above were recorded from 1905 to 1912 (Figure 1). 363 shocks (49%) were of magnitude 4 to 4.9, 256 (35%) of magnitude 5 to 5.9, 87 (12%) of magnitude 6 to 6.9, 22 (3%) of magnitude 7 to 7.9, and 3 of magnitude 8 and above. Only 15 shocks (2%) of magnitude 3 to 3.9 were detected, due to the lack of recording stations: there are none in the western part of Pakistan, the northern region of Chitral and Gilgit or the western Himalayan belt. The only observatory in the northern Pakistan is near Peshawar which is quite far away from northern mountain ranges.

The focal depth of the earthquakes is also shown in Figure 1. The number of earthquakes at 0-50 km, 51 to 100 km, 101 to 200 km, and above 200 km were 238 (32%), 71 (9.5%), 235 (31.5%) and 200 (27%) respectively. Mostly earthquakes of focal depth 100 km or more originate in the Hindu Kush ranges.

As Figure 2 (see page 188) shows, the epicentres of earthquakes of magnitude 6 and above were in the Quetta-Khuzdar-Jacobabad-Fort Munro-Dukl and Chaman areas, the southern coastal area of Makran, in Baluchistan and Sind provinces.

Since the acceleration is the defining parameter of earthquake intensity, much more information regarding the distribution of the acceleration will be needed. This will be possible only with dense instrumentation but unfortunately only two accelerographs have been installed in Pakistan, so there is no information which could be used in assessing the intensity objectively.

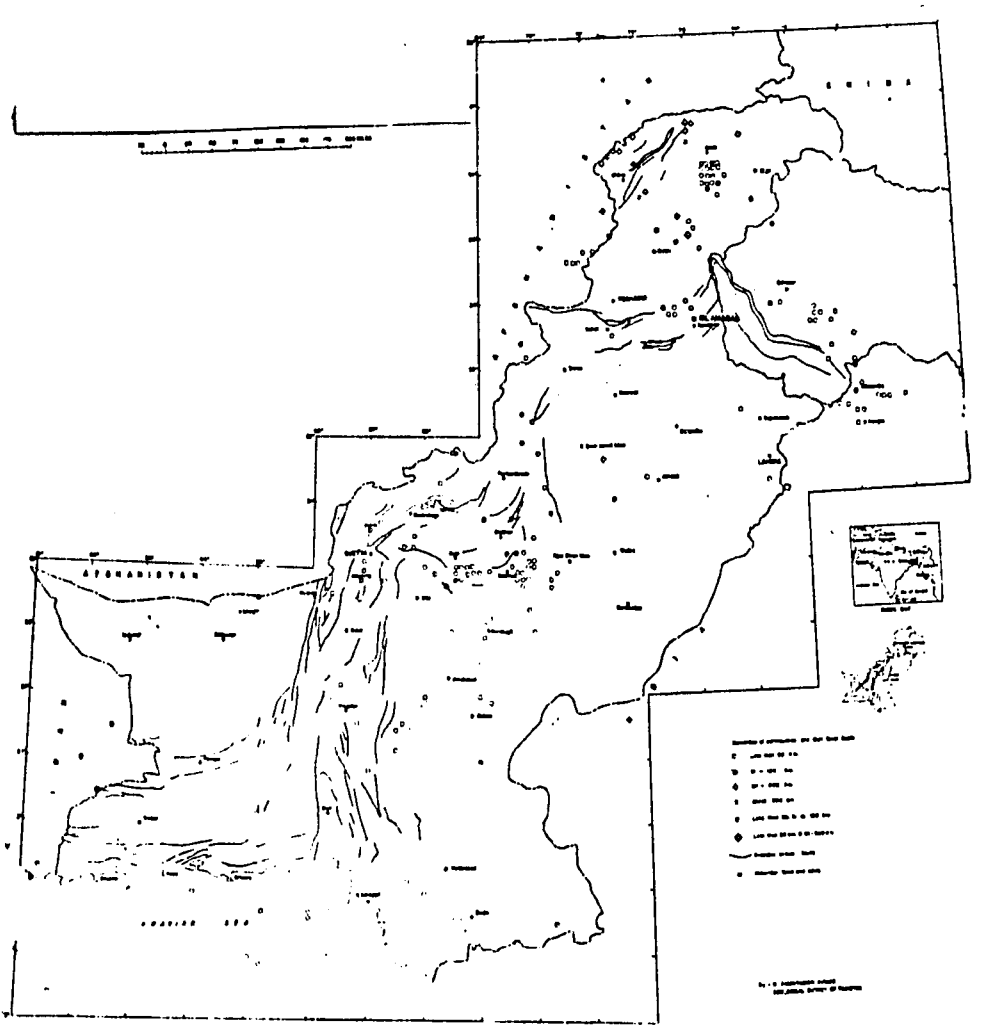

FIGURE 1.

Map Showing the Epicentres of Earthquakes within Pakistan Recorded during 1905-1972 and the Probable Active Faults Inferred

A very important factor in the design of an earthquake proof structure is the maximum seismic intensity to be expected at the site, in the life time of the structure: this must be assessed from data for some major earthquakes

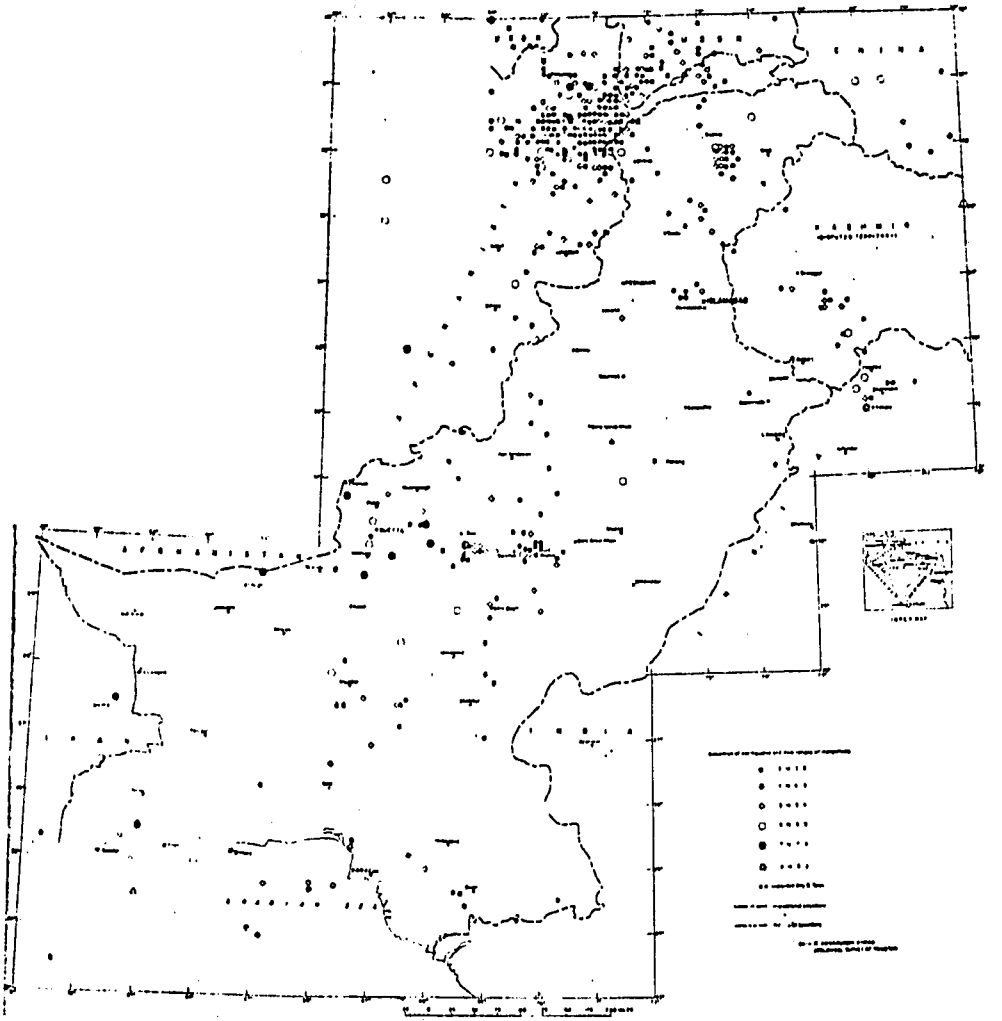

FIGURE 2.

Map of Pakistan and Adjoining Areas Showing the Epic ·tres of Earthquakes of Different Ranges of Magnitudes Recorded during 1905-1972

The isoseismal of the Hindu Kush earthquake of 30th July 1974 (Figure 3) has been prepared on the basis of data of effects of the earthquake observed in different parts of the country. The intensity in Chitral Dir was between 7.5 to 8 on MM scale. The isoseismals swing towards Kohat Mianwali area and then extend south-eastwards towards Punjab plains. The minimum intensity detected in Pakistan was 2 in Multan and

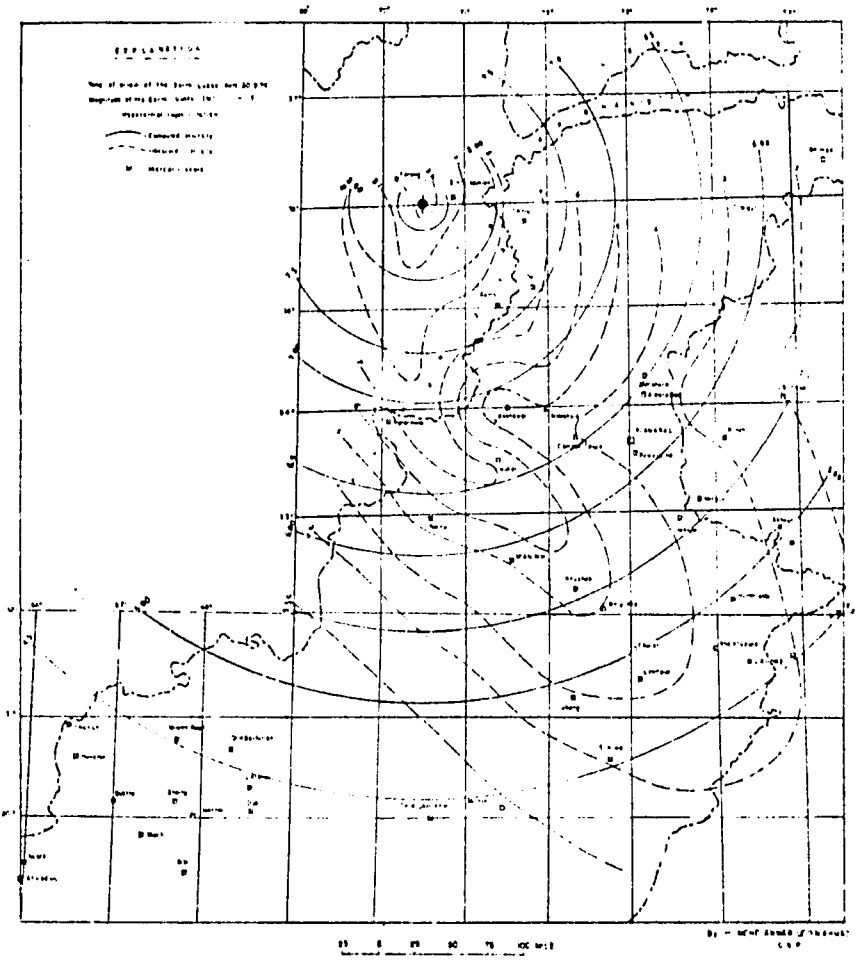

FIGURE 3.

Isoseismals of Hindu Kush Earthquake of 30th July, 1974

(Modified Mercalli Scale)

Dera Ghazi Khan region. The pattern of other earthquakes in Hindu Kush is generally the same except it varies only in the magnitude of the earthquake. For example, the isoseismals of the Quetta earthquakes of 1935[1] and the Kangra earthquake of 1905[2] along with Hindu Kush earthquake of 1974 (Figure 4) also tend to extend towards alluvial plains.

Adequate precise instrumental data on the destructive ground motions that have occurred in the past is not available in many countries of the world. Therefore, the problem of establishing the standards for earthquake-resistant structures is a very serious one. It is necessary to estimate the intensity of the ground motion that might be expected at various locations even if this requires drastic assumptions. Even when intensity data of past shocks are available, it is difficult for a designer to assess whether the future shocks will originate from the some source and whether the ground motion will of the same intensity. A structure designed for a bigger ground motion will cost more, so one has to decide upon the size of the future shocks and maximum intensity expected at the location of structure. In deciding this, the importance of the structure and its expected life must be kept in view. For the qualitative study of the relative structural behaviour the intensities allotted to the corresponding geographical zone are of great value. However, these are based upon damage reports, and the damage is a function of the materials, workmanship, method of construction, type of foundations as well as the geology of the region, size and location of the shock; consequently it is very difficult to make quantitative use of thes information in the design.[2] The instrumental measurement of magnitude which is a function of epicentral distance, ground motion, and total energy released can give objective information which a designer may need: having assumed the size of the shock it will be necessary to make further assumptions in order to estimate the ground acceleration at the site of the structure.

In view of the limited data regarding the intensity of various major earthquakes in Pakistan, an attempt has been made to construct an isoseismal map of Pakistan based upon historical data of the earthquake as well as upon computation of the acceleration by Krishna's method.[3]

The following assumptions have been made:

1. The radiation of energy released from thecentre is uniform in all directions.

2. The shock has the centre of the disturbed mass at a depth of 15 miles below the surface.

3. The intensity of ground motion decreased with the square of the distance from the centre and increased with the cube root of the energy released as suggested by Gutenberg and Richter.[4]

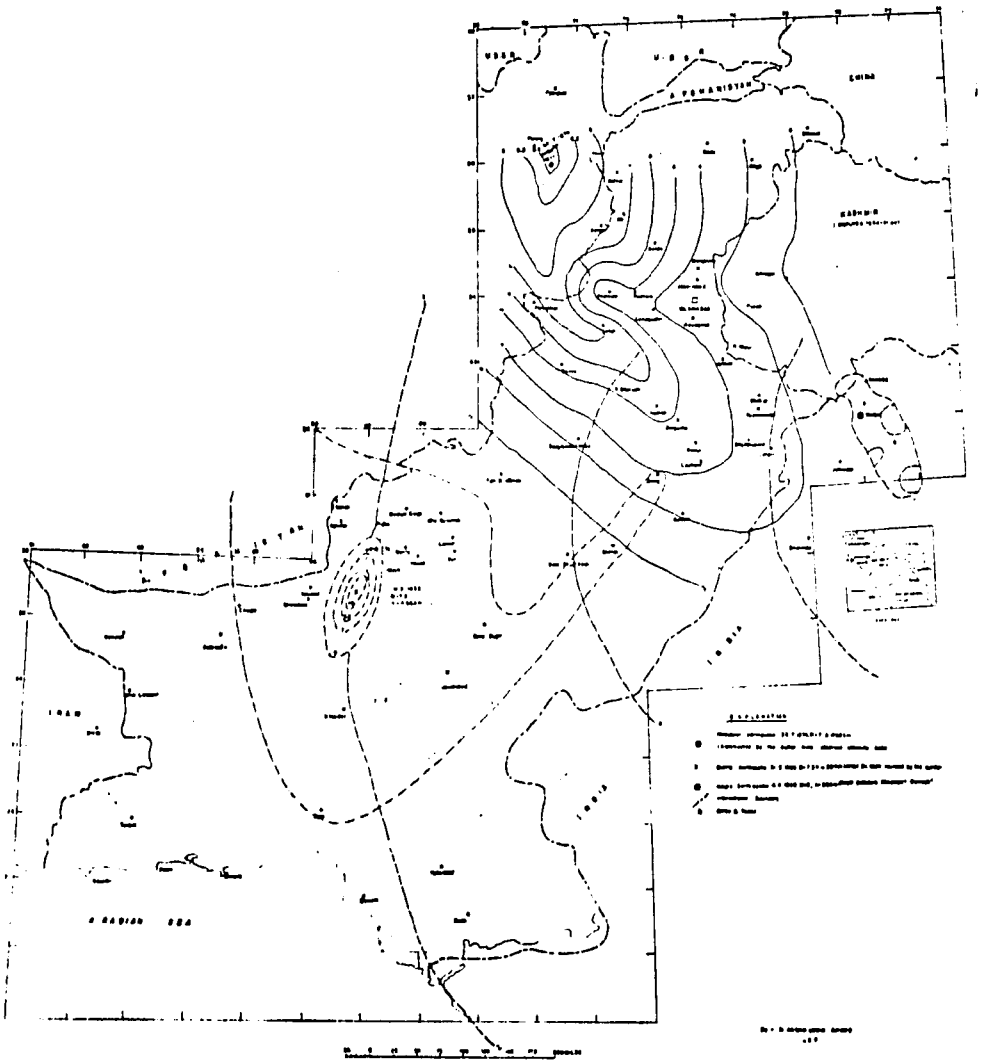

FIGURE 4.

Isoseismal of Some Historical and Recent Earthquakes of Pakistan and Adjoining Areas

(On Modified Mercalli Scale)

The relationships between energy and acceleration[3,4] are:

$$\log_{10}E = 9.4 + 2.14M - 0.054M^2 \tag{1}$$

$$a = C(E)^{1/3} \frac{h}{D^2 + h^2} \tag{2}$$

Where M is the magnitude of the shock, E the energy released in ergs, a the acceleration expected at a point situated at a distance of D from the centre of disturbance at distance h below ground level.

For the El Centro earthquake of May 18th, 1940 when h = 15 miles, D = 30 miles M = 7.1, the strong motion seismograph recorded the maximum ground acceleration equal to .33g. In equation (2), the constant of proportionality can thus be calculated. If log E = A, eliminating C, we have

$$a = (0.33g) \frac{h}{15} \frac{30^2 + 15^2}{D^2 + h^2} 10^{1/3 (A - 21.87)} \tag{3}$$

where the value of the El Centro shock was 21.87

$$\text{or} \quad a = \frac{24.75}{D^2 + h^2} 10^{1/3 (A - 21.87)} \tag{4}$$

From equations (1) and (4) acceleration can be calculated very conveniently for shocks if the magnitude, the focal depth and the distance of the location from epicentre of active fault zone are known.

Krishna[3] observed that the values of acceleration calculated for various shocks in the United States were quite comparable to the actual acceleration recorded by the accelerograph, with very few exceptions. Thus these computed accelerations can be converted into intensities by the following empirical formula[5] :

$$\text{Log} \quad a = \frac{1}{3} - \frac{1}{2} \tag{5}$$

$$\text{or} \quad I = 3 \log a + 1.5 \tag{6}$$

The values of acceleration 30 miles away from the epicentre have been taken for the estimation of the maximum epicentral intensity. Normally the more pronounced effects of the earthquake are at some distance from the epicentre. This distance is usually comparable to the hypocentral depth. The acceleration generated by a particular earthquake at greater distance has also been calculated and these values utilized for the computation of intensities and preparation of the isoseismal map of Pakistan. Figure 5 shows

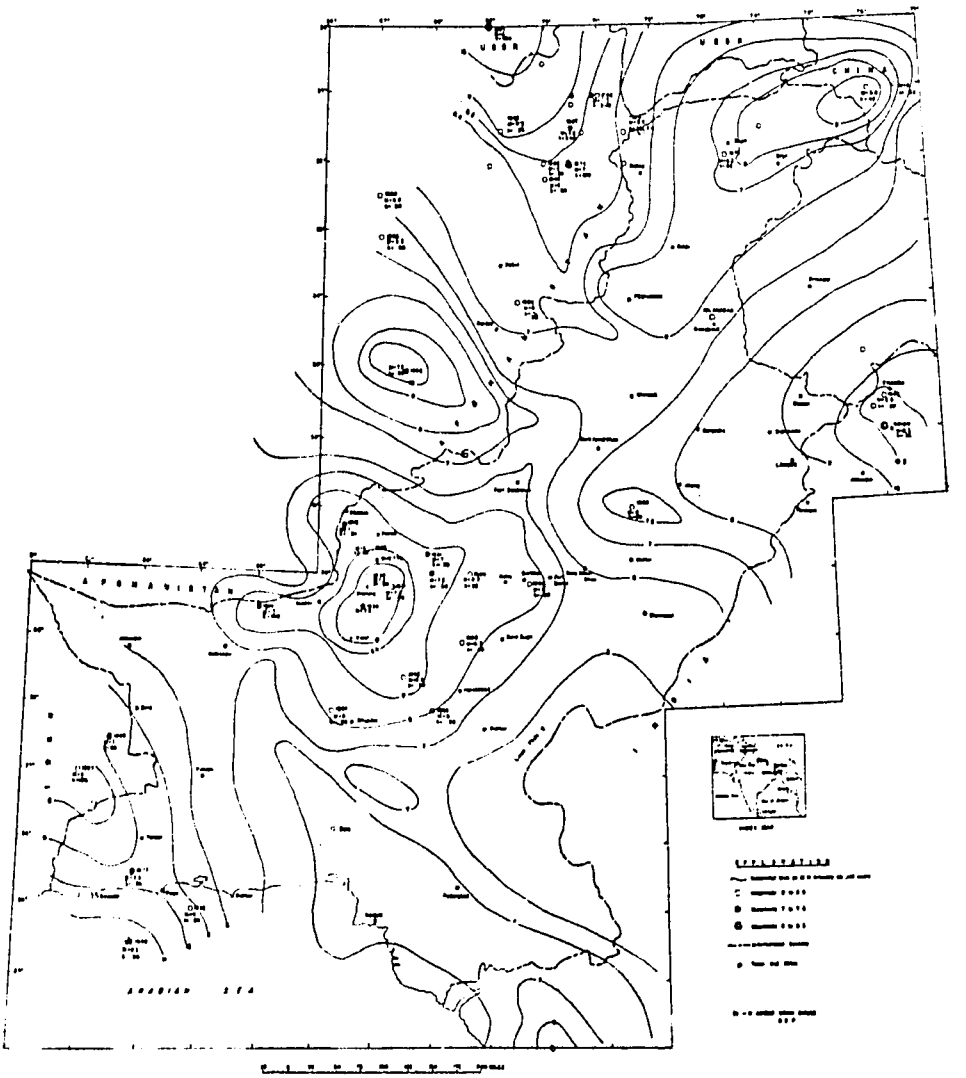

FIGURE 5. Isoseismals of Pakistan on Modified Mercalli Scale of Intensity

isoseismals based on historical and recent data and these calculations.

A comparison of observed and computed intensities for the Hindu Kush shock of 30.7.1974 is given in Figure 3. The computed isoseismals are function of magnitude, hypocentral depth and distance while the observed intensities are the function of the subsoil condition as well. While the observed intensities extend according to superficial geological condition, the computed intensities extend evenly according to inherent assumptions made in the calculations. Both the isoseismal observed and computed match to some reasonable degree. However, it should be noted that intensities determined by the macroseismic effects correspond only to the level of acceleration which persisted long enough to produce permanent effects. These values of accelerations must be less than the maximum acceleration recorded on a seismogram,[5] so, in a way, instrumental records of an earthquake furnish an objective and more reliable data of the maximum acceleration or intensity rating.

In order to prepare the intensity map of Pakistan, the observed intensities of the recorded earthquake in three seismically active zones in and around Pakistan (Quetta 1935, Kangra 1905, Hindu Kush 1974) have been used along with the intensities calculated for different major earthquakes of magnitude 6 and above in various region of Pakistan.

In rating the seismic intensities due weight has been given to the observed effects, so the possible errors in the estimation of intensities caused by neglecting the surface and subsurface geological factors are indirectly compensated to some extent, on a regional scale. In preparing this map, the magnitude of the earthquakes having greatest value in a particular region has been chosen for computation.

SEISMIC ZONING OF PAKISTAN, EXPECTED RANGES OF "g" FACTOR AND DELINEATION OF HAZARD ZONE

The degree of hazard to which different areas these are liable to be subjected are shown in Figure 6. The estimated g factor has also been indicated within each zone: this gives the amount of shaking or induced acceleration due to the earthquakes within or outside these zones. The values of acceleration are set rather higher for the reasons of safety. The higher the value of acceleration of any zone, greater is the degree of hazard in this zone. The intensity of .01 to .05g is assigned to the areas of Hyderabad, Sukkur, Bahawalpur, Dera Ismail Khan and Mianwali. Probably this is the shield area which is quite stable.

The areas within the acceleration range of 0.05 to 0.1g are west and north of Panjgur towards Bela and Dalbandin, Fort Sandeman, Mianwali, Dera Ismail Khan, and south of Peshawar are moderately active than the shield area and, therefore, are somewhat more hazardous.

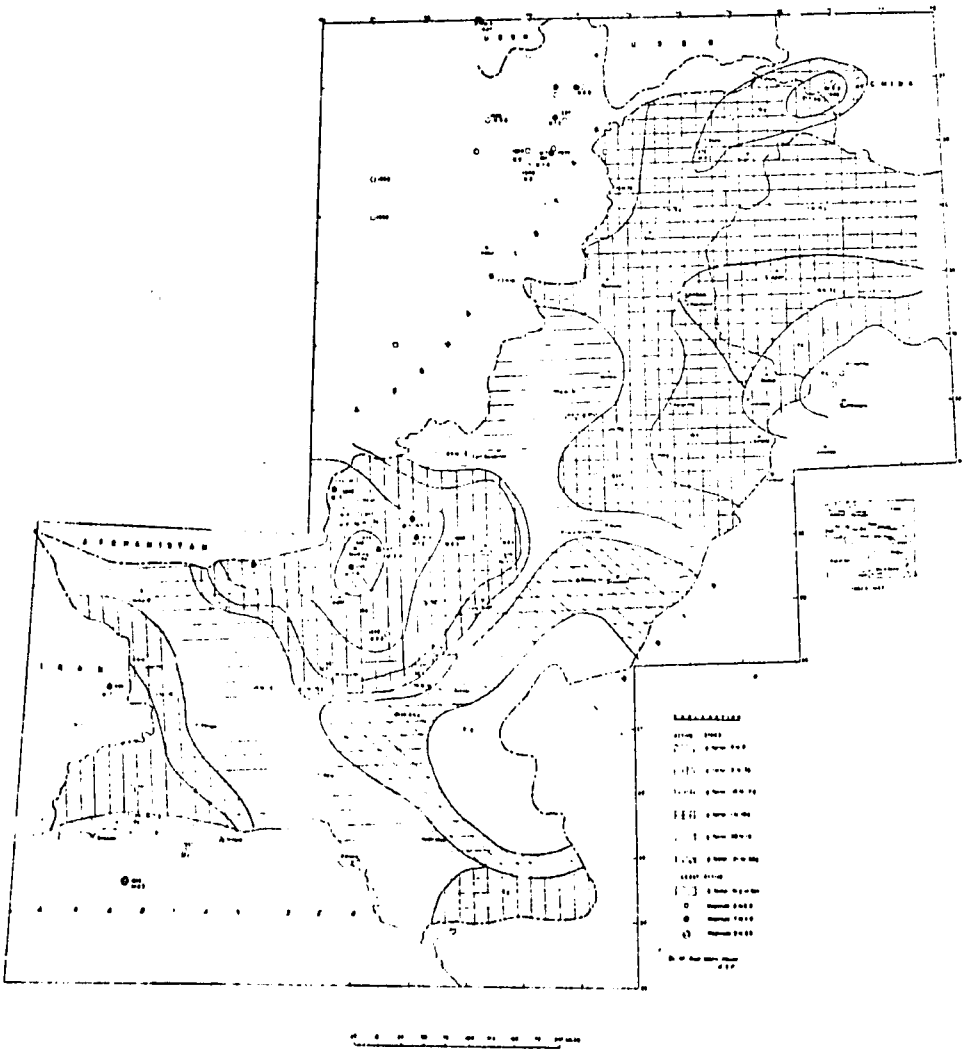

FIGURE 6. Seismic Hazards Zones of Pakistan and Their g Factors

The zones of acceleration .1 to .15 are north of Srinagar in Kashmir, southwest of Sialkot, south and north of Gilgit, Peshawar, Islamabad and Lahore and also the Sind area adjacent to Kutch. These areas can be considered active moderate to severe.

The zones of acceleration .15 to .2g are south of Srinagar in Kashmir, and north and south of Chitral bordering Afghanistan; these are severely active and hazardous.

The region of intensities 9 to 10 corresponding to .3 to .6g are most active and extremely hazardous: the Makran Coastal area, the Quetta-Kalat-Chaman-Duki Burkhan area of Baluchistan, the Hunza area of Gilgit near the Chinese border and north of Sialkot.

APPLICATION OF THE SEISMIC MAPS

The knowledge of various characteristics of earthquakes such as magnitude, intensity, relationship to tectonics and of the hazard zones is very important from the engineering point of view. Its application in the development of building techniques and urban planning can minimize such human sufferings and national losses. Pakistan is in the development stage and various engineering projects such as dams, thermal and nuclear power stations and industrial complexes have to be in regions which are hitherto underdeveloped and sparcely populated. Any mistake in the design schemes of construction stemming from a neglect of the degree of seismic hazard can be extremely dangerous. It is hoped that, these maps will be of use to planners and design engineers.

REFERENCES

1. *W.D. West, Rec. Geol. Serv. India, 69 (1936).*

2. *A. Gansser, "Geology of the Himalayas". Interscience, London, 1964.*

3. *J. Krishna, Proc. 2nd World Cong. Earthq. Eng., Tokyo, 2, 1803 (1960).*

4. *B. Gutenberg and C.F. Richter, Bull. Seismol. Soc. Amer, 46 (1958).*

5. *C.F. Richter, Bull. Seismol. Soc. Amer., 30, 173 (1942).*

DISCUSSION

In reply to Dr. Keightley, Mr. Anwaruddin said that there were two strong motion accelographs, at the Mangla and Tarbela Dams: there were five observatories with seismographs.

MOTION INSTRUMENTATION IN IRAN

Dr. A.A. Moinfar

Many severe earthquakes have occurred in the CENTO Region since 1960. In Iran, there was the Lar earthquake in 1960, the Buin-Zahra earthquake with about twelve fatalities in 1962, the Dasht-E-Bayaz and Ferdous earthquakes which killed more than ten thousand people in 1968, the Gharnaveh in 1970 and Ghir earthquake which killed more than five thousand people in 1972. In Turkey there was the Varto earthquake of 1966, the Modonlu (Adapazarı) earthquake of 1967, the Gediz earthquake of 1970 and the Bordoor and Bingöl earthquakes of 1971 which caused extensive damage to life and property. In Pakistan in 1966 there was the Duki and Balkhan earthquakes in Baluchistan with magnitudes of 6.2 and the Balkhan earthquake 6.8 respectively. The last strong earthquake in the CENTO Region was the Hindu Kush earthquake in Pakistan in 1974 with a magnitude of 7.

There were no ground acceleration records for any of these earthquakes, except in the Ghir earthquake of 10 April 1972 when we recorded ten aftershocks with the only two instruments which were in Iran at the time. The instrumentation of strong motion is very important for CENTO regional countries, so after the Ghir earthquake the Technical Research and Standards Bureau of the Plan and Budget Organization, began a programme of instrumentation in Iran. 146 strong motion accelographs, 75 seismoscopes and 5 ARDETA 100 seismoscopes have been bought by the Bureau. A network of one hundred and thirty instruments is ready for operation in the seismically active regions. Figures 1 and 2 (see the next pages) show the present location of our instruments.

A few of the instruments are on stand-by to be used as portable networks in the event of future strong earthquakes. Results gained from our network will be used for the study of focal mechanism of shocks as well as after shocks and amplification under nonlinear soil condition. There is enough evidence to show that most earthquakes of a magnitude greater than 6 in Iran are associated either with preliminary or secondary faulting. Consequently, the discovery of recent and historical faulting should indicate regions of high seismicity. An energy release map has been drawn by Mr. M. Banisadr for the whole of Iran, 1or 1900-50 and 1950-70 (Figures 3 and 4 on pages 200 and 201). Same method has been used in Figure 4 to draw one for the period of 1950-1970. Figure 5 (see page 202) combines these two figures, the period 1900-1970. If the assumption of uniform stored energy is valid, then earthquakes are more likely to occur in those areas where the gradient of energy released is more than in other areas. This

has been taken into consideration when we are locating our instruments, together with the evidence from large scale tectonics that the eastern and north eastern parts of Iran are of major importance. Since we started our strong motion accelerographs in Iran we have had no strong earthquakes but so far several records have been obtained from small earthquakes, and a comprehensive report on these will be presented later.

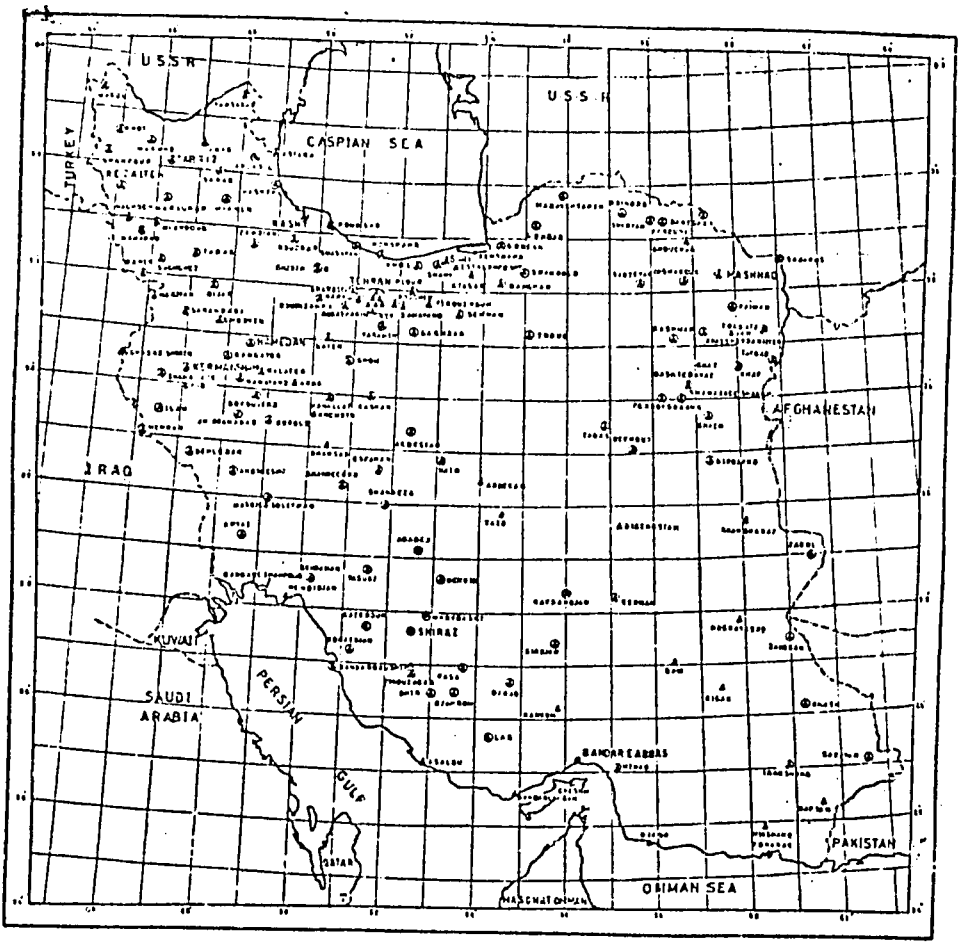

FIGURE 1.

Location of Existing Strong Motion Accelerographs in Iran

Instruments installed ⊕ Instrument to be installed ▲

The ARDETA 100 seismoscope which has been developed in Iran by Aryamehr University and the Technical Research and Standard Bureau will also be discussed later.

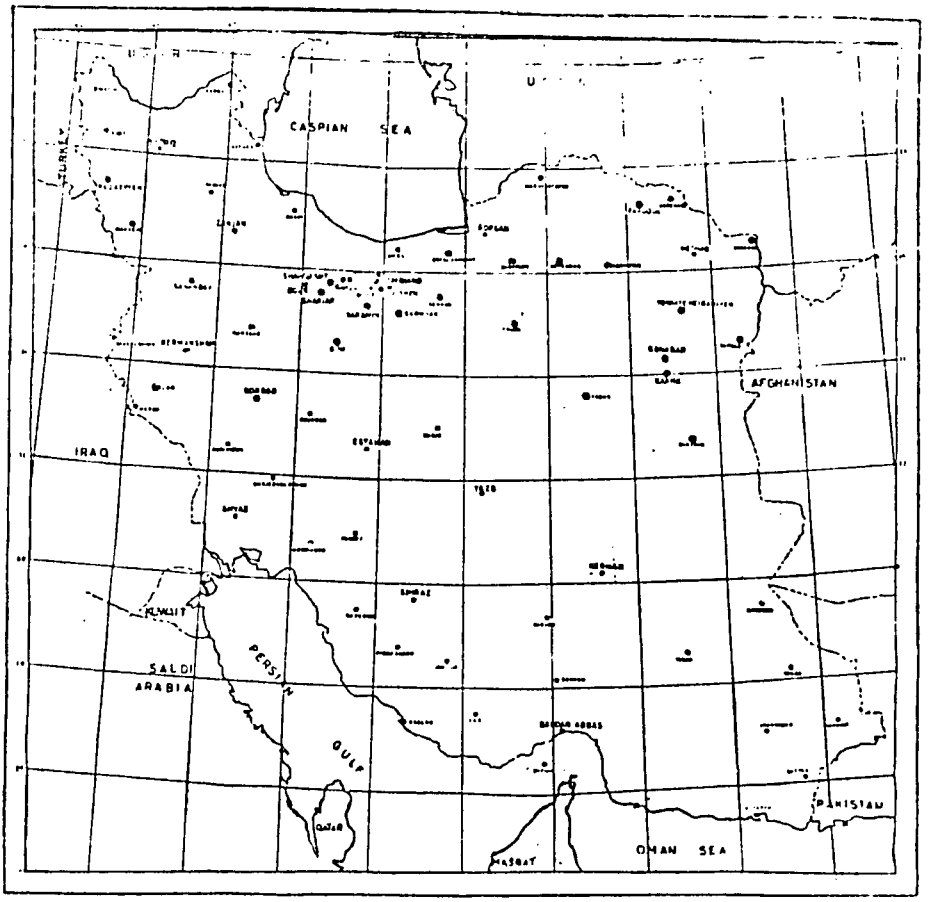

FIGURE 2.

● Location of existing Seismoscope in Iran

■ Location of Existing Ardeta Seismoscope in Iran

◑ Instruments installed ● Instruments to be installed

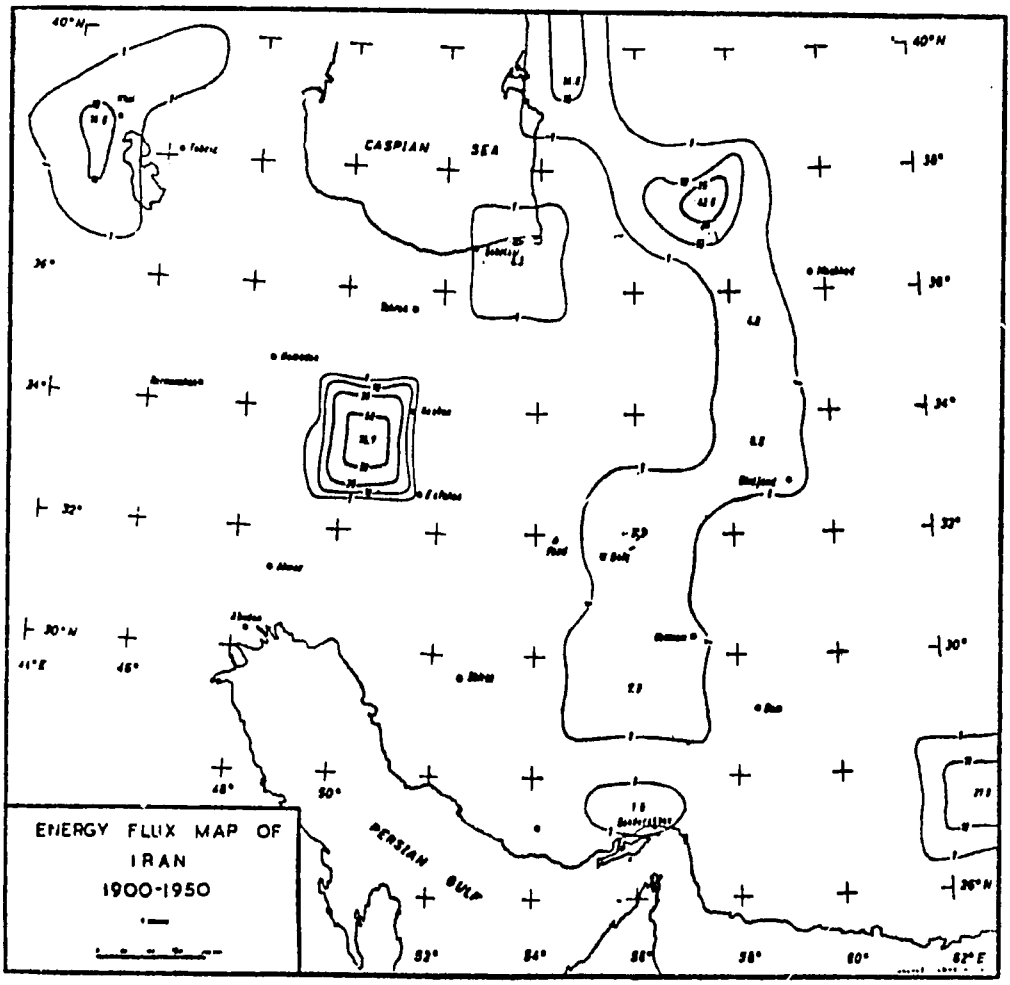

FIGURE 3

There are many obstacles in the instrumentation programme, such as the allocation of funds, monpower, and the accessibility of the sites and the type of energy available there. Merely installing the instruments is not enough: they must be well

taken care of and the results processed and studied. I believe strongly that the CENTO regional countries should take a serious step towards strong motion instrumentation and also there should be a close collaboration between the countries on the results gained by the instruments.

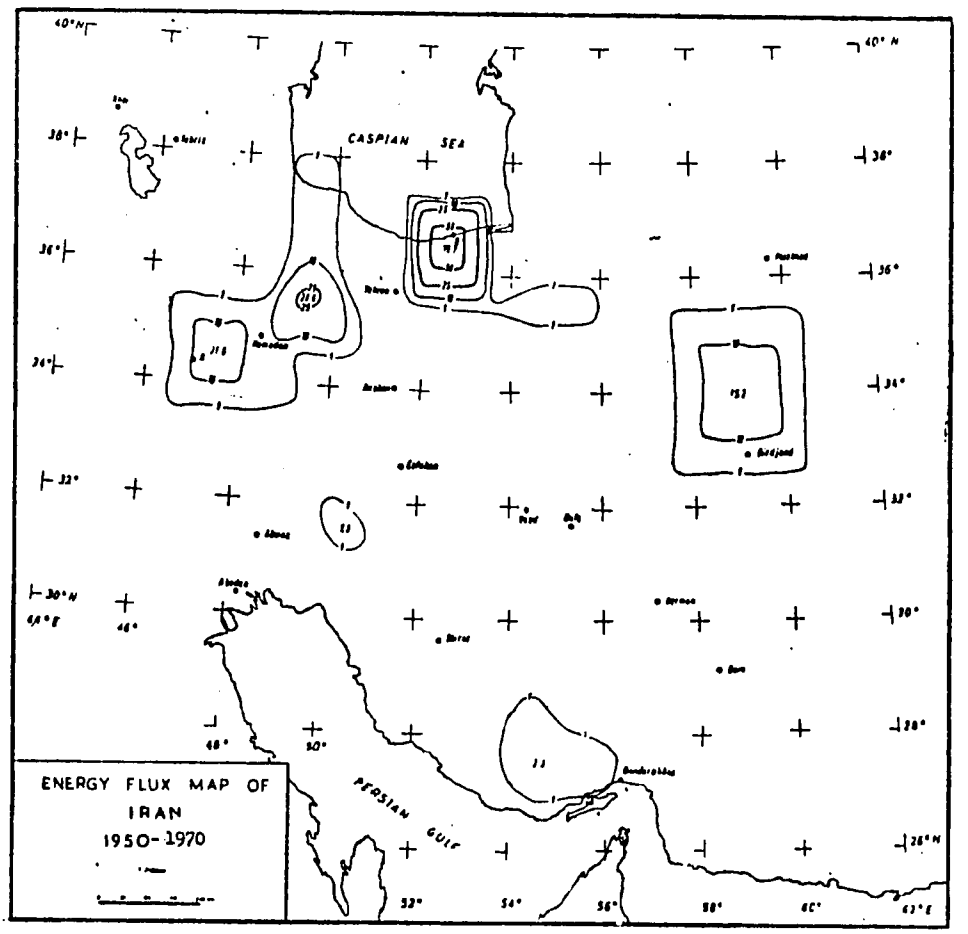

FIGURE 4

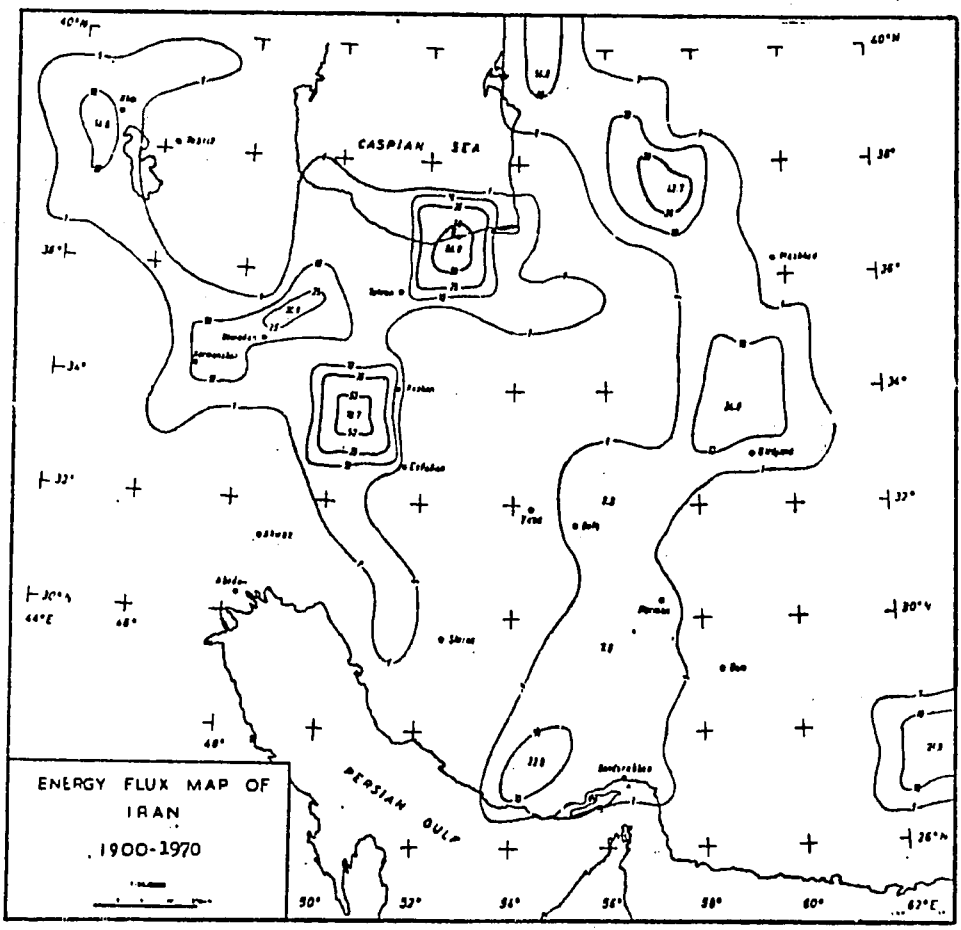

FIGURE 5

DISCUSSION

In reply to Mr. Aytun, Dr. Moinfar said that the strong motion accelerographs were the responsibility of the Plan and Budget Organisation; maintenance was done by a team of three civil engineers and three technicians, in collaboration with Iranian Universities, especially Arya Mehr University.

THE STUDY OF PAST EARTHQUAKES IN IRAN

Mr. M. Banisadr

Apart from a relatively narrow coastal zone, Iran consists mostly of mountain ranges with plateaus ranging from 1200-1600 m upto of 5000 m elevation. The country is highly seismic and in general most earthquakes fall in class d, M between 5.3 and 5.9, with a few falling in class c, and b. Most of the earthquakes in Iran happened very close to existing faults. The thickness of the lines in Figure 1 (see the next page) is an indication of major and minor faults, with some observed movement of the faults.

To study the earthquake activitiy in Iran, one can divide the era into two periods. The first period covers most earthquakes which happened before 1900: there is only very little published information for this era, mostly on an historical basis. Fortunately there are many old manuscripts and books which describe major earthquakes and by referring to these documents one can obtain a great deal of valuable information, although it will never suffice to describe the seismic potential of the region. From this information, we may indicate regions of high and low seismic activity, but we can never predict how these areas will react in the future: possibly regions which are quiet now may be active in the years to come.

The second period is from 1900 to the present. Though there is more information available for this period, it should be treated very cautiously. Upto 1930 instrumental information is not very accurate or complete, due to the uneven spread of population and the lack of seismological stations throughout the world. The instrumental information for this period should be checked against macroseismic information and the local newspapers, and perhaps adjusted. The Technical Research and Standard Bureau jointly with the Imperial College of Science and Technology is doing an extensive study of the earthquakes of this period. An example of such studies is the Silakhor earthquake of January 23, 1909: field investigations showed that the actual epicentral area was several kilometers away from the instrumental calculated epicenter. From the year 1930 to the present, due to an improvement of technology and also to a better spread of population and more instruments being installed around the world, we have more reliable information available. Also by reference to local and foreign newspapers we are able to gather more information for this period. Figure 2 (page 205) shows most earthquakes which have happened in Iran since 1900. The size of the circle is a representation of the magnitude, and hollow circles indicates earthquakes for which the magnitude is not known. Most activity in this period is spread through the northern and western parts of Iran. There are two distinct bands, one starting from northeast and extending

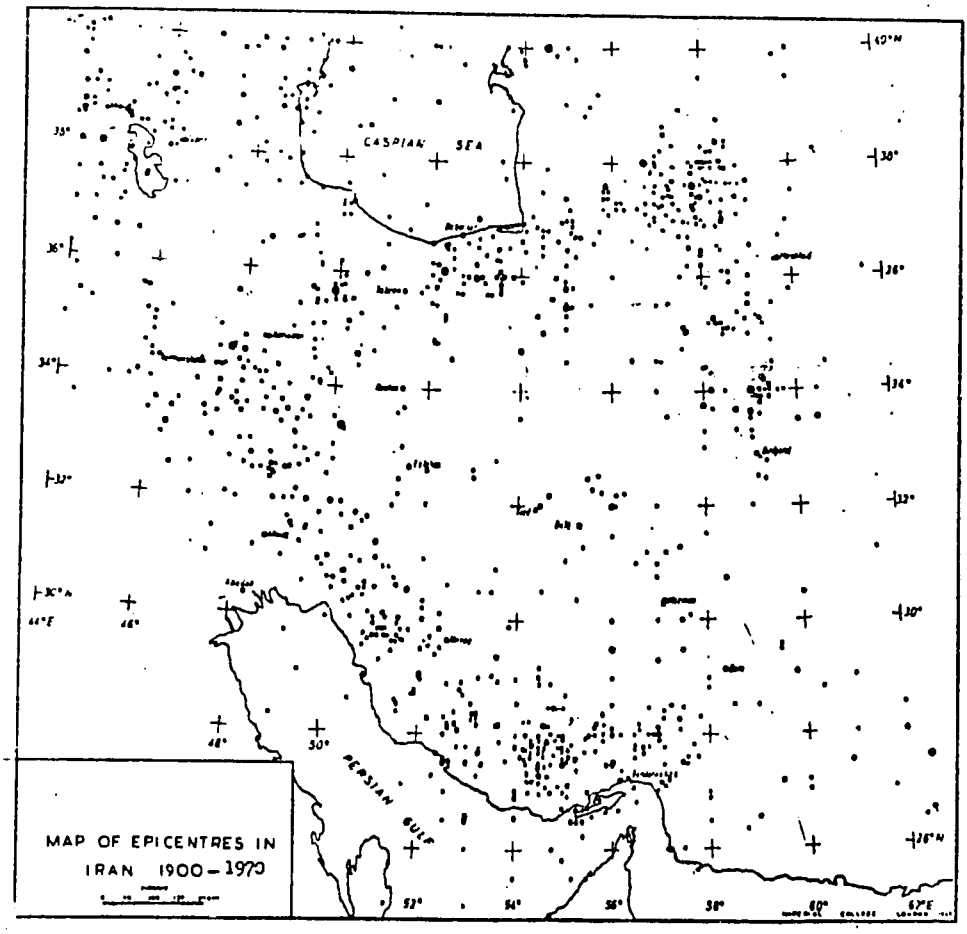

FIGURE 1

towards the north-west along the Alburz mountains and the Caspian coast. The second band starts from the west and extends towards the western and southern parts of Iran along the Zagros range.

Specific prediction of the time and magnitude of future earthquakes at the present time is not possible, but with the conjunction of our existing faults we can suspect that the northern area along the Alburz, and the eastern and western areas of Iran might be the scene of future catastrophic earthquakes.

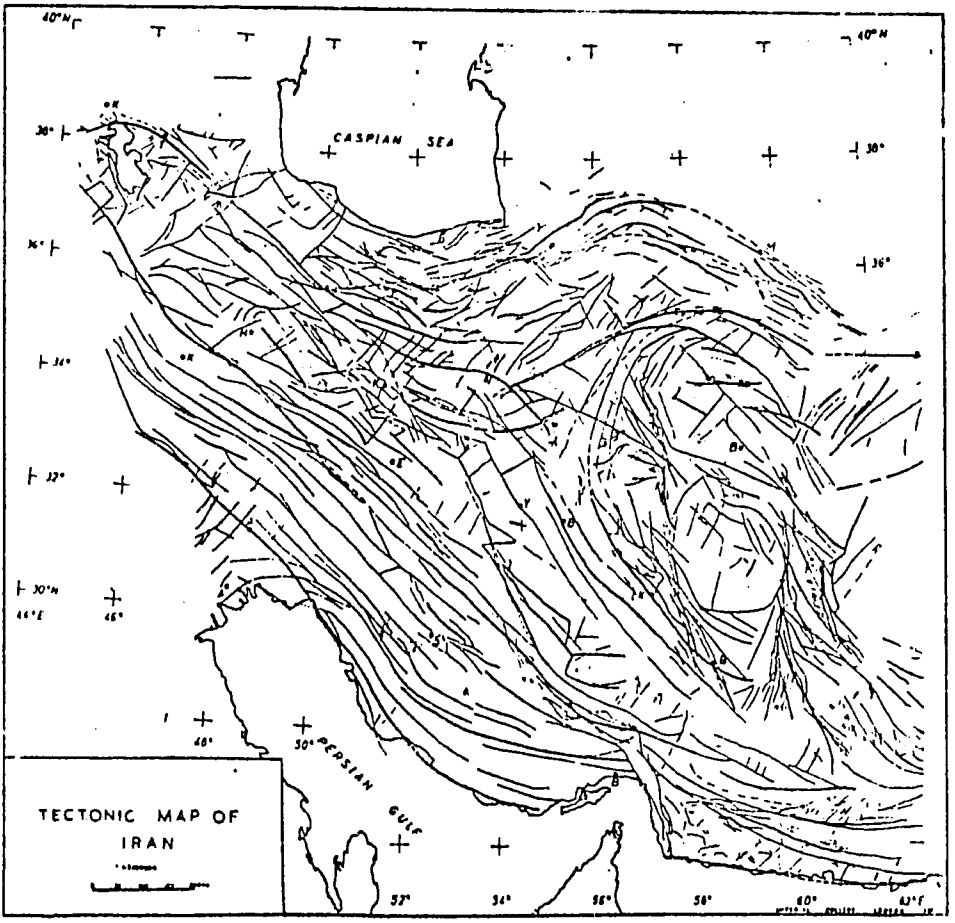

FIGURE 2

THE CORRELATION OF INTENSITY WITH GROUND MOTION

Professor N.N. Ambraseys

Intensity is a convenient means of rating the effect of ground motions on man-made structures, and it has been readily adopted by engineers for design purposes. We now have a multitude of empirical formulae from which we can derive ground accelerations and velocities as a function of intensity: its advantages and limitations for design purposes have been discussed elsewhere.[1] Seismologists and engineers continue to seek a meaningful correlation between intensity and other quantities which can be used directly for design purposes, in spite of repeated warnings against the abuse of such correlations. They hope perhaps that more research may remove some of the weaknesses implicit in such empirical correlations. The purpose of this study is to show that neither wholly disappointed nor wholly fulfilled.

Figure 1 shows a plot of recorded maximum ground accelerations versus reported intensities from 1933 to 1943. The scatter is considerable but there is an obvious trend which, in 1943, would have tempted one to fit a curve through these points and obtain an empirical formula. This is exactly what Gutenberg did to obtain the classical relationship: $\log (a) = 1/3 - 0.5$, which since that time features in every textbook. Figure 2 (page 208) shows a plot similar to that in Figure 1 for the next 20 years, and fitting a curve to this plot is questionable. Today, fitting a curve to such a plot becomes almost impossible as shown in Figure 3. A weak correlation between recorded acceleration and intensity for this worldwide collection of data does exist, but the data scatter is more than one and a half orders of magnitude. The scatter here is associated not only with an obvious weak correlation between intensity and acceleration, but also with the differences that exist between various Intensity Scales (MM, MS, MSK, JMO, RF), between the different types of accelerographs used, and the different earthquake mechanisms and foundation conditions involved.

Until strong-motion data provide a better alternative, the engineer is likely to continue using intensity-acceleration relationships. A study of the data available today from European earthquakes may prove helpful in focussing attention to the degree of empricism implicit in such relationships.

During the last few years the number of strong-motion instruments in operation, especially in Europe and in the Near East, has been increasing rapidly, and there is much new evidence for abnormally high accelerations, some of which has come from relatively small earthquakes. At the present time approximately 500 accelerographs and

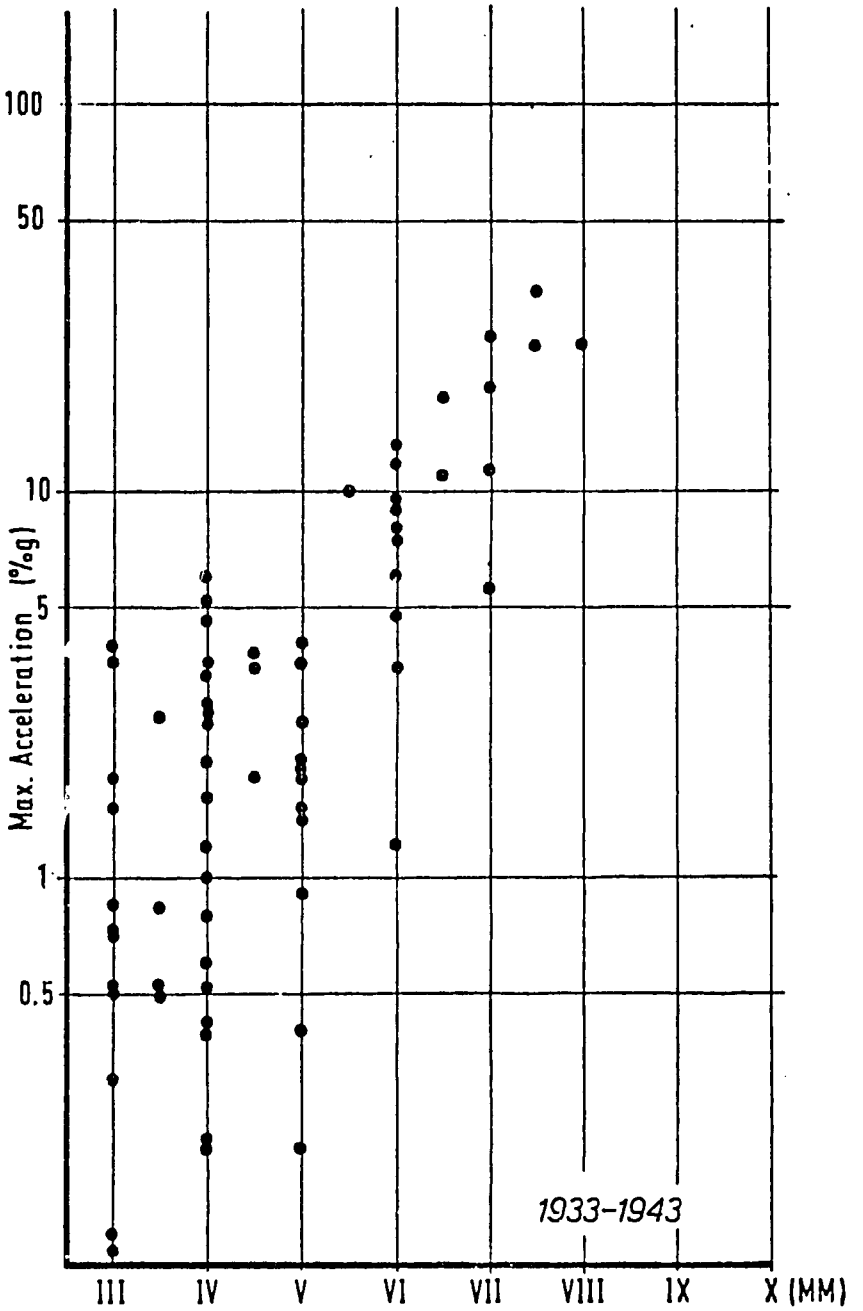
100
50
10
5
1
0.5
Max. Acceleration (‰g)
1933-1943
III
IV
V
VI
VII
VIII
IX
X (MM)

FIGURE 1

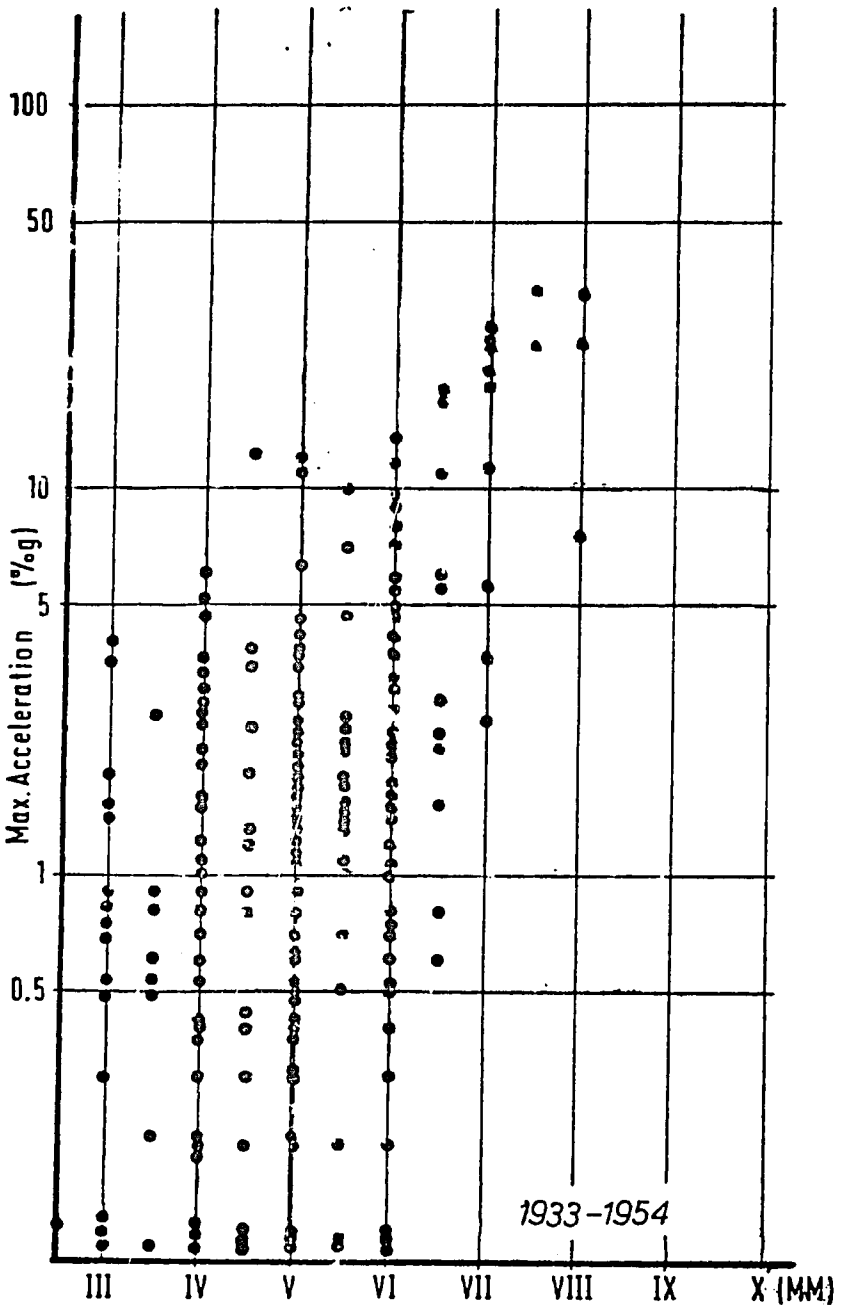
100
50
10
5
1
0.5
Max. Acceleration (%g)
1933-1954
III
IV
V
VI
VII
VIII
IX
X (MM)

FIGURE 2

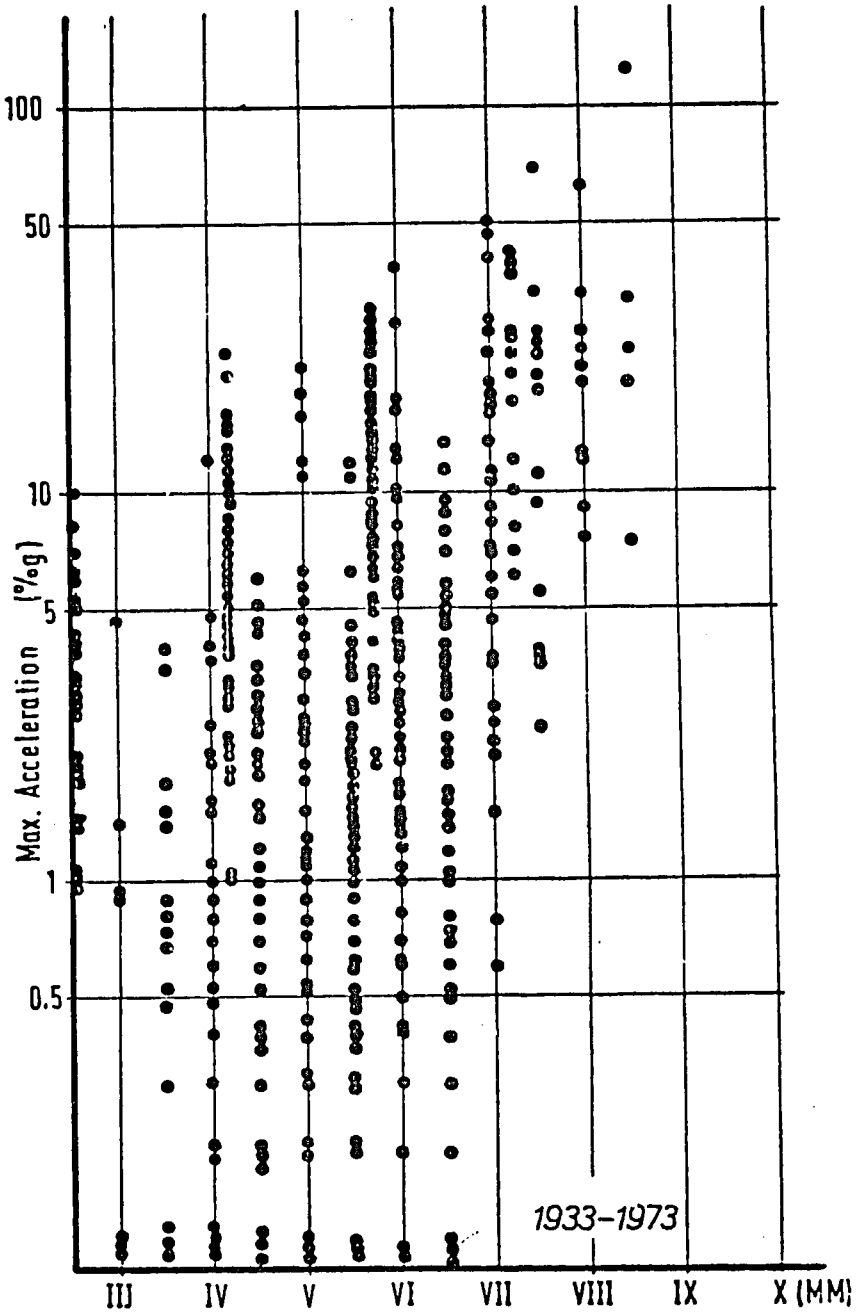
100
50
10
5
1
0.5
Max. Acceleration (%g)
1933–1973
III
IV
V
VI
VII
VIII
IX
X (MM)

FIGURE 3

TABLE 1. NUMBER OF KNOWN STRONG-MOTION INSTRUMENTS IN OPERATION IN EUROPE AND IN THE NEAR EAST (1967 – 1974)

Country	MO–2	SMA–1	AR–240	RFT–250	RMT–280	SMAC–AB	UAR–T	Other	Total	SR–100+	Other	Total	Events recorded
Afghanistan	–	–	–	2	–	–	–	–	2	–	–	–	–
Bulgaria	–	4	–	–	–	–	1	–	5	–	–	–	–
Greece	–	15	–	–	–	2	–	–	17	17	–	17	7
Iran	–	86	1	1	1	1	–	–	90	50	–	50	18
Italy	102	12	10	1	–	–	–	–	125	5	–	5	38
Pakistan	–	–	4	–	–	1	–	–	5	–	–	–	1
Portugal	–	1	–	1	–	1	–	–	3	–	–	–	4
Rumania	7	4	–	–	1	1	–	–	13	2	–	2	–
Switzerland	–	2	–	–	–	–	–	–	2	–	–	–	–
Turkey	–	11	2	–	–	3	–	3	19	13	–	13	1
U.K.	–	3	–	–	–	–	–	–	3	1	–	1	–
U.S.S.R.	–	–	–	–	–	–	–	174	174	–	–	–	–
Yugoslavia	–	118	2	–	–	–	–	–	120	100	70	170	10
						TOTAL			578			258	79

an equal number of simpler devices such as seismoscopes and maximum acceleration recorders are reported to be in operation. Table 1 shows the distribution of the various types of instruments by country; in addition a number of portable accelerograph arrays are available in Iran, Italy and Yugoslavia for the study of aftershock sequences.

The first seismoscope recording was made in Greece on the 1st September 1966, and the first earthquake to be recorded by an accelerograph was a year later in Yugoslavia. Since then, more than 75 earthquakes have been registered by one or more strong-motion instruments. Of the 75 shallow earthquakes recorded, 23 were main shocks and 52 were aftershocks of magnitude between 3.1 and 6.9.

Preliminary data for intensity correlation studies are listed in Table 2 (see the next page). Most of the main shocks and few of the larger aftershocks have been located quite accurately, in some cases independently by near-by local networks. However, not all of the smaller events, particularly those of the Ancona group, could be located with the same accuracy, while only two of the Ghir group could be located at all. Focal distances are also subject to the same uncertainties, these being particularly critical at small value.

The unification of epicentral and local intensities of European and Middle Eastern data presents some difficulties. Intensities in Yugoslavia are invariably given on the Medvedev-Sponheuer-Karnik (MSK) Scale which is also the scale employed in Greece during the period 1965-1967. In Italy, intensity is always expressed in terms of the Mercalli-Sieberg (MS) Scale, while in the rest of the region when no particular scale is specified, earthquake intensity is expressed in terms of the Modified Mercalli (MM) Scale.

For the intensities between IV and VII (MM) it is usually assumed that there is little difference between (MSK) and (MM) ratings. However, for all intensities the difference between (MS) and (MM) ratings is not negligible. The relation between the two scales[2] is

$$I_{MM} = -0.013\,(I_{MS})^2 + 1.068\,(I_{MS}) - 0.902$$

Even when the same scale is used, differences in intensities assigned to main shocks and after shocks are likely to exist. From our experience, intensities of aftershocks in Europe and in the Near East are invariably over-estimated by at least one degree, particularly in the lower range of the scale. A correction of aftershock intensities is not warranted particularly when there is evidence that intensities assigned to a number of the aftershocks have been derived not from field observations, but from the use of empirical Intensity-Magnitude-Focal depth relationships.

TABLE 2. EARTHQUAKES RECORDED ON STRONG-MOTION INSTRUMENTS

		Time	M_L	I	R	a	Location	
1966	Sep. 1	1422	5.5	VIII	15	60.2*	GRC	Megalopolis
	Oct. 29	0239	5.6	IV+	38	9.0*	GRC	Laukas
				V	32	6.0*		Agrinion
				V+	54	30.0*		Mesolonghi
1967	Dec. 2	1244	5.1	V	36	7.4	YUG	Debar
		1418	4.4	IV	42	—	YUG	Debar
	7	1803	4.4	—	41	—	YUG	Debar
1969	Feb. 28	0240	7.5	VI+	330	3.0	PRT	Lisbon
1970	Mar. 28	2102	6.9	III	210	17.1*	TRK	Alibeyköy
	Nov. 21	0850	3.3	V+	6	1.7	ITL	Mignano
				II	18	0.2		Garigliano
	22	0910	3.5	II	18	0.4	ITL	Garigliano
	26	1430	3.1	V	6	1.0	ITL	Mignano
1971	Jan. 6	1320	3.2	V	6	1.1	ITL	Mignano
	Feb. 14	0004	4.0	VI+	11	5.2	ITL	Velfabbrica
1972	Jan. 25	2025	4.2	VII+	21	4.6	ITL	Ancona G
		2322	4.0	VII	9	8.2	ITL	Ancona G
	26	1050	3.9	VII	12	5.9	ITL	Ancona G
	Feb. 4	0242	4.4	VIII+	10	14.7	ITL	Ancona G
		0918	4.4	VIII+	—	12.7	ITL	Ancona G
		1719	4.4	VII+	25	5.8	ITL	Ancona G
		1817	4.0	VII	8	8.7	ITL	Ancona G
		1902	3.9	VII	10	5.4	ITL	Ancona G
		1930	3.5	VI	—	1.9	ITL	Ancona G
	5	0126	4.1	VIII+	8	19.3	ITL	Ancona G
		0214	3.4	VI	—	4.2	ITL	Ancona G
		0349	3.6	VI+	8	7.2	ITL	Ancona G
				VI+	11	4.7	ITL	Ancona V
		0505	3.9	VII	5	9.8	ITL	Ancona G
				VII	5	9.0	ITL	Ancona V
		0530	3.4	V	8	3.0	ITL	Ancona G
		0708	4.2	VII+	14	3.8	ITL	Ancona V
		1233	3.6	VI+	13	0.9	ITL	Ancona V
		1347	3.4	V+	8	3.0	ITL	Ancona V
		1514	4.2	VII+	13	8.6	ITL	Ancona V
		2240	3.6	V+	18	1.0	ITL	Ancona V
	6	0134	4.2	VIII	9	6.6	ITL	Ancona V
				VIII	8	18.6	ITL	Ancona G
		2145	3.9	VI	13	4.5	ITL	Ancona P
	8	1219	4.0	VII	10	11.2	ITL	Ancona P
				VII	9	15.5		Ancona G
				VII	9	7.9		Ancona V
	Mar. 14	2303	3.7	V	16	5.6	ITL	Ancona P
				V	22	2.9		Ancona G
	Apr. 4	0826	3.5	—	—	6.5	ITL	Ancona P
				—	—	11.5		Ancona G
	17	0225	4.5	—	15	22.8	PAK	Geir Mehra
		1230	—	—	—	8.1	IRN	Ghir T1
	18	0821	—	—	—	10.1	IRN	Ghir T1
	22	2043	—	—	—	18.2	IRN	Ghir T1
		2205	—	—	—	11.0	IRN	Ghir T1
	23	2228	4.6	—	—	7.0	IRN	Ghir T1

TABLE 2. (Continued)

		Time	M_L	I	R	a	Location	
	24	0140	—	—	—	7.0	IRN	Ghir T1
1972	Apr. 24	1441	4.6	—	29	9.1	IRN	Ghir T1
				—	29	5.0		Ghir H2
	25	1201	—	—	—	6.7	IRN	Ghir T1
	27	1213	—	—	—	4.8	IRN	Ghir H3
	May 30	2356	3.7	V+	8	4.4	ITL	Ancona G
	Jun. 14	1855	4.5	VII+	6	40.7	ITL	Ancona G
				VII+	11	16.6		Ancona P
				VII+	6	61.0		Ancona R
		2023	3.3	IV+	11	3.0	ITL	Ancona P
		2101	4.2	VII+	6	24.4	ITL	Ancona P
				VII+	6	51.0		Ancona R
				VII+	6	39.0		Ancona G
	15	1010	3.5	V+	5	7.3	ITL	Ancona R
				V+	6	—		Ancona P
	21	0026	—	—	—	—	ITL	Ancona P
		1506	4.0	VII	4	41.5	ITL	Ancona P
				VII	6	22.0		Ancona R
				VII	9	3.0		Ancona T
				VII	6	7.7		Ancona G
	27.	0246	3.4	—	—	4.4	ITL	Ancona G
	Sep. 17	1407	5.6	VII	50	17.2	GRC	Argostoli
				VII	50	12.8*		Argostoli
				V	136	2.5*		Mesolonghi
				V	90	2.5*		Zante
	Oct. 30	1432	5.1	V	27	16.0	GRC	Argostoli
				V	27	7.0*		Argostoli
1973	Jan. 18	0806	—	—	—	—	YUG	Rieka
	Jun. 6	2112	4.5	VI	25	5.6	YUG	Hercegnovi
	Aug. 31	1107	—	—	—	—	IRN	Dorud
	Sep. 17	0406	4.8	—	62	—	IRN	Nowshahr
	Nov. 4	1552	5.8	VII	16	52.3	GRC	Leukas
				VII	16	20.0*		Leukas
		1611	4.5	V	12	7.8	GRC	Leukas
	18	—	—	—	—	—	PRT	Acores
	23	1336	5.0	VI	223	—	PRT	Acores
	Dec. 11	0010	5.0	—	286	—	PRT	Acores
1974	Jan. 11	—	—	—	—	—	IRN	Damavand
	29	1512	4.0	V	20	4.9	GRC	Patras
	Mar. 1	—	—	—	—	—	IRN	Damavand
	10	—	—	—	—	—	IRN	Damavand
	11	2021	4.7	—	134	—	IRN	Shiraz
				—	87	—		Jahrum
	Apr. 11	2102	3.8	—	25	—	IRN	Kazerun
	May 19	—	—	—	—	—	IRN	Keyasar
	23	1951	4.7	VI	14	18.0	YUG	Imotski
	Jun. 30	—	—	—	—	—	IRN	Faruj

Notes : I = Reported intensity of earthquake at recording station. For Italian events (ITL) intensity on (MS) Scale; for Yugoslav events (YUG) intensity on (MSK) Scale.

R = Focal distance of recording station in kilometres.

a = Maximum recorded ground acceleration in (%) of (g). Entries marked with asterisk indicate maximum double amplitude in (mm) of Wilmot seismoscope.

The geological conditions at the site of instruments are known to the extent that only a rough classification of the foundation conditions is possible. Sites have been classified, therefore, in four broad categories, ranging from very soft normally consolidated soils "A" to solid rock, "D"

Of the 99 strong-motion recordings listed in Table 2, copies of half of them were made available for analysis. These records were corrected for base line using parabolic fitting without filtering. For the other half of the recordings peak ground accelerations were extracted from published and unpublished reports.

Figure 4 shows a plot of the recorded maximum horizontal acceleration (solid points) versus reported intensity (MM) at the recording station for the period 1967-1974. The same figure shows a plot of the maximum vertical acceleration (open points) versus I_{MM}. Stars and circles show peak accelerations on "hard ground" (C and D), and "soft ground" (A and B) respectively.

For the 8-year sample of data, a first order approximation of the relation between maximum horizontal acceleration and I_{MM} may be expressed by

$$\log(a_h) = -0.16 + 0.36\,(I_{MM})$$

For the vertical acceleration we have:

$$\log(a_v) = -0.55 + 0.38\,(I_{MM})$$

These two empirical relations are shown in Figure 4 by a solid and broken line respectively; the standard deviation is about 0.7 of the mean. Figure 5 (page 216) shows a plot of the maximum horizontal velocity versus I_{MM}. The data is barely sufficient to define a trend:

$$\log(v_h) = 0.18 + 0.26\,(I_{MM})$$

Considering now the relationship between maximum horizontal and vertical accelerations, the data suggest that with increasing horizontal acceleration the ratio (a_v/a_h) decreases. For the range of $1\%g \leqslant a_h \leqslant 10\%g$, $11\%g \leqslant a_h \leqslant 29\%g$ and $30\%g \leqslant a_h \leqslant 60\%g$ we have, $a_v = 0.67\,(a_h)$, $a_v = 0.53\,(a_h)$ and $a_v = 0.39\,(a_h)$ respectively. For velocities the data is insufficient to give a trend; they do, however, suggest that on the average, the maximum vertical velocity is about 60% of the horizontal.

Concerning the influence of geologic conditions on maximum recorded ground-motions, Figure 4 shows quite clearly that for intensities greater than V, both horizontal and vertical maximum accelerations on "hard ground" are larger by a factor

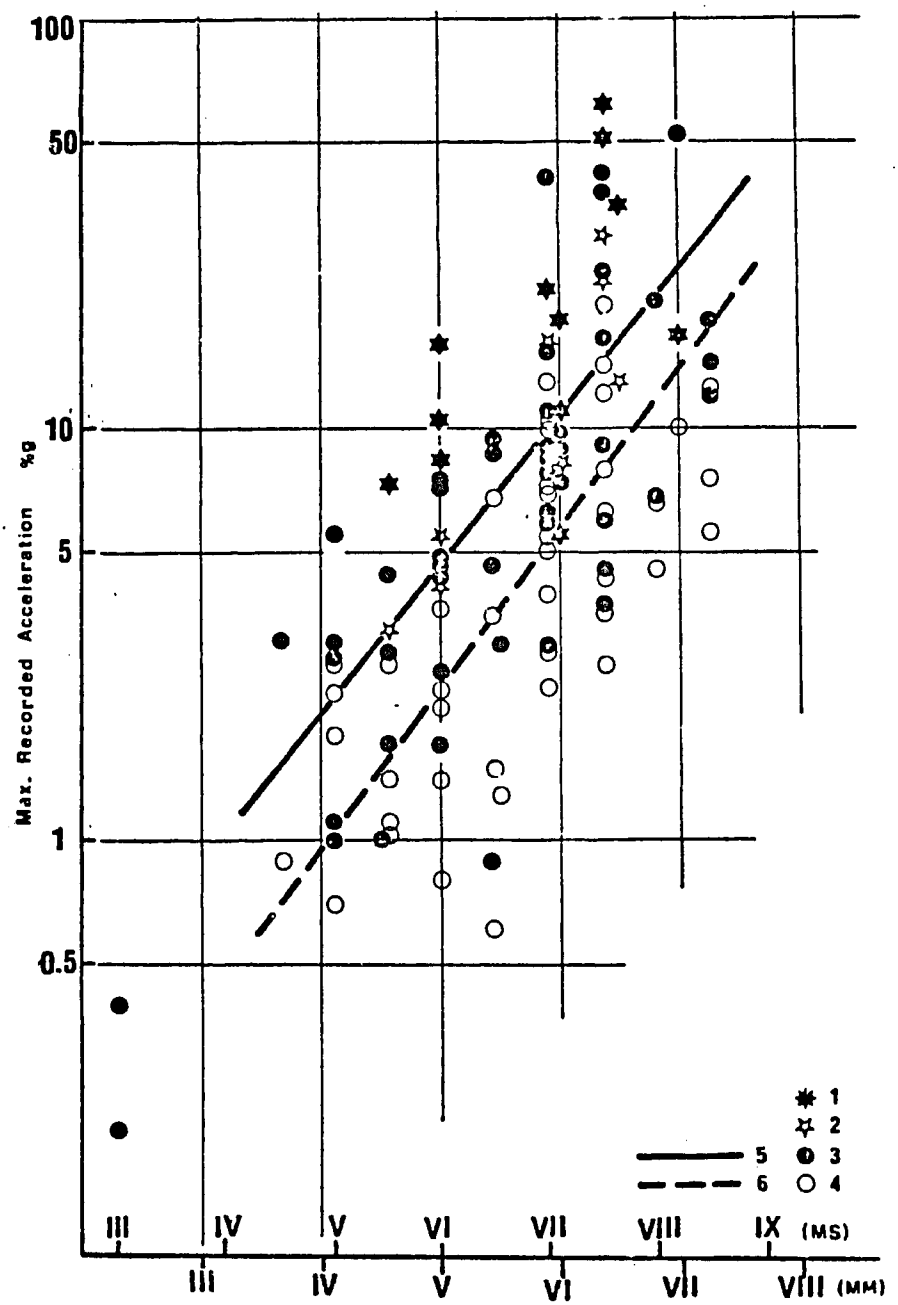
100
50
10
5
1
0.5
Max. Recorded Acceleration %g
III
IV
V
VI
VII
VIII
IX (MS)
III
IV
V
VI
VII
VIII (MM)
1
2
3
4
5
6

FIGURE 4

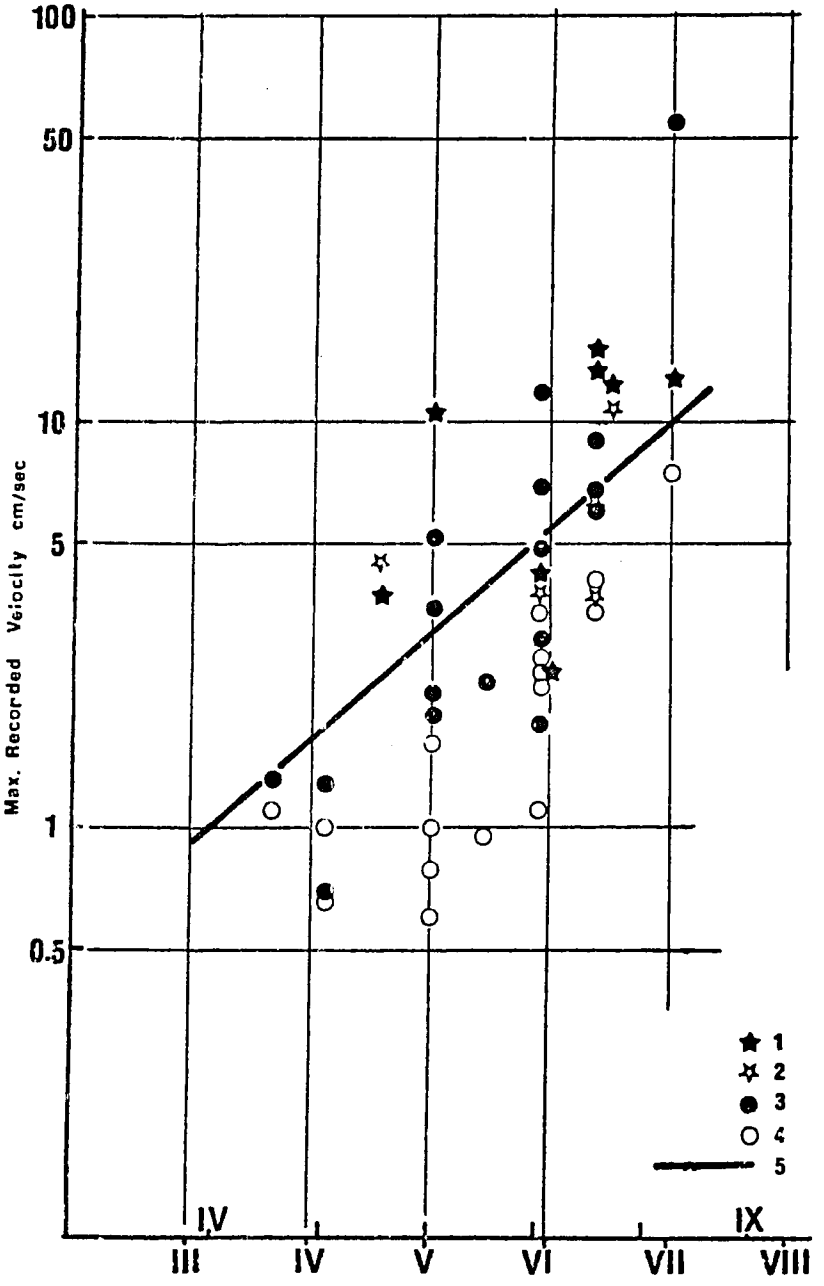
100
50
10
5
1
0.5
Max. Recorded Velocity cm/sec
1
2
3
4
5
IV
IX
III
IV
V
VI
VII
VIII

FIGURE 5

of two than on "soft ground". The same conclusion may be drawn from Figure 5 for peak velocities.

REFERENCES

1. *N. Ambraseys, Proc. 5th World Cong. Earthq., Rome (1973).*

2. *R. Console, F. Peronaci, G. Sist and A. Sonaglia, "Alcune considerazioni sui fenomeni sismici di Ancona", Ist. Naz. Geof. Publ., Rome, 1972.*

RANDOM VIBRATION OF AN ELASTOPLASTIC SYSTEM

Mr. İbrahim Helvacı and Dr. Aybars Gürpınar

The response of nonlinear systems to random excitation is becoming important as earthquake engineering. The incorporation of the ductility factor into earthquake resistant design has made it necessary to study the response of nonlinear systems more carefully. Almost all real physical systems exhibit nonlinearity for sufficiently large motions.

Aproximate methods such as perturbation[1] and equivalent linearization[2,3,4] techniques have been developed to extend linear analysis to certain nonlinear systems. The drawback of such methods is the restriction that the nonlinearities are very small. Exact solutions to nonlinear system response problems can be obtained under certain strict conditions.

Consider the equation of motion of a "nonlinear spring" system.

$$\ddot{x} + \beta \dot{x} + F(x) = f(t) \qquad (1)$$

where x is displacement, t is time, β is the viscous damping per unit mass, F (x) is the nonlinear restoring force per unit mass, and f (t) is the load per unit mass as a function of time. If the dynamical system is represented by a point in the phase space, then its

trajectory in this phase space is identified as a continuous Markov process. The probability law for such a process can be obtained as the fundamental solution to the Fokker-Planck equation,[5]

$$\frac{\partial p_c}{\partial t} = -\sum_i \frac{\partial}{\partial y_i}(a_i P_c) = \frac{1}{2}\sum_i \sum_j \frac{\partial^2}{\partial y_i \partial y_j}(b_{ij} P_c) \tag{2}$$

where $P_c = P_c\ (y, t/x)$ is the transition probability and

$$a_i = \lim_{\Delta t \to o} \frac{E(\Delta \bar{y}_i)}{\Delta t}, \quad b_{ij} = \lim_{\Delta t \to o} \frac{E(\Delta \bar{y}_i \,.\, \Delta \bar{y}_j)}{\Delta t} \tag{3}$$

in which E (.) is the expected value of (.), y_i is the position vector in the phase space.

Caughey[5] obtained the transition probability for a general nonlinear system with one-degree of freedom, the motion of which is governed by Eq. 1 under the conditions that the forcing function is stationary Gaussian with white spectral density having zero mean, i.e.

$$E[\,f(t)\,] = 0 \tag{4a}$$

$$E[\,f(t_1)\,.\,f(t_2)\,] = (W_o/2)\,.\,\delta\,(t_1 - t_2) \tag{4b}$$

where W_o is the white spectral density in $(cm/sec)^2 cps$ and δ (.) is the Dirac delta function. Letting $y_1 = x$ and $y_2 = x$, the transition probability can be obtained as

$$P(y_1, y_2) = C \exp\left\{-\frac{4\beta}{W_o}\left[\frac{y_2^2}{2} + \int_o^{y_1} F(u)\,du\right]\right\} \tag{5}$$

where C is normalizing constant.

Consider the one-degree-of-freedom system having elasto-plastic force-deformation relation shown in Figure 1. If stiffness degradation and rebound phenomenon are neglected and if the forcing function is assumed to be a stationary, Gaussian "white" random process with zero mean. then the restoring force F (x) for the loading zone, i.e., from $-x_y$ to μx_y can be written as

$$F(x) = W_n^2\,[\,X - (x - x_y)\,H\,(x - x_y)] \tag{6}$$

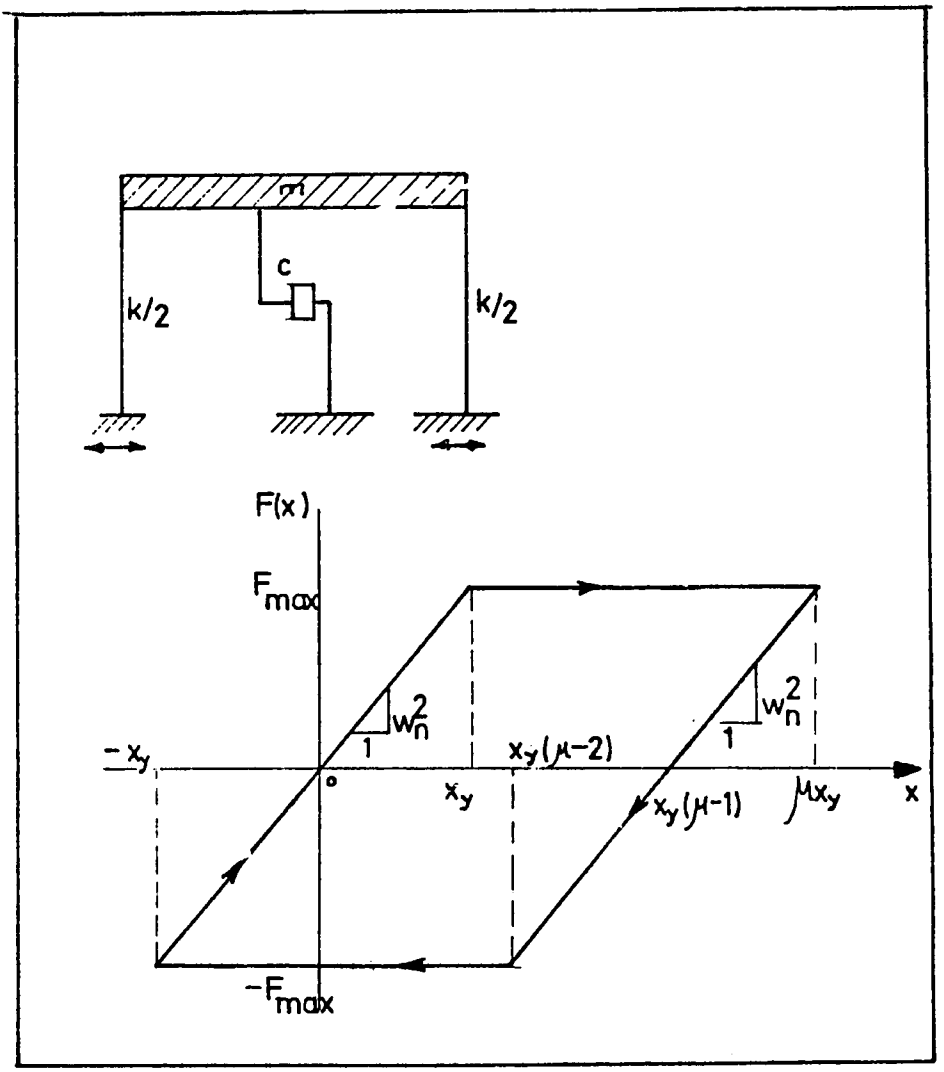

Figure 1. One Degree of Freedom System and Assumed Elasto-Plastic Deflection Diagram.

where W_n is the undamped natural frequency in the elastic zone and H (.) is the Heaviside function. Substituting Eq. 6 into Eq. 5

$$P(y_1, y_2) = C \exp\left\{-A^2 \left[\frac{y_2^2}{w_n^2} + y_1^2 - (y_1 - x_y)^2 H(y_1 - x_y)\right]\right\} \quad (7)$$

Here, $A^2 = 4\xi\, w_n^3/W_o$ where ξ is known as the ratio of critical damping. Using the normality condition,

$$\int_{-\infty}^{\infty} \int_{-x_y}^{\mu x_y} p(y_1 . y_2)\, dy_1 . dy_2 = 1 \quad (8)$$

and substituting for $P(y_1, y_2)$,

$$\frac{1}{C} = \frac{W_n\sqrt{\pi}}{A}\left\{2\int_0^{x_y} \exp(-A^2 y_1^2) dy_1 + \exp(A^2 x_y^2) \int_{+x_y}^{\mu x_y} \exp(-2A^2 x_y . y_1) dy_1\right\} \quad (9)$$

Carrying out the integrations and substituting for C, the final form of $P(y_1, y_2)$ can be written as,

$$p(y_1, y_2) = \frac{A \exp\left\{-A^2\left[\frac{y_2^2}{w_n^2} + y_1^2 - (y_1 - x_y)^2 H(y_1 - x_y)\right]\right\}}{W_n\sqrt{\pi}\left\{\frac{2S_1}{A} + \frac{x_y}{B \exp(B/2)}\left[1 - \exp - B(\mu - 1)\right]\right\}} \quad (10)$$

where, $B = 2A^2 x_y^2$, and (11)

$$S_1 = \sum_{n=o}^{\infty} (-1)^n \frac{(A\, x_y)^{2n+1}}{(2n+1)\,(n!)} \quad (12)$$

It can easily be shown that S_1 converges.

The mean square displacement for loading can be found from the definition:

$$E_1(y_1^2) = \int_{-\infty}^{\infty} \int_{-\infty}^{\infty} y_1^2\, p(y_1, y_2)\, dy_1\, dy_2 \quad (13)$$

by substituting for $P(y_1, y_2)$ from Eq. 10

$$E_l(y^2) = \frac{\dfrac{2S_2}{A^3} + \left(\dfrac{x_y}{B}\right)^3 \left\{ [(B+1)^2+1]e^{-B/2} - [(\mu B+1)^2+1]e^{-B(\mu - \frac{1}{2})} \right\}}{\dfrac{2S_1}{A} + \dfrac{x_y}{Be^{B/2}} - [1 - e^{-B(\mu-1)}]} \tag{14}$$

where,

$$S_2 = \sum_{n=o}^{\infty} (-1)^n \frac{(Ax_y)^{2n+3}}{(2n+3)(n!)} \tag{15}$$

The mean square displacement $E_r(y_1^2)$ for reverse loading can easily be obtained from $E_l(y_1^2)$ and is

$$E_r(y_1^2) = E_l(y_1^2) + x_b^2 \tag{16}$$

where,

$$x_b = X_y(\mu - 1) \tag{17}$$

The general equation (6) for crossing a level a with positive slope is

$$\nu_a^+ = \int_o^{\infty} \dot{x}\, p(a, \dot{x})\, d\dot{x} \tag{18}$$

where ν_a^+ is the expected number of crossing level a with positive slope per unit time, which becomes

$$\nu_{x_y}^+ = \int_o^{\infty} y_2\, p(x_y, y_2)\, dy_2 \tag{19}$$

for the case under consideration. $P(x_y, y_2)$ in Eq. 19 may already be obtained from general form of probability density function, Eq. 10 for $y_1 = x_y$ and $\mu = 1$, and Eq. 19 becomes

$$\nu^{+}_{x_y} = \int_0^{\infty} y_2 \frac{A^2 \exp\left\{-A^2\left[-\frac{y_2^2}{w_n^2} + x^2\right]\right\}}{2\sqrt{\pi}\, w_n S_1} dy_2 \tag{20}$$

which yields

$$\nu_{x_y} = \frac{\sqrt{\pi}}{2 S_1 T_n} \exp(-B/2) \tag{20a}$$

where $T_n = 2\pi/w_n$ is the natural period in the elastic range. Expected time for crossing the yield level is thus

$$E(t_c) = 1/\nu_{x_y} = \frac{2 S_1 \exp(B/2)}{\sqrt{\pi}} T_n \tag{21}$$

Expected time for crossing the barrier for both loading and reverse-loading may be assumed to be equal. This assumption permits the calculation of total time that the system spends in each zone when it is excited by a force of known duration $\underset{\sim}{t}$.

Then, we define time-weighted MSD $\bar{E}(y_1^2)$ as

$$\bar{E}(y^2) = \frac{t_l E_l(y_1^2) + t_r E_r(y_1^2)}{\underset{\sim}{t}} \tag{22}$$

where t_l and t_r the total time spent in loading and reverse-loading, respectively, $\underset{\sim}{t}$ is the duration of excitation (earthquake acceleration), and $\underset{\sim}{t} = t_l + t_r$ holds. Inserting Eq. 17 into Eq. 22, one gets

$$\bar{E}(y_1^2) = E_l(y_1^2) + \frac{t_r}{\underset{\sim}{t}} x_b^2 \tag{23}$$

Nonstationaritl of the response process as a whole is obvious since the first and the second statistical moments (mean and mean-square displacements) are not the same for loading and reverse loading cases. Now, we propose an equivalent-mean that matches the weighted MSD, and variance of the nonstationary process. That is,

$$E(y_1^2) = E_{eq}(y_1^2)$$
$$= V_{eq}(y_1) + [E_{eq}(y_1)]^2 \tag{24}$$

Since we assume equal variances,

$$\overline{E}(y_1^2) = V_l(y_1) + [E_{eq}(y_1)]^2$$
$$= E_l(y_1^2) + [E_{eq}(y_1)]^2 \tag{25a}$$

or

$$[E_{eq}(y_1)]^2 = \overline{E}(y_1^2) - E_l(y_1^2) \tag{25b}$$

Substituting Eq. 23 into Eq. 25b, equivalent-mean is obtained as,

$$E_{eq}(y_1) = \left(\sqrt{\frac{t_r}{\underset{\sim}{t}}}\right) . x_b \tag{26}$$

An equivalent ideal elastic system having the same MSD as the weighted-MSD, $E(y_1^2)$, of the elasto-plastic system can be found under certain assumptions. Keeping the damping unchanged and relying on Caughey's results[3,5] for the elasto-plastic systems, an equivalent period for the corresponding elastic system can be obtained. It can be shown that MSD for an ideal elastic system under the prescribed assumptions is

$$E(y_1^2) = \frac{W_o}{64\,\pi^3 \xi} T_n^3 \tag{27}$$

If we equate this to the weighted MSD, modifying the period,

$$\overline{E}(y_1^2) = \frac{W_o}{64\,\pi^3 \xi} T_{eq} \tag{28}$$

where T_{eq} is the corresponding equivalent period, given as

$$T_{eq} = 4\pi \sqrt[3]{\frac{\xi}{W_o} E(y_1^2)} \tag{29}$$

Results and Discussion

As the first step, the probability density function essential for nondeterministic analysis has been obtained in series form for loading zone of an elasto-plastic system subjected to an earthquake-type excitation having a Gaussian distribution with zero mean and white spectral density. Zero mean assumption for the earthquake acceleration is valid for the cases of practical interest. The white spectral density assumption, however, implies weak stationary which is not strictly true for the earthquake acceleration. It has been shown that the later assumption is good for all damping values especially in the short period range.[7]

Form of the equations for MSD of elasto-plastic system suggests that numerical values must be assigned to the variables involved. For this purpose, the following values and ranges were considered:

$0.005 \leqslant \xi \leqslant 0.10$; $0.10 \leqslant T_n \leqslant 1.0$ sec.; $1.0 \leqslant \mu \leqslant 5.0$; $\underset{\sim}{t} = 30$ sec.
$W_o = 300\ (\text{cm/sec})^2/\text{cps}$.

The last two values correspond, approximately, to the values for the NS component of the El-Centro earthquake in 1940.[8]

The series terms S_1 and S_2, as given by Eq. 12 and 15 respectively, are functions of $(A\ x_y)$, both of which are related to T_n. The relation between A and T_n is given in Eq. 7. It is known that natural period and the yield displacement of a structure are related to each other, and this relation can be expressed as

$$x_y = (C_e \cdot o_\gamma \cdot 4\pi^2)\, T_n^2 \tag{30}$$

where C_e is known as the seismic coefficient. In our analysis, the Code for structures to be Built in the Regions of Hazard of Turkey has been used to determine C_e. The elements which this considers for the earthquake effect on structures, and the corresponding critical values are as follows:

Regional coefficient	$C_o = 0.06$
Foundation coefficient	$\alpha = 1.20$
Building importance coefficient	$\Theta = 1.50$
Structural dynamic coefficient	$\gamma = 1$ for T_n 0.5 sec. $= 0.5/T_n$ 0.5 sec.
Seismic coefficient	$C_e = C_o \cdot \alpha \cdot \gamma \cdot \Theta$ (31)

A computer program has been prepared for the values mentioned above, and the results were given in graphical form (See Figures 3 — 8 on the next pages). The decreasing effect of damping on MSD is obviously due to its energy dissipative character.

From Eq. 30, the yield displacement, which is the point of stiffness discontinuity in the case, increases with period, a measure of the flexibility of a structure. The results we have obtained are in good agreement with those obtained by Yao and Yeh[9] for the relation between the period and MSD, since they showed that system responses increase with the parameter representing the point of stiffness discontinuity (yield displacement) (Figure 2 on page 226).

Figure 3 compares the elasto-plastic and the corresponding elastic responses as given by Eq. 23 and 27, respectively. The elasto-plastic MSD increases with ductiliy factor, and depending on that factor, they are generally greater than the corresponding elastic values particularly for relatively high damping values. This result seems to contradict the results of deterministic analysis of the system. The earthquake response spectra obtained from the existing records indicate that maximum response of an elastoplastic structure is smaller than that of the corresponding elastic system. However, there is no contradiction since the response spectrum corresponds to a maximum amplitude whereas root-mean square value corresponds to average amplitude. Besides, the results we have obtained agree with those obtained by Caughey.[2] Hence, the average amplitude of displacement response for an elasto plastic system is greater, but the maximum amplitude is smaller than that for the corresponding elastic system. This implies that elasto-plastic systems are more susceptible to fatique failure whereas elastic systems may fail due maximum stresses.

The MSD response of an elasto-plastic system is found to be more sensitive to ductility than damping for a given natural period as shown in Figure 4. This can be explained by the fact that the effect of damping is assumed to be the same for both loading and unloading, whereas change in ductility factor shifts the point of equilibrium x_b in the reverse-loading zone. This explanation also holds for Figure 5, plotted for Eq. 26.

Variation of the expected time for crossing the yield level, computed from Eq. 21 is shown in Figure 6. Since the yield level increases with the period, the system needs more time to reach that level. On the other hand, if the system has relatively higher damping values, more energy is dissipated, hence more time is needed for yielding.

The ratio of the period of an ideal elastic system having equal damping and MSD with the elasto-plastic system to the corresponding natural period is computed using Eq. 29, and the results are presented in Figure 7. The higher the damping, the more energy can be transferred to the system from the excitation since some of it will be

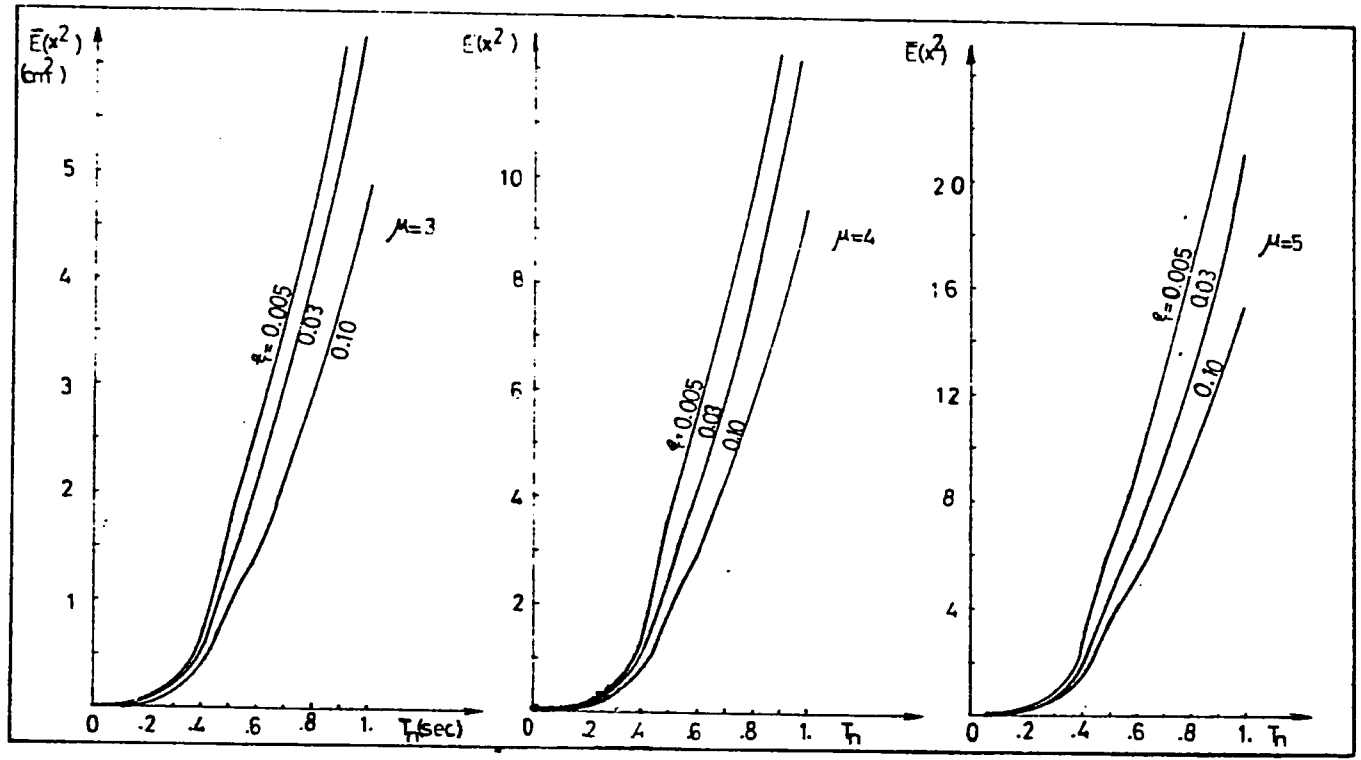

Figure 2.

Time-Weighted Averages of the Mean-Square Displacements

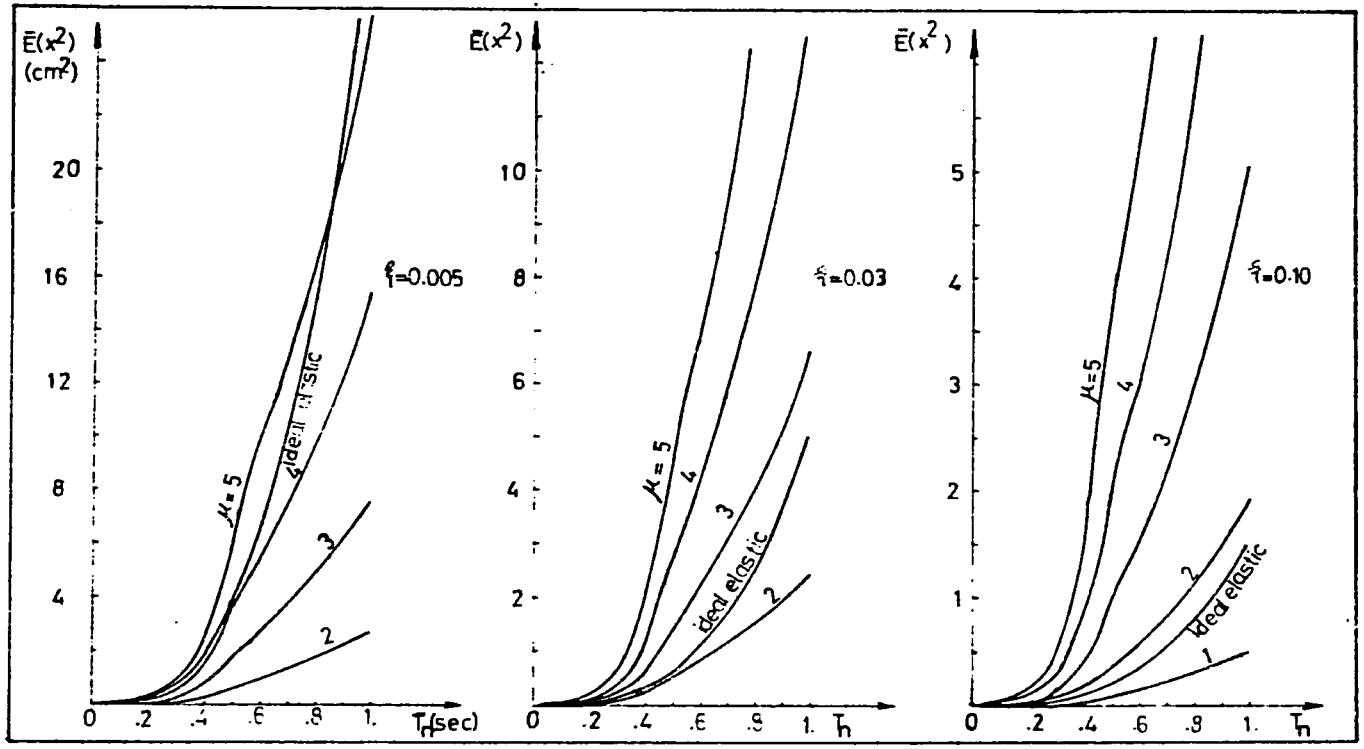

Figure 3.

Mean-Square Displacements for Elastic and Elasto-Plastic Systems

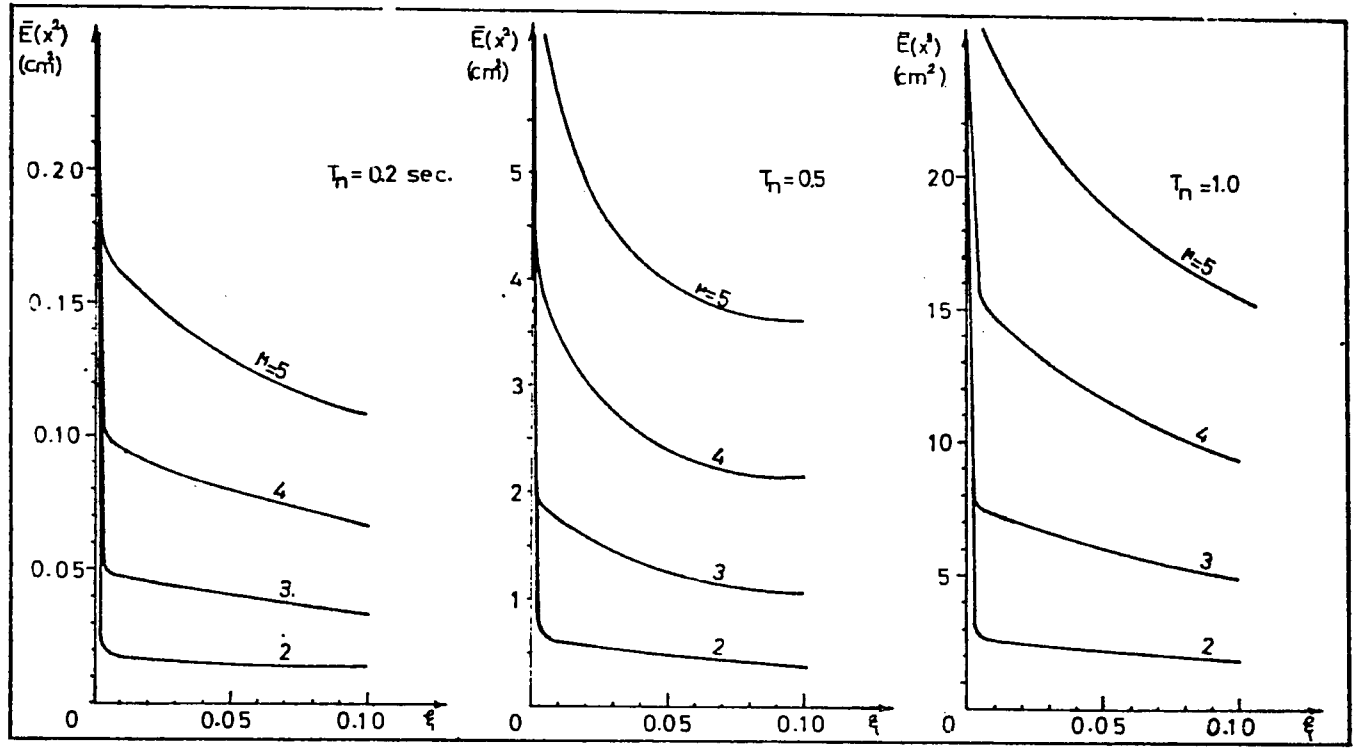

Figure 4.

Damping-Ductility Sensitivity Curves

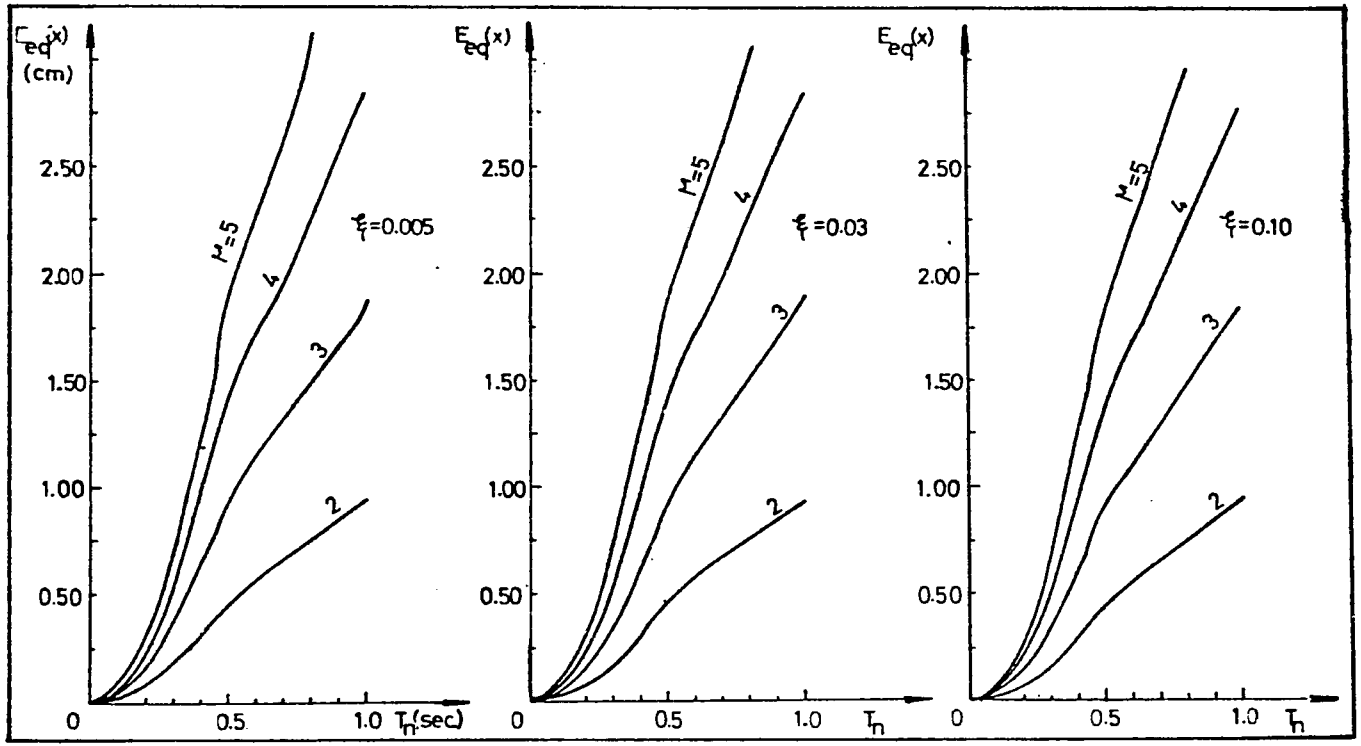

Figure 5.
Equivalent Mean Values

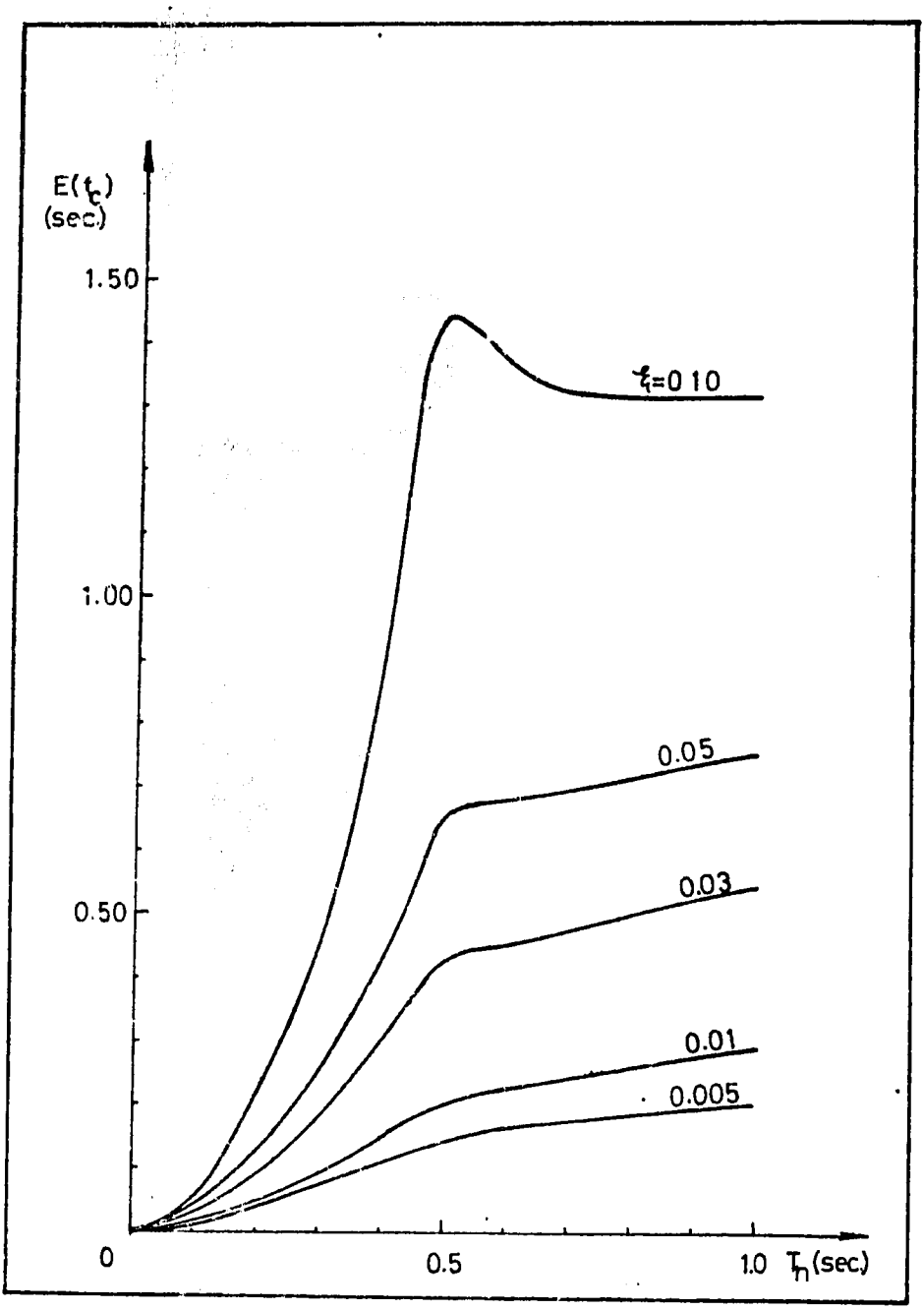

Figure 6. Expected Time for Crossing the Yield Level

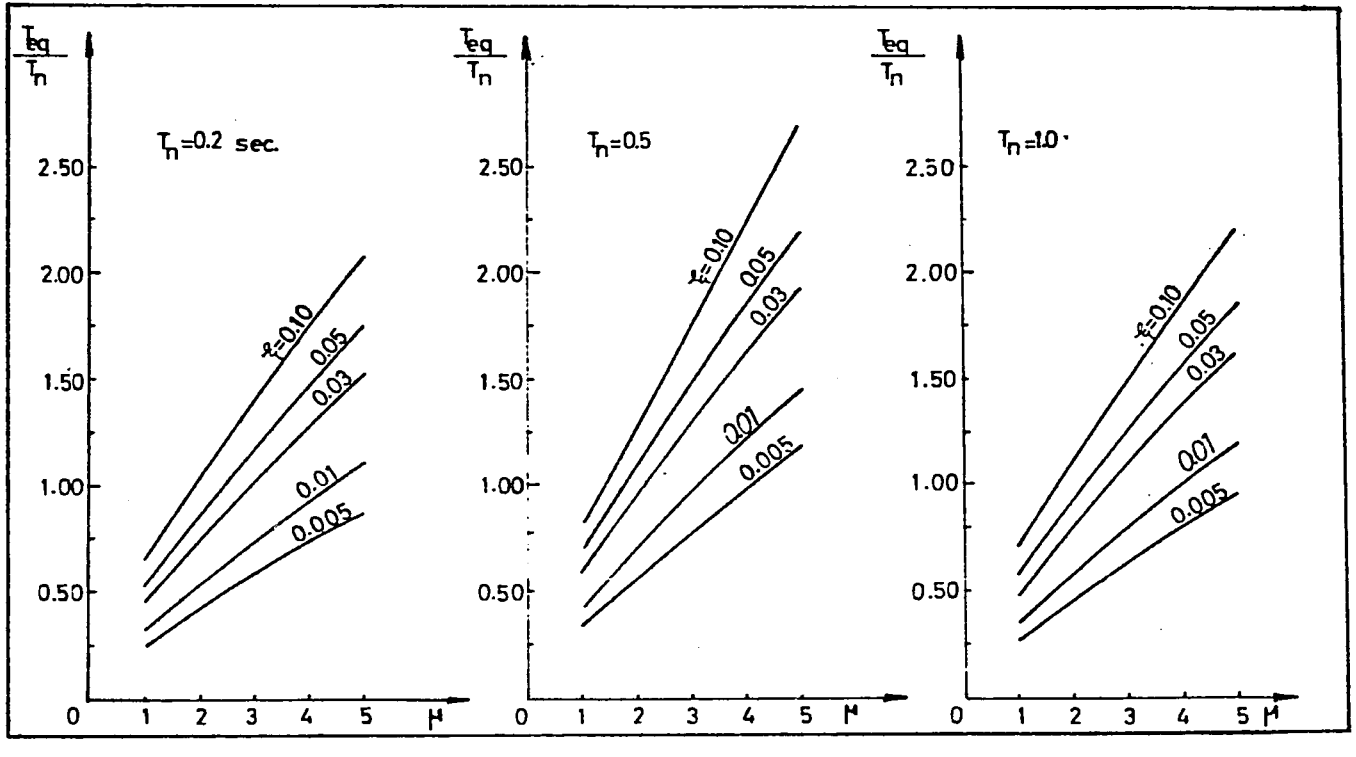

Figure 7.

Period Ratios of Equivalent Ideal Elastic Systems

dissipated during the motion. However, since the linear system is assumed to have the same damping as the elasto-plastic one, it is to absorb more energy which implies a greater area under the force-deflection curve and this, in turn, requires a greater period. Increasing the equivalent period with ductility factor, on the other hand, indicates the decrease in effective stiffness of the elasto-plastic system, a result which had been found previously by Caughey[2] using different techniques.

The results obtained lead to the conclusion that the average amplitude of displacement response of an elasto-plastic system subjected to earthquake-type excitation is greater than the corresponding elastic ystem. This suggests that repeated load as well as the peak response (stress) should be considered as a failure criteria for elasto-plastic systems.

REFERENCES

1. *S.H. Crandall, J. Acoust. Soc. Amer., 35, 1700 (1963).*

2. *T.K. Caughey, J. Appl. Mech., 27, 649 (1960).*

3. *T.K. Caughey, J. Acoust. Soc. Amer., 35, 1706 (1963).*

4. *L.D. Lutes, Proc. Amer. Soc. Civil Eng., EM3, 227 (1970).*

5. *T.K. Caughey, J. Acoust. Soc. Amer., 35, 1683 (1963).*

6. *S.H. Crandall and W.D. Mark, "Random Vibration in Mechanical Systems", Academic Pr., N.Y., 1963.*

7. *J. Penzien, Bull. Int. Inst. Seism. Earthq. Eng., 2, 47 (1965).*

8. *J. Penzien and S.C. Liu, Proc. 4th World Conf. Earthq. Eng., Santiago, A–1, 114 (1968).*

9. *H.Y. Yeh and J.T.P. Yao, Bur. Eng. Res., Univ. New Mexico, Technical Report, 1964.*

DISCUSSION

Professor Ambraseys was doubtful about the provision made for viscous damping: it was necessary to be careful when using the damping coefficient term since it varied according to the nature of the system. Mr. Helvacı said that damping for non-linear systems approached asymptotically the values for the linear system.

RECOMMENDATIONS

1. It is recommended that each Regional Government should appoint a national committee to coordinate activities in earthquake engineering.

2. The CENTO Scientific Coordinating Board is asked to finance visits to the scheme of recent earthquake, soon after the event, by housing engineers and engineering geologists from the other CENTO countries.

3. CENTO is asked to organise a Study Workshop on the site of a previous earthquake. This would enable geologists to map and identify tectonic features, faulting, ground slumping and landslides, and the effect these had; seismologists could study the seismicity before and after the earthquake; engineers could assess any damage still visible and structures which were not damaged, and consider the construction techniques.

4. CENTO is asked to organise panel meetings or symposia on:

(a) Earthquake hazards of dwellings: siting, use of traditional materials, improvement of traditional methods, standardisation and mass production, and costs.

(b) Minimization of earthquake hazards: seismicity earthquake risk active tectonics, implementation of earthquake codes of practice. This meeting would be concerned with rural housing, new towns and villages, and important engineering structures such as dams, power stations, etc.

(c) Predisaster planning.

5. CENTO is asked to organise a short course on earthquake engineering: this could be an interdisciplinary course covering seismology, soil dynamics, geology, etc.

LIST OF PARTICIPANTS

IRAN

Dr. M. Banisadr	Plan and Budget Organisation, Tehran
Dr. K. Moazami Goudarzi	Institute of Geophysics, Tehran University
Dr. Mehram Lashkari	Arya Mehr University, Tehran
Dr. Ali A. Moinfar	Plan and Budget Organisation, Tehran

PAKISTAN

Mr. Anwaruddin Ahmad	Geological Survey of Pakistan, Quetta
Professor S. Nazir Ahmad	University of Engineering and Technology, Lahore
Brig. Mushtaq A. Gill	Ministry of Defence, Mangla

TURKEY

Mr. Ertuğrul Ada	State Waterworks, Ankara
Mr. Hazer Aloc	Karabük Steel Works, Karabük
Mr. Hasan Umar Akay	Middle East Technical University, Ankara
Mr. Mustafa Akınlı	Turkish Electricity Institute
Mr. Nuri Akkaş	Middle East Technical University, Ankara
Mr. Emin Aktan	Middle East Technical University, Ankara
Mr. Ender Arkun	TBTAK, Ankara

Dr. Attila Askar	Bosphorus University, Istanbul
Mr. Yaşar Atan	İstanbul Technical University, İstanbul
Mr. Bilgutay Atila	Middle East Technical University, Ankara
Mr. Ruhi Aydın	State Engineering Academy, Eskişehir
Mr. M. Nuray Aydınoğlu	İstanbul Technical University, İstanbul
Mr. Alkut Aytun	Building Research Institute, Ankara
Mr. Nejat Bayülke	Ministry of Reconstruction and Resettlement
Mr. Mustafa Boyacıyılmaz	State Waterworks, Ankara
Mr. Erol Buluş	State Waterworks, Ankara
Dr. Mehmet Çelebi	Middle East Technical University, Ankara
Dr. Muammer Çetinçelik	Turkish Society of Engineers and Architects, Ankara
Mr. Mesut Çetinçelik	Turkish Society of Engineers and Architects, Ankara
Mr. Murat Dikmen	Middle East Technical University, Ankara
Dr. H. Turan Durgunoğlu	Bosphorus University, İstanbul
Dr. M. Bahadır Eke	State Highways Administration, Ankara
Dr. Selçuk M. Erden	Bosphorus University, İstanbul
Mr. Turhan Erdoğan	Middle East Technical University, Ankara
Mr. Oktay Ergunay	Ministry of Reconstruction and Resettlement
Dr. Ali Erguvanlı	İstanbul Technical University, İstanbul
Mr. Uğur Ersoy	Middle East Technical University, Ankara

Mr. Aybar Ertepınar	Middle East Technical University, Ankara
Mr. Sinan Gencoğlu	Earthquake Research Institute, Ankara
Dr. Polat Gülkan	Middle East Technical University, Ankara
Mr. Ayfer Gürkök	Middle East Technical University, Ankara
Dr. Aybars Gürpınar	Middle East Technical University, Ankara
Mr. Teoman Güzey	Earthquake Research Institute, Ankara
Dr. İbrahim Helvacı	Middle East Technical University, Ankara
Mr. Mehmet İpek	Middle East Technical University
Dr. Muzaffer İpek	İstanbul Technical University, İstanbul
Mr. Can İskender	TBTAK, Ankara
Dr. Bilgin Kaftanoğlu	Middle East Technical University, Ankara
Mr. Ergin Karaesmen	Middle East Technical University, Ankara
Dr. Erhan Karaesmen	Karadeniz Technical University, Trabzon
Dr. H. Faruk Karadoğan	İstanbul Technical University, İstanbul
Dr. Engin Keyder	Middle East Technical University, Ankara
Mr. Uğur Köken	Ministry of Public Works, Ankara
Mr. Süleyman Kovacıoğ	Earthquake Research Institute, Ankara
Professor Vahit Kumbasar	İstanbul Technical University, İstanbul
Dr. Uğur Kuran	State Highways Administration, Ankara
Mr. Taylan Lunel	Middle East Technical University, Ankara
Mr. Oğuz Mutdoğan	Turkish Electricity Institute, Ankara

Dr. Mete Nakiboğlu	Middle East Technical University, Ankara
Dr. Teoman Norman	Middle East Technical University, Ankara
Professor Nuriye Pınar Erdem	State Academy of Engineering, İstanbul
Mr. Burhan Cahit Özdural	Middle East Technical University, Ankara
Dr. Dinçer Özgür	Middle East Technical University, Ankara
Mr. Yener Özkan	Middle East Technical University, Ankara
Mr. Hasan Özyiğit	Middle East Technical University, Ankara
Mr. Bülent Pakman	Middle East Technical University, Ankara
Mr. Hüseyin Sosyal	İstanbul University
Dr. Çetin Soydemir	Middle East Technical University, Ankara
Mr. Ahmet Tabban	Earthquake Research Institute, Ankara
Mr. Duran Tekin	Bosphorus University, İstanbul
Mr. Turgut Tokdemir	Middle East Technical University, Ankara
Professor Semiz Tezcan	Boğaziçi University, İstanbul
Mr. Ayser Türkoğlu	Earthquake Research Institute, Ankara
Mr. İlhami Tüzel	Ministry of Defence, Ankara
Dr. Mehmet Ersen Ülküdaş	Social Security Institute, İzmir
Mr. Rifat Ünal	Middle East Technical University, Ankara
Dr. Coşkun Ünan	Middle East Technical University, Ankara
Dr. Erol Varoğlu	Middle East Technical University, Ankara
Mr. S. Tanvir Wasti	Middle East Technical University, Ankara

Mr. Muammer Yaralıoğlu	State Waterworks, Ankara
Mr. Esat Yarar	Earthquake Research Institute, Ankara
Professor Kasım Yaşar	Middle East Technical University, Ankara
Mr. Tuncay Yaşar	Middle East Technical University, Ankara
Professor Asım Yeğinobalı	Middle East Technical University, Ankara
Mr. Sabahattin Yeşilyurt	Middle East Technical University, Ankara
Professor Müfit Yorulmaz	İstanbul Technical University, İstanbul
Dr. Özal Yüzügüllü	Middle East Technical University, Ankara

UNITED KINGDOM

Professor N. Ambraseys	Imperial College of Science and Technology, London
Mr. J.D.M. Lloyd	Building Research Establishment, Watford

USA

Dr. A. Cakmak	Princeton University, New Jersey
Professor W. Keightley	Montana State University

CENTO

Dr. G.R. Ames	CENTO Scientific Secretary, Tehran

CENTO SCIENTIFIC PROGRAMME PUBLICATIONS

1. High Yielding Wheat: *Panel held in Tehran, December 1970.*

2. Environmental Pollution: *Panel held in Tehran, March 1971.*

3. Food Processing: *Travelling Workshop held in İzmir, Tehran and Lahore, September 1971.*

4. Scientific Laboratories, Organization and Administration: *Travelling Workshop held in Lahore, Tehran and İstanbul, April 1972.*

5. Cereals: *Programme Meeting held in Lahore, December 1972.*

6. Natural Drugs, and their Commercial Utilisation: *Panel Meeting held in Peshawar, December 1972.*

7. Pests and Diseases of Wheat: *Panel Meeting held in Karaj, Iran, February 1973.*

8. Rural Housing: *Symposium held in Ankara, May 1973.*

9. Village Water: *Programme Meeting held in İzmir, November 1973.*

10. Village Water: *Project Report, 1971—1973.*

11. Parasitic Diseases: *Symposium held in Shiraz, December 1973.*

12. Scientific Documentation: *Conference held in Tehran, April 1974.*

13. Economics of Nuclear Power Plants: *Symposium held in Ankara, June 1974.*

14. Cereals: *Programme Meeting held in İzmir, November 1974.*

15. University Services for Industry: *Panel Meeting held in Lahore, December 1974.*

16. Optimum Use of Water in Agriculture: *Panel Meeting held in Lyallpur, March 1975.*

17. **Scientific Research Institutions in the CENTO Region:** *1975 Directory.*

These reports are available free of charge from:

Dr. Geoffrey Ames
CENTO Scientific Secretary
P.O. Bo 1828
Tehran, Iran

or

A. S. Kışlalı
Technical Editor
CENTO
Eski B.M.M. Binası, Ulus
Ankara, Turkey